G-quadruplex recognition and isolation with small molecules

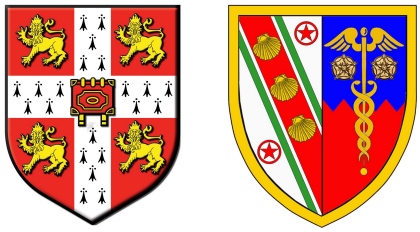

Sebastian Müller

Darwin College

University of Cambridge

A dissertation submitted in partial fulfillment of the requirements for the degree of

Doctor of Philosophy

October 2010

Declaration

I, Sebastian Müller, declare that this thesis titled: 'G-quadruplex recognition and isolation with small molecules' and the work presented therein are my own.

The work described in this thesis was carried out by me in the Department of Chemistry, University of Cambridge, under the supervision of *Professor Shankar Balasubramanian*, between October 2006 and September 2010. This dissertation is the outcome of my own work and includes nothing which is the outcome of work done in collaboration except where specifically indicated in the text.

The work described is original except where indicated by reference, and has not been submitted for any other degree at this or any other university.

This thesis contains fewer than 60,000 words.

Signed: _____

Date: _____

"Res severa verum gaudium."

Seneca

In memory of my father *Frank Harras Müller*.

Acknowledgements

I would like to thank my supervisor *Prof. Shankar Balasubramanian* for the opportunity to conduct my Ph.D. in his research group and for providing me with supervision and organising funding.

Very special thanks go to *Dr. Raphaël Rodriguez* who supervised me on a daily basis throughout my Ph.D. and who has become an invaluable friend.

Special thanks go to my family for their support and love during these last four years, in particular my mother *Heidemarie Ursula Liddy Müller* aka *Herzkäfer*, my father *Hartmut Gerhard Hänsel* aka *Oider Mo* and my brother *Dr. Christian Müller* aka *Dino*.

My thanks also go to my dear friends *Dr. Stéphane Forsik* aka *Le Bunny*, *Dr. Rebecca Rancourt*, *Emily Simon Thomas*, *Barasa Adele Idris-Goudarz* aka *Mercedes*, *Louise Kay* aka *Loo*, *Claudia Crovace*, *Markus Graebig*, *Annelie* and *Robert Matthes* and *Clemens Petzold*. Their friendship has been invaluable during the course of the studies.

My thanks also go to *Cancer Research UK* who have provided me with the funding necessary to conduct this Ph.D.

I would like to thank all my colleagues in the Balasubramanian group for their support, in particular *Dr. Katja Jantos* who gave me a lot of guidance during my first year and *Deborah A. Sanders*.

Furthermore, I would like to thank *Darwin College* and the people of *Darwin College Boat Club* for their support during this degree.

I would like to thank all the people I have worked and collaborated with and who have proof-read the thesis.

Publications

The following work by the author has been published, or is in preparation for publication, as part of, or as mentioned and referenced, in this thesis:

(1) M. Bejugam, M. Gunaratnam, **S. Müller**, D. A. Sanders, S. Sewitz, J. A. Fletcher, S. Neidle, and S. Balasubramanian. Targeting the c-Kit promoter quadruplexes with 6-substituted indenoisoquinolines, a novel class of G-quadruplex stabilising small molecule ligands. *ACS Med. Chem. Lett.*, 2010, DOI: 10.1021/ml100062z (Chapter 1).

(2) **S. Müller**, G. D. Pantoş, R. Rodriguez, and S. Balasubramanian. Controlled-folding of a small molecule modulates DNA G-quadruplex recognition. *Chem. Commun.*, 80-82, 2009 (Chapter 2).

(3) R. Rodriguez, **S. Müller**, J. A. Yeoman, C. Trentesaux, J.-F. Riou, and S. Balasubramanian. A novel small molecule that alters shelterin integrity and triggers a DNA-damage response at telomeres. *J. Am. Chem. Soc.*, 130: 15758-15759, 2008 (Chapter 3).

(4) **S. Müller**, D. A. Sanders, R. Rodriguez, M. Di Antonio, S. Matsis, F. Mauro, and S. Balasubramanian. Small molecules that show selective growth inhibition for cancer cells, low cytotoxicity and induce telomere shortening. *J. Med. Chemistry*, 2010, *in preparation for submission* (Chapter 3).

(5) **S. Müller**, S. Kumari, R. Rodriguez and S. Balasubramanian. Small molecule-mediated G-quadruplex isolation from human cells. *Nature Chem.*, 2010, *in press* (Chapter 4).

Abstract

An increasing interest in non-canonical nucleic acid structures has drawn the attention of the scientific community during the last few decades. One such structure, the G-quadruplex, has been the focus of an increasing number of scientists as G-quadruplexes are believed to play a role in biological processes such as telomere integrity and gene expression. Their existence *in vivo* is largely unproven but they have stimulated a lot of research into small molecules that interact with them. The development of a new class of such molecules is described in this thesis. A member of this family showed to be very selective in stabilising one particular G-quadruplex. The further development of another family of G-quadruplex interacting small molecules is also presented in this thesis and some of their effects *in cellulo* were assessed. Based on the scaffold of this family, an affinity probe was developed, which can mediate the isolation of its nucleic acid targets from human cells. This is the first example of the use of a small molecule with an affinity tag that has been used to isolate a nucleic acid target in a *structure specific* manner from human cells.

Contents

Abbreviations

Abbreviation	Name
2D	two-dimensional
A	absorbance
A	adenine
ADME	absorption, distribution, metabolism and excretion
aka	also known as
al	aliphatic
ALT	alternative lengthening of telomeres
AMP	adenosine 5′-monophosphate
aq.	aqueous
ar	aryl
Ar	argon
ATM	ataxia telangiectasia mutated
ATP	adenosine-5′-triphosphate
ATR	ataxia telangiectasia and Rad3 related protein
BGP1	beta globin protein 1
BML	Bloom's syndrome helicase
BOC	*tert*-butyloxycarbonyl
bp	base pair
C	cytosine
Cbz	carbobenzyloxy
ChIP-seq	chromatin immunoprecipitation DNA sequencing
CNBP	cellular nucleic acid binding protein
cm	centimeter
comp.	complementary
COSY	correlation spectroscopy
cpd.	compound
CyP450	cytochrome P450

Abbreviation	**Name**
d	day
ΔT_m	difference in melting temperature
D_2O	deuterium oxide
DCM	dichloromethane
DIAD	diisopropyl azodicarboxylate
DDR	DNA damage response
DMEM	Dulbecco's modified eagles medium
DMSO	dimethyl sulfoxide
DNA	deoxyribonucleic acid
Dr.	doctor
ds-DNA	double-stranded DNA
equiv.	equivalent(s)
EDTA	ethylenediaminetetraacetate
e.g.	*exempli gratia*
EBr	ethidium bromide
EtOAc	ethyl acetate
EtOH	ethanol
FACS	fluorescence-activated cell sorting
FAM	6-carboxyfluorescein
FANCJ	Fanconi anemia group J protein
FCS	fetal calf serum
FRET	Förster resonance energy transfer
g	gram
G	guanine
GFP	green fluorescent protein
GI_{50}	half maximal inhibitory concentration of growth
GmbH	Gesellschaft mitbürgerlicher Herren
h	hour
H_2O	water
HCl	hydrochloric acid
HCOOH	formic acid
HMBC	heteronuclear multiple bond coherence
HMQC	heteronuclear multiple quantum coherence

Abbreviation	**Name**
hnRNP	heterogeneous nuclear ribonucleoprotein
HPLC	high performance liquid chromatography
hTERT	human telomerase reverse transcriptase
Hz	Hertz
i.e.	*id est*
K	Kelvin
K^+	potassium cation
KCl	potassium chloride
λ	wavelength
LC_{50}	half maximal lethal concentration
LiCl	lithium chloride
Ltd.	Limited
μl	microliter
M	molar
mAU	milli enzyme activity units
Me	methyl
Me_3SiCHN_2	(trimethylsilyl)diazomethane
MeCN	acetonitrile
MeOH	methanol
mer	donates the bases of an oligonucleotide
mg	milligram
$MgSO_4$	magnesium sulfate
min	minute
miRNA	micro RNA
ml	milliliter
mM	millimolar
mmol	millimole
mRNA	messenger RNA
m.p.	melting point
mut.	mutated
N_2	nitrogen
NaCl	sodium chloride
$NaHCO_3$	sodium hydrogen carbonate

Abbreviation	Name
NaOH	sodium hydroxide
NCI	National Cancer Institute
n.d.	not determined
NHE	nuclease hypersensitive element
nm	nanometer
nM	nanomolar
NMR	nuclear magnetic resonance
nOe	nuclear Overhauser effect
NOESY	nuclear Overhauser effect spectroscopy
$p16^{INK4a}$	protein 16 cyclin-dependent kinase inhibitor 4A
p53	protein 53
PA	polyacrylamide
PAGE	polyacrylamide gel electrophoresis
PBS	phosphate buffered saline
PCR	polymerase chain reaction
PD	population doubling
Pd/C	palladium carbon
PDGFR	platelet-derived growth factor receptor
Ph	phenyl
Ph.D.	doctor of philosophy
PM3	Parameterised model number 3
PPh_3	triphenylphosphine
RN_3	azide with a chemical group R
POT1	protection of telomeres 1
PP_i	pyrophosphate
PQS	putative G-quadruplex sequence
Prof.	professor
qPCR	quantitative PCR
Rb	retinoblastoma protein
rDNA	ribosomal DNA
RNA	ribonucleic acid
RNAP	RNA polymerase
ROH	alcohol with a chemical group R

Abbreviation	Name
rpm	rotations per minute
rt	room temperature
s	second
SAR	structure activity relationship
sat.	saturated
SD	standard deviation
$SOCl_2$	thionyl chloride
T	thymine
TAMRA	6-carboxytetramethylrhodamine
TBE	Tris/borate/EDTA
TEA	triethylamine
TEMED	tetramethylethylenediamine
TFA	trifluoroacetic acid
TGI	total growth inhibitory concentration
THF	tetrahydrofuran
TIC	transcription initiation complex
T_m	melting temperature
TPP1	tripeptidyl peptidase 1
TRF1/2	telomeric repeat factor 1/2
Tris	tris(hydroxymethyl)aminomethane
TSS	transcription start site
U.K.	United Kingdom
UTR	untranslated region
UV	ultra-violet
V	volt
WRN	Werner's syndrome helicase

Chapter 1

Introduction

1.1 G-quadruplex nucleic acids

Nucleic acids play fundamental roles in cells and constitute an important class of biological macromolecules. They can adopt complex secondary structures which are functionally important in the cellular context. The discovery of the DNA double helix and $A{\cdot}T$ and $G{\cdot}C$ base pairing in 1953[1–3] paved the way for the burgeoning research on nucleic acids and their importance in genetics. Whereas it is now established that RNA molecules adopt various complex secondary structures, the general belief still holds that DNA exists mainly in its double-stranded helical form with only a few exceptions. It has been known since 1901[4] that guanylic acid can form gels in solution, which suggests molecular interactions between guanines. However, it was not discovered until 1962[5] that guanine-rich sequences can form alternative structures to the double helix proposed by Watson and Crick. It has now been demonstrated by crystallographic[6–10] and NMR spectroscopic[11–15] studies, that single-stranded guanine-rich strands can fold into G-quadruplexes (also termed G-tetraplexes), secondary nucleic acid structures with stacks[5,16,17] of guanine tetrads in their central cores. Each tetrad comprises four Hoogsteen hydrogen-bonded guanines. The hydrogen bonds observed in $A{\cdot}T$ and $G{\cdot}C$ base pairs and those in guanine tetrads are depicted in Figure 1.1. Like B-DNA helices, G-quadruplexes also have a right-handed helical twist but contain around 12 tetrads per turn[18,19] as opposed to 10 base pairs in B-DNA.

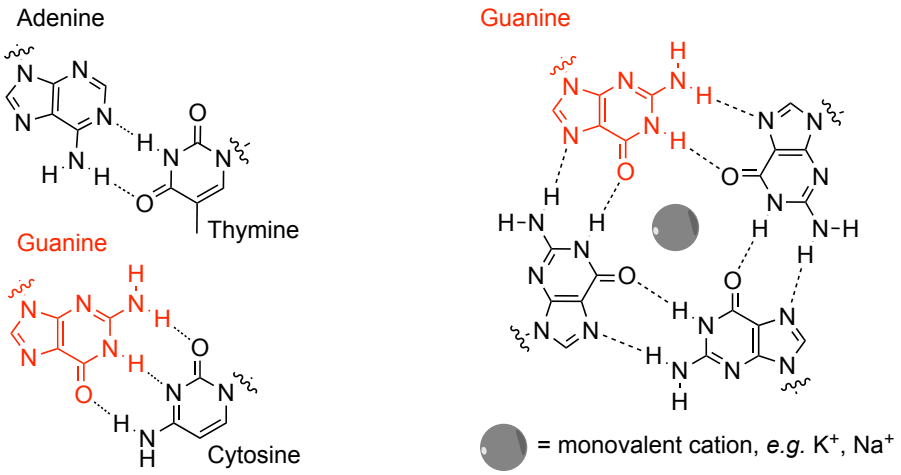

Figure 1.1: Left: $A{\cdot}T$ and $G{\cdot}C$ base pairs. **Right:** Guanine tetrad formed by four guanines and a monovalent cation in the centre. Hydrogen bonds are indicated as dashed lines.

G-quadruplexes can be formed by a single strand (intramolecular) or several strands (intermolecular) and often exhibit dynamic and polymorphic structures[20–22] in solution depending on factors such as cation nature,[8,23] loop (*i.e.*, sequences connecting the tetrads) length and topology,[24,25] DNA concentration, associated proteins and molecular crowding.[26] The DNA strands that run along the periphery of G-quadruplexes can be parallel or antiparallel defining the directionality/polarity of the strands in relation to each other. The angle of the glycosylic bond, as depicted in Figure 1.2, is *syn* if the strands are parallel and *anti* if the strands are antiparallel. The *syn*/*anti* nature of the gycosylic bonds determines the groove widths of G-quadruplexes, whereas the loop lengths highly influence G-quadruplex topology and stability.[24,25] Figure 1.3 depicts examples of schematic views of some parallel and anti-parallel intra-and intermolecular quadruplexes. It is noteworthy that the stacked guanines are neither exactly symmetric nor exactly planar. Depending on the loop length and nature, the guanines of the top and/or bottom tetrad can tilt or buckle to accommodate conformational strain. The size of the cations residing in the centre of G-quadruplexes also highly influence G-quadruplex conformation and topology. For instance, ammonium and potassium ions coordinate between two quartets, whereas the smaller sodium ion

can reside within the plane of a guanosine quartet. G-quadruplex polymorphism gives great scope for the possibility of differential recognition by other molecules, including proteins and synthetic small molecules.

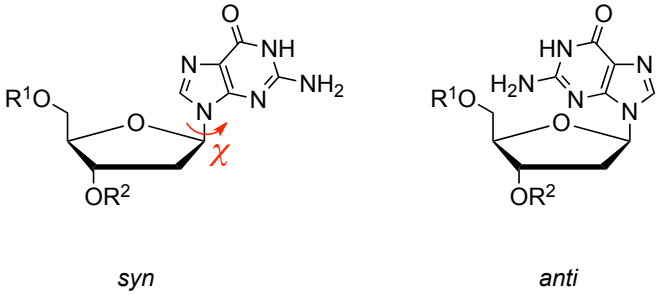

Figure 1.2: Guanosine can adopt *syn* and *anti* conformations. The bond determining the glycosylic angle χ is indicated.

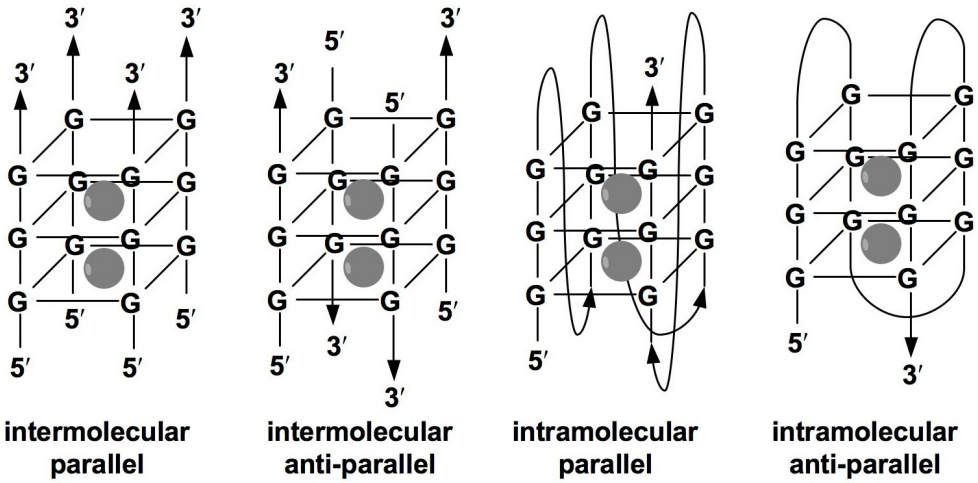

Figure 1.3: Examples of G-quadruplex conformations. Depicted are examples of intra-and intermolecular parallel and anti-parallel G-quadruplexes.

Human chromosome ends (telomeres) possess a repetitive G-rich sequence with a single-stranded overhang of the sequence 5′-$(GGTTAG)_n$-3′. The human telomeric sequence can adopt different G-quadruplex structures depending on cation nature and concentration.[8] It is likely that these structures are dynamic

in their natural context and it has been shown *in vitro* by Ying *et al.* that the parallel and anti-parallel structures of this sequence readily interconvert in solution by using single-molecule fluorescence resonance energy transfer.[27] Figure 1.4 depicts the human telomeric repeat sequence and a schematic view of a possible G-quadruplex conformation it can adopt. Illustrated is an anti-parallel conformation.

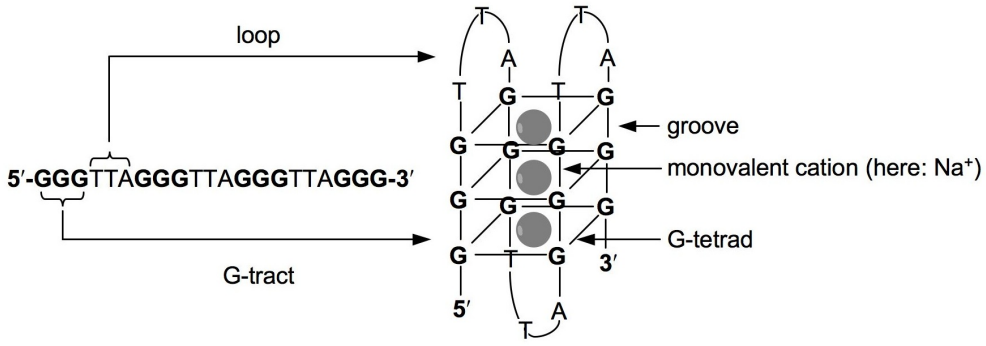

Figure 1.4: Left: Human telomeric sequence. **Right:** Diagram of an antiparallel G-quadruplex that can be formed by this sequence.

In cells, with the exception of the single-stranded telomeric G-overhang, the formation of intramolecular DNA G-quadruplexes is in competition with hybridisation to the complementary strand. In human cells, DNA G-quadruplexes have been hypothesised to form at telomeres,[28] in promoter regions of genes,[29] in parts of rDNA[30] and they are also believed to form throughout the genome during replication,[31] as described in section 1.3. G-quadruplexes can also be formed by G-rich RNA.[32–36] RNA G-quadruplexes tend to be even more stable than their DNA-counterparts and are not in competition with a complementary strand. However, RNA can adopt complex secondary structures such as hairpins, bulges and loops, which can compete with G-quadruplex formation.

Intramolecular G-quadruplexes may be of relevance in biology. An algorithm based on observed stable G-quadruplexes has been proposed: at least four G-tracts of three guanines which are joined by 1-7 bases of any nature, *i.e.*, $GGG(X)_{1\text{-}7}GGG(X)_{1\text{-}7}GGG(X)_{1\text{-}7}GGG$ where X is any nucleobase, are required to form intramolecular G-quadruplexes. Using this algorithm, approxi-

mately 376,000 putative DNA G-quadruplex sequences have been identified in the human genome.[37] This publication was complemented by another study by Todd *et al.*,[38] which was also based on an algorithm to assess intramolecular G-quadruplexes in the genome. Both papers were published back-to-back in the same journal. However, these motifs have not yet been mapped experimentally in the genome and their formation in human cells has not yet been proven. An experimental approach to identify these structures in the human genome could potentially shed light on the existence of G-quadruplexes in human cells.

1.2 G-quadruplex interacting small molecules

It was proposed in 1991 by Zahler *et al.*[28] that telomerase can be inhibited by G-quadruplex formation. Molecules were later identified that inhibit the action of human telomerase[39,40] by interacting with and by stabilising telomeric G-quadruplexes *in vitro*. In 2001 the natural product **telomestatin** (Figure 1.5), isolated from *Streptomyces anulatus*,[41] was found to be a potent inhibitor of telomerase function, which was linked to its G-quadruplex interacting properties. The same molecule was later shown to disrupt the protein complexes associated with telomeres.[42]

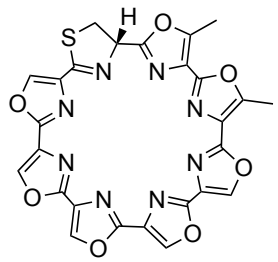

Figure 1.5: Molecular structure of **telomestatin**.

Targeting G-quadruplex DNA is challenging given that this canonical DNA structure is highly polymorphic and not very abundant in comparison with double-stranded DNA. Nonetheless, there are several classes of G-quadruplex interacting

small molecules described in the literature, notably: acridine derivatives,[39,43–51] amidoanthracene derivatives,[52,53] amidofluorenone derivatives,[54] ethidium derivatives,[55] porphyrins,[40,56–59] dibenzophenanthrolines,[60] perylenes,[61,62] quinoxaline derivatives,[63] indoloquinolines,[64] diarylureas,[65,66] isoalloxazines,[67] oxazole-containing macrocycles,[68–71] a family to which telomestatin[41,42] belongs, triazine derivatives,[72,73] acridones,[74,75] quinacridine derivatives,[76–78] triarylpyridines[79] and 2,6-pyridine-dicarboxamide derivatives.[80] This shows, that during the last two decades a great number of publications involving G-quadruplex interacting molecules have emerged developing the field exponentially.[39–104]

Small molecules can interact with G-quadruplexes in potentially different ways, especially given that they are highly polymorphic structures. Interactions with the G-tetrad, an obvious site for ligands designed to target G-quadruplexes generically, can be *via* hydrophobic or *via* stacking interactions. In fact, many G-quadruplex ligands have been designed to contain a flat aromatic scaffold. Structural evidence for the interaction with the tetrads has been reported.[105] Other binding sites for small molecules are the loops[24,25,106] and grooves,[99,107] which are highly variable between different G-quadruplexes. This could potentially be exploited to achieve differential recognition between different G-quadruplexes in order to achieve specificity towards a single one of these structural elements. It is noteworthy that G-quadruplex ligand interactions determined by different experimental techniques can differ. This has been exemplified by studies on the binding of the G-quadruplex interacting small molecule **TMPyP4**, a phenol quaternary ammonium porphyrin which is depicted in Figure 1.6. Whereas solution NMR studies carried out by Patel and co-workers showed how the molecule can interact with the tetrad of a G-quadruplex target,[86] Neidle and co-workers later proposed using X-ray crystallography, that the molecule preferentially interacts with the loops of the nucleic acid target.[59] This molecule has been used in many studies involving G-quadruplexes.[57,108,109] However, it has been observed that **TMPyP4** does not exhibit high selectivity for G-quadruplex DNA over ds-DNA[57,109] in contrast to other G-quadruplex interacting small molecules such as **telomestatin**.[110] Porphyrins such as **TMPyP4** have inspired the synthesis of related G-quadruplex interacting compounds, such as **Se2SAP** (depicted in

Figure 1.6) which was shown to be selective for G-quadruplexes formed in the promoter of the gene *c-Myc*.[58]

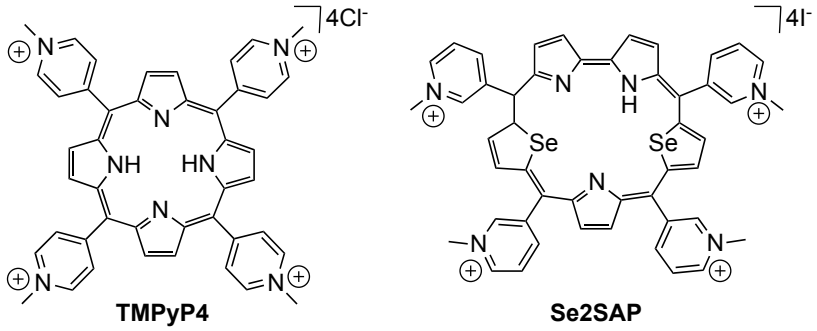

Figure 1.6: Molecular structures of **TMPyP4** and **Se2SAP**.

It is important to note that many of the biological hypotheses in the field are based on experimental data from proposed interactions of chemical agents with these non-canonical DNA structures. There have been a few reports on the development of therapeutic anti-cancer agents based on G-quadruplex ligands, such as **CX-3543**[30,111] which has now entered phase II clinical trials. Other synthetic small molecules which have certainly been milestones in the G-quadruplex field are **BRACO-19**[44,46] and **RHPS4**.[80,105,112,113] However, the latter two have not progressed beyond the experimental stage into clinical trials, despite showing promising anti-tumor growth effects.[46,113,114] These three molecules are illustrated in Figure 1.7.

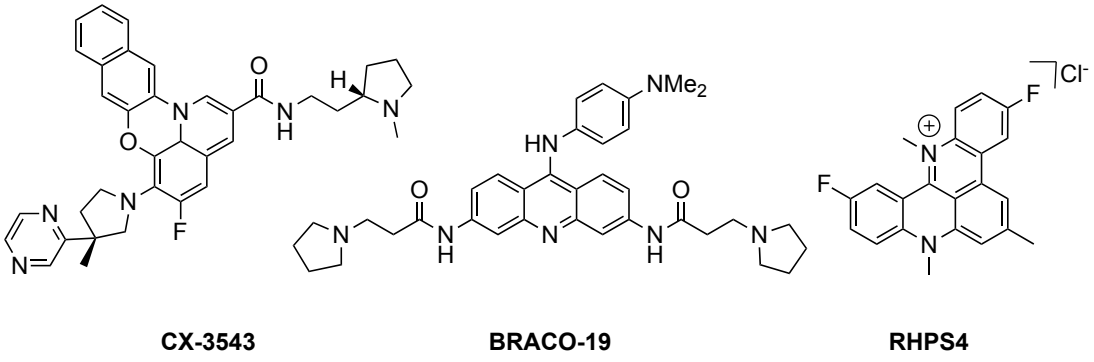

Figure 1.7: Molecular structures of **CX-3543**, **BRACO-19** and **RHPS4**.

Despite the extensive list of reported G-quadruplex interacting small molecules, it would be advantageous to develop new molecules which either exhibit differential cytotoxicity between cancerous and non-cancerous cells as had been demonstrated by 4,5-di-substituted acridone ligands,[75] or show a large concentration dependence on their cytotoxic as compared to growth-inhibitory (cytostatic) properties. Such compounds could target highly proliferative cells, a property that could potentially be exploited in the treatment of cancer. There has been some success in the development of small molecules that show some cancer cell selectivity in short term growth assays, for example substituted diarylureas.[65] The triazine derivative **12459** (Figure 1.8) has been shown to cause long-term growth arrest of human A549 lung carcinoma cells that correlates with telomere shortening and the induction of senescence.[72]

Small molecules are very powerful tools for studying biological processes. There have been a few reports on the development of biochemical tools, such as fluorescent G-quadruplex interacting molecules,[115] that may be used to study these structures *in cellulo*. They may also be exploited to study phases of the cell-cycle since there have been reports of cell-cycle alterations caused by G-quadruplex interacting small molecules.[116,117] The 2,6-pyridine-dicarboxamide **360A** has been shown to cause severe cell cycle alterations and also to induce apoptosis in telomerase-positive glioma cell lines.[117] The structure of the molecule is depicted in Figure 1.8.

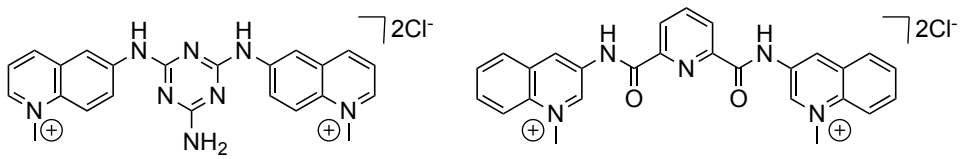

12459 **360A**

Figure 1.8: Molecular structures of **12459** and **360A**.

However, there is still great scope for the development of chemical tools to better study these nucleic acid structures, particularly *in cellulo*. It would for instance be of great interest to develop a G-quadruplex specific small molecule with an affinity tag, which could be used to mediate the isolation of its target from

cells. The initial steps towards the development of such a probe are described in this thesis.

1.3 Biological significance of G-quadruplexes

Despite the mounting evidence that G-quadruplexes can form *in vitro*, only recently has evidence started to accumulate for their existence and function *in cellulo*.[118] DNA as well as RNA G-quadruplexes have now been proposed to play biological roles in cells. Although there is compelling evidence for *in cellulo* G-quadruplex formation in ciliates such as *Stylonichia lemnae* using immunostaining of their telomeric intermolecular G-quadruplexes,[119] the evidence is less direct for human cells as their low concentration of telomeres is believed to have so far precluded visualisation using this technique.[118,120] In addition, human telomeres are heavily sheltered by protein complexes, are highly dynamic and are only believed to form intramolecular quadruplexes. This section will give an overview of the different areas where these structures may play an important biological role, mainly focussing on human cells.

1.3.1 Protein interaction

Proteins have been shown to modulate the formation of G-quadruplexes in *Oxytricha*. The organism's telomere-binding protein functions as a molecular chaperone to promote the formation of higher order complexes of telomeric DNA stabilised by G-tetrads. This has now been observed *in vitro*[121,122] and *in vivo*.[120] There have been reports of proteins interacting with G-quadruplex structures in human cells, supporting their existence *in vivo*. Helicases help maintain genome stability and some helicases, such as BML,[123] WRN[124] and FANCJ[31] have been shown to unwind DNA G-quadruplexes. Recently, it has also been reported that these secondary nucleic acid structures interact with poly(ADP-ribose) polymerase.[125] RNA G-quadruplex protein interactions have also been described in some pioneering work by Moine and co-workers on the fragile X mental retardation protein,[126] which inspired subsequent research on RNA G-quadruplexes.

The telomeric G-quadruplex has also been shown to be unwound by hnRNP proteins.[127] The protein hnRNP A1 has for instance been demonstrated to unfold G-quadruplex DNA in the human *KRAS* promoter.[128] Furthermore, it has been shown that nucleolin interacts with rDNA, which can adopt G-quadruplex structures.[30] The same protein has also been demonstrated to bind to a G-quadruplex in the promoter region of *c-Myc*.[129] These studies show some of the most compelling evidence of the formation of G-quadruplexes in human cells.

1.3.2 Telomeres

The most widely studied DNA G-quadruplexes are those formed from the G-rich strand of human telomeric DNA, which has the sequence $(GGTTAG)_n$. Part of this repeat sequence is single-stranded, the 3′-G-overhang. The human telomere is protected by a protein complex called *telosome*[130] or *shelterin*[131] which protects the DNA from degradation, non-homologous end-joining and the activation of the DNA damage response (DDR) machinery that involves ATM and ATR kinases. Furthermore, it allows the cell to distinguish the G-overhang from DNA strand breaks. Shelterin is a six-protein complex comprising of three DNA-binding proteins (TRF1, TRF2 and POT1), TIN2, which binds to TRF1 and TRF2, Rap1 which interacts with TRF2 and TPP1 which is in contact with TIN2 and POT1 (Figure 1.9).[131] This complex interacts with the double-stranded telomeric repeat and the single-stranded G-overhang. Telomerase is an enzyme active in approximately 85% of human cancers and many immortalised cell-lines that can extend the G-overhang and thus confer infinite proliferative capacity on cells. POT1 interacts with TPP1 to recruit and thereby modulate the activity of telomerase.[132] It has been shown that the G-rich telomeric overhang can fold into G-quadruplexes, rendering it resistant to the extension by telomerase.[28] Telomere shortening, which occurs in the absence of telomerase or if the ALT mechanism malfunctions in ALT-positive[133] tumour cells, appears to be a tumour suppressor mechanism.[134] Telomeres in telomerase- and ALT-negative somatic cells are gradually shortened as the cells progress through the cell-cycle, and once telomeric DNA reaches a critically short length, cells can enter p53 and Rb-dependent replicative cellular senescence and apoptosis. The exact mechanism of cell-cycle

arrest and/or resulting cell death differs between different cells depending on the expression status of tumour suppressor proteins like p53 and Rb. Human cells employ signaling pathways that can down-regulate the cell cycle if DNA-damage occurs, which can give sufficient time for repair prior to cell division,[135] a mechanism crucial to pertain the stability of the genome. The stabilisation of telomeric G-quadruplexes has been proposed to disrupt telomere function and inhibit telomerase.[136] It has been shown that small molecules interacting with this structural element can disrupt shelterin by uncapping POT1 in human HT1080 cells.[42,48] The G-quadruplex interacting small molecules **BRACO-19**, **RHPS4** and **telomestatin** induce rapid replicative senescence in human cancer cells and activate a DDR analogous to that following DNA double-strand breaks. The proteins p53, ATM and $p16^{INK4a}$ have been characterised to be involved in particular in these responses.[46,113,137,138] The telosome and the effect of G-quadruplex formation in the G-overhang are depicted in Figure 1.9.

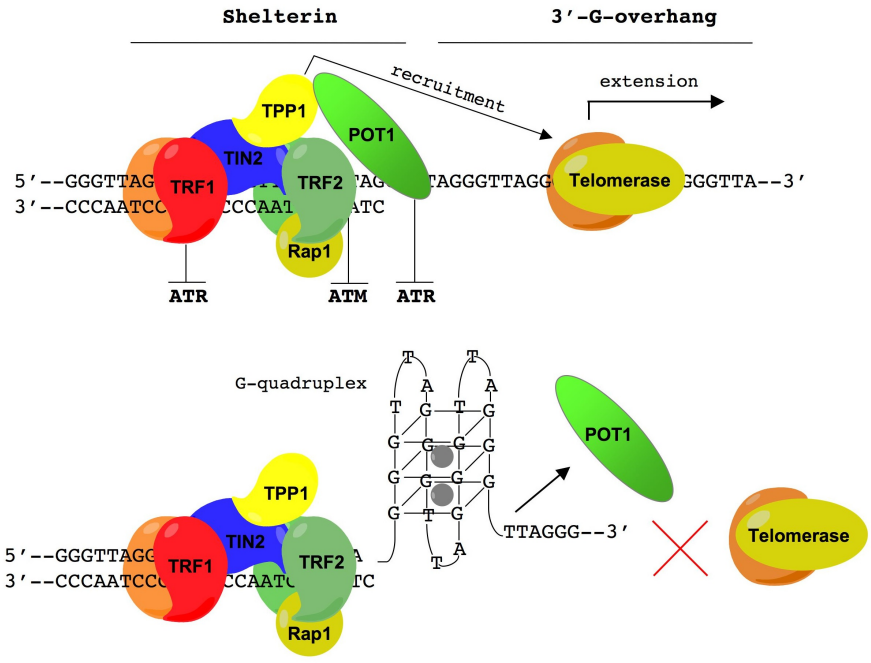

Figure 1.9: Top: Schematic view of shelterin and the G-overhang which gets extended by telomerase in many cancer cells. **Bottom:** G-quadruplex formation uncaps POT1 and prevents extension of the G-overhang by telomerase.

G-quadruplex ligands may not only target telomerase-positive tumourigenic cells and inhibit their proliferation, but can also uncap telomeres in ALT cells.[139] Interestingly, another hypothesis has been proposed as to how a G-quadruplex interacting small molecule may interfere with telomere integrity. The G-quadruplex interacting small molecule **12459** has been found to stabilise RNA G-quadruplexes in the mRNA of hTERT, the catalytic subunit of human telomerase.[140] The molecule has been hypothesised to interfere with the splicing machinery. This molecule also causes telomere shortening and replicative senescence.[72] An RNA G-quadruplex has also been identified in the mRNA of TRF2.[141] A small molecule that interacts with this structure may also interfere significantly with telomere integrity (see section 1.3.5).

It is noteworthy that an alternative model for shelterin exists where the G-overhang has been proposed to invade double-stranded telomeric DNA to displace base pairing with the complementary strand in order to form a *t-loop*[142,143] as depicted in Figure 1.10.

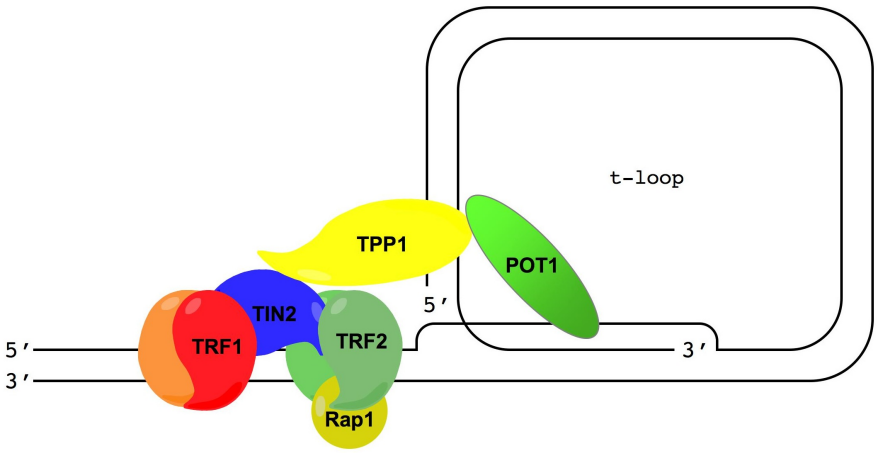

Figure 1.10: T-loop formation at human chromosome ends.

Extensive research is being carried out on the identification and further development of small molecules that interact with telomeric regions in human cells, and which may therefore have an anti-proliferative activity in human cancer cells.[41,46,48,73,144,145]

1.3.3 Replication stalling

G-quadruplexes have been proposed to stall replication forks due to their formation in single-stranded DNA that exists during replication. This is supported by the existence of helicases that unwind G-quadruplex DNA.[31,123,124] This theory was first proposed for BML in 1998 by Sun *et al.*[123] It is possible that when the DNA strands are single-stranded G-quadruplexes form during replication delaying fork progression. The helicases would then help defend genome stability, which would explain the existence of G-quadruplex specific helicases. It has been shown that stabilisation of telomeric quadruplexes perturbs replication of telomeres which can cause activation of ATM and ATR kinases leading to a DNA damage response.[112] Small molecules interacting with G-quadruplexes could interfere with the replication process and cause replication fork stalling at G-rich stretches. A scheme of how replication stalling could be caused by G-quadruplex formation is depicted in Figure 1.11.

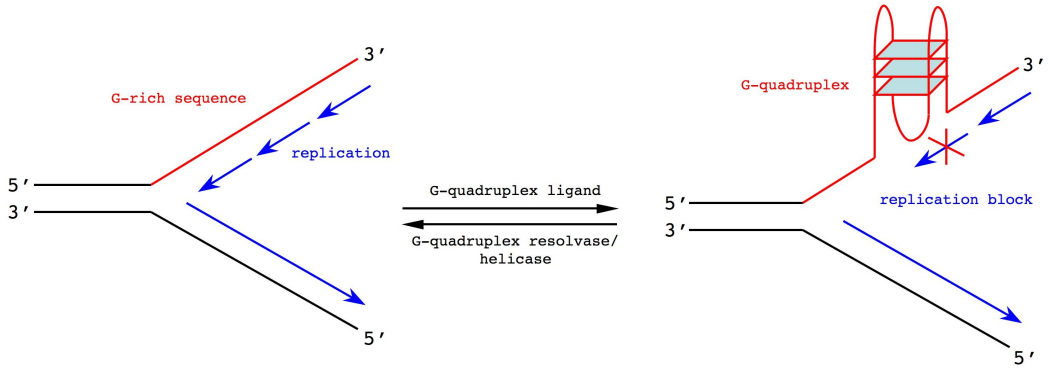

Figure 1.11: G-quadruplex formation stalls the replication fork. **Left:** Replication progressing normally. **Right:** Replication fork stalling due to the formation of G-quadruplexes. A G-quadruplex stabilising molecule would drive the equilibrium to the right.

1.3.4 Transcriptional control

Computational studies have predicted that more than 40% of all promoters of human genes contain a putative G-quadruplex forming sequence (PQS).[29] In

particular, oncogenic promoters are enriched in PQSs by almost 70% using the bioinformatic algorithm described in section 1.1. This prediction has to be taken with precaution, as these numbers have not been confirmed experimentally. However, the hypothesis that these nucleic acid structural elements could have an effect on promoter regulation and hence transcriptional activity has stimulated the research on several PQSs in several genes, such as *c-Myc*,[15,58,84,86,92,146] *c-kit*,[147–149] *VEGF*,[87] *bcl-2*,[150,151], *KRAS*[152,153] and *PDGFR-β*.[154] A schematic view of gene transcription altered by G-quadruplex formation in the promoter is depicted in Figure 1.12. Pioneering studies by Howell *et al.*[155] showed that G-quadruplexes can form in the nuclease hypersensitive region of the chicken *β*-globin gene promoter. A poly(dG)-binding protein called BGP1 has been identified to specifically bind to the G-tract of the *β*-globin gene promoter to activate gene expression.[156] It has been proposed that this G-quadruplex forming region could act as a conformational switch subject to modulation by BGP1. There have been reports that G-quadruplex interacting small molecules can alter gene expression, for instance that of the human genes *c-Myc*,[84,92,157] *c-kit*,[67,104,158] *KRAS*[152] and *bcl-2*.[159] This has been linked to the interaction with the respective promoter G-quadruplexes.

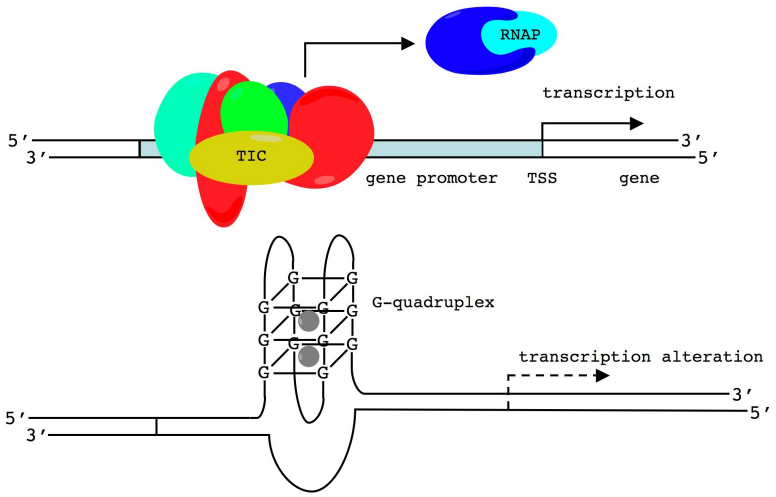

Figure 1.12: Top: Schematic view of an eukaryotic gene with a promoter and transcription initiation complex (TIC). **Bottom:** G-quadruplex formation in the promoter alters transcription possibly through alteration of TIC binding.

However, most of the studies performed only look at the effect of the transcription of a single gene and/or the change in expression of the protein it encodes. A down-regulation of the *c-Myc* gene for example, which encodes for a transcription factor, is inherently linked to the expression of other genes. Hence, if the transcriptional network is influenced as a whole, a change in the transcription and expression of *c-Myc* is highly likely. This makes it difficult to attribute transcriptional alterations to the formation of G-quadruplexes. There have been studies using plasmid constructs with the promoters under investigation,[84] but that system is somewhat removed from chromatinised DNA. For the c-kit promoter sequence, it has been postulated that double-stranded DNA is practically the only species present at pH 7.0, and G-quadruplex formation is only observed at a lower pH that facilitates i-motif formation in the complementary strand *in vitro*.[160] The i-motif is a secondary nucleic acid structure that can be formed by a cytosine-rich strand such as the complementary strand of a G-quadruplex forming sequence. These structures are normally not very stable under physiological conditions. However, it has been demonstrated that G-quadruplexes and the i-motif can form in the *c-Myc* promoter facilitated by DNA superhelicity.[161] Also, it has now been demonstrated that the complementary strand can form intermediate partially folded structures at physiological pH which are i-motif-like in structure.[162]

Transcriptional control in human cells is highly complex. For example, the G-quadruplex forming sequence in the promoter of *c-Myc* is situated in the nuclease hypersensitive element NHE III_1. Proteins, such as CNBP[163] (cellular nucleic acid binding protein), Sp1 transcription factor and hnRNP K[164] (heterogeneous nuclear ribonucleoprotein K) have been shown to interact with the DNA of NHE III_1. Michelotti *et al.*[165] proposed that this NHE III_1 adopts at least three different states as depicted in Figure 1.13.

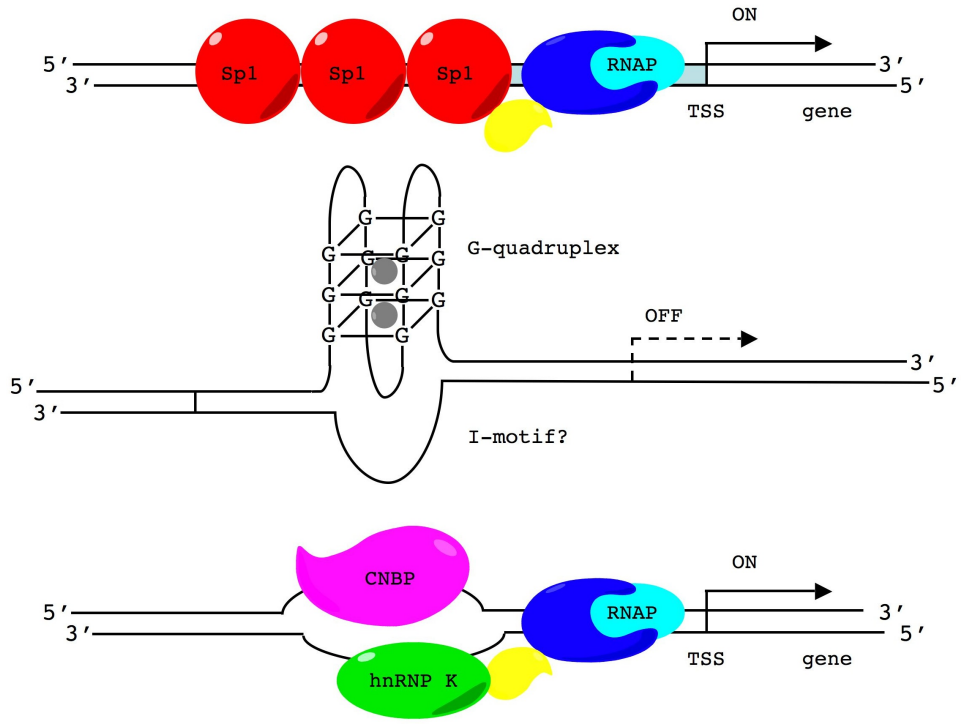

Figure 1.13: Top: Sp1 binding to the NHE III_1 in the promoter of *c-Myc* activates gene transcription. **Middle:** G-quadruplex formation inhibits gene transcription. **Bottom:** CNPB and hnRNP K binding activate gene transcription.

This model illustrates the biological complexity that researchers have to face when trying to understand the involvement of transient DNA structures in gene regulation. Targeting promoter G-quadruplexes is a very active field of research and very promising for the purpose of chemical intervention. However, compelling *in cellulo* evidence of this hypothesis is still missing and it remains a controversy whether transcriptional control influenced by G-quadruplexes occurs *in vivo*.

1.3.5 Translational control

Non-coding *cis*-acting secondary nucleic acid structures in the 5′-UTR, such as hairpins, control mRNA-specific translation.[166] The 3′-UTR of mRNAs is responsible for protein and miRNA binding which influences the stability and transport of the mRNA and can have a role in translation termination.[167] G-

quadruplexes have been proposed to exist as higher order structures in RNA at the 3′[32]-and 5′[126]-UTR regions of mRNA. This stimulated research into bioinformatic predictions[35] of UTR-sequences with a PQS and also work on translational regulation due to G-quadruplexes in mRNA specifically at the 5′-end, as it poses a direct influence on translational control.[34,36,168] It has been shown that a G-quadruplex within the 5′-UTR of certain genes causes a reduction in the translational activity from the corresponding mRNA.[34,169,170] This might be due to interference with the assembly of the translation initiation complex or hindrance of the complex migrating along the 5′-UTR before translation starts. G-quadruplexes could also act as binding sites for proteins that interfere with the initiation of translation. The effect of G-quadruplex formation in the 5′-UTR of mRNA is depicted in Figure 1.14.

It has now also been demonstrated that small molecules interacting with RNA G-quadruplexes in the 5′-UTR can down-regulate translational activity by stabilising this secondary structure, which may add additional steric bulk that can no longer be resolved.[36,141] This may present another way for therapeutic intervention using G-quadruplex interacting small molecules.

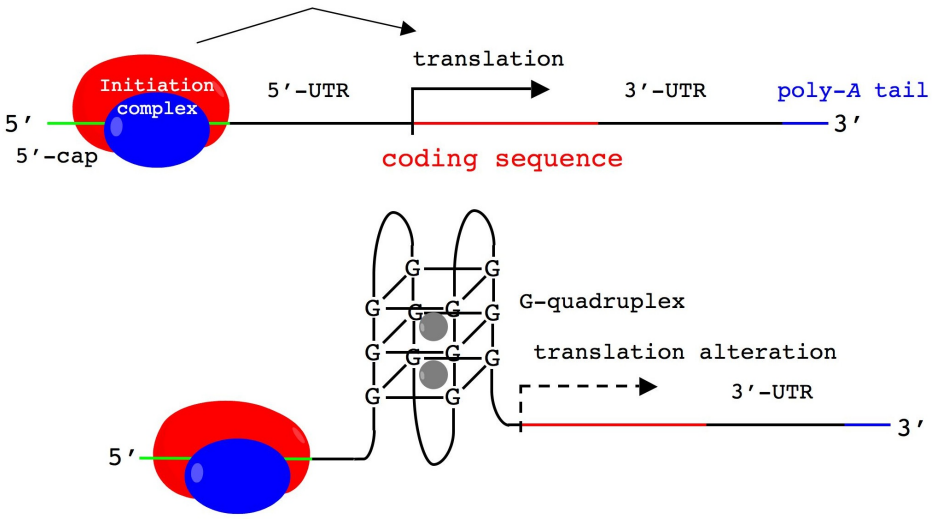

Figure 1.14: Top: Schematic view of an mRNA. **Bottom:** G-quadruplex formation in the mRNA alters translational activity.

1.4 Conclusions and outlook

There has been intensive research on G-quadruplexes during recent decades and a plethora of small molecules has been developed to target these structures. However, there is still limited evidence of their formation in cells and a lot of the molecules reported in the literature have not been or cannot be developed into drugs for chemical intervention as they are not inherently drug-like. Now there is a need for more evidence for the formation of these structures *in cellulo* and also to develop molecules which could potentially be used to improve the human condition, one of the ultimate goals of scientific research. The development of drug-like G-quadruplex interacting small molecules and chemical probes that could help elucidate the underlying biology is the current focus in this scientific field.

The next chapter will describe the synthesis and evaluation of a new family of G-quadruplex interacting small molecules. They have been designed to be able to adopt different conformations influenced by a methyl substitution on the molecular scaffold. The different conformations result in differential recognition of various G-quadruplexes but retain the ability of the molecules to selectively recognise G-quadruplex over double-stranded DNA. Chapter 3 chronicles the synthesis and some biological evaluation of a class of G-quadruplex binding small molecules based on a *N*,*N*′-*bis*(quinolinyl)pyridine-2,6 dicarboxamide scaffold. Chapter 4 outlines the development of a novel chemical probe based on the same scaffold that can mediate the isolation of these nucleic acid structures directly from human cells. The last chapter details all the experimental procedures corresponding to chapters 2, 3 and 4.

Chapter 2

Controlled-folding of a small molecule modulates G-quadruplex recognition

2.1 Background

As outlined in the previous chapter, intensive research has been conducted on the development and synthesis of G-quadruplex interacting small molecules.[39–104] A great number of these synthetic molecules comprise a flat aromatic scaffold. Such a design is aimed at facilitating stacking or hydrophobic interactions with the top or bottom tetrad of their target and thus a flat aromatic molecule can potentially interact with a variety of different G-quadruplexes. However, there are reports of ligands that are in contact with the loops of G-quadruplexes.[59,106] Some of these compounds show excellent selectivity for G-quadruplex DNA over ds-DNA. Many of the scaffolds have attached side chains to enable interactions with the loops of the nucleic-acid targets. However, for a molecule to discriminate between different G-quadruplex targets, the focus on its design should lie in the differences between the desired targets, which are mainly the loops and grooves of G-tetraplexes. Because of the predicted abundance of these non-canonical structures in the genome,[37,38] such discrimination is highly sought after. There are some reports of exploiting loop[106] and groove-recognition[99,107,171] specifically for small molecule G-quadruplex interactions. Neidle and co-workers[106]

showed by X-ray crystallography that disubstituted acridine ligands can interact preferentially with a bimolecular DNA G-quadruplex as these ligands have amino end groups of varying sizes. The diagonal loop in the quadruplex studied results in a large cavity which can accommodate these groups. Thus, loop nature has a significant influence on ligand selectivity for particular quadruplex folds. Derivatives of Distamycin A, a classical ds-DNA binder, have been shown by Moore *et al.* to selectively interact with the grooves of DNA G-quadruplexes.[171] However, these ligands did not show great selectivity for G-quadruplex DNA over ds-DNA. The specificity of G-quadruplex interacting small molecules has been enhanced by varying the nature,[71] position[95] and stereochemistry[68] of attached side chains. There has been some success in the development of molecules that can recognise one particular G-quadruplex topology.[50,64,97,172] For example, Rodriguez *et al.* showed that a small molecule based on a polyamine can induce the formation of the antiparallel conformation of the telomeric G-quadruplex from a mixed population.[50] However, the challenge for compounds to effectively recognise only one particular G-quadruplex from a single sequence still remains. This might be attributed to the fact that the core of many of those molecules is rigid and inflexible, which facilitates interactions with the G-tetrads of all G-quadruplexes. This calls for the exploration of different approaches. An alternative strategy to achieve this goal is presented in this chapter.

2.2 Objectives

The aim of this work was to create a new family of G-quadruplex ligands for which the conformation could be controlled by a simple substitution on a central molecular scaffold. The scaffold was designed to allow a certain degree of conformational freedom which differs to the rigid nature of many other reported G-quadruplex ligands.[93] Although very similar in structure, the molecules were designed in a way that their conformation would differ depending on a methyl substitution on the scaffold. This could influence their potential to stabilise G-quadruplex DNA. The final aim was to investigate if such an approach could be employed to achieve discrimination in stabilisation of the molecules between different G-quadruplex DNA targets.

2.3 Design of the new molecules

As an alternative strategy to achieve discrimination in molecular recognition between different G-quadruplex targets, a 1,3-[di-quinolin-2-yl-diureido] benzene scaffold was devised. It allows flexibility as opposed to the rigid structure of many other reported G-quadruplex interacting molecules,[93] including macrocycles such as **telomestatin**.[41] A new class of molecules was designed which incorporated some of the structural features of some known G-quadruplex binding ligands,[93] such as an aromatic scaffold and positively charged appendages. There is a selection of quinoline-based G-quadruplex ligands that can be found in the literature,[36,110,117,144,173,174] suggesting that quinolines may be a good structural feature of a variety of ligands. Two urea functionalities which link two quinolines to a central benzene core were included, and these urea bonds confer a degree of conformational freedom to these molecules.[175–177] Methyl substituted benzene was used to direct the conformation as a consequence of a possible steric clash with the oxygens of the urea bonds[178] (Figure 2.1).

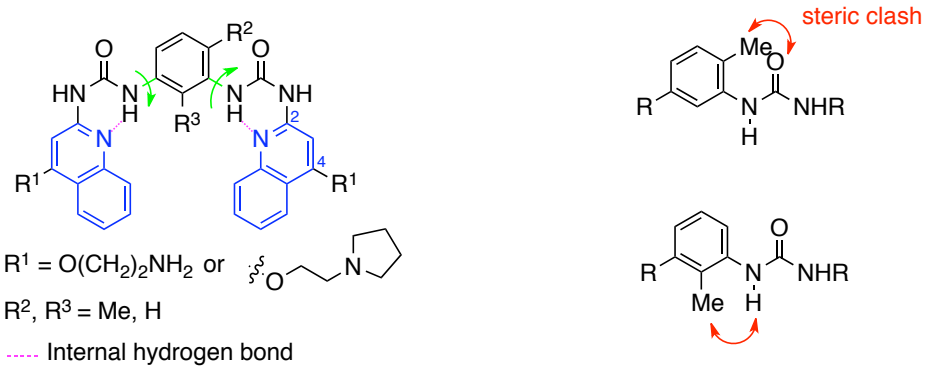

Figure 2.1: Left: Molecular structure of the 1,3-[di-quinolin-2-yl-diureido] benzene scaffold with substitutions at the 4-position of the quinoline moieties. The rotatable bonds are indicated in green and with green arrows. The quinolines are highlighted in blue. The hydrogen bonds that help keep the urea bonds in a plane with the quinoline moieties are highlighted with a dashed line in magenta. **Right:** Steric clash that would arise if the methyl substituent and the oxygens or hydrogens of the urea bonds were in close proximity.

An internal hydrogen bonding network keeps the urea bonds in a plane with the quinoline moieties. It restricts conformational freedom mainly to the bonds as indicated on the scaffold of the new ligand series in Figure 2.1. A methyl group at position R^2 would cause a potential steric clash with the oxygen and force the urea bond on that side of the benzene ring and the quinoline out of the plane. Alternatively, a methyl group at position R^3 would cause steric clash with the internal hydrogen bond network, also forcing the quinolines out of the plane. The figure shows the molecular framework and highlights the steric clash that would arise between the oxygen and a methyl at R^2 and R^3 if in close proximity. The quinolines which constitute part of the molecular scaffold are highlighted in blue. The internal hydrogen bonds restrict rotational freedom of the bond between the 2-position of the quinoline and the nitrogen of the urea bond as indicated in Figure 2.1 in magenta.

Two analogous series of molecules were synthesised: one with primary amine side chains (**1a-3a**) and the other with pyrrolidine appendages (**1b-3b**) as depicted in Figure 2.2. This would allow to also investigate whether the nature of the side chain could influence the nucleic acid recognition properties of the different conformations of the ligands.

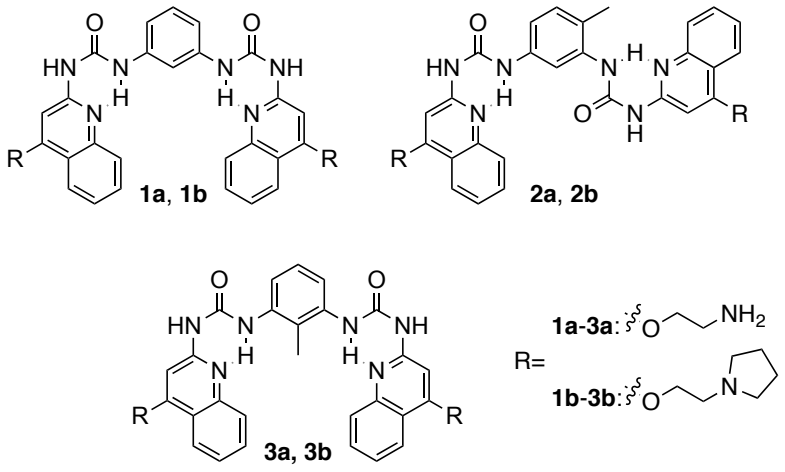

Figure 2.2: Molecular structure of molecules **1a-3b**. Series **a** carries a primary amine and series **b** a pyrrolidine as the terminal group on the chain.

2.4 Synthesis of the molecules

Molecules **1a-3b** were synthesised using a short and high yielding synthetic procedure as depicted in Scheme 2.1. Compounds **1a-3a** were synthesised in three and compounds **1b-3b** in two steps. Firstly, 2-aminoquinolin-4(1*H*)-one (**4**) was reacted with *N*-Boc ethanolamine or *N*-(2-hydroxyethyl)-pyrrolidine under Mitsunobu reaction conditions to obtain the quinoline building-blocks **5a** and **5b** in 53-65% yield.[176] The products were subsequently reacted with commercially available 1,3-phenylene diisocyanate (**6a**), 2,4-toluene diisocyanate (**6b**) or 2,6-toluene diisocyanate (**6c**) to synthesise the desired *bis*-ureas in 86-92% yield. This step required heating at 50 °C overnight. The Boc-protecting groups on the precursors of molecules **1a-3a** were removed in the presence of TFA in DCM. Molecules **1a-3b** were finally purified by HPLC to yield the TFA salts of the products.

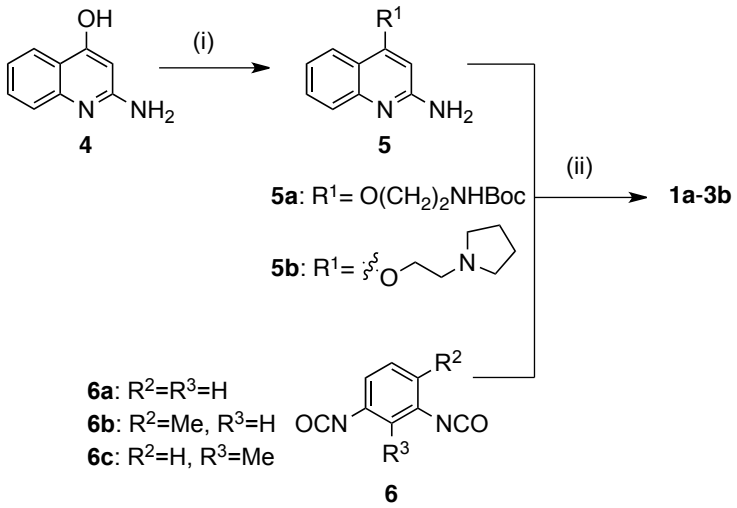

Scheme 2.1: Synthetic scheme of the synthesis of molecules **1a-3b**. (i) *N*-Boc ethanolamine or *N*-(2-hydroxyethyl)-pyrrolidine, PPh_3, DIAD, THF, 0 °C then rt., 3 d; (ii) DCM, 50 °C, overnight; then for **1a**, **2a** and **3a** TFA/DCM, rt, 1 h.

2.5 Folding of the molecules

2.5.1 Molecular modelling

The conformation adopted by a flexible G-quadruplex ligand may have profound implications on its target recognition properties. In order to gain an insight into the folding of the molecules in aqueous solution, molecular modelling of compounds **1a**, **2a** and **3a** was performed using HyperChem® with the PM3 semi-empirical method[179,180] including water as solvent. The rotational barriers for atoms 1-2, 4-5, 7-8 and 10-11, as illustrated for molecule **1a** in Figure 2.3, were calculated. This work was carried out in collaboration with Dr. G. D. Pantoş.

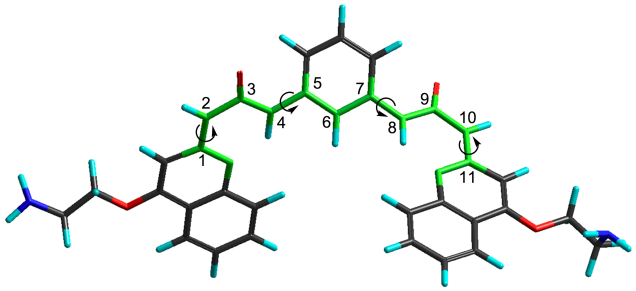

Figure 2.3: Model of molecule **1a** with atom labels. Rotational barriers were calculated for the bonds indicated with an arrow.

Using this method, it was predicted that molecule **1a** has the conformation in aqueous solution as depicted in Figure 2.4. It is a coiled conformation with one of the quinolines pointing out of the plane below the benzene ring and the other above. Displayed are both, the top and the side view. Molecule **2a** shows a twisted conformation, with one of the quinolines pointing upwards; a conformation that is supported by nOe cross-peaks between the hydrogens of the methyl substituent on the benzene ring and one of the hydrogens of one of the quinolines (presented in Figure 2.5). The displayed top and side views show how this conformation is different to that of molecule **1a**.

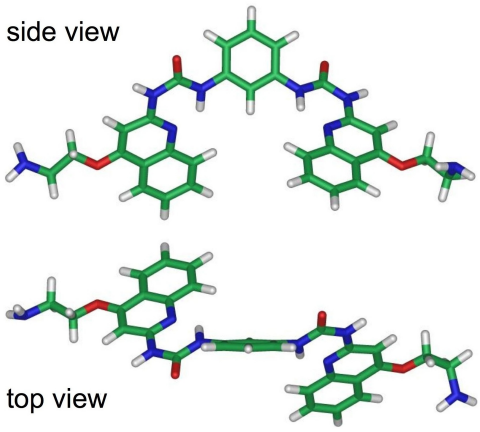

Figure 2.4: Coiled conformation adopted by **1a** in water. Both the side and top view are shown.

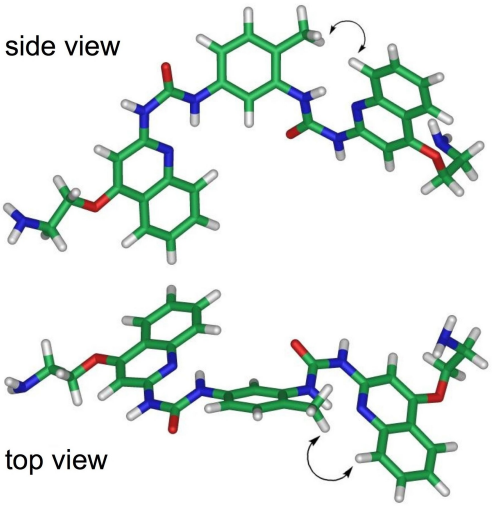

Figure 2.5: Twisted conformation adopted by **2a** in water. The nOe cross-peaks are indicated by arrows. Both the side and top view are illustrated.

The predicted conformation for compound **3a** in water is W-shaped as displayed in Figure 2.6 and also differs from those anticipated for **1a** and **2a**.

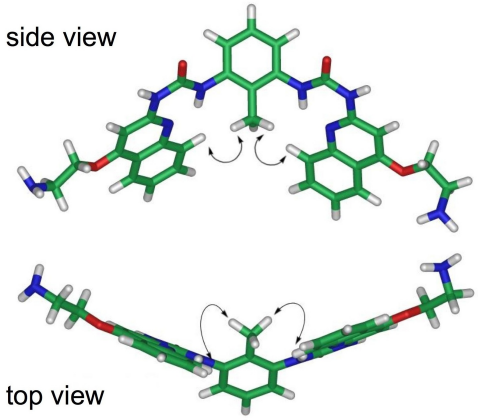

Figure 2.6: W-shaped conformation of **3a** in water. The nOe cross-peaks are indicated by arrows. Both the side and top view are shown.

This was supported experimentally by nOe cross-peaks between the methyl substituent on the benzene ring with hydrogens on both quinolines (see section 2.5.2). The structural data supports the hypothesis that the conformation can be controlled by the methyl substitution on the benzene ring. This predicts that the three molecules adopt different conformations in aqueous solution which could make differential interaction with a nucleic acid target likely.

2.5.2 2D NMR studies

In order to gain experimental support for the proposed folding, I performed 2D NMR experiments in D_2O on molecules **2a** and **3a**. The protons were assigned after performing ^{1}H COSY, ^{1}H NOESY, ^{1}H-^{13}C HMBC and ^{1}H-^{13}C HMQC NMR experiments. The COSY and NOESY spectra of **2a** are depicted in Figure 2.7 and of **3a** in Figure 2.8. The NOESY spectrum displayed in Figure 2.7 shows that hydrogens 4 and 6a interact *via* nOe, placing them in close proximity. This supports the proposed model we obtained by molecular modelling as illustrated in Figure 2.5.

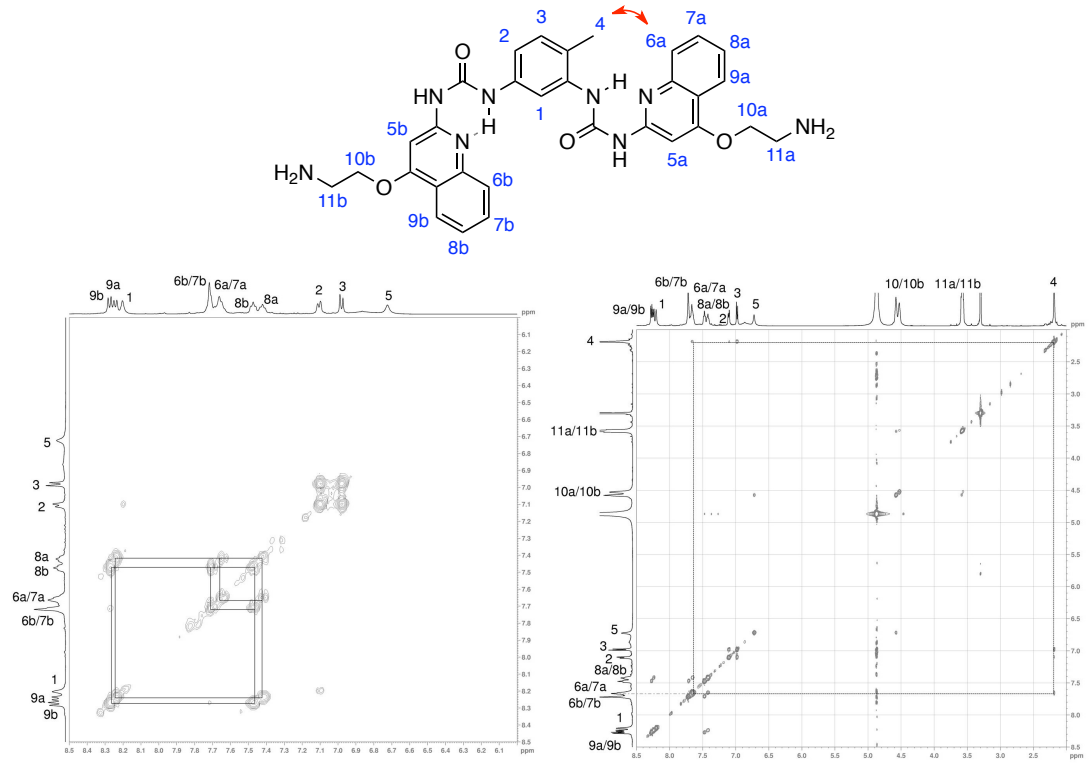

Figure 2.7: Top: Molecular structure of **2a** with labelled hydrogens. The nOe between hydrogens 4 and 6a is indicated with a red arrow. **Bottom left:** COSY of **2a** in D_2O. **Bottom right:** NOESY of **2a** in D_2O.

The NOESY spectrum displayed in Figure 2.8 shows that hydrogens 3 and 5 interact *via* nOe, which suggests that the quinolines are either both pointed downwards, or one pointed upwards and the other downwards. This supports the conformation we obtained by molecular modelling as shown in Figure 2.6, in which both the quinoline moieties are pointed upwards.

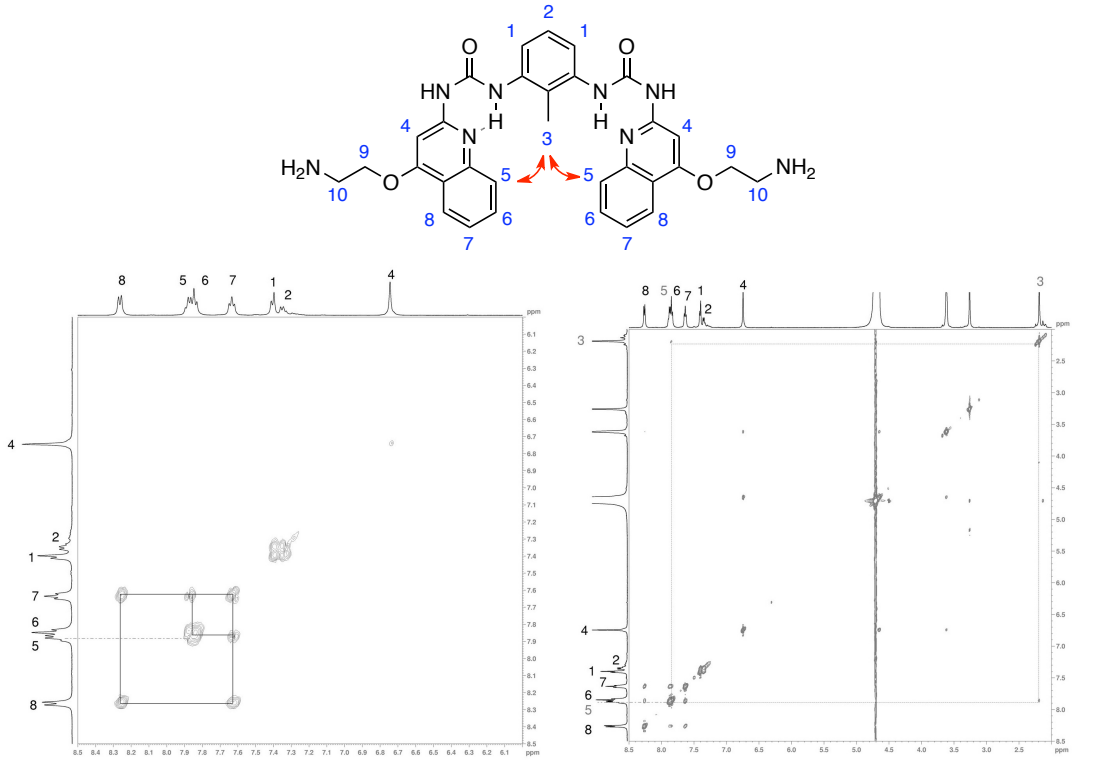

Figure 2.8: Top: Molecular structure of **3a** with labelled hydrogens. The nOe between hydrogens 3 and 5 is indicated with a red arrow. **Bottom left:** COSY of **3a** in D_2O. **Bottom right:** NOESY of **3a** in D_2O.

It was found that molecules **1b**, **2b** and **3b** gave the same results in terms of folding with molecular modelling and NMR experiments as detailed for **2a** and **3a** above. This suggests, that changing the nature of the side chain from a primary amine to a pyrrolidine does not change the folding of the molecules.

2.6 DNA G-quadruplex recognition

It was next explored how distinct folding of these molecules could influence their ability to interact with DNA. This would evaluate the ability of the compounds to stabilise DNA G-quadruplexes and test the hypothesis that controlled-folding can be used to modulate inter-quadruplex specificity of small molecules. Ligand-DNA

interactions were assessed using FRET (Förster Resonance Energy Transfer)-melting experiments.[181]

2.6.1 FRET-melting to assess G-quadruplex stabilisation by small molecules

Energy can be transferred between two fluorophores placed in close proximity. FRET is a non-radiative energy transfer from a donor fluorophore to an acceptor fluorophore and is distance dependent with a typical range of 15 to 60 Å. FRET efficiency can be calculated using equation 2.1:

$$E = \frac{{R_0}^6}{{R_0}^6 + r^6} \tag{2.1}$$

E = FRET efficiency, R_0 = Förster distance in Å, where energy transfer between fluorophores is 50%, r = distance between the fluorophores in Å.

This phenomenon was exploited by J.-L. Mergny and J.-C. Maurizot[181] to develop an assay that allows assessing G-quadruplex stabilisation potentials of small molecules. An oligonucleotide, which has a donor chromophore on one end and an acceptor chromophore on the other, is used in this assay. These are in close proximity when the strand is in a folded conformation, *e.g.* a G-quadruplex as depicted in Figure 2.9. Excitation of the donor fluorophore will result in non-radiative energy transfer from the donor to the acceptor fluorophore if the oligonucleotide is folded. If the strand is unfolded, the fluorophores are too far apart for efficient FRET to occur. Exploiting the fact that elevated temperatures drive the equilibrium towards the unfolded form, heat is supplied to the system. By following the fluorescence emission of the fluorophores upon excitation and heating, information about the folding of the oligonucleotide can be inferred. A graph of temperature against relative fluorescence is then plotted. The temperature at the inflection point of the sigmoidal graph is the temperature at which half the population of the oligonucleotide is folded into its secondary structure. It is also termed melting temperature or T_m. This technique can also be applied for other structures, such as DNA hairpins. By measuring the T_m upon increasing amounts of small molecule, the change in melting temperature (ΔT_m) can

be obtained at a given ligand concentration. However, attaching fluorophores on the oligonucleotides may significantly affect the kinetics of folding and unfolding. Also, any compound can potentially interact with with the fluorophores and thus influence their excitation and emission properties. The technique is depicted in Figure 2.9.

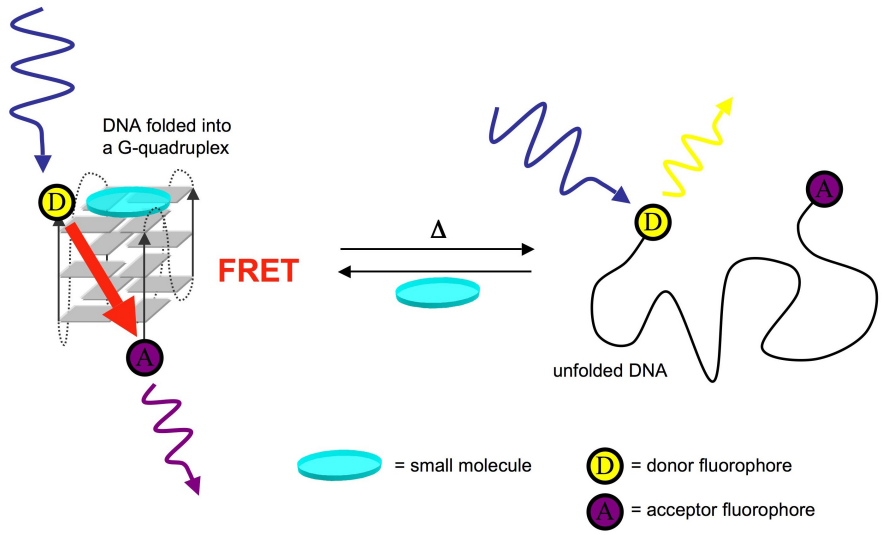

Figure 2.9: Drawing of a FRET system with an oligonucleotide that can fold into a G-quadruplex structure. FRET efficiency decreases heavily when the G-quadruplex (on the left) is unfolded (right).

The stability of a secondary nucleic acid structure is dependent on the sequence and length of the oligonucleotide and thus, different oligonucleotides exhibit different melting temperatures (T_m). Therefore, different amounts of energy are needed to induce the same shift in melting temperature. Hence, it is difficult to directly compare ΔT_m values induced by a small molecule on different G-quadruplex targets, although comparisons have been made in the literature before.[65] It has to be noted that experimental conditions are limited to a maximum temperature of 95 °C. Hence, the biggest measurable change in melting temperature ($\Delta T_{m(max)}$) is calculated as shown by equation 2.2:

$$\Delta T_{\mathrm{m(max)}} \quad = \quad 95\ ^{\circ}\mathrm{C} - T_{\mathrm{m(0)}} \tag{2.2}$$

$\Delta \mathrm{T_{m(max)}}$ = maximal shift in melting temperature, $\mathrm{T_{m(0)}}$ = melting temperature of the oligonucleotide in absence of small molecule.

2.6.2 FRET-melting studies on molecules 1a-3b

Using FRET melting, the aptitude of compounds **1a-6b** to stabilise an array of biologically relevant G-quadruplex forming DNA sequences was determined, namely: the human telomeric G-quadruplex (H-telo), sequences from the promoter regions of *c-kit* [147–149] (including the two G-quadruplex forming sequences C-kit1 and C-kit2), *c-Myc* [15,58,84,86,92,146] and *k-ras* [152,153] (the sequences can be found in Chapter 5). The thermal shift profiles, in which changes in melting temperature ($\Delta \mathrm{T_m}$) are plotted as a function against ligand concentration, are depicted for molecules **1a-3b** in Figure 2.10.

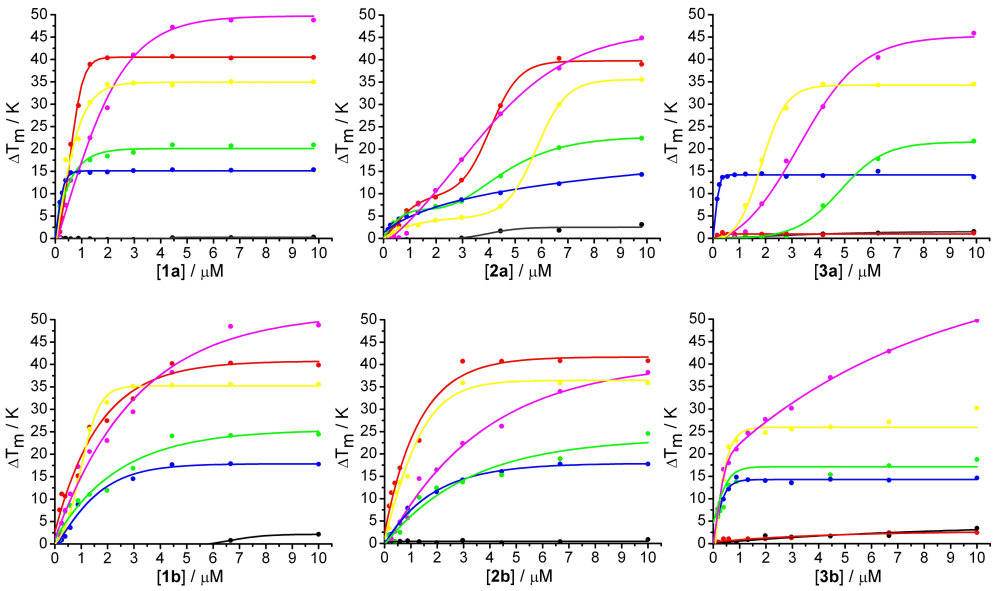

Figure 2.10: Thermal shift profiles for molecules **1a**, **2a** and **3a** obtained by FRET-melting: ● (H-telo), ● (C-kit1), ● (C-kit2), ● (C-myc), ● (K-ras) and ● (ds-DNA).

Tables showing ΔT_m at 1 μM ligand as conventionally quoted in the literature[68,79,93,96,181] (Table 2.1) and [ligand] in μM at half maximal ΔT_m (Table 2.2) are displayed for compounds **1a-3b** to help compare the thermal shift profiles. It was found that the melting shift profiles of all the G-quadruplexes studies varied greatly between molecules **1a**, **2a** and **3a** as illustrated in Figure 2.10. This implies that the folding of these ligands could influence their molecular mode of interaction. It is possible that the methyl group interacts with the target DNA influencing the FRET-melting results. It is a relatively small and unfunctionalised chemical group and unlikely to be the main contributor to the vast differences in stabilisation seen between the molecules. The melting shift profiles for molecules **1b**, **2b** and **3b** also vary (Figure 2.10), but the differences are not as pronounced as for the molecules carrying a primary amine. No detectable stabilisation of ds-DNA with any of the ligands was detected at the concentrations used, which is consistent with a high level of discrimination between quadruplex and ds-DNA.

	ΔT_m (K)					
Target[1]	**1a**	**2a**	**3a**	**1b**	**2b**	**3b**
H-telo	27.3±0.3[2]	2.8±0.3	3.9±0.4	16.7±0.5	20.0±0.5	25.9±0.5
C-kit1	34.0±0.4	6.6±0.7	0.0±0.3	19.8±0.4	20.1±0.3	0.7±0.3
C-kit2	16.2±0.9	4.2±0.2	1.0±0.8	9.3±0.6	6.1±0.2	14.9±0.7
C-myc	17.7±0.4	6.2±0.4	14.1±0.3	7.5±0.5	7.1±0.4	13.8±0.5
K-ras	16.7±0.5	4.0±0.4	2.7±0.3	16.0±0.6	9.4±0.4	20.8±0.3
ds-DNA	0.0±0.2	0.0±0.1	0.0±0.4	0.0±0.2	0.5±0.5	0.4±0.3

Table 2.1: ΔT_m at 1 μM ligand in K.

Molecule **1a** caused a very high ΔT_m value for each of the G-quadruplexes studied (corresponding to $\Delta T_{m(max)}$). Although these are very high stabilisation potentials, there is very little discrimination between different G-quadruplexes. The stabilisation temperature of the human telomeric G-quadruplex with a ΔT_m of 27.3±0.3 K is in the range of the most potent ligands reported in the literature,[110,144] for example a quinoline macrocycle that showed 33.8 K at 1 μM.[110]

[1]The T_m of the quadruplexes in 60 mM K^+ in the absence of ligand ($T_{m(0)}$) are: 59.4 °C (H-telo), 54.5 °C (C-kit1), 72.7 °C (C-kit2), 79.3 °C (C-myc), 45.9 °C (K-ras), 62.7 °C (ds-DNA); measurements could be taken up to 95.0 °C under the experimental conditions.

[2]Errors were calculated as SD of three independent experiments.

Compound **1a** exhibits the highest ΔT_m that can be measured with this method for all the G-quadruplexes tested which is visualised by the plateauing of the curves in Figure 2.10. The concentrations needed to achieve this saturation were 2.8 μM for H-telo, 2.0 μM for C-kit1, 2.5 μM for C-kit2, 0.8 μM for C-myc and 5.0 μM for K-ras. Ligand **2a** did not exhibit strong stabilisation potentials at lower concentrations for any of the G-quadruplex targets investigated, but good stabilisation at higher concentrations. Much higher ligand concentrations were required to reach saturation of the curves as compared to molecule **1a**, indicating that this ligand is less potent as a G-quadruplex stabilising molecule. In contrast, **3a** showed selective stabilisation for one of the G-quadruplexes investigated. $\Delta T_{m(max)}$ for the C-myc quadruplex was measured at 0.4 μM whereas much higher concentrations of ligand were needed to stabilise the other targets significantly. Table 2.2 displays the concentrations needed to induce half the maximal ΔT_m.

	cpd. (μM)					
Target	**1a**	**2a**	**3a**	**1b**	**2b**	**3b**
H-telo	0.5	5.6	1.9	1.0	0.9	0.5
C-kit1	0.6	3.7	>10.0	1.1	0.9	>10.0
C-kit2	0.4	3.4	4.8	1.2	1.9	0.5
C-myc	0.2	2.3	0.2	1.0	1.0	0.3
K-ras	1.5	4.0	3.7	2.0	3.6	1.5
ds-DNA	>10.0	>10.0	>10.0	>10.0	>10.0	>10.0

Table 2.2: [Compound] in μM at half maximal ΔT_m.

Striking is the comparison of molecules **2a** and **3a**. Whereas 0.2 μM of compound **1a** were required to induce half the maximal stabilisation for C-myc (see Table 2.2), the other targets required much higher concentrations. Similar concentrations were needed as compared to ligand **3a** to achieve maximal stabilisation for C-kit2 and K-ras, but higher concentrations for H-telo, as half the maximum stabilisation was reached at 5.6 μM as compared to 1.9 μM. Ligand **3a** did not stabilise the C-kit1 G-quadruplex at any of the concentrations measured. To the best of my knowledge, this was the first example of a molecule that caused a large ΔT_m for one or more G-quadruplexes, yet no detectable stabilisation for another.

These results demonstrate, that it is possible to achieve differential recognition and even quadruplex specificity by controlling the folding of a particular molecular scaffold.

The G-quadruplex stabilisation potential was altered when the side chains were changed from primary amines to pyrrolidines. This substitution reduced the stabilisation properties of molecules of type **1** but enhanced those of type **2** and **3**. Compound **3b** did not stabilise the C-kit quadruplex like its analogue **3a**, which could be a general recognition property of molecules of this scaffold with a W-shaped conformation. However, this compound showed better stabilisation for all the other G-quadruplexes studied by FRET-melting than **3a** (see Table 2.1). These results demonstrate that it is possible to combine controlled-folding with side chain variation to fine-tune the molecular recognition properties of a particular scaffold. It is possible that the conformation of the ligands changes from our predicted structures when interacting with the nucleic acids, as the molecules are inherently flexible.

2.7 Conclusions and future work

It has been demonstrated that a simple methyl substitution of molecules with a 1,3-[di-quinolin-2-yl-diureido] benzene scaffold can influence their folded conformation. This hypothesis was supported by molecular modelling and confirmed by NMR spectroscopy experiments. The new compounds stabilise G-quadruplexes selectively over ds-DNA which was assessed by FRET-melting experiments. Some of the compounds compare favourably to the most potent ligands reported in the literature as assessed by this method. Controlling the ligand conformation has an effect on the molecular recognition properties of a compound towards nucleic acid targets. This can be fine-tuned by varying the side chains of the molecules. This approach was successfully implemented to obtain a G-quadruplex ligand that preferentially stabilises one particular G-quadruplex out of the nucleic acid targets studied. These studies did not reveal how the ligands interact with the G-quadruplexes, but I postulate that they most likely interact with the loops of the target. That could be investigated with additional NMR spectroscopic studies, which would help understand how the compounds can be derivatised further to achieve differential recognition of G-quadruplex targets.

To further explore how the conformation of molecules with a 1,3-[di-quinolin-2-yl-diureido] benzene scaffold could be influenced by substitutions on the benzene ring, potentially leading to differential G-quadruplex recognition, the molecules depicted in Figure 2.11 could be synthesised. These two molecules have have two and three methyl substitutions, respectively. This would constrict the conformations of the ligands further to that of the mono-substituted compounds **2a**, **2b**, **3a** or **3b**.

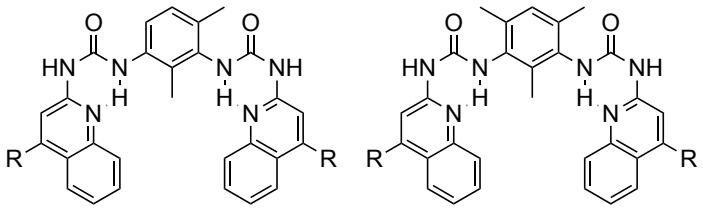

Figure 2.11: Possible molecules with two or three methyl substitutions on the central benzene ring.

Furthermore, the methyl groups could be changed to bulkier groups (such as ethyl) to exaggerate the potential steric clash influencing the conformation adopted by the molecules. Ligand **3a**, which stabilised the C-myc G-quadruplex preferentially as assessed by FRET-melting, might also influence *c-Myc* expression by stabilising the promoter G-quadruplex of the gene. The data presented in this chapter might also be useful to design new ligands to achieve better inter-G-quadruplex discrimination.

However, during the course of these studies another family of small molecules based on quinolines was developed in our lab and was found to have striking biological implications in human cells. Research was therefore directed towards these compounds and will be the theme of the remaining chapters of this thesis.

Chapter 3

N,N′-Bis(quinolinyl)pyridine-2,6 dicarboxamides: G-quadruplex interacting small molecules and their cellular effects

3.1 Background

Our group previously reported on a small molecule, named **pyridostatin**,[144] based on a *N,N′-bis*(quinolinyl)pyridine-2,6 dicarboxamide scaffold as depicted in Figure 3.1. The ligand was designed by Dr. Raphaël Rodriguez based on structural features of other potent G-quadruplex binding molecules, with particular emphasis on: 1) the ability to adopt a mainly flat conformation facilitated by an internal hydrogen bonding network,[182] 2) an electron-rich aromatic surface with alkoxy-substituents carrying positively charged aliphatic amines and 3) the presence of nitrogen lone pairs able to hydrogen-bond a molecule of water in the middle, which helps the scaffold adopt a flat conformation.[183] The internal hydrogen bonds give the molecule a flat character with some flexibility[182] that can facilitate binding. As discussed in section 1.1 (Chapter 1), the tetrad is not exactly planar. A flat molecule which is not completely rigid has therefore better chances to interact with the aromatic surface of the G-tetrad. Quinolines were incorporated into the molecular scaffold, which is similar to that presented

in Chapter 2, but does not allow as much conformational freedom as molecules of the 1,3-[di-quinolin-2-yl-diureido] benzene family. The scaffold was designed to be able to generally interact with G-quadruplex structures and not primarily to achieve inter-quadruplex selectivity. The molecule was shown to stabilise the telomeric G-quadruplex with a ΔT_m of 35.0 K in 60 mM K^+ as assessed by FRET-melting. The molecule also exhibited negligible stabilisation of ds-DNA and its G-quadruplex stabilisation potential was hardly altered by the presence of 25 mole equivalents of competitor ds-DNA. These data represent the highest induced shift in T_m for the telomeric G-quadruplex by a small molecule to date assessed by this method, with a very high level of selectivity over ds-DNA. **Pyridostatin** is structurally related to **360A**[173] (depicted in Figure 1.8) but the latter may not adopt the same conformation in solution as it cannot form the same internal hydrogen-bond network and is electron-poor.

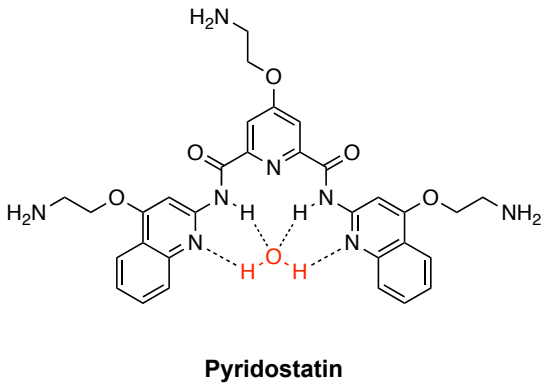

Figure 3.1: Molecular structure of **pyridostatin**. Water (in red) can hydrogen-bond in the centre as depicted.

It has been demonstrated that **telomestatin** uncaps POT1 from telomeres leading to loss of telomeric DNA and senescence in human HT-1080 tumour cells.[42] HT-1080GFP-POT1 transfected cells were used in the study presented here, to assess the effect of **pyridostatin** on POT1 uncapping. This work was carried out by Dr. Raphaël Rodriguez and Dr. Jean-François Riou. It was found that after 72 h incubation of the cells with 1 μM **pyridostatin**, a concentration where most of the cells were still viable, the fluorescent green signal associated with telomeres decreased dramatically.[144] It was postulated that the folding of

the G-overhang into quadruplexes induced by the small molecule led to POT1 uncapping from telomeres in cells as depicted in Figure 3.2.[1] Unprotected telomeres have been associated with nuclear foci of γH2AX, a phosphorylated histone that is an early DNA-damage marker. It was demonstrated that **pyridostatin** induced DNA-damage as seen by immunofluorescence microscopy against γH2AX which was partially colocalised with GFP-POT1 at telomeres (Figure 3.3).

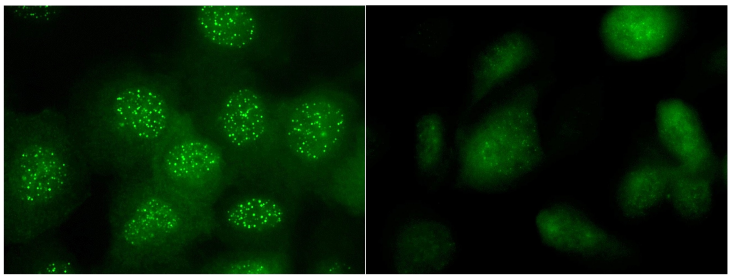

Figure 3.2: POT1 uncapping by **pyridostatin**. **Left:** HT-1080 cells after 72 h without treatment. **Right:** HT-1080 cells treated with 1 μM **pyridostatin** after 72 h. The number of green dots associated with GFP-POT1 decreases dramatically.

This suggests that the removal of POT1 by the compound induces a DNA damage response. However, partial colocalisation could be indicative that the DDR may be triggered elsewhere in the genome, possibly due to the interaction of the molecule with other G-quadruplexes throughout the genome.

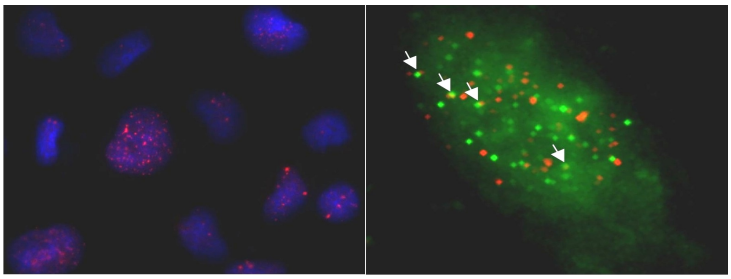

Figure 3.3: Left: DNA damage shown by red foci of γH2AX. **Right:** Partial colocalisation with GFP-POT1 as indicated with arrows.

[1] Pictures for Figure 3.2 and Figure 3.3 have been adopted from the literature. [144]

The interaction of G-quadruplex ligands with telomeres can not only lead to POT1-uncapping and telomere shortening,[42,48,144] but also to replicative senescence in certain tumour cell lines, such as HT-1080.[44,57,72,82,138] Moreover, another molecule based on the *N,N′-bis*(quinolinyl)pyridine-2,6 dicarboxamide scaffold has also been shown to interact with the NRAS RNA G-quadruplex in the 5′-UTR of the mRNA, altering translation,[36] a process that is described in Chapter 1 in section 1.3.5. **Pyridostatin** did not cause the same selective effect. This suggests that different molecules based on this scaffold interact with different G-quadruplexes and the recognition might be fine-tuned to preferentially target certain G-quadruplexes. These results prompted us to develop this family of compounds in our laboratory by synthesising **pyridostatin** analogues and comparing their biophysical and cellular effects. Compounds targeting telomeres are particularly promising for the development of anti-cancer drugs, as they might have anti-proliferative effects.

3.2 Objectives

The aim of this work was to design and synthesise G-quadruplex interacting small molecules based on the *N,N′-bis*(quinolinyl)pyridine-2,6 dicarboxamide scaffold and evaluate them for their potential to stabilise G-quadruplex DNA. Furthermore, the prospect was to investigate the effect of the compounds on telomere biology. The aim was also to assess the growth-inhibitory and cytotoxic properties of these molecules and carry out initial investigations as to whether they could potentially be developed into drug molecules.

3.3 Synthesis of pyridostatin analogues

Based on the *N,N′-bis*(quinolinyl)pyridine-2,6 dicarboxamide scaffold, 28 small molecules were synthesised in 2-7 steps. In order to gain an insight into structure activity relationships (SAR) of the potential interactions of the compounds with DNA, the nature and length of the side chains R^1 and R^2, as depicted in Scheme 3.1, was varied. It was decided to keep the oxygen on the 4-substitution on the quinoline moieties for all the molecules as it had been proven to be an excellent structural feature by the successful design of **pyridostatin** and by the

molecules presented in Chapter 2. This would keep the electron density of the quinoline moieties the same.

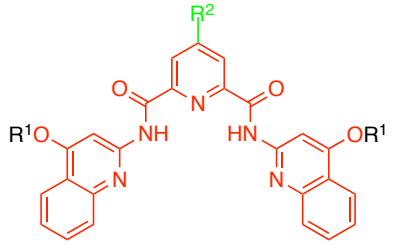

Scheme 3.1: *N,N′-bis*(quinolinyl)pyridine-2,6 dicarboxamide scaffold (highlighted in red) with side chains. The nature and length of the side chains R^1 and R^2, highlighted in black and green respectively, were altered in order to gain an insight into the SAR of the molecules with G-quadruplex targets.

3.3.1 First generation molecules

A list of first generation ligands, which encompasses compounds **18**-**37**, was synthesised. The scaffold can be assembled from one pyridine-based building block and two quinoline-based building blocks, followed by any necessary modifications to obtain the desired target G-quadruplex ligands. The pyridine building block used was either the commercially available 2,6-pyridinedicarbonyl dichloride (**7**), or was obtained from chelidamic acid (**8**) as illustrated in Scheme 3.2, Scheme 3.3 and Scheme 3.4.

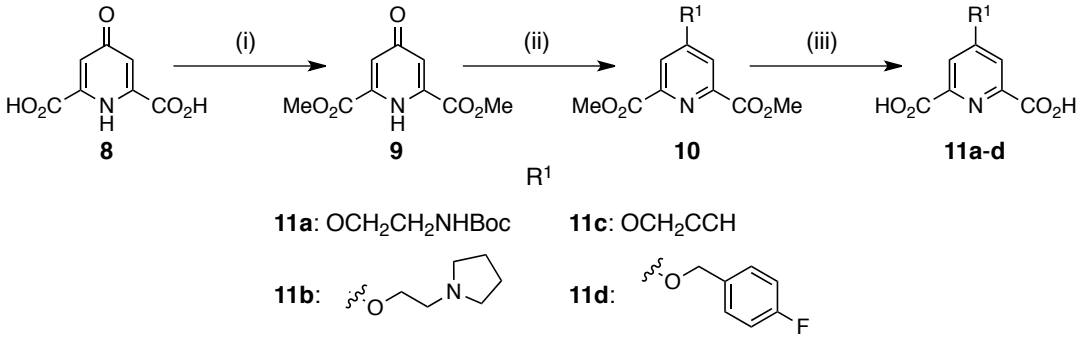

Scheme 3.2: (i) $SOCl_2$, MeOH, 0 °C, 1h; then **8**; then rt, overnight; (ii) PPh_3, DIAD, THF, 0 °C, 1 h; then ROH, rt, 3 d; (iii) NaOH, MeOH, H_2O, rt, 1 h.

Pyridine building-blocks **11a-d** were synthesised as depicted in Scheme 3.2. The acid groups of compound **8** were first protected as methyl esters using $SOCl_2$/MeOH. The alcohol on the 4-position of the resulting chelidamic dimethyl ester (**9**) was derivatised using Mitsunobu reaction conditions. The products were purified by column chromatography and the resulting intermediates **10** were deprotected using base catalysed ester hydrolysis to obtain **11a-d** in 57-77% yield over two steps.

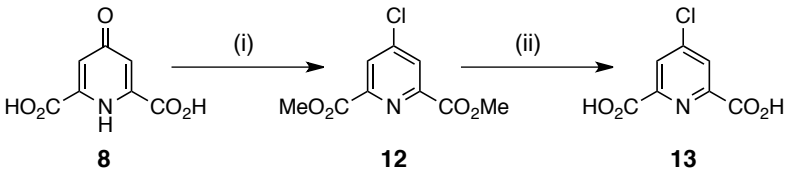

8 **12** **13**

Scheme 3.3: (i) $SOCl_2$, MeOH, 0 °C, 1 h; then **8**; then reflux, overnight; (ii) NaOH, MeOH, H_2O, rt, 1 h.

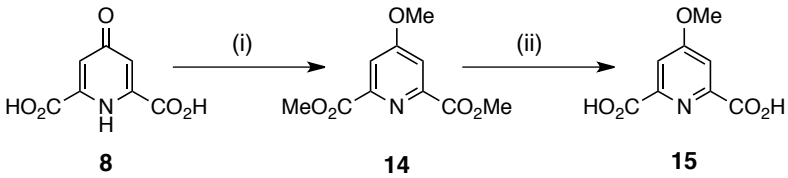

8 **14** **15**

Scheme 3.4: (i) Me_3SiCHN_2, PhMe/MeOH, rt, 30 min; (ii) NaOH, MeOH, H_2O, rt, 1 h.

Whilst following a published procedure[184] to obtain the chelidamic acid dimethyl ester (**9**), dimethyl 4-chloropyridine-2,6 dicarboxylate (**12**) was obtained as a by-product as shown in Scheme 3.3. Compound **12** was obtained in mediocre yield (28%). Thus, it was facile to easily obtain *N*,*N*′-*bis*(quinolinyl)pyridine-2,6 dicarboxamides with a chlorine substituent at the 4-position on the pyridine ring. It was later found that the reaction yielded exclusively **9** in high yield (85%) when stirred at rt overnight and not refluxed as described in the literature.[184] The diacid (**13**) was obtained from **12** analogous to the procedure to obtain **11a-d**. Me_3SiCHN_2 was used to synthesise the dimethyl 4-methoxypyridine-2,6 dicarboxylate (**14**) in 90% yield. The diester was subsequently hydrolysed using

basic conditions to afford 4-methoxypyridine-2,6 dicarboxylate (**15**) as illustrated in Scheme 3.4. The quinoline-based building blocks were prepared using the two routes depicted in Scheme 3.5 and Scheme 3.6. Two of the molecules (**5a** and **5b**) were previously presented in Chapter 2 (Scheme 2.1). Mitsunobu reaction conditions were employed (Scheme 3.5), analogous to the synthesis of the pyridine building-blocks, to afford the products in 53-71% yield.

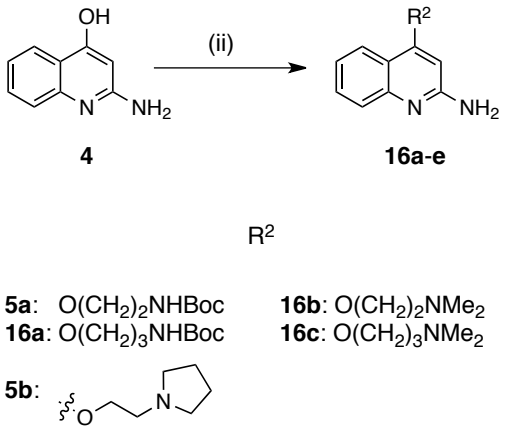

Scheme 3.5: (i) PPh_3, DIAD, THF, 0 °C, 1 h; then ROH, rt, 3 d.

A quinoline building block with a methoxy substituent at position 4 (**17**) was synthesised using Me_3SiCHN_2 as depicted in Scheme 3.6.

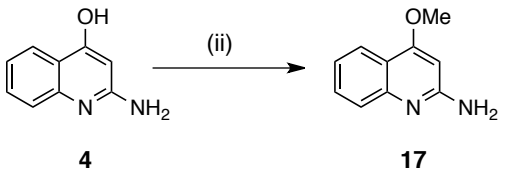

Scheme 3.6: (i) Me_3SiCHN_2, PhMe/MeOH, rt, 30 min.

To assemble molecules with a *N,N′-bis*(quinolinyl)pyridine-2,6 dicarboxamide scaffold, one mole equivalent of the pyridine building-blocks (**7**, **11a-e**, **13** or **15**) was reacted with two identical mole equivalents of the synthesised quinoline building-blocks (**16a-e** or **17**). Two different routes were employed as depicted in Scheme 3.7 and Scheme 3.8.

Five molecules with the desired scaffold (**18-22**), without a substituent present on the 4-position of the pyridine ring, were synthesised (Scheme 3.7). The commercially available 2,6-pyridinedicarbonyl dichloride (**7**) was used as the pyridine building block. Yields increased significantly by adding TEA to the acyl chloride prior to coupling. The primary amines of compounds **18** and **19** were obtained by removing the Boc-protecting group with TFA/DCM. All final compounds were purified using HPLC to obtain pure products for subsequent biophysical and biological evaluation and molecules **18-22** were obtained in 62-82% yield.

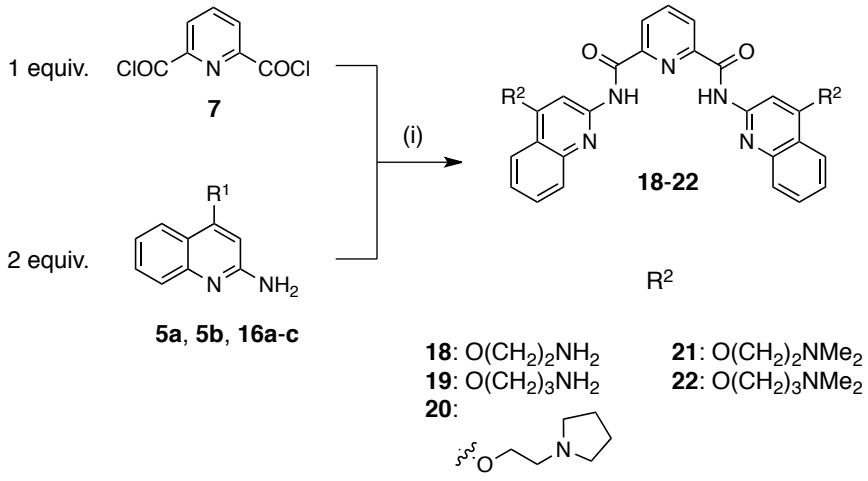

Scheme 3.7: (i) TEA, DCM, rt, overnight; then for **18** and **19**, TFA/DCM, rt, 1 h.

The *N*,*N*′-*bis*(quinolinyl)pyridine-2,6 dicarboxamides **23-37** were synthesised as illustrated in Scheme 3.8. One equivalent of the pyridine building blocks **11a-d**, **13** and **15** were reacted with two equivalents of the quinoline building blocks **5a**, **5b**, **16a-c** and **17** to obtain molecules with the desired scaffold. Different coupling strategies were attempted and it was found that the strategy using Ghosez' reagent (1-chloro-*N*,*N*,-2-trimethylpropenylamine) was very facile and gave satisfactory yields. The coupling products could be precipitated from hot MeCN to yield the desired intermediates or final products. The final compounds **23-25**, **27**, **28**, **31**, **32** and **36** were obtained by removing the Boc-protecting groups with TFA/DCM. All the final compounds were also purified using HPLC to obtain the pure products, which were used in subsequent biological analyses, in 53-93% yield.

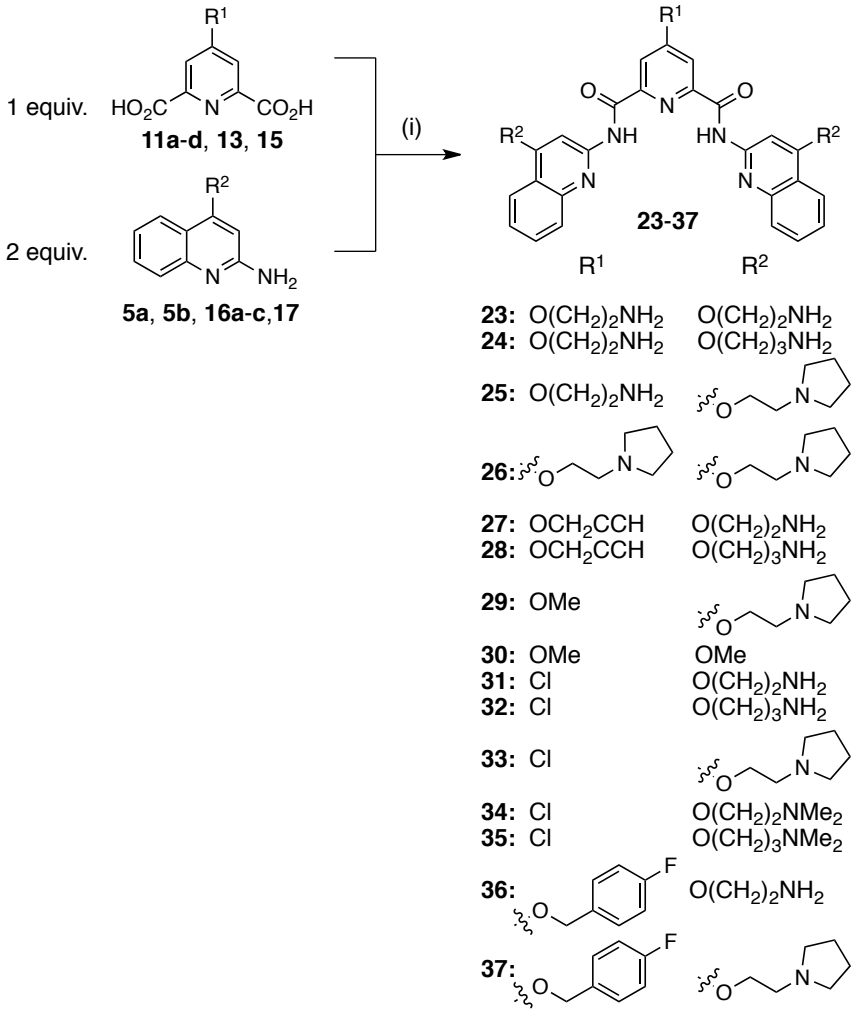

Scheme 3.8: (i) 1-chloro-*N*,*N*,-2-trimethylpropenylamine, DCM, 2 h; then TEA, 0 °C, 1 h; then rt, overnight.

3.3.2 Second generation molecules

In order to introduce further functionalities, a strategy was applied to derivatise the side chain on the pyridine ring after the scaffold had been assembled. For that reason, molecules **27** and **28**, both containing an alkyne side chain on the pyridine ring of the scaffold, were used as starting materials. This would allow for the reaction with azides *via* a copper-catalysed 1,3-Huisgen cycloaddition using copper(II) sulfate pentahydrate and sodium ascorbate ('click chemistry') to easily

synthesise *N,N′-bis*(quinolinyl)pyridine-2,6-di carboxamides with more complex appendages in just one additional synthetic step. It is precedented in the literature to use click chemistry to assemble G-quadruplex ligands.[66,101] Compounds **38-46** were prepared using this procedure, which is depicted in Scheme 3.9. This strategy enabled the introduction of sugar moieties on molecules **42-44**. Two analogues (**45** and **46**) carrying a derivative of a nucleobase were synthesised by reacting zidovudine with **27** and **28**.

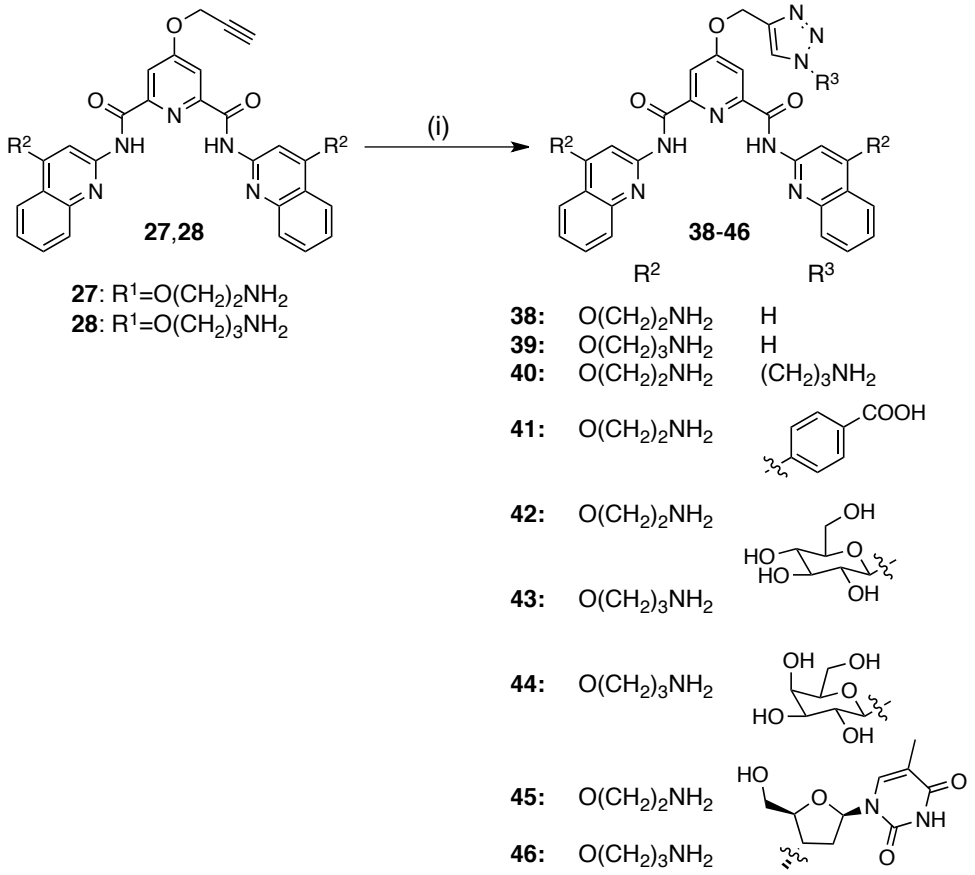

Scheme 3.9: (i) copper(II) sulfate pentahydrate, sodium ascorbate, rt, 10 min; RN_3, rt, overnight.

The sugar moieties of molecules **42-44** were chosen as sugars present a high potential for hydrogen bonding to nucleic acid targets. The thymine on **45** and **46** can also potentially hydrogen-bond with the desired nucleic acid targets. A

nucleobase is an obvious choice as a side chain of a nucleic acid interacting small molecule based on the old Latin saying *similia similibus solvuntur*. The design of molecules **38** and **39** would allow potential comparisons of the G-quadruplex interacting effects of the triazole moiety compared with the attached side chains.

The synthesis of the library of *N,N′-bis*(quinolinyl)pyridine-2,6 dicarboxamides was achieved in reasonably high yields and with high purity in 2-7 steps, which renders the employed strategy very attractive. It has been demonstrated how side chain substitution could be achieved before and after the assembly of the final scaffold.

3.4 G-quadruplex stabilisation

In order to assess the interaction of molecules **18-46** with DNA G-quadruplexes, a FRET-melting assay was performed on five different quadruplex targets (H-telo, C-kit1,[148] C-kit2,[149] C-myc,[15,84,86,146] Bcl-2[150] and K-ras[152,153]) and one double-stranded DNA sequence for comparison (the sequences can be found in Chapter 5). The biological data, which will be discussed later, is focussed on the telomeres and the biophysical discussion will therefore mainly focus on H-telo. The ΔT_m values at 1 μM ligand obtained by FRET melting experiments can be found in Table 3.1 for H-telo and ds-DNA and for the promoter G-quadruplexes studied in Appendix A (Table A.1). All the melting shift profiles can be found in Appendix A (Figure A.1, Figure A.2 and Figure A.3).

Most of the molecules of this family show very good stabilisation of the telomeric quadruplex but no significant stabilisation of ds-DNA at the concentration range studied. Most of the compounds also stabilise the other G-quadruplex targets with high ΔT_m values. Ligands **23-26** cause maximal stabilisation for H-telo at 1 μM ligand. They all have an amine functionality on a two-carbon aliphatic chain on R^1. Compounds **31**, **32** and **25**, which have a chlorine substituent at R^1, and molecules **43** and **44**, which have a sugar functionality at that position, also exhibit maximal stabilisation of this quadruplex target. Other compounds with a chlorine or hydrogen substituent at this position also show considerable changes in the stabilisation temperature ranging from 22±0.9 K (**20**) to 31.4±0.8 K (**19**). Ligands with an alkyne functionality on R^1 exhibit moderate ΔT_m for H-telo. The 4-fluorobenzyloxy-substitution on R^1 on ligands **36** and **37** resulted

in a huge drop in ΔT_m values compared to other analogues. Molecules **38**-**46** which have a 1,2,3-triazole side chain exhibited varying stabilisation potentials. Whereas molecules **38**-**42** showed moderate ΔT_m values, the sugar and thymidine derivatives showed very high values for the quadruplexes studied.

ΔT_m (K)			ΔT_m (K)		
compound	**H-telo**	**ds-DNA**	**compound**	**H-telo**	**ds-DNA**
18	28.4±0.8[1]	0.0±0.1	**33**	24.3±0.6	0.1±0.1
19	35.7±0.8	0.1±0.2	**34**	27.9±0.6	0.0±0.1
20	22.0±0.9	0.0±0.1	**35**	35.9±0.3	0.3±0.2
21	30.0±0.6	0.3±0.2	**36**	8.8±0.5	0.3±0.1
22	35.5±1.2	0.8±0.3	**37**	4.3±0.3	0.0±0.2
23	34.8±0.6	0.5±0.2	**38**	10.1±0.6	0.0±0.1
24	35.1±0.9	0.9±0.2	**39**	13.2±0.8	0.0±0.1
25	35.5±0.9	0.4±0.1	**40**	18.8±0.6	0.0±0.1
26	35.5±0.8	0.9±0.2	**41**	6.3±0.4	0.0±0.1
27	16.0±1.0	0.0±0.1	**42**	30.0±1.0	0.0±0.2
28	18.3±0.5	0.0±0.1	**43**	35.5±0.7	0.4±0.1
29	12.5±1.1	1.0±0.3	**44**	35.5±1.0	0.4±0.1
30	0.5±0.4	0.0±0.2	**45**	32.0±0.4	0.0±0.1
31	35.5±0.9	0.0±0.0	**46**	32.2±0.6	0.0±0.0
32	35.5±0.7	0.4±0.0			

Table 3.1: ΔT_m at 1 μM ligand in K measured by FRET-melting against H-telo and ds-DNA for **18**-**46**.

The general trend of decreasing stabilisation for H-telo at the R^1 position is: $O(CH_2)_2NH_2$ > 2-pyrrolidinoethyloxy > sugar functionalities > Cl > H > OCH_2CCH > OMe > 4-fluorobenzyloxy. Positively charged functionalities and sugars gave the highest values, which could be due to their potential for electrostatic or hydrogen bonding interactions with the nucleic acid target, possibly the loops and phosphate backbones of the quadruplexes. Since ligands with chlorine and hydrogen substitution at R^1 also gave very high stabilisation potentials, this position does not seem to be crucial to ensure good interactions with quadruplex nucleic acids. However, substitution with uncharged, aromatic or aliphatic side chains adversely affects the stabilisation potentials of the molecules, which could

[1]Errors were calculated as standard deviation of three independent experiments.

be due to repulsion.

The nature of the primary amine side chain at R^2 did not greatly affect the G-quadruplex stabilisation potential of the molecules. There was only a slight general trend at this position with greater stabilisation observed for NH_2 > pyrrolidine > NMe_2. Comparing ΔT_m values for **18-22**, **31-35** and **42-44**, which are three series where R^1 is unaltered in each case, shows that a three-carbon side chain on position R^2 gives slightly higher stabilisation potentials than two-carbon side chains. Compound **30** does not have any amine functionality at either position R^1 or R^2. This eliminated the stabilisation potential for any of the quadruplex targets almost entirely.

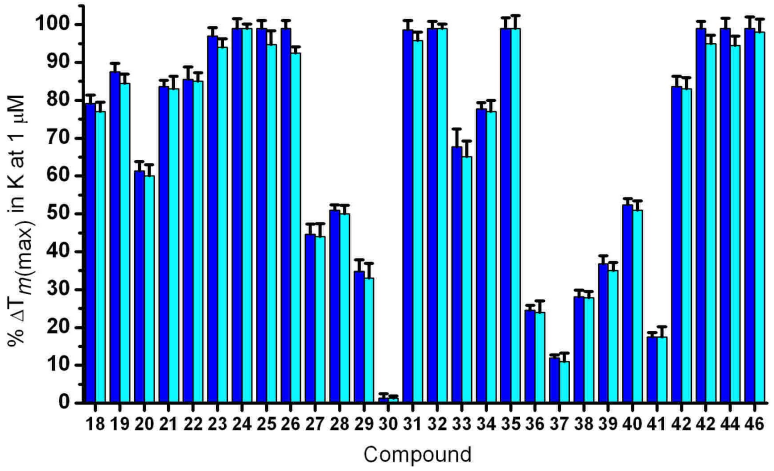

Figure 3.4: FRET competition results at 1 μM **18-46** for H-telo in the presence of 50 mole equivalents of DNA competitor. Values are expressed as $\%\Delta T_{m(max)}$, which is the maximum measurable change in T_m where $T_{m(max)}$ is 95 °C. $\Delta T_{m(max)}$ is therefore 35.5 K for H-telo. Dark blue: $\Delta T_{m(max)}$ in the absence of ds-DNA; cyan: $\Delta T_{m(max)}$ in the presence of ds-DNA competitor.

In order to further assess the selectivity of these compounds for G-quadruplex DNA over ds-DNA, I performed a FRET-melting assay on the H-telo quadruplex in the presence of an excess of ds-DNA as depicted in Figure 3.4. 50 mole equivalents of a DNA competitor, which can form an intramolecular hairpin or inter-molecular duplex, were added. Thus, at least 25 mole equivalents of ds-DNA were present in these experiments. The melting profiles for the H-telo quadru-

plex were not affected and the stabilisation temperatures were almost unaltered. The ΔT_m values determined in the absence and presence of ds-DNA competitor normalised against $\Delta T_{m(max)}$ are illustrated Figure 3.4.

These results demonstrate that the *N,N′-bis*(quinolinyl)pyridine-2,6 dicarboxamides are very effective and selective G-quadruplex stabilising ligands in the presence of an excess of ds-DNA. This also suggests their likely interaction with telomeric G-quadruplexes *in cellulo*, validating the design. The data suggests that these molecules could potentially interact with a variety of G-quadruplex targets in cells.

3.5 Short-term growth inhibition

Molecules **18**-**46** were assessed for their ability to inhibit cell growth using a luminescent cell viability assay (CellTiter-Glo™ by Promega®)[185] after 72 h of exposure of the cells to the compounds at eight different doses. This would allow an initial indication as to whether these compounds may cause a mechanistic effect in cells. Growth inhibition was determined for a panel of three human cancer cell lines: HeLa[186] (cervical adenocarcinoma), HT-1080[187] (fibrosarcoma) and U2OS[188] (osteosarcoma). The growth inhibition of WI-38 cells which is a non-cancerous, normal and untransformed cell line was also assessed.[189,190] The luminescent assay determines the average number of viable cells in culture based on the quantification of ATP present, which signals the presence of metabolically active cells. The supplied reagent mixture lyses the cells to liberate all the ATP into solution. As a detection method beetle luciferin is used, which is converted into luminescent oxyluciferin by the enzyme luciferase (see Scheme 3.10).

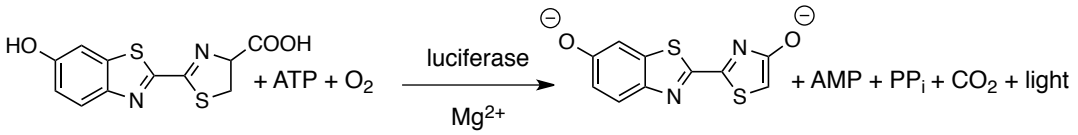

Scheme 3.10: Oxidation of luciferin into oxyluciferin by luciferase.

Experiments were performed in triplicate using three independent repeats. GI_{50} values (*i.e.* the ligand concentration needed to induce 50% of the signal as com-

pared to the untreated cells) were determined by plotting the concentration of ligand against % of cells observed at 72 h compared to the untreated control (which was set to 100%). A dose-response curve was fitted to the values and an example is given for compound **23** (**pyridostatin**) for HT-1080 cells in Figure 3.5.

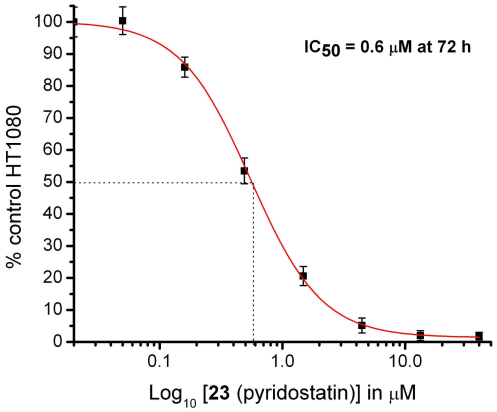

Figure 3.5: GI_{50} results for HT-1080 cells treated with different doses of **23** (**pyridostatin**).[a]

[a]Errors were calculated as the SD of triplicates of the experiment.

The GI_{50} values against the four cell lines of compounds **18-46** are tabulated in Table 3.2, which shows the selectivity ratios of the cancer cell lines against the normal cell line. Molecules **18-29** and **31-38** cause growth inhibition at high nanomolar to low micromolar concentrations against this panel of cell lines. Notably, compounds **27-46** which contain a triazole at position R^1, generally exhibit higher GI_{50} values by a factor of 10 or more compared to analogues **18-29** and **31-37**. Ligand **30**, as the only molecule without amine functionalities at either R^1 or R^2, did not show any significant growth inhibition at the concentrations used. Compound **25**, which carries a 2-aminoethoxy side chain at position R^1 and a 2-pyrrolidineoethoxy substituent at R^2, causes the lowest GI_{50} for all the cell lines ranging from 0.2 to 0.5 µM (Figure 3.6).

Many of the *N,N′-bis*(quinolinyl)pyridine-2,6 dicarboxamides cause growth inhibition at lower concentrations for the cancer cell lines investigated than the normal cell line WI-38. Strikingly, **23** (**pyridostatin**) shows a 18.5-fold selectivity for HT-1080 cells over WI-38 cells. The most selective compounds for

HeLa (5.2-fold) and U2OS (6.0-fold) over WI-38 cells are **38** and **33**, respectively (Figure 3.6).

	GI_{50} (μM)				
					Selectivity ratio
Compound	**HeLa**	**HT-1080**	**U2OS**	**WI-38**	**HeLa/HT-1080/U2OS/WI-38**
18	1.2±0.3[1]	0.3±0.1	0.7±0.2	1.1±0.3	0.9/3.4/1.7/1.0
19	1.4±0.4	1.1±0.2	1.5±0.3	1.6±0.2	1.1/1.5/1.1/1.0
20	3.0±0.2	0.6±0.1	0.8±0.3	3.1±0.6	1.0/5.5/4.0/1.0
21	2.2±0.3	3.3±0.3	2.3±0.5	2.1±0.4	1.0/0.6/0.9/1.0
22	3.0±0.3	2.6±0.3	2.1±0.3	2.1±0.5	0.7/0.8/1.0/1.0
23	2.5±0.5	0.6±0.1	16.8±1.0	11.1±1.6	4.4/18.5/0.7/1.0
24	13.7±1.0	6.8±0.3	14.1±1.3	10.6±1.6	0.8/1.6/0.8/1.0
25	0.3±0.1	0.2±0.0	0.2±0.1	0.5±0.1	1.4/2.6/2.6/1.0
26	2.3±0.2	2.2±0.2	2.1±0.3	2.1±0.2	0.9/1.0/1.0/1.0
27	5.2±0.4	4.7±0.5	4.9±0.7	4.0±0.5	0.8/0.9/0.8/1.0
28	3.6±0.3	2.6±0.2	2.3±0.2	3.5±0.4	1.0/1.3/1.5/1.0
29	3.9±0.2	1.5±0.2	1.6±0.3	3.9±0.4	1.0/2.6/2.4/1.0
30	>40.0	>40.0	>40.0	>40.0	n.d.[2]
31	1.5±0.2	1.8±0.2	0.8±0.1	1.6±0.2	1.1/0.9/2.0/1.0
32	0.7±0.1	0.6±0.1	0.3±0.1	0.6±0.1	0.9/1.0/2.0/1.0
33	4.7±0.4	3.4±0.2	2.3±0.3	13.7±1.9	2.9/4.0/6.0/1.0
34	3.2±0.2	2.2±0.1	2.2±0.5	4.0±0.4	1.3/1.8/1.8/1.0
35	1.6±0.2	1.8±0.2	1.8±0.5	3.6±0.7	2.3/2.0/2.0/1.0
36	9.6±0.8	1.6±0.2	5.6±0.8	4.9±1.2	0.5/3.1/0.9/1.0
37	13.0±1.1	8.5±0.3	5.8±0.7	11.4±2.4	0.9/1.3/2.0/1.0
38	7.7±0.7	13.5±1.5	>40.0	39.7±3.7	5.2/3.0/n.d./1.0
39	>40.0	35.2±3.3	>40.0	>40.0	n.d.
40	>40.0	>40.0	>40.0	>40.0	n.d.
41	>40.0	>40.0	>40.0	>40.0	n.d.
42	>40.0	>40.0	>40.0	>40.0	n.d.
43	>40.0	23.5±2.3	24.3±4.3	19.2±2.6	n.d./0.8/0.8//1.0
44	38.2±3.5	23.5±2.7	16.8±2.3	29.7±3.3	0.8/1.3/1.8/1.0
45	>40.0	>40.0	>40.0	>40.0	n.d.
46	38.2±2.1	20.9±1.5	>40.0	>40.0	n.d.

Table 3.2: GI_{50} in μM after 72 h incubation of the stated cell lines with compounds **18-46**. Selectivity given as $GI_{50.WI\text{-}38}/GI_{50.cancer\ cell\ line}$.

[1]Errors were calculated as SD of three independent experiments.

[2]Value was not determined as the maximum compound concentration used was 40 μM.

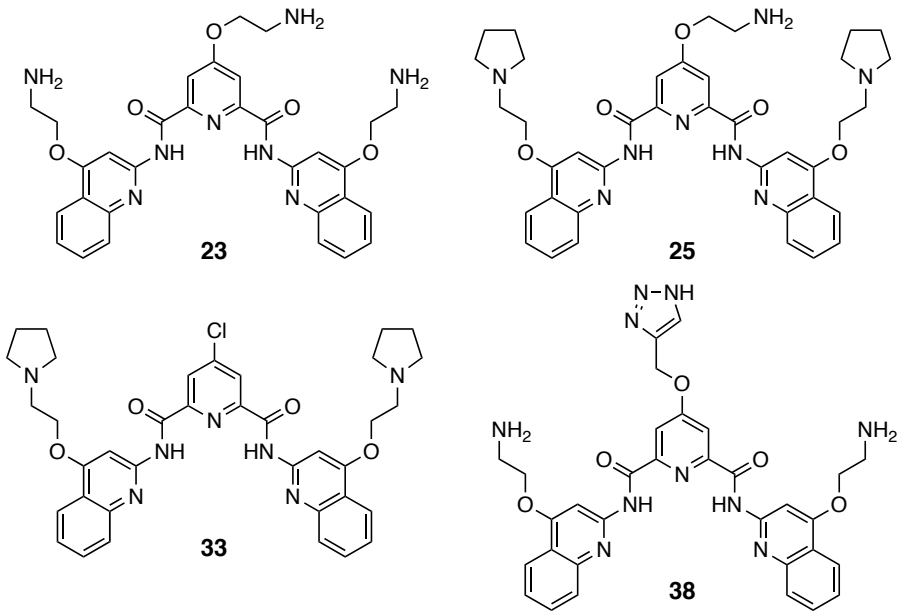

Figure 3.6: Molecular structures of **23** (**pyridostatin**), **25**, **33** and **38**. **23** is most selective for HT-1080 cells, **25** gives the lowest GI_{50} for all the cell lines, **33** is most selective for U2OS cells and **38** is most selective for HeLa cells.

Compound **9** has a hydrogen and **22** a chlorine at position R^1 and both molecules have a pyrrolidine-containing side chain at position R^2. They are more selective towards the cancer cell lines than other analogues that carry a hydrogen or chlorine at position R^1. This suggests that the nature of the substitution at R^2 has a considerable effect on growth inhibitory properties. The varying growth inhibition of different cell lines may be exploited to develop molecules selective for a particular cancer. Upon incubation of cells with the compounds at their GI_{50} values, an elevated level of cell death compared to the untreated control was not observed (assessed by a Trypan blue nuclear exclusion assay), suggesting that the compounds may cause growth inhibition but are not generally toxic at these concentrations. Factors such as differential cellular uptake, metabolism and off-target effects (*i.e.*, targets other than G-quadruplexes) may contribute to the GI_{50} values measured. Therefore, I did not try to correlate G-quadruplex stabilisation to the GI_{50} values.

3.6 Long-term growth inhibition

The following studies were performed on HT-1080 cells, the same cell line that had been used to study the effects on telomeres and shelterin by **pyridostatin** as described earlier.[144] I investigated the long-term growth effects on HT-1080 cells of the following molecules: **18-20**, **22**, **23**, **25**, **26**, **31-33**, **35-38** and **44**. The cells were incubated for up to 30 days with the compounds at their respective GI_{50}. Cells were counted every third or fourth day and replated at the initial density. Population doublings (PD) were calculated using the following formula (3.1):

$$PD = \frac{ln(n_1/n_2)}{ln2} \tag{3.1}$$

n_1 = initial number of cells, n_2 = final number of cells.

As discussed in section 3.5, an increase in cell death was not observed at these concentrations for any of the compounds, suggesting that these concentrations are *subcytotoxic*. These concentrations were used to facilitate a comparison of the long-term growth effects between different *N,N′-bis*(quinolinyl)pyridine-2,6 dicarboxamides. The PDs were plotted against days of treatment for the different compounds and the graph is illustrated in Figure 3.7. Some of the molecules caused a strong reduction of PD, indicating a long-term growth arrest of HT-1080 cells, notably **23**, **31** and **33** after 6 days, **25** after 12 days, **26** and **37** after 18 days and **36** and **44** after 24 days of exposure. Compounds **31** and **33** both have a chlorine substitution at position R^1 and **23**, **25** and **26** have an amine side chain at that position. Compound **44** has a glucosyl side chain at R^1. Compounds which have a hydrogen at this position (**18**, **19**, **20** and **22**) did not show a decrease in PD over the time period measured. The two compounds which have a 4-fluorobenzyloxy-substitution at position R^1 (**36** and **37**) also caused long-term growth arrest. The latter two compounds do not exhibit a high stabilisation of the telomeric G-quadruplex by FRET-melting (ΔT_m of 8.8 and 4.3 K at 1 μM, respectively), whereas **23**, **25**, **26**, **31**, **33** and **44** showed high shifts in melting temperature (all around 35.0 K at 1 μM) as discussed in section 3.4. This implies that an interaction of the molecules with the telomeric

G-quadruplex may not be the main contributor or sole cause of the long-term growth inhibitory effects observed.

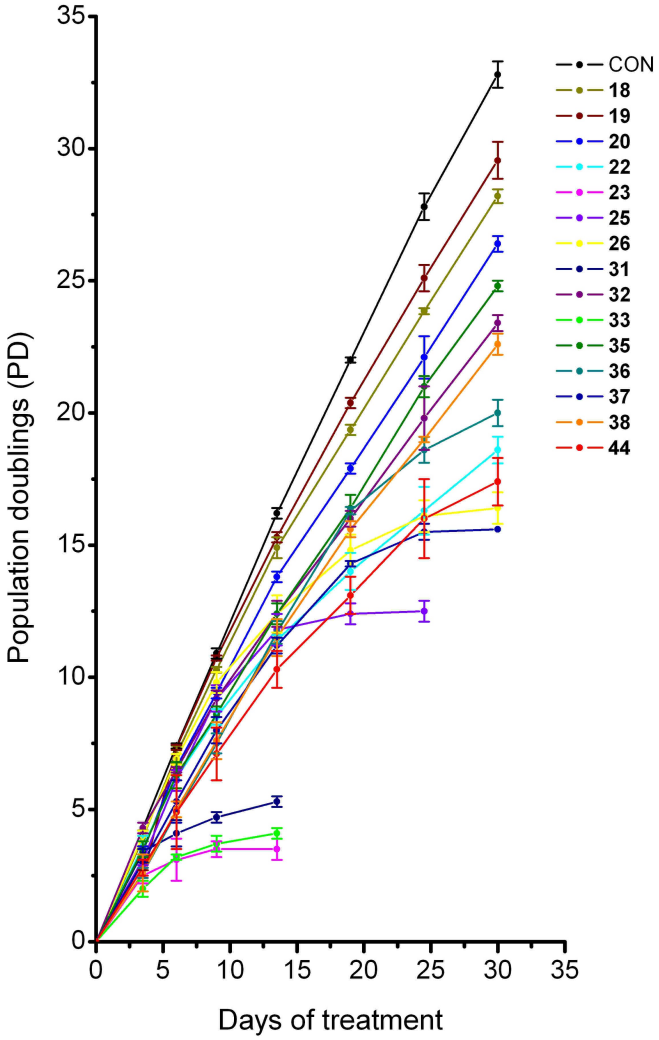

Figure 3.7: Long term growth studies of compounds **18-20**, **22**, **23**, **25**, **26**, **31-33**, **35-38** and **44** on HT-1080 cells. CON donates control cells which were not treated with compound. Measurements were taken at the respective GI_{50} values of the compounds. The errors are the SD of three independent experiments.

3.7 Telomere shortening

It was previously demonstrated that compound **23** (**pyridostatin**) disrupts shelterin by uncapping POT1.[144] The effect of **23** on telomere length was not assessed in that initial study. In order to assess the effect of the *N*,*N*′-*bis*(quinolinyl)-pyridine-2,6 dicarboxamides on telomere length, it was chosen to perform a non-denaturing hybridisation assay[42] to detect the telomeric 3′-G-overhang of HT-1080 cells treated with a selection of the compounds (see Figure 3.8).

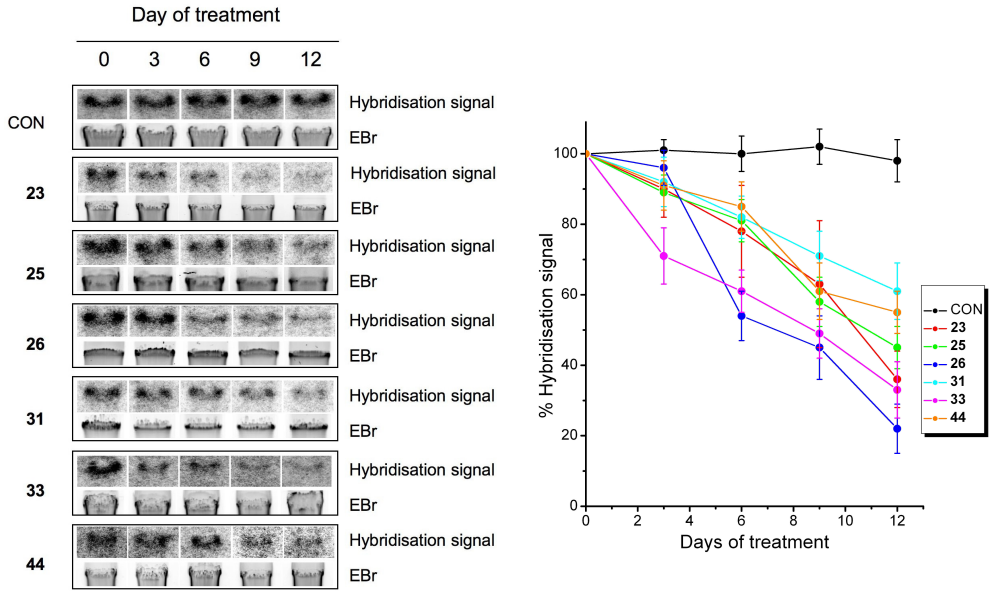

Figure 3.8: Telomere shortening assessed for **23**, **25**, **26**, **31**, **33** and **44** for HT-1080 cells by a non-denaturing hybridisation assay. CON represents DNA from cells grown in the absence of compound. **Left:** Hybridisation gel radiograph and EBr fluorescent picture. **Right:** graph showing the %hybridisation signal against days of treatment. The radiograph signal was normalised against the fluorescence signal. The errors are the SD of three different experiments.

The HT-1080 cell line is telomerase-positive and thus maintains the same telomere length in culture. This assay was performed using a selection of six compounds (**23**, **25**, **26**, **31**, **33** and **44**). which have shown supportive biophysical data for telomeric G-quadruplex interaction, short-term growth arrest at high nanomolar to low micromolar concentrations and long-term growth inhibitory effects for HT-1080 cells. The DNA of cells incubated with the respective com-

pounds at their GI_{50} was extracted after 3 days, 6 days, 9 days and 12 days of exposure. Cells were split and replated at their initial density with the GI_{50} of the respective compound at each time point to avoid increased cell stress due to confluency. The DNA was hybridised for 16 h with a [γ-^{32}P] ATP-labelled oligonucleotide of the sequence (5′-$(CCCTAA)_3CCC$-3′), which is complementary to the 3′-G-overhang. The hybridised DNA was run on an agarose gel which was subsequently stained with EBr and the resulting radiograph was compared to the fluorescence intensity. The assay was also performed on a control cell sample which was treated under the same conditions but in the absence of compound. The radiographs and fluorescent images are displayed in Figure 3.8. This figure also shows a graph of the relative %hybridisation signals normalised against the EBr signal of each sample as an average of three independent experiments. It was found that the five compounds investigated caused a significant decrease in the hybridisation signal whereas the control was unaffected. This is further *in cellulo* proof that members of the *N,N′-bis*(quinolinyl)pyridine-2,6 dicarboxamide family can target the telomeres.

3.8 Cellular senescence of HT-1080 cells

Small molecules interacting with telomeric G-quadruplexes can cause shelterin disruption and telomere shortening.[44,57,72,82,138] As a consequence, certain cells can undergo replicative cellular senescence.[72] It has been postulated that there seems to be a minimal or critical mean telomere length necessary to maintain cell division in cells.[72] It is also established that HT-1080 cells undergo senescence as a consequence of POT1 knockdown.[191] This suggests, that a compound causing POT1 uncapping from the telomeres would also cause a senescent phenotype in this cell line. It was examined if compounds **23**, **25**, **26**, **31**, **33** and **44**, each of which caused 3′-G-overhang shortening, induce replicative cellular senescence in HT-1080 cells. Senescent cells usually exhibit an enlarged cell-size and exhibit a pH-dependent β-galactosidase activity which can be detected histochemically at pH 6.[192] This enzyme catalyses the cleavage of 5-bromo-4-chloro-3-indolyl-β-D-galactopyranoside (**X-Gal**) to yield galactose and 5-bromo-4-chloro-3-hydroxyindole; the latter oxidises to the blue dye 5,5′-dibromo-4,4′-dichloro-indigo which can be observed visually. The reaction scheme for this

reaction is displayed in Figure 3.9.

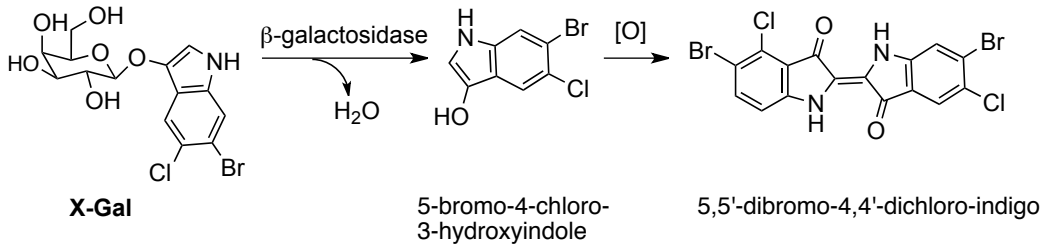

Figure 3.9: Reaction scheme of β-galactosidase catalysed hydrolysis of **X-gal**.

A senescence β-galactosidase staining assay was performed on cells treated with the aforementioned compounds to assess replicative cellular senescence. HT-1080 cells were incubated with the respective compounds at their GI_{50} for 4 days, split and replated at the initial density and compound concentration for another 4 days.

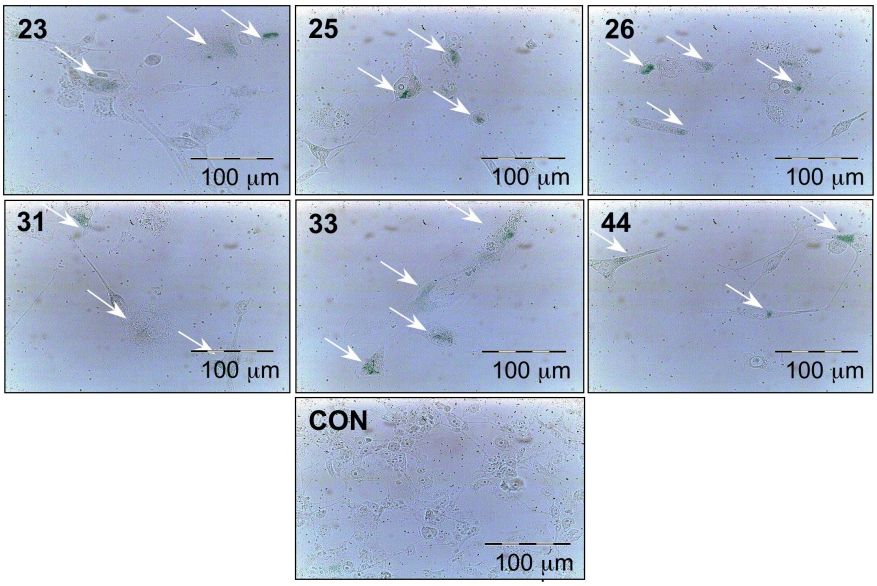

Figure 3.10: Cell pictures showing HT-1080 cells incubated with **23**, **25**, **26**, **31**, **33** and **44** for 8 d. CON donates cells grown in the absence of compound. Arrows indicate blue staining due to 5,5′-dibromo-4,4′-dichloro-indigo indicating β-galactosidase activity characteristic of senescent cells.

Morphological examination of the cells after treatment of compound for 8 days showed an increased proportion of flat giant cells with an over-expression of β-galactosidase activity, which is characteristic of replicative cellular senescence in cultured cells.[193] Figure 3.10 illustrates blue staining of cells treated with compounds **23**, **25**, **26**, **31**, **33** and **44** and the absence of blue colouring in the control cells which were not treated with compound. Also, there is an obvious increase of the cell size, which has been attributed to be a characteristic of senescent cells.[72,193] This data qualitatively shows that compounds **23**, **25**, **26**, **31**, **33** and **44** induce replicative cellular senescence in HT-1080 cells which is likely to be linked to shelterin disruption and consequently the shortening of the telomeres.

3.9 Drug development

Some of the compounds were sent to the **N**ational **C**ancer **I**nstitute of the United States (NCI) and Cancer Research Technology® Ltd. to perform cell-growth and ADME studies, respectively. The data obtained so far are presented in this section. I did not not perform the experiments and the data can be found in the appendix of this thesis.

3.9.1 NCI cell line screen

Six of the synthesised *N*,*N*′-*bis*(quinolinyl)pyridine-2,6 dicarboxamides (**20**, **22**, **23** (**pyridostatin**), **25**, **26** and **31**) were sent to the NCI for a developmental therapeutics program.[194] Other structures were not submitted, as these were the only compounds synthesised at the time. This screen implemented by the NCI is designed to identify compounds with promising growth inhibition of cancer cells and also to assess their general toxicity. Compounds that are promising in these screens are then taken forward for therapeutic development. These compounds were tested for growth inhibition in a single dose assay (10 μM) against a panel of 60 cancer cell lines. Four of the compounds (**20**, **25**, **26** and **31** which are depicted in Figure 3.11) gave sufficient growth arrest to be selected for the second round of testing, *i.e.*, a five-point dosing assay. GI_{50} values were taken after 48 h incubation of the cells with the compounds.

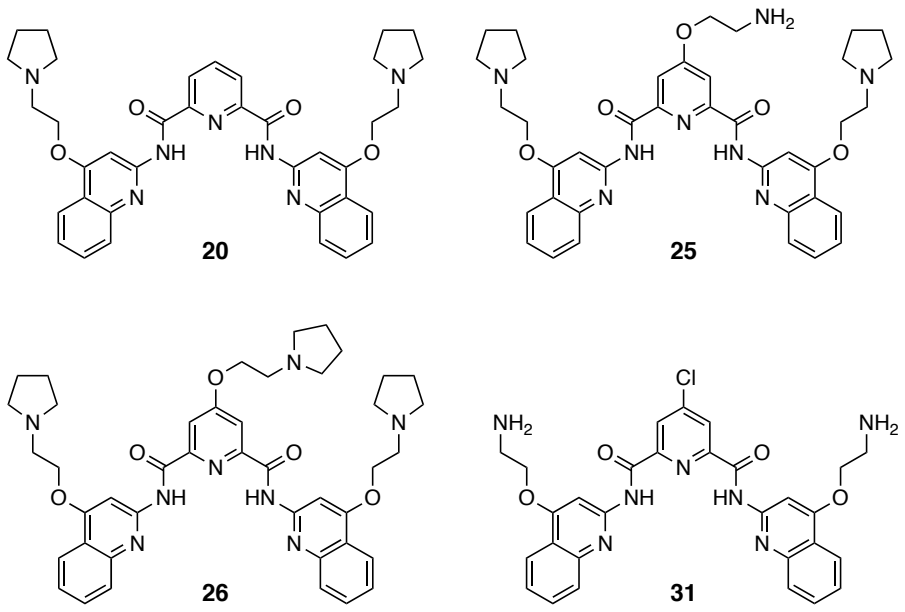

Figure 3.11: Molecular structures of **20**, **25**, **26** and **31** which were selected by the NCI for further testing.

The summarised data can be found in Appendix B. Generally, these four compounds gave high nanomolar to low micromolar GI_{50} values for the cancer cell lines investigated. Strikingly, the GI_{50} was in most cases two magnitudes lower than the LC_{50} (lethal concentration 50, *i.e.*, concentration of drug resulting in a 50% reduction in the measured protein at the end of the drug treatment as compared to that at the beginning), which confirmed the earlier observations of no elevated cell death at the growth inhibitory concentrations as compared to the control. For example, the LC_{50} values induced by **25** for the leukemia cell lines tested were greater than 1.00×10^4 μM, whereas the GI_{50} values were 2.26-3.08 $\times 10^6$ μM. The data imply that the compounds target certain cellular pathways. I propose that these compounds mainly act in a *cytostatic* and not *cytotoxic* manner. This is a very good starting point for potential drug development, but, perhaps more importantly, for the creation of chemical tools to dissect and study the biochemical pathways involving G-quadruplexes. The NCI is currently deciding whether to take the compounds forward for further evaluation, which would involve a hollow fibre cancer model in mice.[194]

3.9.2 ADME studies

Compounds **20**, **21**, **22** and **23** (Figure 3.12) were sent to Cancer Research Technology® Ltd. for ADME studies which assessed pharmacokinetic parameters (as the abbreviation defines: **a**bsorption, **d**istribution, **m**etabolism and **e**xcretion). The four compounds were selected from the compounds of the family which had been synthesised at the time based on the following selection criteria: 1) quantity available and 2) structural diversity in side chains and absence and presence of the substitution on the pyridine ring.

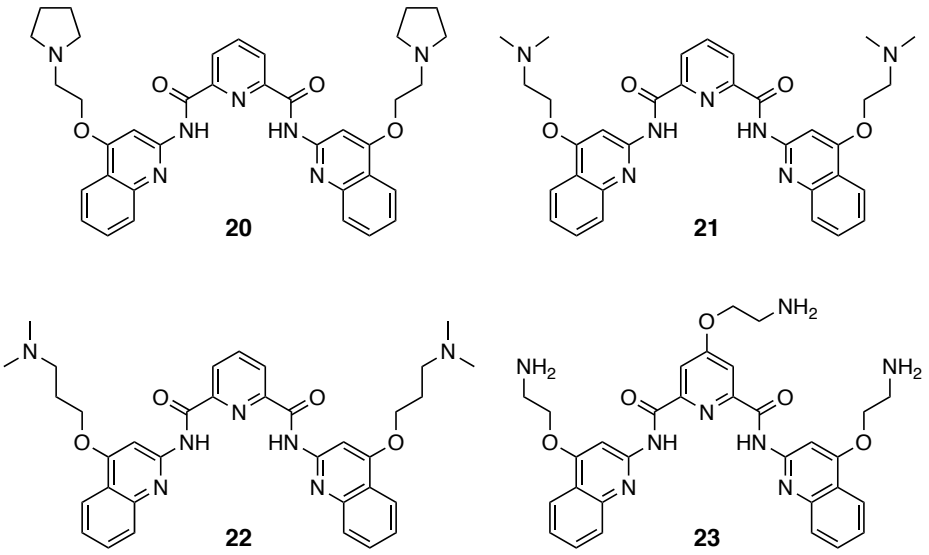

Figure 3.12: Molecular structure of compounds **20**, **21**, **22** and **23** for which ADME studies were performed.

Drug levels and kinetics of exposure upon drug administration are crucial parameters to assess potential drug candidates. The studies presented herein address some of those parameters. An indication of the performance and potential pharmacological activity of the compounds is given and the summarised data can be found in Appendix C. There are certain thresholds for each criterion that should be fulfilled by a potential drug candidate. These are stated in Table C.1. Only compounds **20** and **22** show sufficient solubility (according to the ADME guidelines). The cell permeability is slightly too low for all the compounds investigated but the efflux ratio is sufficient for all the compounds, except for **22**.

None of the compounds causes any inhibition *in vitro* of the CyP450s studied (see Appendix C, Table C.1). The cell redox systems are therefore not necessarily directly affected by the *N,N′-bis*(quinolinyl)pyridine-2,6 dicarboxamides. Plasma binding of these compounds is high for all the compounds, which may reduce their effectiveness in reaching their DNA targets they have been designed for (G-quadruplexes). All the compounds show little microsome turnover in human cells and mediocre microsome turnover in mouse cells. This suggests that the compounds are not predicted to be highly metabolised *in vivo* but may effectively reach their nucleic acid target without being degraded. The compounds exhibit minimal hERG binding. This protein is part of the ion channels which control K^+ ion efflux. Inhibition of these channels can lead to cardiac and muscle dysfunctions with concomitant risk of sudden death.[195] Compounds **20**, **21**, **22** and **23** show considerable muscarinic receptor binding inhibition. Inhibition of these G protein-coupled acetylcholine receptors renders the compounds potential neurotoxins. All four compounds possess amine side chains which may bind to the receptors similarly to the potent inhibitor muscarine (Figure 3.13).

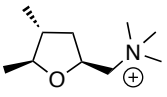

Figure 3.13: Molecular structure of muscarine.

Muscarinic receptor-binding could potentially be circumvented by changing primary or tertiary amines to more sterically hindered amines, or cyclic secondary amines. This may not significantly reduce G-quadruplex interaction as I believe the interaction of the amine side chains is mainly by electrostatic or hydrogen-bond interactions.

3.10 Conclusions, future work and outlook

A small family of *N,N′bis*(quinolinyl)pyridine-2,6 dicarboxamides was synthesised based on the scaffold of **pyridostatin**,[144] a small molecule that had been shown by our group to interact with G-quadruplexes and cause a shelterin disruption followed by a γH2AX response in human HT-1080 cancer cells. A high-yielding and

efficient synthetic route involving 2-7 steps was employed to obtain these molecules. The compounds were evaluated for their potential to stabilise G-quadruplex structures *in vitro* and their effects on cell growth were investigated. Strikingly, elevated levels of cell death were not observed at their GI_{50} concentrations even at long-term exposure of the compounds. It was demonstrated that it is possible to fine-tune the cellular effects of these compounds by changing the side chains on the scaffold. A selection of the compounds was shown to induce long-term growth arrest which was linked to their interaction with telomeric G-quadruplexes leading to G-overhang shortening and replicative cellular senescence. Some of the compounds were sent to the NCI and some of these have been selected for further evaluation in their implemented anti-cancer screening assays. The data suggest that the compounds have cytostatic growth inhibitory properties. The initial ADME studies have shown that the compounds fulfill some but not all the criteria usually desired for a drug. However, simple changes on the ligand such as side chain nature and position and introduction of asymmetry could be applied to develop the pharmacokinetic properties of the molecule. The data obtained suggests that *N,N′-bis*(quinolinyl)pyridine-2,6 dicarboxamides are potential drug candidates.

The data demonstrate that molecules of this type have promising anti-cancer properties which we propose to be linked to their interaction with G-quadruplexes. This makes them very good tools to further study the underlying biology involving these nucleic acid targets in cells. The results indicate that the compounds act mainly in a *cytostatic* and not *cytotoxic* manner and it would be of immediate interest to investigate their cytostatic effects using FACS and cell-cycle markers. Furthermore, **pyridostatin**[144] triggered a DDR at telomeres and other genomic regions, as assessed by immunofluorescent staining of γH2AX. We are currently investigating in our laboratory the exact mechanisms of DNA damage caused by compounds of this type. Interestingly, recent evidence suggests that the 5′-UTR of TRF2 mRNA has a G-quadruplex which can be targeted by small molecules to down-regulate translational activity.[141] *N,N′-Bis*(quinolinyl)pyridine-2,6 dicarboxamides including **pyridostatin** have been shown to target RNA G-quadruplexes in the 5′-UTR of another gene,[36] which makes it likely that these compounds also affect translational levels of TRF2. This would have a profound effect on shelterin.

The next chapter describes a small molecule based on the *N,N′-bis*(quinolinyl)pyridine-2,6 dicarboxamide that can selectively recognise and pull down G-quadruplex DNA with the final goal to isolate from cells and directly analyse G-quadruplex forming-sequences in the human genome.

Chapter 4

Small molecule-mediated G-quadruplex isolation from human cells

4.1 Background

For the purpose of target discovery and validation, natural products and their related affinity matrices have been used for the isolation of cellular proteins.[196] The recent development of massively parallel Illumina sequencing[197] has enabled the genome-wide analysis of transcription factor binding loci using ChIP-seq,[198,199] a methodology that involves the immunoprecipitation of chromatin-transcription factor complexes followed by sequencing of the associated DNA fragments. Such an approach requires the use of an antibody against the transcription factor of interest to identify the captured nucleic acids. To the best of my knowledge, no small organic molecules have yet been reported that can be used to isolate a particular nucleic acid motif in a *structure-dependent* manner. Although the existence of G-quadruplexes *in vitro* is beyond reasonable doubt and they are believed to play a role in telomere maintenance,[28] gene expression[67,84] and replication stalling,[112] their actual formation in human cells remains elusive and unproven.

Until now, scientists have heavily relied on bioinformatic studies about G-quadruplex loci and their prevalence in the genome.[35,37] It would be advantageous to develop chemical tools which can recognise and ultimately isolate these

nucleic acid motifs. Yet, no such technology is available. A chemical probe which could perform the aforementioned task could potentially be used to perform experiments analogous to Chip-seq,[198,199] by isolating and ultimately sequencing G-quadruplex nucleic acids. This could lead to the the identification of the actual G-quadruplex forming sequences in cells and would constitute further evidence for their formation *in vivo*.

4.2 Objectives

The aim of this work was to develop, synthesise and evaluate small molecule G-quadruplex probes that can be used to isolate G-quadruplex forming nucleic acid sequences from solution. The design of the probes was based on the scaffold of the small molecules presented in Chapter 3. It was intended to synthesise a small library of G-quadruplex probes with an affinity tag and evaluate them for their potential to stabilise G-quadruplexes. These probes were intended to be used to design and optimise an *in vitro* assay for G-quadruplex isolation. The final aim was to apply such an approach to isolate these non-canonical DNA structures from human cells in order to validate this novel method. This approach could ultimately be used to isolate G-quadruplex forming nucleic acid sequences from human cells and such a methodology could potentially identify possible druggable and biologically relevant G-quadruplexes.

4.3 Small molecule probes

4.3.1 Design and synthesis

A G-quadruplex affinity probe would have to possess several structural and functional features: 1) the ability to recognise various G-quadruplex structures with a high level of specificity over ds-DNA; 2) an affinity tag to allow the pull-down of DNA fragments; 3) the capacity to release the DNA fragments intact for subsequent analysis and 4) a detectable biological activity that can be related to its interaction with G-quadruplexes. Depending on the strength of the interaction between the probe and G-quadruplex targets, reversible covalent cross-linking may also be required. When using ChIP-seq,[198,199] proteins of interest are com-

monly cross-linked with formaldehyde. A small library of probes was designed based on the *N,N′-bis*(quinolinyl)pyridine-2,6-dicarboxamide scaffold which was described in Chapter 3. As was demonstrated in section 3.4 (Chapter 3), many compounds with this scaffold show good stabilisation of various G-quadruplexes, suggesting a broad selectivity towards G-quadruplex DNA. That makes this platform an ideal candidate to base a G-quadruplex affinity probe on. As an affinity tag it was decided to introduce a biotin moiety, which allows pull-down with streptavidin matrices.[200] The small library consists of the seven molecules **47**-**53** (Figure 4.1).

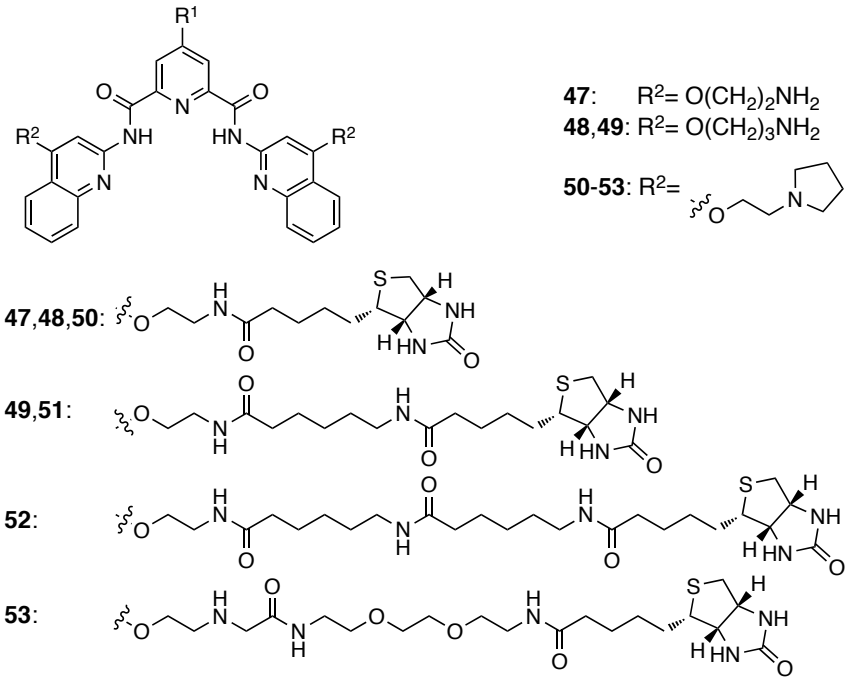

Figure 4.1: Molecular structures of biotinylated probes **47**-**53**.

The scaffold was kept unaltered and the biotin moiety was attached *via* a linker at position R^1. Attaching the tag at this position retains the symmetry of the molecule and is thus synthetically more facile than attaching it on one of the quinolines. I also attached two alternative side chains at position R^2. Primary amines would potentially allow for formaldehyde cross-linking of the probe with the exocyclic primary amines of the guanines of G-quadruplexes. However, this

procedure is novel and would require the amines of the probe and the target to be in close proximity to each other. Therefore, compounds **47** and **48** were synthesised to potentially explore that strategy. Since we did not know anything about the exact molecular spacing required between an affinity tag and a potential probe to successfully isolate the resulting complex with streptavidin, I varied the length and nature of the spacer that connects the biotin tag to the scaffold. Molecules **47-49** were synthesised as illustrated in Scheme 4.1.

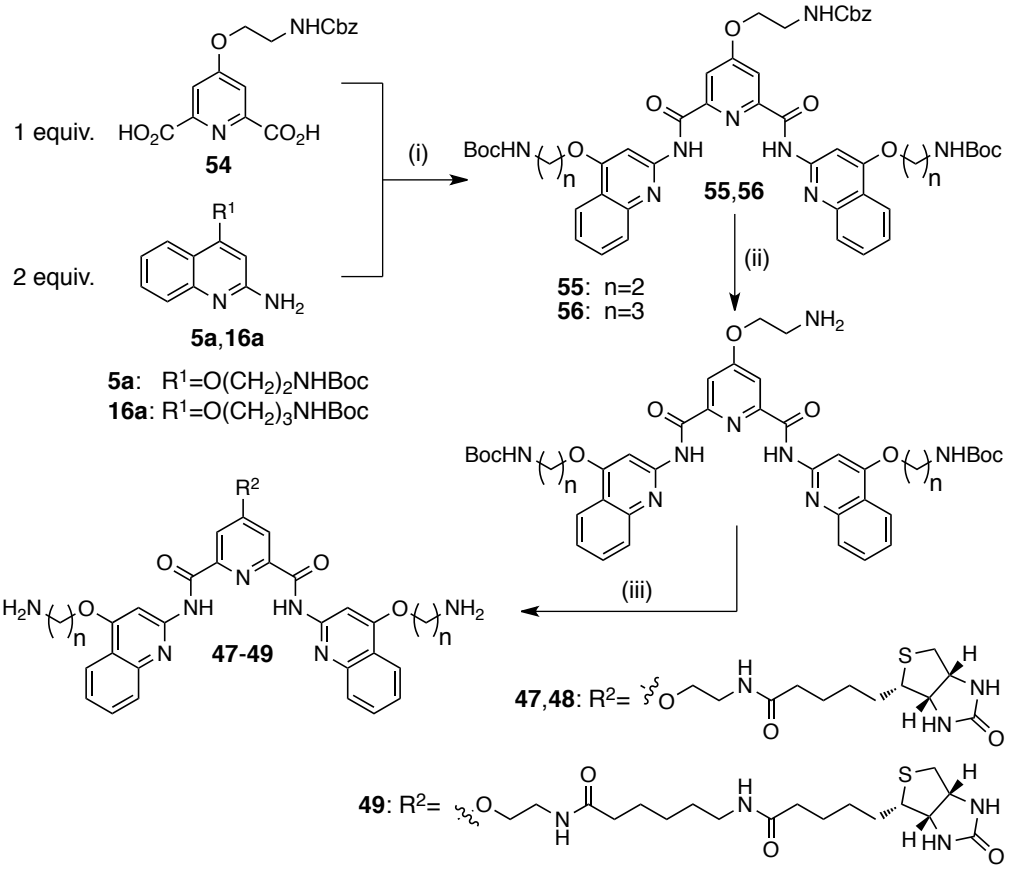

Scheme 4.1: (i) 1-chloro-*N*,*N*,-2-trimethylpropenylamine, DCM, rt, 2 h; then TEA, 0 °C, 1 h; then rt., overnight; (ii) Pd/C, H_2, λ, 1 h; for **47** and **48** (+)-biotin *N*-hydroxysuccinimide ester, TEA, DCM, rt, 2 h, for **49** (+)-biotinamidohexanoic acid *N*-hydroxysuccinimide ester, TEA, rt, 2 h; then DCM/TFA, rt, 2 h.

One equivalent of the pyridine building block **54** was reacted with two equivalents of the quinoline building block **5a** using 1-chloro-*N*,*N*,-2-trimethylpropenyl-

amine and TEA, analogous to the procedure described in Chapter 3, section 3.3. The resulting product was purified by precipitation from hot MeCN. The Cbz-protecting group was removed by hydrogenation using H_2, Pd/C under microwave conditions. Strong reaction conditions were necessary as intermediates **55** and **56** are very insoluble in a variety of organic solvents. The subsequent reactions with the respective hydrosuccinamide biotin esters was achieved at rt using TEA to afford the final compounds in 90-93% yield. Compounds **50-53** were prepared using the procedures as displayed in Scheme 4.2.

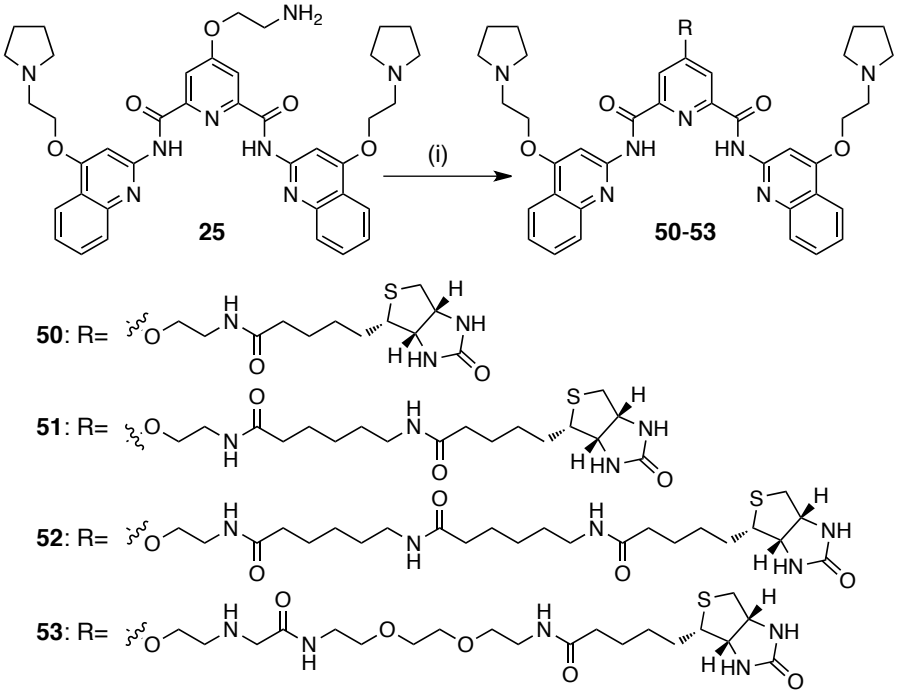

Scheme 4.2: (i) **50** (+)-biotin *N*-hydroxysuccinimide ester, TEA, DCM, rt, 2 h, or **51** (+)-biotinamidohexanoic acid *N*-hydroxysuccinimide ester, TEA, rt, 2 h, or **52** (+)-biotinamidohexanoyl-6-aminohexanoic acid N-hydroxysuccinimide ester, TEA, rt, 2 h, for **53** (+)-biotin polyetheleneoxide iodoacetamide, TEA, 100°, 2 h.

Compound **25**, a *N,N′-bis*(quinolinyl)pyridine-2,6-dicarboxamide described in Chapter 3, section 3.3, was used as starting material. This compound has two pyrrolidine side chains on the quinoline moieties and a primary amine side chain at R^1. Coupling with the respective hydrosuccinamide biotin esters was achieved

using TEA at rt in 90-99% yield. The reaction with (+)-biotin polyetheleneoxide iodoacetamide to afford compound **53** required a large excess of TEA, *i.e.*, very basic conditions, and heating to 100 °C. A much lower yield of 47% was reported for this reaction.

4.3.2 Biophysical evaluation

The biotinylated molecules **47-53** were evaluated for their potential to stabilise the G-quadruplexes H-telo, C-kit1, C-kit2 and C-myc and double-stranded DNA using a FRET-melting assay (The sequences can be found in Chapter 5). The ΔT_m values at 1 μM ligand are displayed in Table 4.1.

	ΔT_m (K)				
Compound	**H-telo**	**C-kit1**	**C-kit2**	**C-myc**	**ds-DNA**
47	34.8±0.5[1]	39.1±0.7	14.7±0.7	16.9±0.7	2.0±0.3
48	30.5±0.6	38.6±0.5	9.7±0.5	13.2±0.5	1.0±0.2
49	21.5±0.7	13.1±0.5	19.5±0.6	7.3±0.4	1.5±0.2
50	27.0±0.9	23.5±0.9	8.7±0.8	9.9±0.7	0.0±0.0
51	20.0±0.5	19.0±0.7	7.1±0.9	8.8±0.6	0.0±0.0
52	15.0±0.7	20.5±0.5	5.4±0.3	9.1±0.5	0.0±0.1
53	30.1±0.6	12.6±1.0	15.6±0.6	8.1±0.4	0.3±0.0

Table 4.1: ΔT_m at 1 μM ligand in K measured by FRET-melting against H-telo, C-kit1, C-kit2, C-myc and ds-DNA for **47-53**.

The data demonstrates that compounds **47-53** stabilise all the G-quadruplex targets evaluated. Molecule **47** shows very high stabilisation temperatures for the quadruplex targets and causes the highest stabilisation for H-telo, C-kit1 and C-myc out of the series of ligands. Compounds **49** and **53** have higher ΔT_m values for C-kit2. It is striking that the compounds with the pyrrolidine side chains do not exhibit any stabilisation of ds-DNA whereas some stabilisation of double-stranded DNA was detected for **47-49**, which have a primary amine at this position. This might be due to additional hydrogen bonding interactions with the free lone pairs of the DNA bases. According to this data, compound **47**, with its very high stabilisation potentials for the various G-quadruplex targets,

[1]Errors were calculated as SD of three independent experiments.

could be the best candidate for the G-quadruplex isolation studies. However, since this compound shows some stabilisation for ds-DNA, compounds **50-53** are more selective and hence might be more suitable.

4.3.3 Short-term growth inhibition

The biotinylated compounds were evaluated for their potential to inhibit the growth of four different cell lines, analogous to the study on the other *N,N′-bis*(quinolinyl)pyridine-2,6-dicarboxamides presented in Chapter 3, section 3.5. The data are summarised in Table 4.2.

	GI_{50} (μM)			
Compound	**HeLa**	**HT-1080**	**U2OS**	**WI-38**
47	18.0±1.3[1]	16.4±1.7	>40.0	32.1±2.3
48	>40.0	21.6±2.0	>40.0	>40.0
49	25.7±3.7	30.2±2.3	>40.0	16.2±1.8
50	25.4±2.3	8.4±1.5	29.8±2.0	27.4±3.0
51	25.3±1.9	22.6±2.3	34.2±2.9	22.0±1.9
52	>40.0	38.8±3.7	>40.0	>40.0
53	7.9±1.2	13.4±1.2	8.8±0.9	10.6±1.1

Table 4.2: GI_{50} in μM after 72 h incubation of the stated cell-lines with compounds **47-53**.

The GI_{50} values for the biotinylated compounds were observed to be on average about one order of magnitude higher than of most of the *N,N′-bis*(quinolinyl)-pyridine-2,6-dicarboxamides presented earlier but similar to those induced by the derivatives with a triazole attached to the side chain of the pyridine ring (see Table 3.2). The higher GI_{50} values could be attributed to differential uptake into the cells, lower solubility or different metabolism of the compounds in the cells. Compounds **47-49** and **52** showed values higher than 40.0 μM for one or more cell-lines. Ligand **53** showed low micromolar GI_{50} values and is the most potent of the seven candidates, suggesting it to be the most suitable compound for further studies, providing the biological mechanism of action is analogous to that of the non-biotinylated molecules.

[1]Errors were calculated as SD of three independent experiments.

4.3.4 G-quadruplex isolation

A pull-down assay was developed to isolate G-quadruplex DNA from solution using the biotinylated molecules developed and magnetic beads coated with streptavidin. The assay consists of the following steps:

(1) Using the biotinylated probe to incubate a solution containing nucleic acids folded into G-quadruplexes and non-G-quadruplex nucleic acids.
(2) Incubation of that solution with streptavidin-coated magnetic beads.
(3) Isolation of the G-quadruplex bound biotinylated probe by magnetic separation.
(4) Recovery of the G-quadruplex nucleic acids from the beads in a new buffer-containing solution.

A picture of that assay is depicted in Figure 4.2.

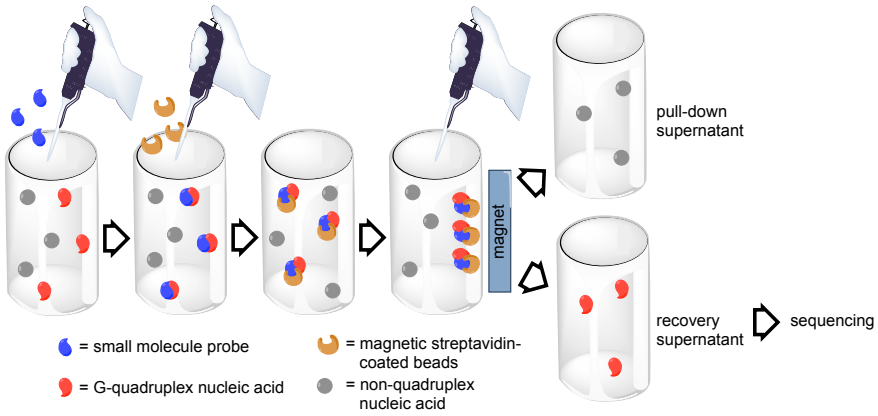

Figure 4.2: Schematic drawing of G-quadruplex isolation with a small molecule.

Firstly, it was investigated whether the compounds can selectively isolate G-quadruplex DNA from solution. Three G-quadruplex targets, C-kit1, C-kit2 and C-myc (these G-quadruplexes were discussed in the previous chapters and the sequences can be found in Table 4.4), and one ds-DNA control of the sequence 5′-CAA TCG GAT CGA ATT CGA TCC GAT TG-3′ were chosen for this investigation. Annealed DNA samples were incubated with various concentrations of compounds **47**-**53**. This resulting solution was then incubated with streptavidin-

coated magnetic beads and subsequently the supernatant isolated after incubation for 15 min. The resulting solution was analysed by UV and the absorbance values at 260 nm were recorded. A starting concentration of 2 μM DNA was used for each experiment and the concentrations of oligonucleotide of the supernatants after pull-down were determined using the Beer-Lambert law (equation 4.1).

$$A = l \times \epsilon \times c \tag{4.1}$$

A = absorbance; l = pathlength in cm; ϵ = molar extinction coefficient in M^{-1} cm^{-1}, c = concentration in M.

The G-quadruplex DNA concentration of the solutions decreased using increasing amounts of biotinylated probe. On the contrary, the concentration of ds-DNA was unaltered. By plotting 1/[ligand] against [DNA] (that remained in solution), it was established that the relationship was inversely proportional for the concentration range used, as a straight line could be fitted on the graph. The gradient of those graphs gives values of nM DNA/μM compound. The values for each target corresponding to the different compounds were compared in order to establish if there was a difference in pull-down between molecules **47**-**53**. These values were termed *pull-down constants* and all the values obtained are tabulated in Table 4.3. Figure 4.3 portrays the graph obtained for molecule **53** as an example.

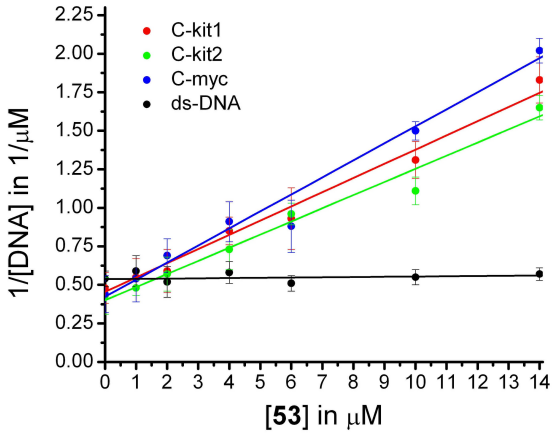

Figure 4.3: Plot of 1/[DNA] against [**53**] for C-kit1, C-kit2, C-myc and ds-DNA. The gradients of the graphs donate the *pull-down constants*.

The *pull-down constants* displayed in Table 4.3 suggest that molecules **49** and **53** can mediate G-quadruplex isolation most efficiently from solution. It is striking that all the compounds very selectively facilitate G-quadruplex DNA pull-down with *constants* ranging from 22.8±0.7 to 110.9±5.5 $n\mathrm{M}_{\mathrm{compound}}/\mu\mathrm{M}_{\mathrm{DNA}}$ and that they do not mediate the isolation of ds-DNA. However, the compounds with the primary amine side chains (**47-49**) also pull down a small amount of ds-DNA (between 0.4 and 1.0 $n\mathrm{M}_{\mathrm{compound}}/\mu\mathrm{M}_{\mathrm{DNA}}$). These accumulated data suggest that molecule **53** is the most suitable probe for this *in vitro* pull-down study out of the series synthesised.

Compound	C-kit1	C-kit2	C-myc	ds-DNA
47	43.9±1.8[1]	26.1±0.8	28.5±0.9	0.4±0.0
48	31.1±0.9	22.8±0.7	33.8±0.9	0.6±0.5
49	110.9±5.5	61.6±3.1	129.6±7.8	1.0±0.2
50	41.1±2.5	9.9±0.4	26.8±0.8	0.0±0.0
51	42.6±2.6	24.1±1.4	25.2±0.8	0.0±0.0
52	21.7±1.1	39.4±1.2	41.1±1.6	0.1±0.0
53	88.6±4.4	72.5±2.2	109.9±3.3	0.0±0.0

Table 4.3: Pull-down constants in $n\mathrm{M}_{\mathrm{compound}}/\mu\mathrm{M}_{\mathrm{DNA}}$ for **47-53** for C-kit1, C-kit2, C-myc and ds-DNA.

4.3.5 Selection of a competent probe

A small library of seven biotinylated small molecules based on the *N,N′-bis*(quinolinyl)pyridine-2,6-dicarboxamide scaffold has been synthesised. The compounds very selectively stabilise G-quadruplex DNA as shown by FRET-melting experiments. These compounds also induced short-term growth inhibition of four cell lines and can be used to isolate small synthetic G-quadruplex oligonucleotides from solution. The FRET-melting data suggest that **50-53** are most selective for G-quadruplex DNA over ds-DNA. It was also found that only compounds **47**, **48** and **53** were very soluble in water. From the short-term growth assays it was concluded that **53** is the most suitable probe for cellular investigations. The preliminary pull-down studies presented in section 4.3.4 suggested that **49** and

[1]Errors were calculated as SD of three independent experiments.

53 are the most efficient molecules for G-quadruplex isolation. Based on these results, **53** (Figure 4.4) was chosen as a small molecule probe to further investigate its aptitude to mediate G-quadruplex DNA pull-down on more complex systems *in vitro* and also on human genomic DNA isolated from cells, which will be presented hereafter.

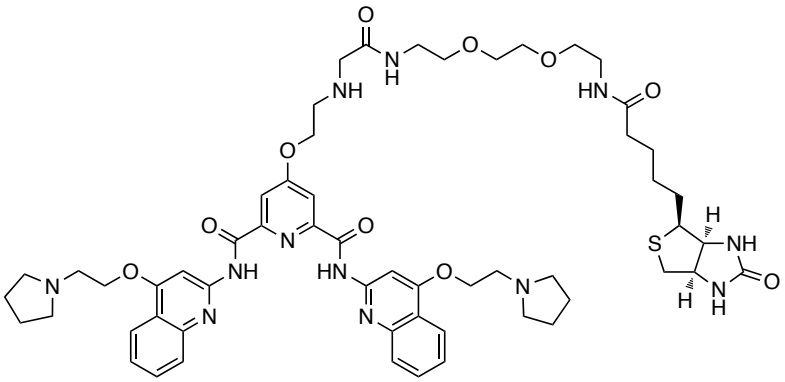

Figure 4.4: Molecular structure of **53**, the molecule chosen to perform more detailed pull-down studies.

The G-quadruplex forming sequences presented in this chapter have all been established in the literature to form G-quadruplexes under the experimental conditions used, and thus constitute good systems to study the *structure-dependency* of the pull-down experiments.

4.4 G-quadruplex isolation and recovery

Further studies on the pull-down properties of **53** were performed on a variety of G-quadruplex and ds-DNA targets. Magnetic streptavidin beads different to those used for the previous studies were employed. They are more costly but more efficient in isolating biotinylated molecules from solution, as their loading capacity and purity is higher. It was therefore concluded to be beneficial to switch to that system for more detailed studies. These beads produce different pull-down efficiencies compared to the beads used for the preliminary studies presented in section 4.3.4.

4.4.1 FRET-melting with ds-DNA competition

Good selectivity of **53** for G-quadruplex DNA over ds-DNA is an essential feature a G-quadruplex affinity probe has to possess. Therefore, I evaluated the G-quadruplex stabilisation properties of compound **53** in the presence of an excess of ds-DNA. A FRET-melting assay was performed for H-telo, C-kit1, C-kit2 and C-myc in the presence of 200 mole equivalents of unlabelled ds-DNA competitor oligonucleotide. The sequence (5′-CAA TCG GAT CGA ATT CGA TCC GAT TG-3′) can form a hairpin and is self-complementary, *i.e.*, two strands can hybridise to form a double helix, and therefore at least 100 mole equivalents of ds-DNA were present in these experiments. The results of these experiments are depicted in Figure 4.5.

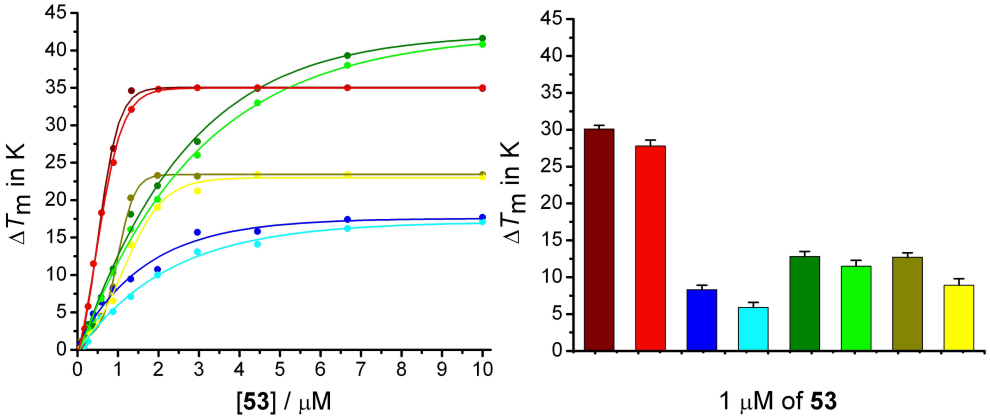

Figure 4.5: Left: Thermal shift profile induced by molecule **53** in presence and absence of ds-DNA competitor. **Right:** Bar chart of ΔT_m values at 1 μM **53**. (●) H-telo; (●) H-telo + ds-DNA; (●) C-myc; (●) C-myc + ds-DNA; (●) C-kit1; (●) C-kit1 + ds-DNA; (●) C-kit2; (●) C kit2 + ds-DNA.

The effect of the double stranded DNA on the ΔT_m induced by **53** was small, as can be seen by the thermal shift profiles illustrated in Figure 4.5. The figure also shows (on the right) that the ΔT_m at 1 μM **53** only dropped slightly, which is consistent with a good selectivity of the compound for G-quadruplex over ds-DNA. The results imply that this biotinylated probe can very selectively recognise and stabilise G-quadruplex DNA in the presence of a large excess of ds-DNA.

4.4.2 Short sequence isolation and recovery

In order to further investigate the aptitude of molecule **53** to mediate the isolation of small G-quadruplex forming oligonucleotides, further experiments were conducted. The work presented in this section was carried out with the help of Dr. Raphaël Rodriguez and Dr. Sunita Kumari. An initial oligonucleotide concentration of 5 μM was used and a pull-down assay was performed on the following G-quadruplexes: H-telo, C-kit1, C-kit2, C-myc[1] (these G-quadruplexes were discussed in the previous chapters and the sequences can be found in Table 4.4) and also on ds-DNA. The UV titration results are displayed in Figure 4.6. As the figure shows, six different concentrations of compound **53** were used in this assay, which had been prepared in serial dilution: 0.0 μM, 3.0 μM, 4.5 μM, 6.5 μM, 10.0 μM and 15 μM. The amplitude of the graph of the pull-down supernatant decreases for G-quadruplex forming DNA (H-telo, C-kit1, C-kit2 and Pu22) using increasing amounts of the small molecule. The amplitude of the graph corresponding to the respective recovery supernatants increases, respectively. This indicates that an increasing amount of compound **53** has been used to isolate an increasing amount of DNA that can fold into G-quadruplexes. The UV signal corresponding to the double stranded DNA (ds-DNA) was untouched using increasing amounts of the probe, for both, the supernatants of pull-down and recovery. This suggests that the probe selectively mediates G-quadruplex DNA isolation but no ds-DNA pull-down at these concentrations.

It was found that the oligonucleotides pulled-down could only be recovered from the magnetic beads using denaturing conditions such as 8 M LiCl and heat or 8 M urea. It has been shown before that urea has a destabilising effect on G-quadruplex structures.[201] Li^+ ions have been proposed not to destabilise G-quadruplexes,[202] but adding a high molarity of LiCl might displace the K^+ ions from the G-quadruplex structures, lowering their thermal stability. This would rationalise, why heating was required in conjunction with 8 M LiCl to recover the G-quadruplexes under investigation. Washing or heating in the presence of buffer-containing solution did not release *any* DNA.

This demonstrates that the complex formed between G-quadruplex DNA and

[1] We used a mutated sequence of the C-myc quadruplex established in the literature, which only forms a single conformation, making subsequent gel analyses easier.[15] This mutated C-myc G-quadruplex is also termed Pu22.

53 is very strong. Therefore, it was concluded that for these experiments cross-linking of the small molecules with the oligonucleotide targets would not be essential as initially proposed and commonly used in Chip-seq protocols.[198,199]

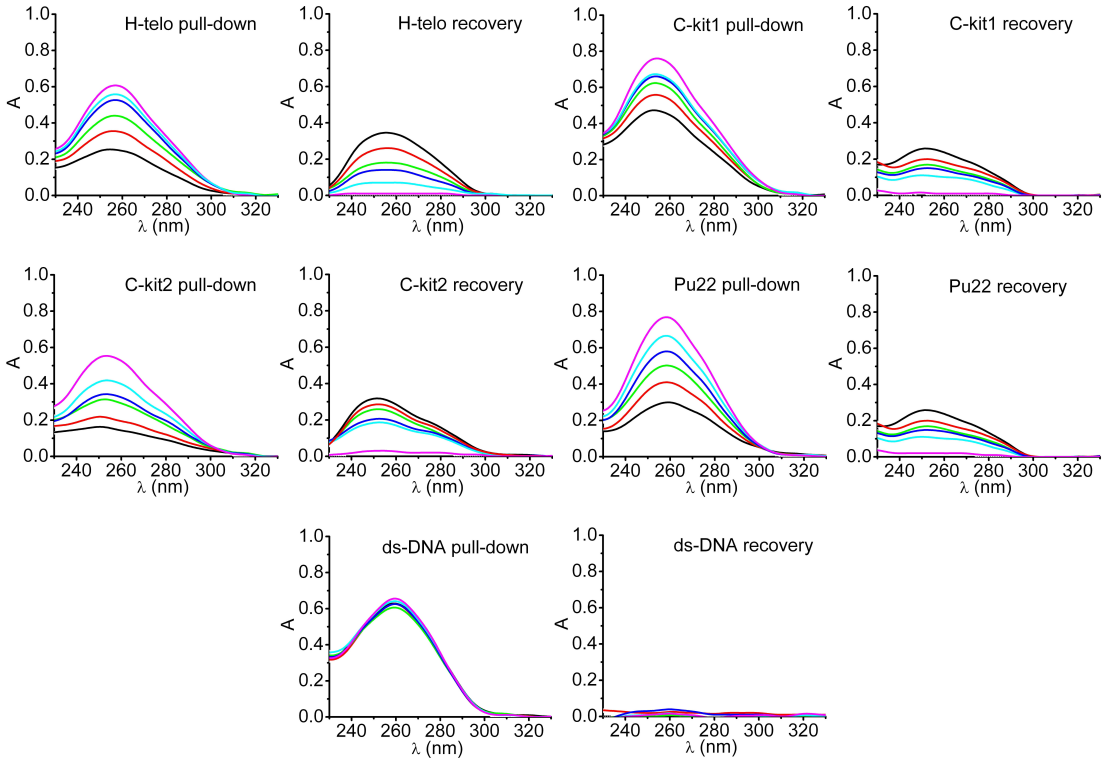

Figure 4.6: UV traces of pull-down experiments with DNA-targets with increasing amounts of probe **53**: (•) 0.0 μM; (•) 3.0 μM; (•) 4.5 μM; (•) 6.5 μM; (•) 10.0 μM; (•) 15.0 μM.

In order to assess the integrity of the recovered oligonucleotide and investigate if G-quadruplex DNA can be isolated from solution in the presence of ds-DNA using the developed methodology, we performed the same experiment with 2.5 μM G-quadruplex DNA and 2.5 μM ds-DNA and analysed the resulting supernatant and recovery solutions by PAGE. The oligonucleotides were recovered from beads using 8 M urea and purified prior to PAGE analysis using G-25 (GE-Healthcare®) columns. The results are displayed in Figure 4.7. As the gels in this figure illustrate, the bands corresponding to G-quadruplex DNA (H-telo, C-kit1, C-kit2 and Pu22) in the pull-down supernatants decrease in intensity upon an increase

of **53** used. This demonstrates that larger molarities of **53** isolate more of G-quadruplex DNA. The intensities of the bands corresponding to ds-DNA do not change. The amount of G-quadruplex DNA recovered from the beads increases as more of the compound is used in the assay, whereas there is a complete absence of bands corresponding to ds-DNA in all the gels. This is consistent with an increase of isolated G-quadruplex DNA but not ds-DNA when using greater amounts of the small molecule. Furthermore, these results show that the oligonucleotides are intact after pull-down and also that the assay is selective for G-quadruplex DNA for a 1:1 solution of G-quadruplex DNA:ds-DNA.

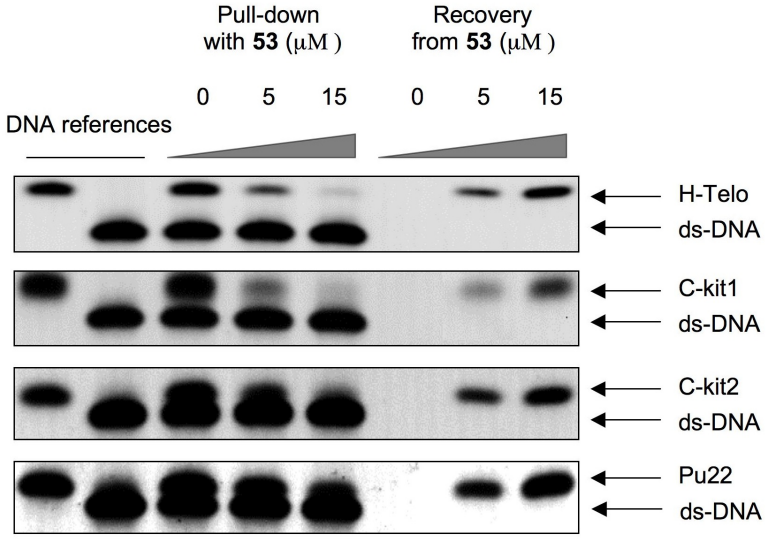

Figure 4.7: PAGE results showing pull-down of four different G-quadruplex DNAs form a 1:1 mixture with ds-DNA. Only G-quadruplex DNA is isolated and not ds-DNA.

It was next explored whether this assay could also be employed to isolate RNA G-quadruplexes formed by synthetic RNA oligonucleotides. As a G-quadruplex target, the one situated in the 5′-UTR of the mRNA of the gene *N-ras*[34] was chosen and as a control the assay was performed on a RNA sequence that can adopt a hairpin as secondary structure (for the sequences see Table 4.4). The experiments were analysed by UV and the results are displayed in Figure 4.8. The figure shows a strong decrease in the amplitudes of the UV spectra corresponding to the N-ras G-quadruplex upon larger amounts of **53** used. The amplitudes of the recovery solutions increase in a dose-dependent manner, indicating more

nucleic acid being isolated. The results presented in Figure 4.8 show that there was very little pull-down of the control hairpin sequence using 15 μM **53** and negligible changes in amplitude using smaller amounts of the compound. It is noteworthy that the recovery of RNA from beads could not be achieved with 8 M LiCl as this was found to degrade the RNA (a disappearance of the band shift was observed using PAGE and the UV signal at 260 nm disappeared after the oligonucleotide had been incubated for 10 min with 8 M LiCl). However, recovery of the oligonucleotide from beads was successfully achieved using 8 M urea.

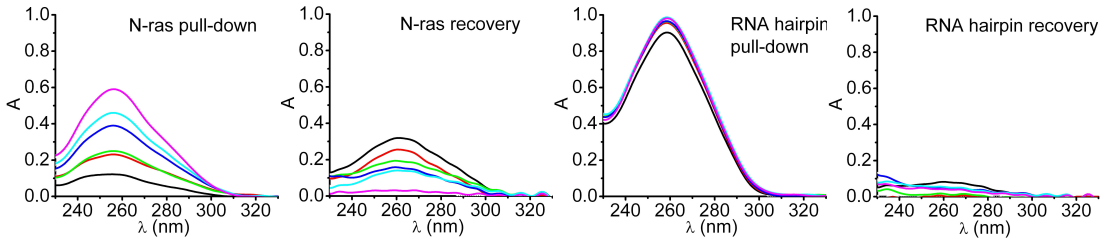

Figure 4.8: UV traces of pull-down experiments with RNA-targets with increasing amounts of probe **53**: (•) 0.0 μM; (•) 3.0 μM; (•) 4.5 μM; (•) 6.5 μM; (•) 10.0 μM; (•) 15.0 μM.

These results suggest that the methodology can also be applied to isolate RNA G-quadruplexes as the N-ras G-quadruplex is pulled down and the RNA hairpin is almost untouched. This further demonstrates that the assay works in a *structure-dependent* manner. However, it was decided to focus the studies and methodology development presented hereafter on DNA targets.

4.4.3 Long sequence isolation and recovery

Classical Chip-Seq experiments[198,199] implement shearing or micrococcal digestion of genomic DNA isolated from cells in order to obtain DNA fragments bound to the protein target of interest, which are sequenced subsequently. If this technology is to be applied to fragments of genomic DNA to isolate G-quadruplex-forming sequences, it would be necessary to 1) isolate longer fragments (normally shearing of genomic DNA yields fragments of the size of approximately 100-500 bp) and 2) isolate these fragments in the presence of the complementary DNA strand. I applied this *in vitro* pull-down methodology on a variety of longer

oligonucleotide sequences to investigate the applicability of the methodology. It was evaluated if compound **53** could mediate the isolation of longer strands of the telomeric sequence $(5'\text{-TTAGGG-}3')_n$ from solution and the assay was performed on a 50-mer and 100-mer oligonucleotide. The experiments on long oligonucleotides were performed on a 5 µM starting concentration for the 50-mer and and a 1 µM concentration for the 100-mer. The lower concentration for the longer oligonucleotide was chosen for practical reasons, *i.e.*, the large amount of DNA required for the experiment. Furthermore, the molar extinction coefficient for longer sequences is higher and thus measuring the UV spectra at lower concentrations of longer sequences is more facile than for shorter sequences. The aptitude of **53** to mediate pull-down was investigated at three concentrations corresponding to 0, 1 and 3 mole equivalents of the DNA concentration used. The results of these experiments are highlighted in Figure 4.9.

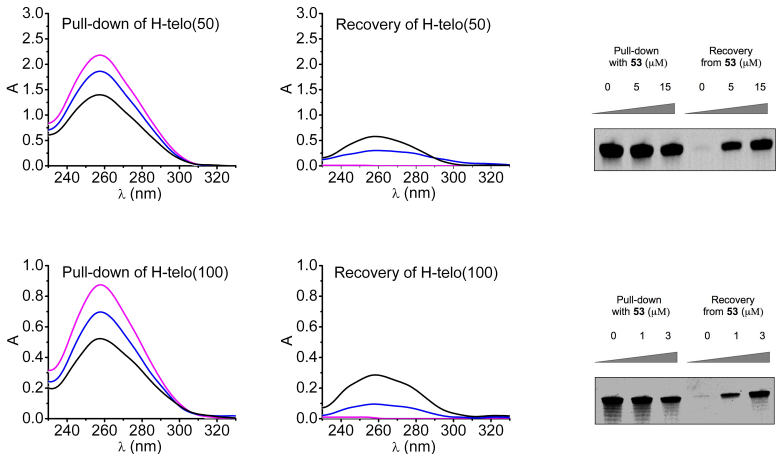

Figure 4.9: Isolation of a H-telo 50-mer and 100-mer with **53** and recovery from **53**. **Left:** UV spectra of pull-down and recovery solutions. **Right:** PAGE analyses of the solutions. (•) 0 equivalents **53**, (•) 1 equivalent **53** and (•) 3 equivalents **53**.

This experiment revealed the possibility to isolate single stranded sequences of the single-stranded telomeric G-overhang from solution. The UV graphs in Figure 4.9 show that the DNA is isolated in a dose-dependent manner using **53**. The PAGE presented in Figure 4.9 illustrate that the DNA is intact after recovery from beads. It is noteworthy that this sequence can form multiple G-quadruplexes which may

favour the pull-down of these oligonucleotides.

These encouraging results prompted me to explore this assay on a longer oligonucleotide with a single G-quadruplex forming sequence. I chose to perform studies on the wild-type C-myc sequence and selected a 51-mer oligonucleotide (C-myc(51)) with the G-quadruplex forming sequence positioned in the middle of the sequence. The natural genomic DNA sequence was used for these experiments. In order to investigate if the probe could isolate G-quadruplex forming sequences in the presence of the complementary strand, pull-down experiments were also performed with **53** on the complementary sequence (comp. C-myc(51)) and on both strands annealed together in solution. The sequences are depicted in Figure 4.10. The G-quadruplex forming sequence is highlighted in red.

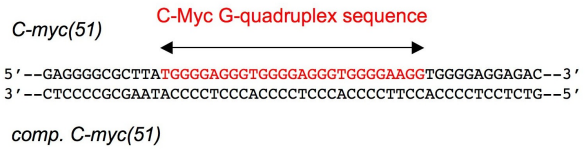

Figure 4.10: C-myc(51) and comp. C-myc(51) sequences with the C-myc G-quadruplex forming sequence highlighted in red.

The results of these experiments are displayed in Figure 4.11. The UV graphs in the figure demonstrate that DNA could only be isolated if the G-quadruplex forming strand was present. Strikingly, the assay could also isolate this sequence if the complementary strand was present. It is noteworthy that the DNA recovered in the presence of the complementary strand, as depicted on the bottom right gel in Figure 4.11, shows a larger proportion of the single stranded DNA containing the G-quadruplex forming sequence. These results imply that is is possible to isolate 51-mer C-myc DNA of the G-quadruplex forming sequence in the absence and presence of the complementary strand. This provides further evidence that the probe **53** acts in a *structure-dependent* manner and targets G-quadruplexes selectively.

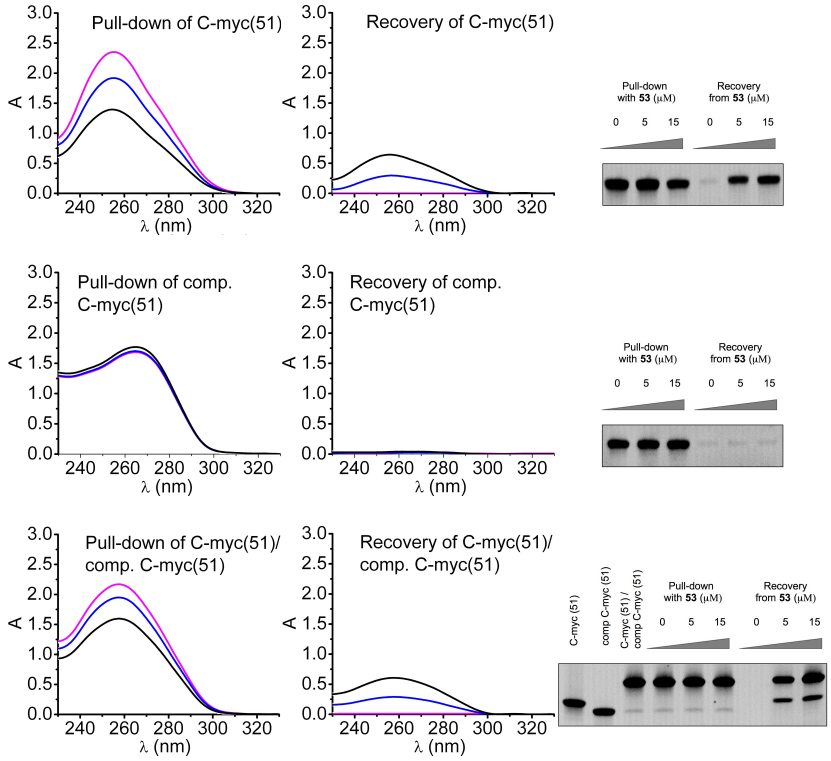

Figure 4.11: Isolation of C-myc(51) with **53** and recovery from **53** in the absence and presence of the complementary strand. Pull-down and recovery of comp. C-myc(51) is also displayed. **Left:** UV spectra of pull-down and recovery solutions. **Right:** PAGE analyses of the solutions. (•) 0 equivalents **53**, (•) 1 equivalent **53** and (•) 3 equivalents **53**.

The assay was also performed on a 101-mer oligonucleotide, which was designed on the same principles as its shorter counterpart as depicted in Figure 4.12. The G-quadruplex forming sequence is again highlighted in red.

C-myc(101)

C-Myc G-quadruplex sequence

5'--CACGCCCTCTGCTTTGGGAACCCGGGAGGGGCGCTTATGGGGAGGGTGGGGAGGGTGGGGAAGGTGGGGAGGAGACTCAGCCGGGCAGCCGAGCACTCTAG--3'
3'--GTGCGGGAGACGAAACCCTTGGGCCCTCCCCGCGAATACCCCTCCCACCCCTCCCACCCCTTCCACCCCTCCTCTGAGTCGGCCCGTCGGCTCGTGAGATC--5'

comp. C-myc(101)

Figure 4.12: C-myc(101) and comp. C-myc(101) sequences with the C-myc G-quadruplex forming sequence in red.

It was found that it is possible to isolate C-myc(101) with and without its complementary strand but the pull-down was weaker than for C-myc(51) as can be seen in Figure 4.13. The results suggest that this assay can be used to isolate oligonucleotides from solution of up to at least 101 bp in length, if the oligonucleotide contains a G-quadruplex forming sequence.

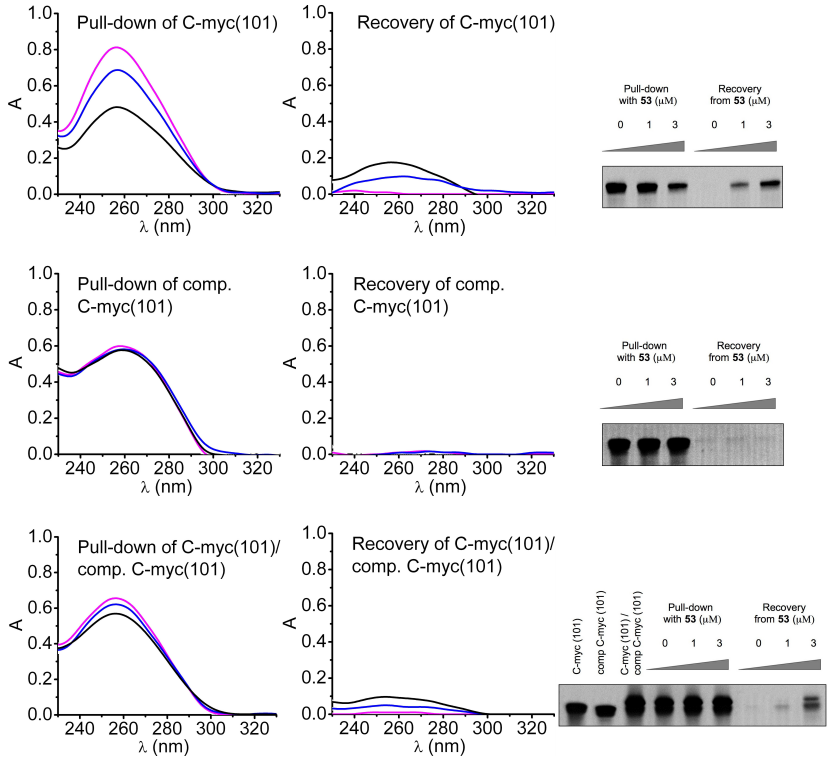

Figure 4.13: Isolation of C-myc(101) with **53** and recovery from **53** in the absence and presence of the complementary strand. Pull-down and recovery of comp. C-myc(101) is also displayed. **Left:** UV spectra of pull-down and recovery solutions. **Right:** PAGE analyses of the solutions. (•) 0 equivalents **53**, (•) 1 equivalent **53** and (•) 3 equivalents **53**.

The stabilisation of G-quadruplexes by **53** as has been demonstrated by FRET-melting experiments presented in sections 4.3.2 and 4.4.1, suggesting that the compound induces the formation of G-quadruplexes by driving the equilibrium towards their formation. This would, in fact, be expected for any small molecule interacting with G-quadruplexes. However, if the small molecule can

drive the population in one direction, it is implied that the G-quadruplex population already exists. The data therefore imply that G-quadruplexes may form in the presence of their complementary DNA strand. The formation of these structures might be favoured by annealing the DNA in 60 mM KCl. However, the experiments clearly show that it is possible to isolate G-quadruplex forming DNA from more complex systems using our methodology. The results and the dose-dependency on the small molecule suggest that the C-myc quadruplex is in dynamic equilibrium with double-stranded DNA. The PAGE show that the the complementary strand is also being isolated if the experiment is performed in the presence of the G-quadruplex forming strand. This is expected since the base pairs of the quadruplex flanking sequences pair with the complementary DNA-strand.

4.4.4 Quadruplex mutations abrogate pull-down

Following this, it was explored if a mutated sequence of the C-myc G-quadruplex containing sequences, which does not allow for the formation of this secondary structure, would have an effect on the pull-down mediated by **53**. A mutated C-myc sequence (mut. C-myc(51)) was used (depicted in Figure 4.14). Each G-tract was mutated to ensure that the sequence could not form a G-quadruplex.[37]

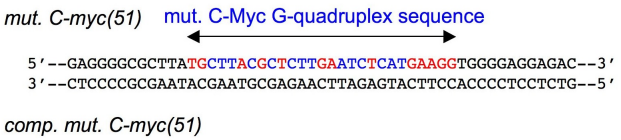

Figure 4.14: Mut. C-myc(51) and comp. mut. C-myc(51) sequences. Mutations are highlighted in blue.

The results of the experiments using the mutated 51-mer and its complementary strand are illustrated in Figure 4.15. Neither the sequences including the mutated quadruplex, nor its complementary strand could be isolated as the figure shows. Furthermore, DNA was also not isolated if both sequences were present as demonstrated by the UV graphs and PAGE presented in Figure 4.15. These results demonstrate that a G-quadruplex forming sequence is required to isolate

DNA and they also constitute further evidence that ds-DNA pull-down is not mediated by **53**.

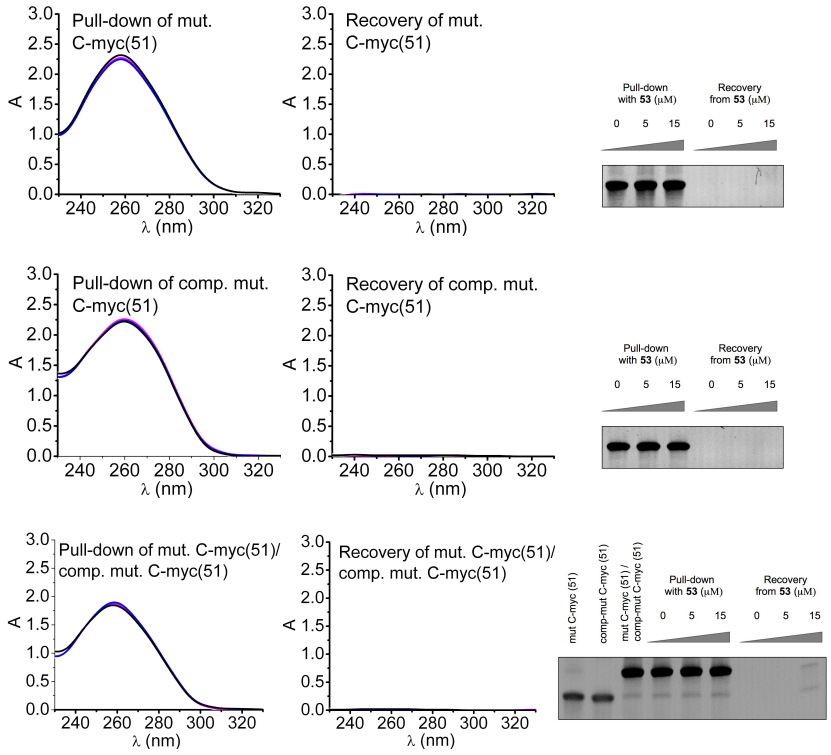

Figure 4.15: Isolation of mut. C-myc(51) with **53** and recovery from **53** in the absence and presence of the complementary strand. Pull-down and recovery of comp. mut. C-myc(51) is also displayed. **Left:** UV spectra of pull-down and recovery solutions. **Right:** PAGE analyses of the solutions. (•) 0 equivalents **53**, (•) 1 equivalent **53** and (•) 3 equivalents **53**.

Analogous experiments were performed using a 101-mer and its complementary strand as displayed in Figure 4.16. The results of the experiments are shown in Figure 4.17.

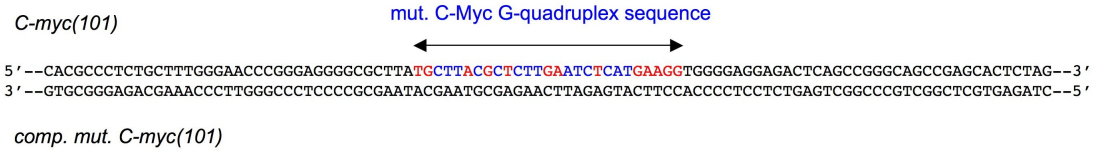

Figure 4.16: Mut. C-myc(101) and comp. mut. C-myc(101) sequences. Mutations are highlighted in blue.

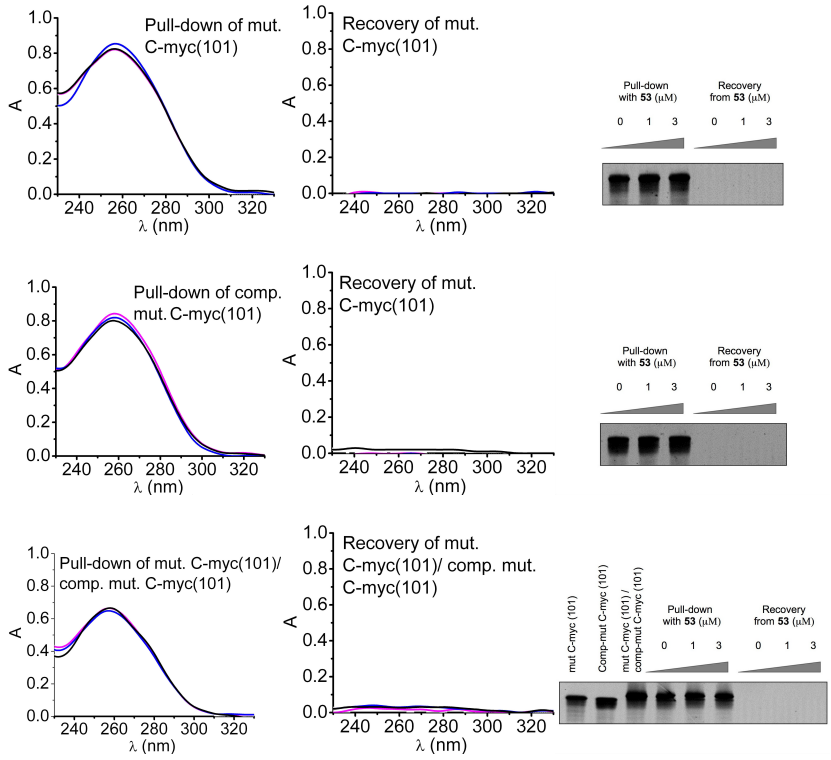

Figure 4.17: Pull-down of mut. C-myc(101) with **53** and recovery from **53** in the absence and presence of the complementary strand. Pull-down and recovery of comp. mut. C-myc(101) is also displayed. **Left:** UV spectra of pull-down and recovery solutions. **Right:** PAGE analyses of the solutions. (•) 0 equivalents **53**, (•) 1 equivalent **53** and (•) 3 equivalents **53**.

Analogous to the results preformed on the mutated 51mer, DNA could not be isolated using **53**. The UV graphs and PAGE results illustrated in Figure 4.17 display that pull-down was completely abrogated compared to the wild type sequence used in the experiments presented in Figure 4.13. These experiments also served as a ds-DNA control since the mutated sequences are expected to exclusively form a double-stranded DNA-helix upon hybridisation in solution. It was observed that the pull-down was completely abrogated due to the mutations, further giving evidence to our hypothesis that the assay can be applied to isolate G-quadruplexes and is *structure-dependent*.

A summary of all the sequences studied and the outcome of the pull-down experiments can be found in Table 4.4. The table shows how quadruplex-forming sequences are a requirement for pull-down to occur. It has to be noted that there is a window of specificity for this assay. I observed some pull-down of all the sequences when the assay was performed with very high equivalents of small molecule compared to the DNA. This might be because **53** carries three positive charges at pH 7.4 and some interaction with the negatively charged phosphate groups of any nucleic acid molecule would be expected at high concentrations of the biotinylated ligand. Therefore, a low ratio of small molecule equivalents to DNA[1] was maintained to ensure specificity towards G-quadruplexes. It is also noteworthy that various sequences presented here are G-rich without a G-quadruplex forming motif and were not pulled down. This suggests that the pull-down is not due to the G-richness of the sequence but rather to the formation of G-quadruplexes, *i.e.*, is *structure-dependent*.

[1]At least one order of magnitude below concentrations where any traces of pull-down of sequences without a G-quadruplex forming sequence could be seen.

Table 4.4: Oligonucleotide sequences studied in nucleic acid isolation experiments.

	Name (mer)[#]	Sequence (5´ to 3´)[†]	PQS[‡]	Pull-down[¶]
1	H-telo(21)	– GGG TTA GGG TTA GGG TTA GGG–	+	+
2	C-kit1(21)	– GGG AGG GCG CTG GGA GGA GGG–	+	+
3	C-kit2(20)	– GGG CGG GCG CGA GGG AGG GG–	+	+
4	Pu22(22)	– TGA GGG TGG GTA GGG TGG GTA A–	+	+
5	C-myc(27)	– TGG GGA GGG TGG GGA GGG TGG GGA AGG–	+	+
6	ds-DNA(26)	– CAA TCG GAT CGA ATT CGA TCC GAT TG–	–	–
7	N-ras(18)	– GGG AGG GGC GGG UCU GGG–	+	+
8	RNA hairpin(24)	– CUA CAG UAC AGA UCU GUA CUG UAG–	–	–
9	H-telo(50)	– TTA GGG TTA GGG TTA GGG TTA GGG TTA GGG TTA GGG TTA GGG TTA GGG TT–	+	+
10	C-myc(51)	– GAG GGG CGC TTA TGG GGA GGG TGG GGA GGG TGG GGA AGG TGG GGA GGA GAC–	+	+
11	comp. C-myc(51)	– GTC TCC TCC CCA CCT TCC CCA CCC TCC CCA CCC TCC CCA TAA GCG CCC CTC–	–	–
12	C-myc(51) / comp. C-myc(51)	– GAG GGG CGC TTA TGG GGA GGG TGG GGA GGG TGG GGA AGG TGG GGA GGA GAC– – GTC TCC TCC CCA CCT TCC CCA CCC TCC CCA CCC TCC CCA TAA GCG CCC CTC–	+	+
13	mut. C-myc(51)	– GAG GGG CGC TTA TGC TTA CGC TCT TGA ATC TCA TGA AGG TGG GGA GGA GAC–	–	–
14	comp. mut. C-myc(51)	– GTC TCC TCC CCA CCT TCA TGA GAT TCA AGA GCG TAA GCA TAA GCG CCC CTC–	–	–
15	mut. C-myc(51) / comp. mut. C-myc(51)	– GAG GGG CGC TTA TGC TTA CGC TCT TGA ATC TCA TGA AGG TGG GGA GGA GAC– – GTC TCC TCC CCA CCT TCA TGA GAT TCA AGA GCG TAA GCA TAA GCG CCC CTC–	–	–
16	H-telo(100)	– TTA GGG TTA GGG TTA GGG TTA GGG TTA GGG TTA GGG TTA GGG TTA GGG TTA GGG TTA GGG TTA GGG TTA G–	+	+
17	C-myc(101)	–C ACG CCC TCT GCT TTG GGA ACC CGG GAG GGG CGC TTA TGG GGA GGG TGG GGA GGG TGG GGA AGG TGG GGA GGA GAC TCA GCC GGG CAG CCG AGC ACT CTA G–	+	+
18	comp. C-myc(101)	–C TAG AGT GCT CGG CTG CCC GGC TGA GTC TCC TCC CCA CCT TCC CCA CCC TCC CCA CCC TCC CCA TAA GCG CCC CTC CCG GGT TCC CAA AGC AGA GGG CGT G–	–	–
19	C-myc(101) / comp. C-myc(101)	–C ACG CCC TCT GCT TTG GGA ACC CGG GAG GGG CGC TTA TGG GGA GGG TGG GGA GGG TGG GGA AGG TGG GGA GGA GAC TCA GCC GGG CAG CCG AGC ACT CTA G– –C TAG AGT GCT CGG CTG CCC GGC TGA GTC TCC TCC CCA CCT TCC CCA CCC TCC CCA CCC TCC CCA TAA GCG CCC CTC CCG GGT TCC CAA AGC AGA GGG CGT G–	+	+
20	mut. C-myc(101)	–C ACG CCC TCT GCT TTG GGA ACC CGG GAG GGG CGC TTA TGC TTA CGC TCT TGA ATC TCA TGA AGG TGG GGA GGA GAC TCA GCC GGG CAG CCG AGC ACT CTA G–	–	–
21	comp. mut. C-myc(101)	–C TAG AGT GCT CGG CTG CCC GGC TGA GTC TCC TCC CCA CCT TCA TGA GAT TCA AGA GCG TAA GCA TAA GCG CCC CTC CCG GGT TCC CAA AGC AGA GGG CGT G–	–	–
22	mut. C-myc(101) / comp. mut. C-myc(101)	–C ACG CCC TCT GCT TTG GGA ACC CGG GAG GGG CGC TTA TGC TTA CGC TCT TGA ATC TCA TGA AGG TGG GGA GGA GAC TCA GCC GGG CAG CCG AGC ACT CTA G– –C TAG AGT GCT CGG CTG CCC GGC TGA GTC TCC TCC CCA CCT TCA TGA GAT TCA AGA GCG TAA GCA TAA GCG CCC CTC CCG GGT TCC CAA AGC AGA GGG CGT G–	–	–

#: the symbol / defines a 1:1 mixture of the oligonucleotide and its complementary strand.

†: oligonucleotides highlighted in red correspond to the wild type C-myc sequences, mutations are highlighted in blue.

‡: + indicates motifs that contain a PQS and - indicates motifs that do not contain a PQS.

¶: + indicate motifs pulled down by **53** and symbols - indicates motifs that remained in the supernatant after a pull-down experiment.

4.4.5 Pull-down enhancement with pyridostatin

The pull-down assay was performed in the presence of **pyridostatin** (**23**). Interestingly, it was observed that the addition of **23** to the DNA prior to isolation studies enhances the pull-down efficiency of **53**. As a control experiment, compound **23** does not mediate any isolation in the absence of **53**. The results of the experiment are displayed in Figure 4.18.

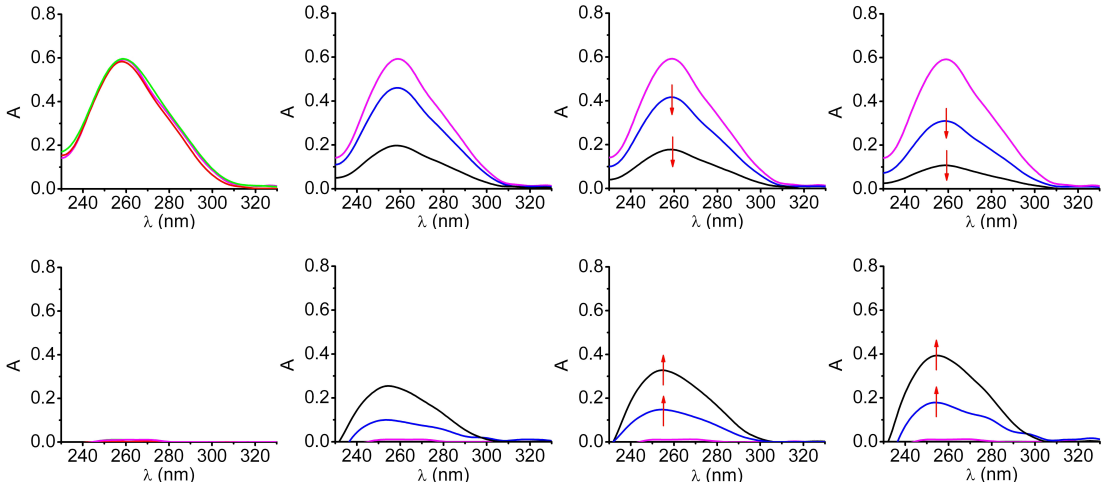

Figure 4.18: Top left: Pull-down supernatant using (•) 0.0 μM, (•) 10.0 μM and (•) 20.0 μM **23**. **Top second from left:** Pull-down supernatant using (•) 0.0 μM, (•) 5.0 μM and (•) 15.0 μM **53**. **Top second from right:** Pull-down supernatant using (•) 0.0 μM **53**/10.0 μM **23**, (•) 5.0 μM **53**/10.0 μM **23** and (•) 15.0 μM **53**/10.0 μM **23**. **Top right:** Pull-down supernatant using (•) 0.0 μM **53**/20.0 μM **23**, (•) 5.0 μM **53**/20.0 μM **23** and (•) 15.0 μM **53**/20.0 μM **23**. **Bottom row:** Corresponding recoveries of the top row. Red arrows mark increase in DNA pull-down by decreasing the DNA concentrations in the pull-down supernatant and increasing the DNA concentrations of the recovery solutions.

Figure 4.18 shows that the amplitude of the UV signal corresponding to the DNA in the supernatant decreases if the assay is performed with an equimolar concentration of **53** but increasing amounts of **pyridostatin** (**23**), indicative of an increased pull-down efficiency. Complementary to these results, the amplitudes of the UV signals in the recovery solutions get bigger if more **pyridostatin** (**23**) is added to the assay, indicative of more G-quadruplex DNA isolated. This result can be rationalised by the fact that DNA prone to fold into G-quadruplex motifs is in dynamic equilibrium with its single coiled counterpart. The equilibrium can be driven by the presence of a G-quadruplex stabilising small molecule. **Pyridostatin** (**23**) may act co-operatively with molecule **53** by driving the DNA towards G-quadruplex folding in solution prior to pull-down with the biotinylated probe.

Although we could relate the apparent phenotype of HT-1080 cells caused

by **53** with that induced by **pyridostatin** (**23**), the latter compound was much more active in cells and also at lower concentrations. Also, the long term growth effect was more pronounced for the lead molecule. Furthermore, **pyridostatin** (**23**) showed a greater aptitude to stabilise G-quadruplexes as assessed by FRET-melting studies.[144] The observed co-operative effect between the compounds for the pull-down could be exploited to isolate genomic G-quadruplex forming DNA. One could incubate cells with **pyridostatin** (**23**) and then isolate the DNA. The pull-down could then be conducted *in vitro* using **53**. We are currently investigating the feasibility of such an approach in our laboratory.

4.4.6 Cellular effects of the probe

It was demonstrated that it is possible to pull down G-quadruplex forming oligonucleotides *in vitro* using the biotinylated probe **53**. The major objective of this project was to utilise this small molecule to recognise and isolate G-quadruplexes from cells. Such an approach could help identify druggable G-quadruplexes. A preliminary characterisation of the cellular effects of **53** was performed and they were compared to those of the lead molecule **pyridostatin** (**23**), which had been identified to interact with the telomeric G-quadruplex.[144] All the studies presented here were performed at the GI_{50} of the compounds. It was initially observed that incubation of HT-1080 cells with compounds **23** and **53** caused phenotypic changes not seen in the untreated control cells. Upon incubation with the compounds the cells enlarged with an obvious increase of the cytoplasmic to nucleoplasmic ratio (see Figure 4.19).

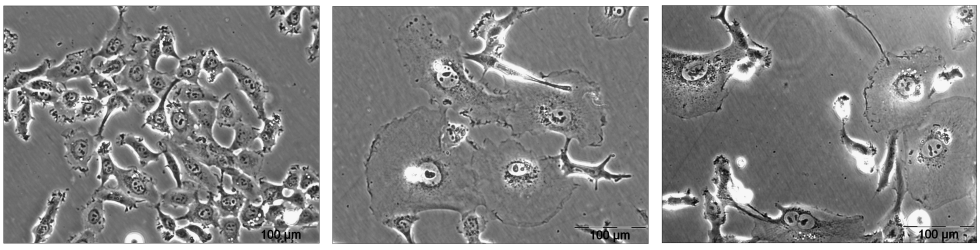

Figure 4.19: Pictures of cells after 12 d. **Left:** Untreated control HT-1080 cells. **Center:** HT-1080 cells incubated with **23**. **Right:** HT-1080 cells incubated with **53**.

An increase of this ratio is characteristic of senescent cells[193] and implies a

cytostatic effect of the compounds. Cells were split and replated at the appropriate compound concentration every 4^{th} day. I also performed experiments on HT-1080 cells, analogous to those presented in Chapter 3, for other *N,N′-bis*(quinolinyl)pyridine-2,6-dicarboxamides. It was investigated if **53** causes long-term growth inhibition and G-overhang attrition leading to replicative senescence. The results of these experiments are summarised in Figure 4.20.

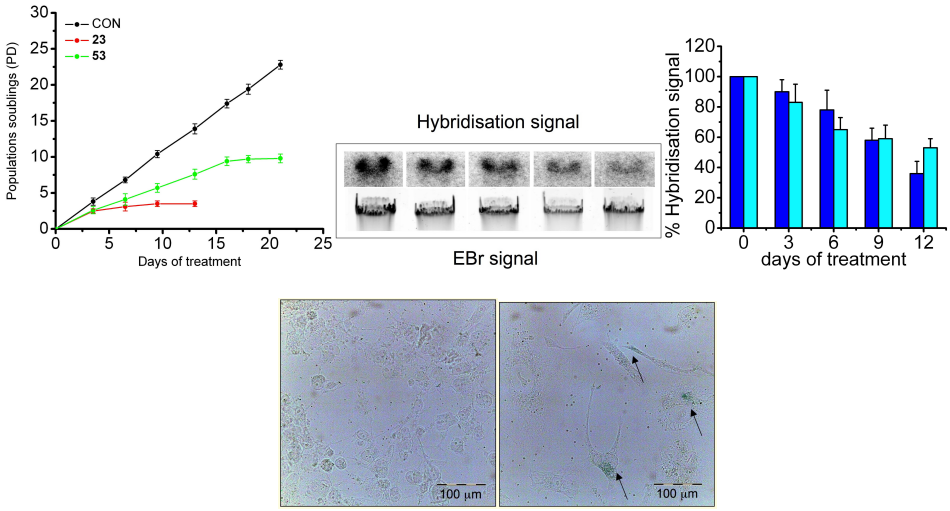

Figure 4.20: Top left: Long-term growth curves of HT-1080 cells treated with **23**, **53** and control (CON) cells without ligand treatment. **Top center:** G-overhang shortening shown for DNA isolated from HT-1080 cells treated with **53** over 12 d. **Top right:** Histogram showing average hybridisation signal of four independent experiments for DNA isolated from HT-1080 cells treated with (•) **23** and (•) **53**. **Bottom left:** Senescence β-galactosidase assay performed on control cells and **bottom right:** Performed on cells treated with **53** for 8 d. Arrows indicate blue staining due to 5,5′-dibromo-4,4′-dichloro-indigo indicating β-galactosidase activity characteristic of senescent cells. (For results for **23** see Chapter 3).

The data obtained suggest that **53** has cellular effects on HT-1080 cells analogous to those induced by **pyridostatin** (**23**), exemplified by the fact that both compounds cause telomere shortening, replicative cellular senescence and induce the same apparent cellular phenotype upon exposure. The data suggests that **53** may be a G-quadruplex interacting small molecule, which can recognise these structures in cells. This makes this probe a suitable candidate to mediate the

pull-down of G-quadruplexes from human cells. It should therefore be possible to isolate biologically relevant and/or druggable DNA and RNA G-quadruplexes from human cells using this probe and the methodology that was presented earlier in this chapter.

4.4.7 Genomic DNA pull-down

Currently, we are exploring the aptitude of the pull-down assay to isolate G-quadruplexes from human cells in our laboratory. It is an ongoing project and preliminary results are discussed in this section. The initial experiments were performed on genomic, non-chromatinised DNA. Although, this system is still removed from the natural state of DNA, it is a good choice to study the methodology in a more complex environment than the one used for the *in vitro* studies presented earlier in this chapter.

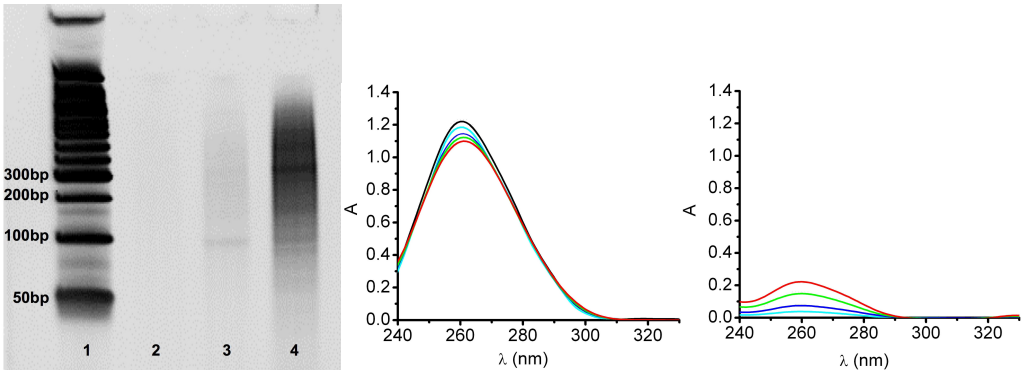

Figure 4.21: Pull-down and recovery from genomic DNA. **Left:** PA gel showing: lane 1) DNA ladder; lane 2) recovery from beads after pull-down with 0.0 μM **53**; lane 3) recovery from beads after pull-down with 1.0 μM **53**; 4) supernatant of pull-down before the experiment. **Center:** pull-down of genomic DNA with **53**. **Right:** Recovery of genomic DNA from **53**. (●) 0.0 μM, (●) 0.5 μM, (●) 1.0 μM, (●) 2.0 μM , (●) 4.0 μM **53**.

Genomic DNA was isolated from HT-1080 cells and associated proteins and RNA were removed by using protease K and RNase A, respectively. The DNA was sheared by sonication; a procedure which yields DNA fragments of approximately 100-500 bp in length. Each sample contains DNA of approximately 6×10^6 cells. Since shearing nicks the DNA at random *foci*, any single PQS will be within

varying DNA sizes in the range of these fragments. It was possible to isolate DNA using our established methodology and the results are displayed in Figure 4.21. The genomic DNA concentration was calculated from the average fragment size. For the pull-down experiments displayed in Figure 4.21, a DNA concentration of 0.52 μM was used; a concentration in relation to that of **53** well within the window of specificity seen in the earlier experiments.

These preliminary results were very encouraging. However, the experiments do not give any insight into the composition of the DNA isolated. We thought of three practical ways to assess the content of the DNA pull-down: 1) sequencing of the fragments, 2) nucleobase digestion and investigation of the G-content of the pull-down and 3) specific qPCR on selected sequences like the telomeric one or the promoter region of *c-myc* which are suspected to form G-quadruplexes.

Option 1) is the ultimate goal, but is very resource consuming and it would be better to have a simpler way to investigate if there is a PQS enrichment in the recovered DNA from beads before performing DNA-sequencing. Option 2) would only give a very crude way of assessing G-richness. Option 3) would give a very good overview on the feasibility of the assay and can easily be applied to a selection of targets. We are currently investigating the composition of the genomic DNA fragments isolated by qPCR in our laboratory, which will be presented in the next section.

4.4.8 Isolation of the telomeric G-quadruplex

The work presented in this section has been carried out in collaboration with Dr. Sunita Kumari and Dr. Raphaël Rodriguez. For this study we decided to assess the DNA composition of the supernatant after pull-down mediated by increasing amounts of **53**. The genomic DNA was sonicated and a final concentration of 0.52 μM DNA (using an average fragment size of 300 bp as suggested by the gel shown in Figure 4.21) was used for the studies. We performed the pull-down assay using 0, 2.6, 5.2 and 10.4 μM **53**. Subsequently, we performed qPCR experiments on the telomeric sequence and on the sequence of a control gene *36B4* using the supernatants after pull-down. The *36B4* gene, which does not contain a G-quadruplex forming sequence, is located on chromosome 12 and encodes for the acidic ribosomal phosphoprotein PO. The qPCR conditions for these sequences,

including the primers used, are established in the literature.[203] The results of these experiments are illustrated in Figure 4.22. This methodology allowed us to compare the Cp values of the amplification reactions and directly relate them to the control reaction (no compound). The experiments showed that increasing amounts of **53** reduced the amount of telomeric sequence in the supernatant in a dose-dependent manner, whereas the quantity of control gene *36B4* remained unaffected (Figure 4.22 on the left). It is noteworthy that we did not relate the absolute amplifications of the telomeric sequence and *36B4*. Despite the fact that the primer efficiencies were comparable, the copy numbers of the sequences are different. Thus, we only performed an intrinsic comparison of each target with its control PCR reaction of the pull-down experiment performed using no compound. Specific qPCR amplification performed on the DNA recovered form beads further demonstrated the presence of telomeric DNA in the pull-down extracts as seen in Figure 4.22 on the right. The primers used gave a major amplification product of 76 bp but also longer fragments as visualised by the gel. These results indicate that compound **53** is capable of selectively mediating G-quadruplex DNA isolation from cells. It is possible that nucleic acid fragments comprising similar sequences found elsewhere in the genome than telomeres may also have been isolated.

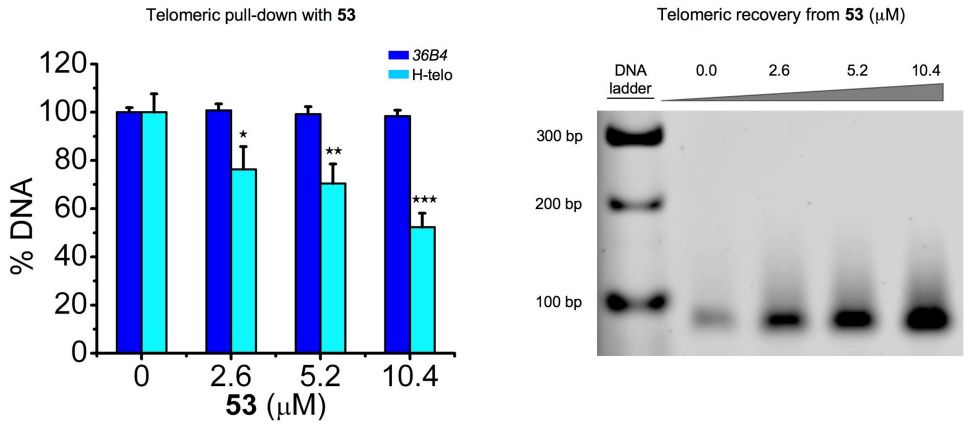

Figure 4.22: Results of the qPCR experiments performed on H-telo and *36B4*. **Left:** Bar chart showing the relative percentage of remaining telomeric sequence and *36B4* control gene in supernatants after pull-down performed on 0.52 μM genomic DNA (n=5). **Right:** Agarose gel showing the PCR amplification products of telomeric sequences after DNA recovery from **53**. SD: $\star$ p $\leq$ 0.05, $\star\star$ p $\leq$ 0.01, $\star\star\star$ p $\leq$ 0.0001.

The outcome of the experiments presented in sections 4.4.3 and 4.4.4 suggested that the pull-down assay may be applied to G-quadruplexes in the presence of their complementary strand. We have now started investigating G-quadruplex targets other than the telomeric one and are currently examining the feasibility to selectively isolate genomic DNA sequences containing promoter G-quadruplexes from genes such as *c-kit* and *c-Myc*, using qPCR as detection method.

4.5 Conclusions, future work and outlook

The successful design and synthesis of biotinylated G-quadruplex stabilising small molecules has been demonstrated. The molecules showed good stabilisation of a variety of G-quadruplex targets as assessed by FRET-melting experiments. Based on these molecules, an *in vitro* assay was developed that can isolate DNA fragments containing G-quadruplexes from solution selectively over ds-DNA. One of the probes was shown to cause phenotypic cellular effects analogous to those of the established G-quadruplex ligand **pyridostatin**.[144] The results suggest that the assay can be used to isolate G-quadruplexes from genomic DNA, as demonstrated by the successful isolation of the telomeric G-quadruplex forming sequence from genomic DNA of human HT-1080 cells. This platform provides a starting point to map all G-quadruplex forming sequences in the human genome. Thus, this approach could be used to identify all G-quadruplex forming sequences in a genome and this information might ultimately supersede the bioinformatic studies on the prevalence of G-quadruplexes in the genome.[37] Such an outcome may help steer and focus the research efforts in the G-quadruplex field.

Indubitably, there is a limitation to this approach. A molecule may induce the formation of G-quadruplexes and identified targets may therefore be wrongly attributed to be of biological significance. However, this is the case for other studies involving small molecules. Also, a small molecule can only drive an equilibrium towards the formation of one population. Therefore any identified G-quadruplex by this method would form in the absence of the small molecule, even though its population in the equilibrium might be small.

Thus I conclude that our methodology offers a good approach to identify possible biologically relevant and/or druggable G-quadruplexes in the human genome. The new methodology presented in this chapter can also be applied to isolate

RNA G-quadruplexes, as the results of the experiments presented in section 4.4.2 imply. However, RNA sequencing is far from trivial due to the various extremely stable secondary structures RNA can adopt.

It has been demonstrated that **53** targets telomeres in cells. This evidence suggests that the compound 1) penetrates into the cells and 2) interacts with DNA at telomeres. This suggests that it might be possible to incubate the cells with compound **53** and isolate G-quadruplexes from the cells. This route is very challenging as the probe will have to fulfill a plethora of properties which have not yet been fully assessed:
1) It would have to stay intact and not be metabolised.
2) The detection of the isolated DNA has to be sensitive enough to detect a potentially very small amount of DNA.
3) The interactions of the G-quadruplexes with the probe have to be strong enough to survive all the isolation steps. With the current system in place, there is no covalent interaction between the probe and the target. It may be necessary to explore the potential of formaldehyde or glutaraldehyde cross-linking, which may require the usage of the probes with primary amines as presented earlier in the chapter.

Furthermore, the experiments performed in section 4.4.5 suggest that an alternative approach is feasible: the isolation of G-quadruplexes with **53** *in vitro* from DNA isolated from cells treated with **23**.

Ultimately, the DNA isolated using one of those approaches will have to be sequenced to identify the G-quadruplex sequences isolated. This part would have to be addressed using methodologies such as Illumina[197] sequencing technology. Despite these challenges lying ahead, the system and methodology developed is functional as shown extensively *in vitro* in this chapter and by the successful isolation the telomeric G-quadruplex forming sequence.

Since, we have shown that human telomeric DNA is a molecular target for **53**, it provides further evidence for the formation of G-quadruplexes at human telomeres.

Chapter 5

Experimental

5.1 Synthesis

5.1.1 General experimental

All solvents and reagents were purified by standard techniques reported in Armarego, W.L.F., Chai, C.L.L., Purification of Laboratory Chemicals, 5^{th} edition, Elsevier, 2003; or used as supplied from commercial sources (Sigma-Aldrich® or Alfa-Aesar®). NMR spectra were acquired on Bruker DRX-400, Bruker DPX-400 and DRX-500 instruments using deuterated solvents as detailed and at ambient probe temperature (300 K). Notation for the ^{1}H-NMR spectral splitting patterns includes: singlet *(s)*, doublet (*d*), triplet (*t*), broad (*br*) and multiplet/overlapping peaks (*m*). Signals are quoted as δ values in ppm, coupling constants (J) are quoted in Hz and rounded to the nearest 0.5 Hz. Proton assignments are supported by ^{1}H-COSY, ^{1}H-^{13}C HMBC and ^{1}H-^{13}C HMQC where necessary. Data analysis for NMR was performed using TopSpin® software. Mass spectra were recorded on Micromass Q-Tof (ESI) spectrometer. TLC was performed on Merck Kieselgel 60 F254 plates, and spots were visualised under UV light. Flash chromatography (FC) was performed using Merck Kieselgel 60 at rt under a positive pressure of N_2 or Ar using previously distilled solvents. Melting points were recorded using a Griffin® melting point apparatus and were recorded for crystalline compounds only and not for salts or precipitates. HPLC purification was carried out using a Varian® Pursuit™ C18, 5 μ column (250.0 × 21.2 mm) and a gradient elution with H_2O/MeCN containing 0.1% TFA at a flow

rate of 12.0 ml/min or a Varian® Pursuit™ C18, 5 μ column (250.0 × 10.0 mm) and a gradient elution with H_2O/MeCN containing 0.1% TFA at a flow rate of 4.6 ml/min. $[\alpha]_D^{20}$ values were recorded on a Perkin Elmer® 241 polarimeter. All labelled DNA oligonucleotides were purchased from Eurogentec® Ltd. and all unlabelled oligonucleotides were purchased from IBA® GmbH. Reagents for cell-based studies were purchased from GIBCO® unless stated otherwise. Luminescence was recorded on a Berthold Detection Services® Orion II Microplate Luminometer. Fluorescent readings for FRET experiments were performed using a Roche® LightCycler™ 480 System RT-PCR. A NanoDrop™ 1000 spectrometer (Thermo Scientific®) was used to record UV spectra and quantify DNA. Gel imaging was performed using a UVP® Bio Doc-it™ imaging system. Cell imaging was performed with an Olympus® microscope fitted with a colour camera. Final data analysis was performed using the Microsoft Office™ package unless stated otherwise.

5.1.2 Procedures

This section describes general procedures for the synthesis of some of the compounds. Structures and analytical data are presented in section 5.1.3.

Procedure for 1a-3b

G1: Two equivalents of **5a** (for **1a**, **2a** and **3a**) or **5b** (for **1b**, **2b** and **3b**) were dissolved in dry chloroform (2 ml) and one equivalent of 1,3-diisocyanatobenzene **6a** (for **1a** and **1b**), 2,4-toluene diisocyanate **6b** (for **2a** and **2b**) or 2,6-toluene diisocyanate **6c** (for **3a** and **3b**) was added. The mixture was heated to 50 °C and allowed to stir overnight. The solvent was removed *in vacuo* and the mixture redissolved in DCM (3 ml) and TFA (1 ml). The mixture was allowed to stir for 1 h and then the solvent removed *in vacuo* to yield a pale yellow solid. Compounds were purified by HPLC (gradient: 10% MeCN/90% H_2O, 0.1% TFA to 100% MeCN, 0.1% TFA over 30 min, R_t=13.0-16.0 min) to yield the TFA salts of the products as white powders.

Procedure for 18-22

G2: One mole equivalent of 2,6-pyridine dicarboxyldichloride (**7**) was dissolved in DCM and cooled to 0 °C under argon. TEA was added dropwise and the solution allowed to warm to rt and stirred for 30 min. Typically, 2.2 mole equivalents of **5a**, **5b** or **16a-16c** was added and the solution allowed to stir overnight under argon. The solvent was removed *in vacuo*. The intermediate for **18** and **19** was precipitated from hot MeCN, filtered, dried using $MgSO_4$ and deprotected using a 1:2 mixture of TFA/DCM (10-100 ml). The final compounds were purified using HPLC (gradient: 10% MeCN/90% H_2O, 0.1% TFA to 100% MeCN, 0.1% TFA over 30 min, R_t=12.0-13.5 min) to yield the TFA salt of the product.

Procedure for 23-37

G3: One mole equivalent of **11a-d**, **13** or **15** were dissolved in DCM and 1-chloro-*N*,*N*,-2-trimethylpropenylamine was added slowly and the reaction allowed to stir at rt for 2 h. The solution was then cooled to 0 °C. TEA was added dropwise and the solution was allowed to warm to rt and stirred for 1 h. Typically, 2.2 mole equivalents of **5a**, **5b** or **16a-16c** was added and the solution stirred under argon at rt overnight. The solvent was removed *in vacuo*. The intermediate for **23-25**, **27**, **28**, **31**, **32** and **36** was precipitated from hot MeCN, filtered, dried and deprotected using TFA/DCM (1:2). The final compounds were purified using HPLC (gradient: 10% MeCN/90% H_2O, 0.1% TFA to 100% MeCN, 0.1% TFA over 30 min, R_t=12.0-13.5 min) to yield the TFA salt of the product.

Procedure for 38-46

G4: **27** or **28** was dissolved in a 1:2 mixture of ^{t}BuOH/H_2O (1-3 ml). Copper(II) sulfate pentahydrate and sodium ascorbate were added and the solution left to stir for 10 min. The respective azide was added and the solution was allowed to stir overnight under argon. The solvent was removed *in vacuo* and the product purified by HPLC (gradient: 10% MeCN/90% H_2O, 0.1% TFA to 100% MeCN, 0.1% TFA over 30 min, R_t=13.0-14.5 min) to yield the TFA salt of the product.

5.1.3 Synthesised molecules

For each compound synthesised the molecular structure is depicted. Some protons are numbered on a few of the molecules for clarity. Additional abbreviations used int he annotations: al = aliphatic, ar = aromatic, T = thymidinyl.

1,3-[Di(4-{2-amino-ethoxy}quinolin-2-yl)diureido]benzene (1a)

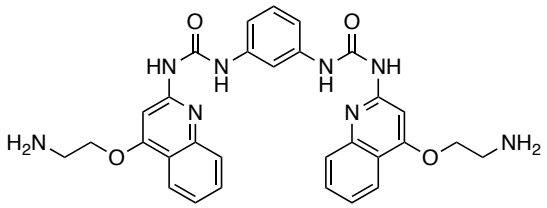

Following procedure **G1**, **5a** (133 mg, 0.440 mmol) was reacted with 1,3- phenylene diisocyanate (**6a**, 35 mg, 0.220 mmol) to afford the TFA salt of the title compound (**1a**·$2CF_3CO_2H$, 154 mg, 0.190 mmol, 86%). **^{1}H-NMR** (500 MHz, D_2O) $\boldsymbol{\delta_H}$ 8.31 (2H, *dd*, *J* 8.0, 1.0 Hz, C<u>H</u> (ar)), 7.78 (2H, *dd*, *J* 8.0, 1.0 Hz, C<u>H</u> (ar)), 7.69 (2H, *ddd*, *J* 8.0, 6.5, 1.0 Hz, C<u>H</u> (ar)), 7.60 (1H, *s*, C<u>H</u> (ar)), 7.48 (2H, *ddd*, *J* 8.0, 6.5, 1.0 Hz, C<u>H</u> (ar)), 7.35 (2H, *d*, *J* 8.0 Hz, C<u>H</u> (ar)), 7.20 (1H, *t*, *J* 8.0 Hz, C<u>H</u> (ar)), 6.69 (2H, *s*, C<u>H</u> (ar)), 4.59 (4H, *t*, *J* 5.0 Hz, OC<u>H_2</u>), 3.61 (4H, *t*, *J* 5.0 Hz, $OCH_2C\underline{H_2}$); **^{13}C-NMR** (125 MHz, D_2O) $\boldsymbol{\delta_C}$ 163.0, 162.5, 154.1, 153.9, 139.8, 134.2, 130.7, 127.5, 127.4, 124.1, 118.9, 116.1, 111.0, 93.1, 68.0, 39.7; **HRMS (ES)** calculated for $C_{30}H_{31}N_8O_4$ ($[M+H]^+$) m/z: 567.2463, found 567.2456.

1,3-[Di(4-{2-pyrrolidinyl-ethoxy}quinolin-2-yl)diureido]benzene (1b)

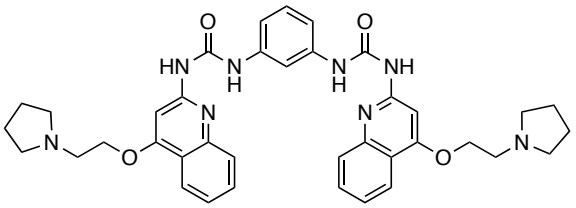

Following procedure **G1**, **5b** (56 mg, 0.220 mmol) was reacted with 1,3 phenylene diisocyanate (**6a**, 18 mg, 0.110 mmol) to afford the TFA salt of the title compound (**1b**·2CF_3CO_2H, 90 mg, 0.1 mmol, 91%). **^{1}H-NMR** (500 MHz, D_2O) $\boldsymbol{\delta_H}$ 8.23 (2H, *dd*, *J* 8.0, 1.0 Hz, C<u>H</u> (ar)), 8.05-8.01 (1H, *m*, C<u>H</u> (ar)), 7.90 (2H, *dd*, *J* 8.5, 1.0 Hz, C<u>H</u> (ar)), 7.77 (2H, *ddd*, *J* 8.5, 7.0, 1.0 Hz, C<u>H</u> (ar)), 7.47 (2H, *ddd*, *J* 8.0, 7.0, 1.0 Hz, C<u>H</u> (ar)), 7.40-7.38 (2H, *m*, C<u>H</u> (ar)), 7.36-7.32 (1H, *m*, C<u>H</u> (ar)), 6.94 (2H, *s*, C<u>H</u> (ar)), 4.55 (4H, *t*, *J* 4.0 Hz, OC<u>H_2</u>), 3.81 (4H, *t*, *J* 4.0 Hz, $OCH_2C\underline{H_2}$), 3.76-3.66 (4H, *m*, $NC\underline{H_2}CH_2CH_2$), 3.31-3.19 (4H, *m*, $NC\underline{H_2}(CH_2)_2$), 2.14-2.03 (4H, *m*, $NCH_2C\underline{H_2}CH_2$), 1.97-1.86 (4H, *m*, $NCH_2C\underline{H_2}CH_2$); **^{13}C-NMR** (125 MHz, D_2O) $\boldsymbol{\delta_C}$ 161.7, 153.6, 152.2, 139.5, 131.2, 129.7, 125.5, 124.3, 122.3, 117.9, 117.4, 115.1, 112.7, 94.9, 65.0, 54.2, 53.9, 23.0; **HRMS (ES)** calculated for $C_{38}H_{43}N_8O_4$ ($[M+H]^+$) m/z: 675.3407, found 675.3411.

2,4-[Di(4-{2-amino-ethoxy}quinolin-2-yl)diureido]toluene (2a)

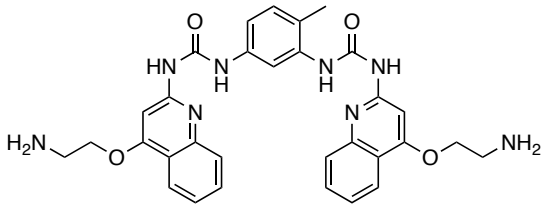

Following procedure **G1**, **5a** (118 mg, 0.4 mmol) was reacted with 2,4-toluene diisocyanate (**6b**, 34 mg, 0.2 mmol) to afford the TFA salt of the title compound (**2a**·2CF_3CO_2H, 150 mg, 0.180 mmol, 90%). **^{1}H-NMR** (500 MHz, D_2O) $\boldsymbol{\delta_H}$ 8.28 (1H, *dd*, *J* 8.5, 1.0 Hz, C<u>H</u> (ar)), 8.24 (1H, *dd*, *J* 8.5, 1.0 Hz, C<u>H</u> (ar)), 8.20 (1H, *s*,

CH (ar)), 7.75-7.70 (2H, *m*, CH (ar)), 7.70-7.62 (2H, *m*, CH (ar)), 7.50-7.45 (1H, *m*, CH (ar)), 7.45-7.40 (1H, *m*, CH (ar)), 7.13-7.09 (1H, *m*, CH (ar)), 7.00-6.96 (1H, *m*, CH (ar)), 6.75-6.70 (2H, *m*, CH (ar)), 4.60-4.50 (4H, *m*, OCH_2), 3.61-3.53 (4H, *m*, OCH_2CH_2), 2.19 (3H, *s*, CH_3); **^{13}C-NMR** (125 MHz, D_2O) $\boldsymbol{\delta_C}$ 163.2, 162.9, 162.6, 162.3, 154.3, 153.89 153.8, 137.3, 134.5, 134.0, 131.8, 127.4, 126.9, 126.8, 124.3, 124.0, 122.0, 119.6, 119.5, 118.9, 118.7, 117.2, 116.6, 114.0, 93.3, 93.1, 67.9, 67.6, 39.7, 39.6, 18.2; **HRMS (ES)** calculated for $C_{31}H_{33}N_8O_4$ ($[M+H]^+$) m/z: 581.2619, found 581.2637.

2,4-[Di(4-{2-pyrrolidinyl-ethoxy}quinolin-2-yl)diureido]toluene (2b)

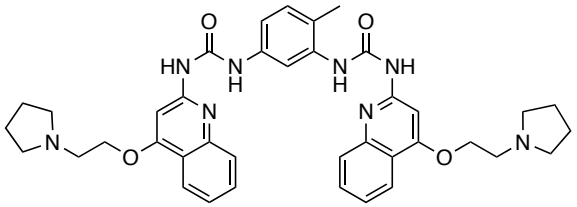

Following procedure **G1**, **5b** (49 mg, 0.2 mmol) was reacted with 2,4-toluene diisocyanate (**6b**, 17 mg, 0.1 mmol) to afford the TFA salt of the title compound (**2b**·$2CF_3CO_2H$, 85 mg, 0.090 mmol, 90%). **^{1}H-NMR** (500 MHz, D_2O) $\boldsymbol{\delta_H}$ 8.42 (1H, *s*, CH (ar)), 8.22 (2H, *br d*, *J* 8.5 Hz, CH (ar)), 7.80 (1H, *d*, *J* 8.0 Hz, CH (ar)), 7.84 (1H, *d*, *J* 8.0 Hz, CH (ar)), 7.78-7.74 (2H, *m*, CH (ar)), 7.49-7.43 (3H, *m*, CH (ar)), 7.27-7.23 (1H, *m*, CH (ar)), 7.00 (1H, *s*, CH (ar)), 6.81 (1H, *s*, CH (ar)), 4.60-4.50 (4H, *m*, OCH_2), 3.85-3.78 (4H, *m*, OCH_2CH_2), 3.75-3.66 (4H, *m*, $NCH_2(CH_2)_2$), 3.30-3.20 (4H, *m*, $NCH_2(CH_2)_2$), 2.57 (3H, *s*, CH_3), 2.13-2.04 (4H, *m*, $NCH_2CH_2CH_2$), 1.97-1.87 (4H, *m*, $NCH_2CH_2CH_2$); **^{13}C-NMR** (125 MHz, D_2O) 161.6, 161.4, 153.8, 153.5, 152.5, 152.2, 146.0, 137.7, 137.1, 131.2, 131.1, 130.6, 130.5, 125.6, 125.5, 124.2, 124.1, 122.4, 122.3, 121.4, 119.7, 117.9, 117.8, 115.1, 113.7, 111.2, 92.8, 92.7, 64.4, 64.3, 54.2, 52.7, 22.7, 22.4, 18.3; **HRMS (ES)** calculated for $C_{39}H_{45}N_8O_4$ ($[M+H]^+$) m/z: 689.3564, found 689.3569.

2,6-[Di(4-{2-amino-ethoxy}quinolin-2-yl)diureido]toluene (3a)

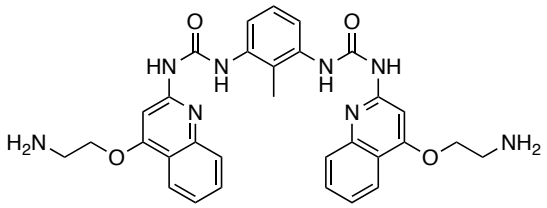

Following procedure **G1**, **5a** (97 mg, 0.320 mmol) was reacted with 2,6-toluene diisocyanate (**6c**, 28 mg, 0.160 mmol) to afford the TFA salt of the title compound (**3a**·2CF_3CO_2H, 117 mg, 0.140 mmol, 88%). **^{1}H-NMR** (500 MHz, D_2O) $\boldsymbol{\delta_H}$ 8.26 (2H, *dd*, *J* 8.5, 1.0 Hz, C<u>H</u> (ar)), 7.88 (2H, *dd*, *J* 8.5, 1.0 Hz, C<u>H</u> (ar)), 7.84 (2H, *ddd*, *J* 8.5, 6.5, 1.0 Hz, C<u>H</u> (ar)), 7.64 (2H, *ddd*, *J* 8.5, 6.5, 1.0 Hz, C<u>H</u> (ar)), 7.41 (2H, *d*, *J* 8.0 Hz, C<u>H</u> (ar)), 7.35 (1H, *d*, *J* 8.0 Hz, C<u>H</u> (ar)), 6.74 (2H, *s*, C<u>H</u> (ar)), 4.65 (4H, *t*, *J* 5.0 Hz, OC<u>H_2</u>), 3.62 (4H, *t*, *J* 5.0 Hz, OCH_2C<u>H_2</u>), 2.40 (3H, *s*, C<u>H_3</u>); **^{13}C-NMR** (125 MHz, D_2O) $\boldsymbol{\delta_C}$ 162.1, 161.8, 154.9, 154.2, 137.1, 134.7, 127.6, 127.4, 124.4, 123.3, 119.0, 118.8, 116.5, 93.3, 68.0, 39.6, 13.3; **HRMS (ES)** calculated for $C_{31}H_{33}N_8O_4$ ($[M+H]^+$) m/z: 581.2619, found 581.2637.

2,6-[Di(4-{2-pyrrolidinyl-ethoxy}quinolin-2-yl)diureido]toluene (3b)

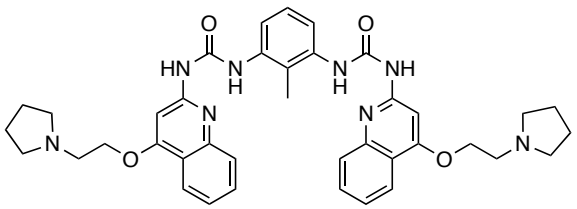

Following procedure **G1**, **5b** (62 mg, 0.220 mmol) was reacted with 2,6-toluene diisocyanate (**6c**, 21 mg, 0.120 mmol) to afford the TFA salt of the title compound (**3b**·2CF_3CO_2H, 103 mg, 0.110 mmol, 92%); **^{1}H-NMR** (500 MHz, D_2O) $\boldsymbol{\delta_H}$ 8.23 (2H, *dd*, *J* 8.0, 1.0 Hz, C<u>H</u> (ar)), 7.88 (2H, *dd*, *J* 8.0, 1.0 Hz, C<u>H</u> (ar)), 7.79 (2H, *d*, *J* 8.0 Hz, C<u>H</u> (ar)), 7.76 (2H, *ddd*, *J* 8.0, 6.5, 1.0 Hz, C<u>H</u> (ar)), 7.48 (2H, *ddd*, *J* 8.0, 6.5, 1.0 Hz, C<u>H</u> (ar)), 7.23 (1H, *t*, *J* 8.0 Hz, C<u>H</u> (ar)), 6.87

(2H, *s*, C<u>H</u> (ar)), 4.55-4.52 (4H, *m*, OC<u>H</u>$_2$), 3.86-3.79 (4H, *m*, OCH$_2$C<u>H</u>$_2$), 3.76-3.65 (4H, *m*, NC<u>H</u>$_2$(CH$_2$)$_2$), 3.30-3.20 (4H, *m*, NC<u>H</u>$_2$(CH$_2$)$_2$), 3.56 (3H, *s*, C<u>H</u>$_3$), 2.13-2.04 (4H, *m*, NCH$_2$C<u>H</u>$_2$CH$_2$), 1.96-1.88 (4H, *m*, NCH$_2$C<u>H</u>$_2$CH$_2$); **^{13}C-NMR** (125 MHz, D$_2$O) 161.8, 153.6, 152.6, 145.0, 137.4, 131.2, 126.0, 125.2, 124.1, 122.4, 119.8, 117.9, 117.2, 114.7, 112.5, 92.7, 64.4, 54.1, 52.7, 22.7, 13.6; **HRMS (ES)** calculated for $C_{39}H_{45}N_8O_4$ ([M+H]$^+$) m/z: 689.3564, found 689.3574.

4-(2-*tert*-Butoxycarbonylamino-ethoxy)-quinolin-2-ylamine (5a)

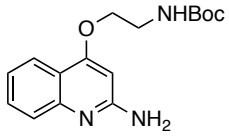

2-Aminoquinolin-4(1*H*)-one (**4**, 1.0 g, 6.2 mmol), *N*-Boc-ethanolamine (1.5 g, 9.3 mmol) and triphenylphosphine (3.3 g, 12.6 mmol) were dissolved in freshly distilled THF (100 ml) and cooled to 0 °C. DIAD (1.8 ml, 9.4 mmol) was added dropwise under argon. The mixture was allowed to warm to rt and stirred for 3 d. The solvent was removed *in vacuo* and the product purified by column chromatography (90% EtOAc, 10% MeOH) to obtain the title compound as a white powder (1.2 g, 4.0 mmol, 65%). **^{1}H-NMR** (500 MHz, CDCl$_3$) $\boldsymbol{\delta_H}$ 7.97 (1H, *dd*, *J* 8.0, 1.0 Hz, C<u>H</u> (ar)), 7.59 (1H, *dd*, *J* 8.5, 1.0 Hz, C<u>H</u> (ar)), 7.54 (1H, *ddd*, *J* 8.5, 7.0, 1.0 Hz, C<u>H</u> (ar)), 7.23 (1H, *ddd*, *J* 8.0, 7.0, 1.0 Hz, C<u>H</u> (ar)), 6.02 (1H, *s*, C<u>H</u> (ar)), 5.00 (1H, *br s*, N<u>H</u>Boc), 4.71-4.69 (2H, *m*, OC<u>H</u>$_2$), 4.17-4.13 (2H, *m*, N<u>H</u>$_2$), 3.69-3.66 (2H, *m*, OCH$_2$C<u>H</u>$_2$), 1.47 (9H, *s*, C<u>H</u>$_3$); **^{13}C-NMR** (125 MHz, CDCl$_3$) $\boldsymbol{\delta_C}$ 162.3, 158.0, 155.9, 148.5, 130.3, 125.7, 122.0, 121.6, 117.5, 90.1, 79.8, 67.5, 39.8, 28.4; **HRMS (ES)** calculated for $C_{16}H_{22}N_3O_3$ ([M+H]$^+$) m/z: 304.1650, found 304.1668.

4-(2-Pyrrolidinyl-ethoxy)-quinolin-2-ylamine (5b)

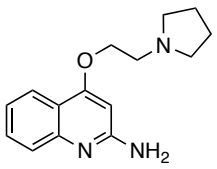

2-Aminoquinolin-4(1*H*)-one (**4**, 1.5 g, 9.4 mmol), *N*-(2-hydroxyethyl)-pyrrolidine (1.7 g, 14.5 mmol) and triphenylphosphine (4.9 g, 18.6 mmol) were dissolved in freshly distilled THF (100 ml) and cooled to 0 °C. DIAD (2.7 g, 14.1 mmol) was added dropwise under argon. The mixture was allowed to warm to rt and stirred for 3 d. The solvent was removed *in vacuo* and the product purified by column chromatography (87% EtOAc, 10% MeOH, 3% TEA) to obtain the title compound as a pale yellow powder (1.3 g, 5.0 mmol, 53%). **^{1}H-NMR** (400 MHz, CD_3OD) $\boldsymbol{\delta_H}$ 8.00 (1H, *dd*, *J* 8.0, 1.0 Hz, C<u>H</u> (ar)), 7.53 (1H, *dd*, *J* 8.0, 1.5 Hz, C<u>H</u> (ar)), 7.48 (1H, *ddd*, *J* 8.0, 6.5, 1.0 Hz, C<u>H</u> (ar)), 7.20 (1H, *ddd*, *J* 8.0, 6.5, 1.5 Hz, C<u>H</u> (ar)), 6.28 (1H, *s*, C<u>H</u> (ar)), 4.33 (2H, *t*, *J* 5.5 Hz, OC<u>H_2</u>), 3.10 (2H, *t*, *J* 5.5 Hz, OCH_2C<u>H_2</u>), 2.81-2.73 (4H, *m*, NC<u>H_2</u>$(CH_2)_2$), 1.94-1.82 (4H, *m*, NCH_2C<u>H_2</u>CH_2); **^{13}C-NMR** (100 MHz, CD_3OD) $\boldsymbol{\delta_C}$ 163.0, 160.3, 148.0, 130.2, 124.1, 121.9, 121.6, 110.8, 90.4, 67.6, 54.8, 54.6, 23.3; **HRMS (ES)** calculated for $C_{15}H_{20}N_3O$ ($[M+H]^+$) m/z: 258.1606, found 258.1611.

Chelidamic acid dimethyl ester (9)

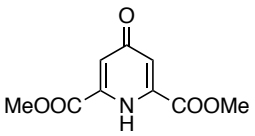

MeOH (100 ml) was cooled to -10 °C. $SOCl_2$ (40 ml) was added slowly and dropwise under stirring. Chelidamic acid (**8**, 10.0 g, 54.6 mmol) was added and the resulting mixture stirred at rt overnight. The solvent was removed *in vacuo*. The product was dissolved in H_2O (100 ml). The crude product crashed out, was filtered and recrystallised from hot EtOH to obtain the title compound as white

crystals (9.1 g, 43.2 mmol, 85%). **M.p.** 168.5-169.0 °C; **^{1}H-NMR** (400 MHz, CD_3OD) $\boldsymbol{\delta_H}$ 7.39 (2H, *br s*, C<u>H</u>), 3.92 (6H, *s*, C<u>H</u>$_3$). The spectroscopic data were in agreement with the literature.[184]

4-(2-((*tert*-Butoxycarbonyl)amino)ethoxy)pyridine-2,6 dicarboxylate (11a)

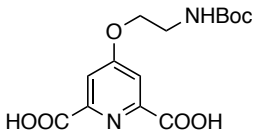

Compound **9** (1.5 g, 7.1 mmol), *N*-Boc-ethanolamine (1.7 g, 10.5 mmol) and triphenylphosphine (3.7 g, 14.1 mmol) were dissolved in freshly distilled THF (50 ml) and cooled to 0 °C. DIAD (1.9 ml, 9.9 mmol) was added dropwise under argon. The mixture was allowed to warm to rt and stirred for 3 d. The solvent was removed *in vacuo* and the product purified by column chromatography (50% EtOAc, 50% petroleum ether) to obtain the dimethyl ester of the title compound as a white powder. This compound was dissolved in MeOH (50 ml) and deprotected by slowly adding a solution of NaOH (0.4 g, 10.6 mmol) in H_2O (50 ml). The solvent was evaporated *in vacuo* and the remaining solid dissolved in H_2O. The solution was acidified with 5% HCOOH (aq.) and extracted with EtOAc. The organic layer was dried over $MgSO_4$, filtered, and the solvent removed *in vacuo* to obtain the title compound as a white powder (1.5 g, 4.6 mmol, 64%). **^{1}H-NMR** (500 MHz, CD_3OD) $\boldsymbol{\delta_H}$ 7.86 (2H, *s*, C<u>H</u> (ar)), 4.26 (2H, *t*, *J* 5.0 Hz, OC<u>H</u>$_2$), 3.49 (2H, *t*, *J* 5.0 Hz, OCH$_2$C<u>H</u>$_2$), 1.42 (9H, *s*, C<u>H</u>$_3$); **^{13}C-NMR** (125 MHz, CD_3OD) $\boldsymbol{\delta_C}$ 169.4, 167.0, 158.4, 150.3, 115.2, 80.5, 69.6, 40.7, 28.6; **HRMS (ES)** calculated for $C_{14}H_{17}N_2O_7$ ($[M\text{-}H]^-$) m/z: 325.1041, found 325.1046.

4-(2-(Pyrrolidin-1-yl)ethoxy)pyridine-2,6 dicarboxylate (11b)

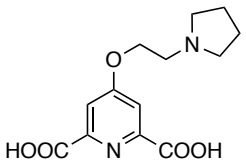

Compound **9** (1.0 g, 4.7 mmol), *N*-hydroxyethyl-pyrrolidine (0.8 ml, 9.4 mmol) and triphenylphosphine (2.5 g, 9.4 mmol) were dissolved in freshly distilled THF (50 ml) and cooled to 0 °C. DIAD (1.8 ml, 9.4 mmol) was added dropwise under argon. The mixture was allowed to warm to rt and stirred for 3 d. The solvent was removed *in vacuo* and the product purified by column chromatography (50% EtOAc, 49% petroleum ether, 1% TEA) to obtain the dimethyl ester of the title compound as a white powder. This compound was dissolved in MeOH (50 ml) and deprotected by slowly adding a solution of NaOH (0.4 g, 10.3 mmol) in H_2O (50 ml). The solvent was evaporated *in vacuo* and the remaining solid dissolved in H_2O. The product was purified by HPLC (gradient: 10% MeCN/90% H_2O, 0.1% TFA to 100% MeCN, 0.1% TFA over 30 min, R_t=7.0-7.5 min) to obtain the TFA salt of the title compound (**11b**·CF_3CO_2H, 1.3 g, 3.1 mmol, 66%). **^{1}H-NMR** (400 MHz, D_2O) $\boldsymbol{\delta_H}$ 7.39 (2H, *s*, C<u>H</u> (ar)), 4.21 (2H, *t*, *J* 5.5 Hz, OC<u>H</u>$_2$), 2.94 (2H, *t*, *J* 5.5 Hz, OCH$_2$C<u>H</u>$_2$), 2.71-2.59 (4H, *m*, NC<u>H</u>$_2$(CH$_2$)$_2$), 1.75-1.62 (4H, *m*, NCH$_2$C<u>H</u>$_2$CH$_2$); **^{13}C-NMR** (100 MHz, D_2O) $\boldsymbol{\delta_C}$ 173.2, 166.8, 155.3, 111.7, 66.6, 54.1, 53.9, 23.1; **HRMS (ES)** calculated for $C_{13}H_{16}N_2NaO_5$ ([M+Na]$^+$) m/z: 303.0951, found 303.0962.

4-(Prop-2-yn-1-yloxy)pyridine-2,6 dicarboxylate (11c)

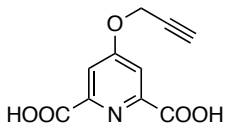

Compound **9** (0.8 g, 3.5 mmol), propargyl alcohol (0.3 ml, 4.6 mmol) and triphenylphosphine polymer bound (1.6 g, 3.0 mmol loading/ g) were added to freshly

distilled THF (50 ml) and cooled to 0 °C. DIAD (0.9 ml, 4.9 mmol) was added dropwise under argon. The mixture was allowed to warm to rt and stirred for 3 d. The solution was filtered and the solvent was removed *in vacuo* and the product purified by column chromatography (50% EtOAc, 50% petroleum ether) to obtain the dimethyl ester of the title compound as a white powder. This compound was dissolved in MeOH (50 ml) and deprotected by slowly adding a solution of NaOH (0.3 g, 7.7 mmol) in H_2O (50 ml). The solvent was evaporated *in vacuo* and the remaining solid dissolved in H_2O. The solution was acidified with 5% HCOOH (aq.) and extracted with EtOAc. The organic layer was dried over $MgSO_4$, filtered, and the solvent removed *in vacuo* to obtain the title compound as a white powder (0.6 g, 2.7 mmol, 77%). **^{1}H-NMR** (400 MHz, CD_3OD) $\boldsymbol{\delta_H}$ 7.95 (2H, *s*, C<u>H</u> (ar)), 5.04 (2H, *d*, *J* 2.5 Hz, OC<u>H</u>$_2$), 3.16 (1H, *t*, *J* 2.5 Hz, C<u>H</u>); **^{13}C-NMR** (100 MHz, CD_3OD) $\boldsymbol{\delta_C}$ 167.1, 165.9, 149.5, 114.4, 78.8, 76.8, 56.5; **HRMS (ES)** calculated for $C_{10}H_8NO_5$ ($[M+H]^+$) m/z: 222.0402, found 222.0398.

4-(4-Fluoro-benzyloxy)-pyridine-2,6 dicarboxylate (11d)

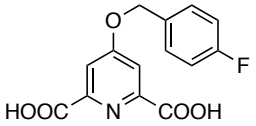

Compound **9** (0.7 g, 3.5 mmol), (4-fluorophenyl)methanol (0.6 g, 4.6 mmol) and triphenylphosphine (1.8 g, 7.0 mmol) were dissolved in freshly distilled THF (50 ml) and cooled to 0 °C. DIAD (1.0 ml, 5.0 mmol) was added dropwise under argon. The mixture was allowed to warm to rt and stirred for 3 d. The solvent was removed *in vacuo* and the product purified by column chromatography (50% EtOAc, 50% petroleum ether) to obtain the dimethyl ester of the title compound as a white powder. This compound was dissolved in MeOH (50 ml) and deprotected by slowly adding a solution of NaOH (0.3 g, 7.7 mmol) in H_2O (50 ml). The solvent was evaporated *in vacuo* and the remaining solid dissolved in H_2O. The solution was acidified with 5% HCOOH (aq.) and extracted with EtOAc. The organic layer was dried over $MgSO_4$, filtered, and the solvent removed *in vacuo* to obtain the title compound as a white powder (0.7 g, 2.0 mmol, 57%).

^{1}H-NMR (400 MHz, $CDCl_3$) $\boldsymbol{\delta_H}$ 7.88 (2H, *s*, C<u>H</u> (ar)), 7.45-7.40 (2H, *m*, C<u>H</u> (ar)), 7.14-7.07 (2H, *m*, C<u>H</u> (ar)), 5.20 (2H, *s*, OC<u>H</u>$_2$), 4.01; **^{13}C-NMR** (100 MHz, $CDCl_3$) $\boldsymbol{\delta_C}$ 166.5, 165.8, 162.9 (*d*, *J* 246 Hz), 149.9, 130.5, 122.7 (*d*, *J* 8 Hz), 115.8 (*d*, *J* 22 Hz), 114.7, 70.1; **HRMS (ES)** calculated for $C_{16}H_{11}FNO_5$ ($[M+H]^+$) m/z: 292.0621, found 292.0632.

Dimethyl 4-chloropyridine-2,6 dicarboxylate (12)

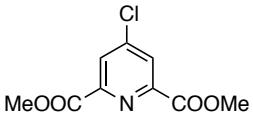

Chelidamic acid (**8**, 10.0 g, 54.6 mmol) was dissolved in $SOCl_2$ (100 ml) and refluxed overnight. The solvent was removed *in vacuo* and a yellow solid was obtained, which was quenched with freshly distilled MeOH (100 ml) at 0 °C. The excess solvent was then removed *in vacuo*. The crude product was dissolved in sat. aq. $NaHCO_3$ solution (200 ml) and extracted with EtOAc (100 ml) to afford the title compound as a white powder (3.5 g, 16.1 mmol, 28%). **^{1}H-NMR** (500 MHz, $CDCl_3$) $\boldsymbol{\delta_H}$ 8.28 (2H, *s*, C<u>H</u> (ar)), 4.02 (6H, *s*, C<u>H</u>$_3$); **^{13}C-NMR** (125 MHz, $CDCl_3$) $\boldsymbol{\delta_C}$ 164.1, 149.4, 146.8, 128.3, 53.5; **HRMS (ES)** calculated for $C_9H_9ClNO_4$ ($[M+H]^+$) m/z: 230.0215, found 230.0206.

4-Chloropyridine-2,6 dicarboxylate (13)

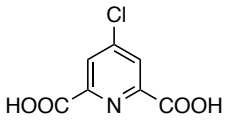

Compound **12** (1.0 g, 4.3 mmol) was dissolved in MeOH (100 ml) and deprotected by slowly adding a solution of NaOH (0.4 g, 9.5 mmol) in H_2O (100 ml). The solvent was evaporated *in vacuo* and the remaining solid dissolved in H_2O. The solution was acidified with 5% HCOOH (aq.) and extracted with EtOAc. The

organic layer was dried over $MgSO_4$, filtered, and the solvent removed *in vacuo* to obtain the title compound as a white powder (0.9 g, 4.3 mmol, 99%). **^{1}H-NMR** (500 MHz, CD_3OD) $\boldsymbol{\delta_H}$ 8.34 (2H, *s*, C<u>H</u> (ar)); **^{13}C-NMR** (125 MHz, $CDCl_3$) $\boldsymbol{\delta_C}$ 166.1, 150.6, 148.5, 129.0; **HRMS (ES)** calculated for $C_7H_5ClNO_4$ ($[M+H]^+$) m/z: 201.9901, found 201.9894.

Dimethyl 4-methoxypyridine-2,6 dicarboxylate (14).

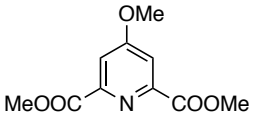

Chelidamic acid (**8**, 0.2 g, 1.1 mmol) was dissolved in a 3:2 mixture of PhMe:MeOH (50 ml). Me_3SiCHN_2 (2 M, 1.8 ml, 3.5 mmol) was added dropwise and the reaction left to stir for 30 min at rt. The solvent was removed *in vacuo* and the crude product dissolved in sat. aq. $NaHCO_3$ solution. The aqueous layer was extracted with EtOAc and the organic layer dried over $MgSO_4$, filtered, and the solvent removed *in vacuo* to obtain the product as a white powder (0.2 g, 0.9 mmol, 90%). **^{1}H-NMR** (400 MHz, DMSO-d_6) $\boldsymbol{\delta_H}$ 7.60 (2H, *s*, C<u>H</u> (ar)), 3.84 (3H, *s*, OC<u>H</u>$_3$), 3.77 (6H, *s*, COOC<u>H</u>$_3$); **^{13}C-NMR** (100 MHz, DMSO-d_6) $\boldsymbol{\delta_C}$ 167.6, 165.2, 149.9, 114.3, 56.7, 53.0; **HRMS (ES)** calculated for $C_{10}H_{12}NO_5$ ($[M+H]^+$) m/z: 226.0715, found 226.0721.

4-Methoxypyridine-2,6 dicarboxylate (15).

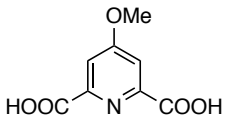

Compound **14** (0.2 g, 0.9 mmol) was dissolved in MeOH (50 ml) and deprotected by slowly adding a solution of NaOH (0.1 g, 1.9 mmol) in H_2O (50 ml). The solvent was evaporated *in vacuo* and the remaining solid dissolved in H_2O. The

solution was acidified with 5% HCOOH (aq.) and extracted with EtOAc. The organic layer was dried over $MgSO_4$, filtered, and the solvent removed *in vacuo* to obtain the title compound as a white powder (0.2 g, 0.9 mmol, 99%). **^{1}H-NMR** (400 MHz, CD_3OD) $\boldsymbol{\delta_H}$ 7.58 (2H, *s*, C<u>H</u> (ar)), 3.84 (3H, *s*, C<u>H</u>$_3$); **^{13}C-NMR** (125 MHz, $CDCl_3$) $\boldsymbol{\delta_C}$ 168.0, 165.7, 150.2, 113.7, 56.6; **HRMS (ES)** calculated for $C_8H_6NO_5$ ($[M\text{-}H]^-$) m/z: 196.0246, found 196.0237.

4-(2-*tert*-Butoxycarbonylamino-propoxy)-quinolin-2-ylamine (16a)

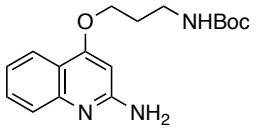

2-Aminoquinolin-4(1*H*)-one (**4**, 1.0 g, 6.2 mmol), *N*-Boc-propanolamine (1.6 g, 9.1 mmol) and triphenylphosphine (3.3 g, 12.6 mmol) were dissolved in freshly distilled THF (10 ml) and cooled to 0 °C. DIAD (1.8 ml, 9.4 mmol) was added dropwise under argon. The mixture was allowed to warm to rt and stirred for 3 d. The solvent was removed *in vacuo* and the product purified by column chromatography (90% EtOAc, 10% MeOH) to obtain the title compound as a white powder (1.4 g, 4.4 mmol, 71%). **^{1}H-NMR** (400 MHz, CD_3OD) $\boldsymbol{\delta_H}$ 7.98 (1H, *dd*, *J* 8.0, 1.0 Hz, C<u>H</u> (ar)), 7.55-7.45 (2H, *m*, C<u>H</u> (ar)), 7.19 (1H, *ddd*, *J* 8.0, 6.5, 1.0 Hz, C<u>H</u> (ar)), 6.42 (1H, *s*, C<u>H</u> (ar)); 4.21 (2H, *t*, *J* 6.0 Hz, OC<u>H</u>$_2$), 3.40-3.30 (2H, *m*, $OCH_2C\underline{H}_2$), 2.15-2.04 (2H, *m*, $O(CH_2)_2C\underline{H}_2$), 1.43 (9H, *s*, C<u>H</u>$_3$); **^{13}C-NMR** (100 MHz, CD_3OD) $\boldsymbol{\delta_C}$ 163.0, 160.2, 157.6, 148.0, 130.2, 124.1, 122.0, 121.5, 117.7, 90.3, 79.0, 66.3, 37.5, 29.7, 27.8; **HRMS (ES)** calculated for $C_{17}H_{24}N_3O_3$ ($[M+H]^+$) m/z: 318.1812, found 318.1824.

4-(2-(Dimethylamino)ethoxy)quinolin-2-amine (16b)

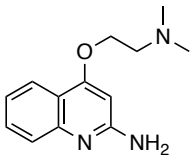

2-Aminoquinolin-4(1*H*)-one (**4**, 1.0 g, 6.3 mmol), 3-dimethylaminoethanol (0.7 g, 7.8 mmol) and triphenylphosphine (3.3 g, 12.6 mmol) were dissolved in freshly distilled THF (100 ml) and cooled to 0 °C. DIAD (1.2 g, 5.9 mmol) was added dropwise under argon. The mixture was allowed to warm to rt and stirred for 3 d. The solvent was removed *in vacuo* and the product purified by column chromatography (87% EtOAc, 10% MeOH, 3% TEA) to obtain the title compound as a pale yellow powder (1.0 g, 4.3 mmol, 68%). **^{1}H-NMR** (400 MHz, CD_3OD) $\boldsymbol{\delta_H}$ 8.01 (1H, *dd*, *J* 8.0, 1.0 Hz, C<u>H</u> (ar)), 7.55-7.43 (2H, *m*, C<u>H</u> (ar)), 7.20 (1H, *ddd*, *J* 8.0, 6.5, 1.0, C<u>H</u> (ar)), 6.27 (1H, *s*, C<u>H</u> (ar)); 4.31 (2H, *t*, *J* 5.5 Hz, OC<u>H</u>$_2$), 2.95 (2H, *t*, *J* 5.5 Hz, $OCH_2C\underline{H}_2$), 2.43 (6H, *s*, C<u>H</u>$_3$); **^{13}C-NMR** (100 MHz, CD_3OD) $\boldsymbol{\delta_C}$ 162.8, 160.0, 148.0, 130.3, 123.9, 122.0, 121.7, 117.6, 90.5, 66.5, 57.7, 45.1; **HRMS (ES)** calculated for $C_{13}H_{18}N_3O$ ($[M+H]^+$) m/z: 232.1444, found 232.1449.

4-(3-Dimethylaminopropoxy)quinolin-2-amine (16c)

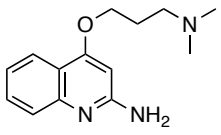

2-Aminoquinolin-4(1*H*)-one (**4**, 1.0 g, 6.3 mmol), 3-dimethylamino-1-propanol (0.8 g, 7.8 mmol) and triphenylphosphine (3.3 g, 12.6 mmol) were dissolved in of freshly distilled THF (100 ml) and cooled to 0 °C. DIAD (1.2 g, 5.9 mmol) was added dropwise under argon. The mixture was allowed to warm to rt and stirred for 3 d. The solvent was removed *in vacuo* and the product purified by column chromatography (87% EtOAc, 10% MeOH, 3% TEA) to obtain the title

compound as a pale yellow powder (1.0 g, 4.1 mmol, 65%). **^{1}H-NMR** (400 MHz, CD_3OD) $\boldsymbol{\delta_H}$ 7.95 (1H, *dd*, *J* 8.0, 1.5 Hz, C<u>H</u> (ar)), 7.55-7.45 (2H, *m*, C<u>H</u> (ar)), 7.20 (1H, *ddd*, *J* 8.0, 6.5, 1.5 Hz, C<u>H</u> (ar)), 6.25 (1H, *s*, C<u>H</u> (ar)); 4.22 (2H, *t*, *J* 5.5 Hz, OC<u>H$_2$</u>), 2.65-2.60 (2H, *m*, OCH_2C<u>H$_2$</u>), 2.34 (6H, *s*, C<u>H$_3$</u>), 2.18-2.10 (2H, *m*, $O(CH_2)_2C$<u>H$_2$</u>); **^{13}C-NMR** (100 MHz, CD_3OD) $\boldsymbol{\delta_C}$ 162.9, 160.0, 147.9, 130.2, 123.9, 121.7, 121.6, 117.6, 90.4, 66.7, 56.3, 44.5, 26.9; **HRMS (ES)** calculated for $C_{14}H_{20}N_3O$ ($[M+H]^+$) m/z: 246.1600, found 246.1601.

4-Methoxyquinolin-2-ylamine (17)

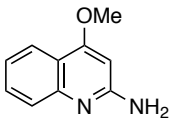

2-Aminoquinolin-4(1*H*)-one (**4**, 0.3 g, 1.9 mmol) was dissolved in a solution of PhMe:MeOH (50 ml). Me_3SiCHN_2 (2 M, 2.0 ml, 4.0 mmol) was added dropwise and the reaction left to stir for 30 min at rt. The solvent was removed *in vacuo* and the crude product dissolved in aq. NaOH (0.1 M) solution. The aq. layer was extracted with EtOAc and the organic layer dried over $MgSO_4$, filtered, and the solvent removed *in vacuo* to obtain the product as a white powder (0.2 g, 1.1 mmol, 55%). **^{1}H-NMR** (400 MHz, CD_3OD) $\boldsymbol{\delta_H}$ 7.93 (1H, *br d*, *J* 8.5 Hz, C<u>H</u> (ar)), 7.53-7.44 (2H, *m*, C<u>H</u> (ar)); 7.21-7.15 (1H, *m*, C<u>H</u> (ar)), 6.26 (1H, *s*, C<u>H</u> (ar)), 3.23 (3H, *s*, C<u>H$_3$</u>); **^{13}C-NMR** (100 MHz, CD_3OD) $\boldsymbol{\delta_C}$ 163.8, 160.5, 148.1, 130.1, 124.1, 122.7, 121.6, 118.7, 89.8, 89.8; **HRMS (ES)** calculated for $C_{10}H_{11}N_2O$ ($[M+H]^+$) m/z: 175.0871, found 175.0861.

N^2,N^6-*bis*(4-(2-Aminoethoxy)quinolin-2-yl)pyridine-2,6 dicarboxamide (18)

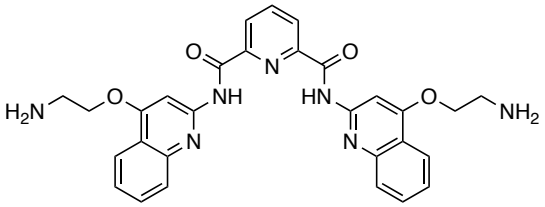

Following procedure **G2**, **7** (50 mg, 0.245 mmol), **5a** (150 mg, 0.495 mmol) and TEA (75 µl, 0.539 mmol) were reacted to afford the TFA salt of the title compound as a white powder (**18**·2CF_3CO_2H, 120 mg, 0.151 mmol, 62%). **^{1}H-NMR** (400 MHz, CD_3OD) $\boldsymbol{\delta_H}$ 8.70 (2H, *d*, *J* 8.0 Hz, C<u>H</u> (ar)), 8.56 (2H, *dd*, *J* 8.0, 1.0 Hz, C<u>H</u> (ar)), 8.46 (1H, *t*, *J* 8.0 Hz, C<u>H</u> (ar)), 8.20 (2H, *s*, C<u>H</u> (ar)), 8.14 (2H, *br d*, *J* 8.5 Hz, C<u>H</u> (ar)), 8.02 (2H, *ddd*, *J* 8.5, 7.0, 1.0 Hz, C<u>H</u> (ar)), 7.76 (2H, *ddd*, *J* 8.0, 7.0, 1.0 Hz, C<u>H</u> (ar)), 4.83 (4H, *t*, *J* 5.0 Hz, OC<u>H_2</u>), 3.72 (4H, *t*, *J* 5.0 Hz, OCH_2C<u>H_2</u>); **^{13}C-NMR** (100 MHz, CD_3OD) $\boldsymbol{\delta_C}$ 166.5, 164.3, 151.4, 147.9, 141.2, 141.0, 134.9, 127.5, 127.0, 123.3, 122.5, 119.0, 94.3, 66.9, 38.8; **HRMS (ES)** calculated for $C_{29}H_{28}N_7O_4$ ($[M+H]^+$) m/z: 538.2197, found 538.2183.

N^2,N^6-*bis*(4-(3-Aminopropoxy)quinolin-2-yl)pyridine-2,6 dicarboxamide (19)

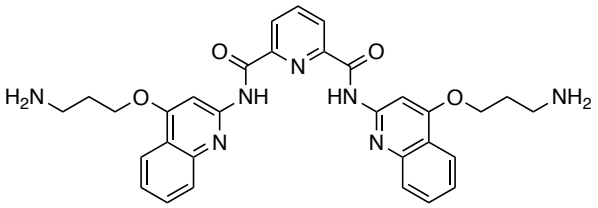

Following procedure **G2**, **7** (50 mg, 0.245 mmol), **16a** (150 mg, 0.473 mmol) and TEA (75 µl, 0.539 mmol) were reacted to afford the TFA salt of the title compound as a white powder (**19**·2CF_3CO_2H, 150 mg, 0.891 mmol, 77%). **^{1}H-NMR** (400 MHz, CD_3OD) $\boldsymbol{\delta_H}$ 8.69 (2H, *d*, *J* 8.0 Hz, C<u>H</u> (ar)), 8.48 (1H, *t*,

J 8.0 Hz, C<u>H</u> (ar)), 8.39 (2H, *br d*, *J* 8.5 Hz, C<u>H</u> (ar)), 8.16-8.11 (4H, *m*, C<u>H</u> (ar)), 8.05-8.00 (2H, *m*, C<u>H</u> (ar)), 7.78-7.73 (2H, *m*, C<u>H</u> (ar)), 4.74-4.68 (4H, *m*, OC<u>H</u>$_2$), 3.40-3.34 (4H, *m*, OCH$_2$C<u>H</u>$_2$), 2.52-2.44 (4H, *m*, O(CH$_2$)$_2$C<u>H</u>$_2$); **^{13}C-NMR** (100 MHz, CD$_3$OD) $\boldsymbol{\delta_C}$ 167.4, 163.7, 151.3, 147.8, 141.1, 140.2, 133.8, 127.6, 127.1, 123.0, 121.9, 119.1, 94.3, 67.9, 37.1, 27.0; **HRMS (ES)** calculated for $C_{31}H_{32}N_7O_4$ ([M+H]$^+$) m/z: 566.2510, found 566.2498.

N^2,N^6*bis*(4-(2-(Pyrrolidin-1-yl)ethoxy)quinolin-2-yl)pyridine-2,6 dicarboxamide (20)

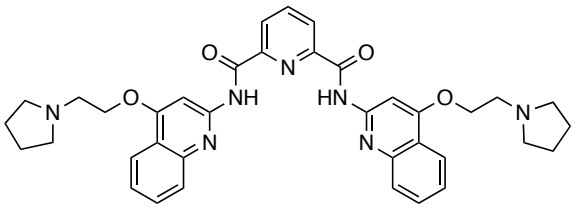

Following procedure **G2**, **7** (50 mg, 0.245 mmol), **5b** (151 mg, 0.587 mmol) and TEA (75 µl, 0.539 mmol) were reacted to afford the TFA salt of the title compound as a pale yellow powder (**20**·2CF$_3$CO$_2$H, 175 mg, 0.200 mmol, 82%). **^{1}H-NMR** (400 MHz, CD$_3$OD) $\boldsymbol{\delta_H}$ 8.46 (2H, *d*, *J* 8.0 Hz, C<u>H</u> (ar)), 8.38 (1H, *t*, *J* 8.0 Hz, C<u>H</u> (ar)), 8.33 (2H, *br d*, *J* 8.0 Hz, C<u>H</u> (ar)), 8.19 (2H, *s*, C<u>H</u> (ar)), 7.98 (2H, *br d*, *J* 8.5 Hz, C<u>H</u> (ar)), 7.83 (2H, *ddd*, *J* 8.5, 7.0, 1.0 Hz, C<u>H</u> (ar)), 7.57 (2H, *ddd*, *J* 8.0, 7.0, 1.0 Hz, C<u>H</u> (ar)), 4.66 (4H, *t*, *J* 4.0 Hz, OC<u>H</u>$_2$), 3.85 (4H, *t*, *J* 4.0 Hz, OCH$_2$C<u>H</u>$_2$), 3.81-3.69 (4H, *m*, NC<u>H</u>$_2$(CH$_2$)$_2$), 3.38-3.28 (4H, *m*, NC<u>H</u>$_2$(CH$_2$)$_2$), 2.17-2.04 (4H, *m*, NCH$_2$C<u>H</u>$_2$CH$_2$), 2.04-1.88 (4H, *m*, NCH$_2$C<u>H</u>$_2$CH$_2$); **^{13}C-NMR** (100 MHz, CD$_3$OD) $\boldsymbol{\delta_C}$ 163.8, 162.1, 158.9, 158.5, 152.8 147.2, 131.1, 127.0, 126.5, 125.1, 122.5, 119.0, 95.6, 64.8, 54.6, 53.1, 23.0; **HRMS (ES)** calculated for $C_{37}H_{40}N_7O_4$ ([M+H]$^+$) m/z: 646.3142, found 646.3168.

N^2,N^6-*bis*(4-(2-(Dimethylamino)ethoxy)quinolin-2-yl)pyridine-2,6 dicarboxamide (21)

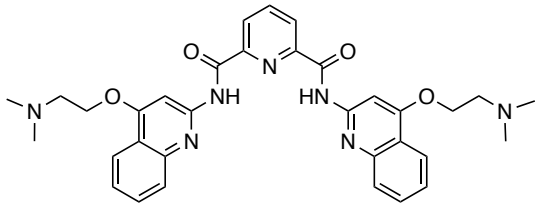

Following procedure **G2**, **7** (50 mg, 0.245 mmol), **16b** (113 mg, 0.489 mmol) and TEA (75 µl, 0.539 mmol) were reacted to afford the TFA salt of the title compound as a white powder (**21**·2CF_3CO_2H, 138 mg, 0.168 mmol, 68%). **^{1}H-NMR** (400 MHz, CD_3OD) $\boldsymbol{\delta_H}$ 8.70 (2H, *d*, *J* 8.0 Hz, C<u>H</u> (ar)), 8.50-8.48 (3H, *m*, C<u>H</u> (ar)), 8.24 (2H, *s*, C<u>H</u> (ar)), 8.14 (2H, *br d*, *J* 8.0 Hz, C<u>H</u> (ar)), 8.03-7.98 (2H, *m*, C<u>H</u> (ar)), 7.76-7.72 (2H, *m*, C<u>H</u> (ar)), 4.98-4.92 (4H, *m*, OC<u>H_2</u>), 3.98-3.93 (4H, *m*, OCH_2C<u>H_2</u>), 3.16 (12H, *s*, C<u>H_3</u>); **^{13}C-NMR** (100 MHz, CD_3OD) $\boldsymbol{\delta_C}$ 165.6, 163.5, 151.5, 147.9, 142.1, 141.0, 133.5, 127.4, 126.9, 123.2, 119.1, 118.1, 94.6, 64.7, 56.2, 43.2; **HRMS (ES)** calculated for $C_{33}H_{36}N_7O_4$ ($[M+H]^+$) m/z: 594.2829, found 594.2825.

N^2,N^6-*bis*(4-(3-(Dimethylamino)propoxy)quinolin-2-yl)pyridine-2,6 dicarboxamide (22)

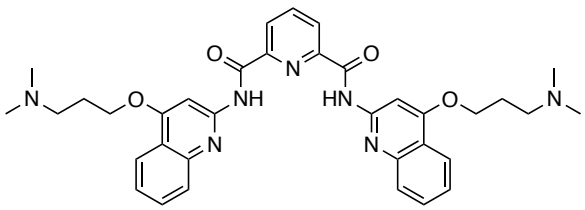

Following procedure **G2**, **7** (50 mg, 0.245 mmol), **16c** (120 mg, 0.489 mmol) and TEA (75 µl, 0.539 mmol) were reacted to afford the TFA salt of the title compound as a white powder (**22**·2CF_3CO_2H, 148 mg, 0.174 mmol, 71%). **^{1}H-NMR** (400 MHz, CD_3OD) $\boldsymbol{\delta_H}$ 8.66 (2H, *d*, *J* 8.0 Hz, C<u>H</u> (ar)), 8.45 (1H, *t*, *J* 8.0 Hz, C<u>H</u>

(ar)), 8.41 (2H, *br d*, *J* 8.0 Hz, CH (ar)), 8.16-8.05 (4H, *m*, CH (ar)), 8.04-8.00 (2H, *m*, CH (ar)), 7.78-7.73 (2H, *m*, CH (ar)), 4.72-4.66 (4H, *m*, OCH_2), 3.60-3.51 (4H, *m*, OCH_2CH_2), 3.04 (12H, *s*, CH_3), 2.62-2.50 (4H, *m*, $O(CH_2)_2CH_2$); **^{13}C-NMR** (100 MHz, CD_3OD) $\boldsymbol{\delta_C}$ 167.5, 163.7, 151.2, 147.7, 141.0, 140.0, 133.8, 127.6, 127.2, 123.3, 121.7, 119.0, 94.3, 67.7, 55.1, 42.6, 24.5; **HRMS (ES)** calculated for $C_{35}H_{40}N_7O_4$ ($[M+H]^+$) m/z: 622.3123, found 622.3119.

4-(2-Aminoethoxy)-N^2,N^6-*bis*(4-(2-aminoethoxy)quinolin-2-yl) pyridine-2,6 dicarboxamide (23, pyridostatin)

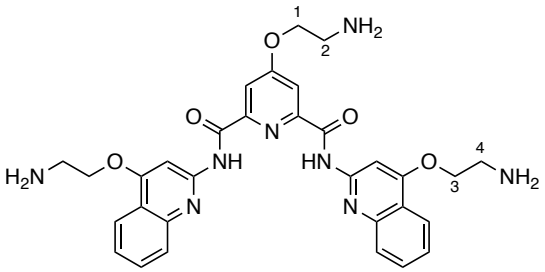

Following procedure **G3**, **11a** (110 mg, 0.337 mmol), **5a** (205 mg, 0.675 mmol), TEA (103 µl, 0.742 mmol) and 1-chloro-*N*,*N*,-2-trimethylpropenyl-amine (98 µl, 0.742 mmol) were reacted to afford the TFA salt of the title compound as a white powder (**23**·$3CF_3CO_2H$, 210 mg, 0.224 mmol, 66%). **^{1}H-NMR** (400 MHz, CD_3OD) $\boldsymbol{\delta_H}$ 8.43 (2H, *dd*, *J* 8.0, 1.0 Hz, CH (ar)), 8.16 (2H, *s*, CH (ar)), 8.16 (2H, *s*, CH (ar)), 7.98 (2H, *dd*, *J* 8.0, 1.0 Hz, CH (ar)), 7.83 (2H, *ddd*, *J* 8.0, 7.0, 1.0 Hz, CH (ar)), 7.61 (2H, *ddd*, *J* 8.5, 7.0, 1.0 Hz, CH (ar)), 4.68 (4H, *t*, *J* 5.5 Hz, OCH_2 (3)), 4.57 (2H, *t*, *J* 5.0 Hz, OCH_2 (1)), 3.63 (4H, *t*, *J* 5.5 Hz, OCH_2CH_2 (4)), 3.51 (2H, *t*, *J* 5.0 Hz, OCH_2CH_2 (2)); **^{13}C-NMR** (125 MHz, CD_3OD) $\boldsymbol{\delta_C}$ 169.0, 165.0, 164.0, 152.9, 151.9, 146.7, 132.9, 126.8, 126.8, 123.6, 120.5, 113.7, 95.7, 66.9, 66.7, 39.9, 39.9; **HRMS (ES)** calculated for $C_{31}H_{33}N_8O_5$ ($[M+H]^+$) m/z: 597.2574, found 597.2550.

4-(2-Aminoethoxy)-N^2,N^6-*bis*(4-(3-aminopropoxy)quinolin-2-yl)-pyridine-2,6 dicarboxamide (24)

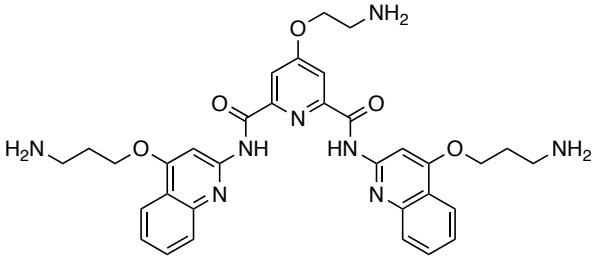

Following procedure **G3**, **11a** (76 mg, 0.223 mmol), **16a** (150 mg, 0.473 mmol), TEA (71 µl, 0.413 mmol) and 1-chloro-*N*,*N*,-2-trimethylpropenyl-amine (68 µl, 0.413 mmol) were reacted to afford the TFA salt of the title compound as a white powder (**24**·3CF_3CO_2H, 178 mg, 0.184 mmol, 79%). **^{1}H-NMR** (400 MHz, CD_3OD) $\boldsymbol{\delta_H}$ 8.37 (2H, *br d*, *J* 8.0 Hz, C<u>H</u> (ar)), 8.23 (2H, *s*, C<u>H</u> (ar)), 8.19 (2H, *s*, C<u>H</u> (ar)), 8.10 (2H, *br d*, *J* 8.0 Hz, C<u>H</u> (ar)), 8.02-7.95 (2H, *m*, C<u>H</u> (ar)), 7.76-7.69 (2H, *m*, C<u>H</u> (ar)), 4.73-4.61 (6H, *m*, OC<u>H_2</u>), 3.59-3.49 (2H, *m*, OCH_2C<u>H_2</u>N), 3.41-3.35 (4H, *m*, OCH_2C<u>H_2</u>CH_2), 2.52-2.42 (4H, *m*, $O(CH_2)_2C$<u>H_2</u>); **^{13}C-NMR** (100 MHz, CD_3OD) $\boldsymbol{\delta_C}$ 162.7, 157.9, 151.1, 149.9, 143.0, 132.7, 130.2, 128.1, 126.2, 123.1, 122.3, 118.9, 112.7, 93.9, 69.1, 66.9, 36.8, 26.7; **HRMS (ES)** calculated for $C_{33}H_{37}N_8O_5$ ($[M+H]^+$) m/z: 625.2887, found 625.2865.

4-(2-Aminoethoxy)-N^2,N^6-*bis*(4-(2-(pyrrolidin-1-yl)ethoxy) quinolin-2-yl)-pyridine-2,6 dicarboxamide (25)

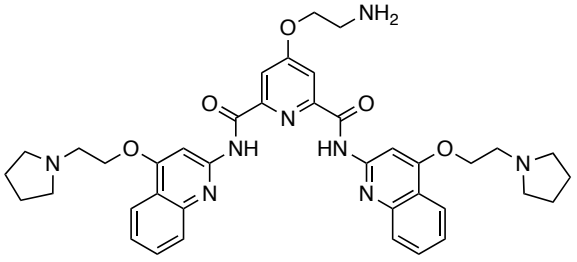

Following procedure **G3**, **11a** (230 mg, 0.705 mmol), **5b** (360 mg, 1.399 mmol), TEA (216 µl, 1.552 mmol) and 1-chloro-*N*,*N*,-2-trimethylpropenyl-amine (205

µl, 1.552 mmol) were reacted to afford the TFA salt of the title compound as a white powder (**25**·3CF_3CO_2H, 550 mg, 0.525 mmol, 74%). **^{1}H-NMR** (400 MHz, CD_3OD) $\boldsymbol{\delta_H}$ 8.48 (2H, *br d*, *J* 8.0 Hz, CH (ar)), 8.21 (2H, *s*, CH (ar)), 8.17 (2H, *s*, CH (ar)), 8.12 (2H, *br d*, *J* 8.0 Hz, CH (ar)), 8.01 (2H, *ddd*, *J* 8.0, 6.5, 1.0 Hz, CH (ar)), 7.75 (2H, *ddd*, *J* 8.0, 6.5, 1.0 Hz, CH (ar)), 4.98-4.93 (4H, *m*, $OCH_2CH_2NCH_2$), 4.69-4.63 (2H, *m*, $OCH_2CH_2NH_2$), 4.07-3.99 (4H, *m*, $OCH_2CH_2NCH_2$), 3.97-3.85 (4H, *m*, $NCH_2(CH_2)_2$), 3.61-3.53 (2H, *m*, $OCH_2CH_2NH_2$), 3.48-3.34 (4H, *m*, $NCH_2(CH_2)_2$), 2.36-2.08 (8H, *m*, NCH_2CH_2-CH_2); **^{13}C-NMR** (100 MHz, CD_3OD) $\boldsymbol{\delta_C}$ 168.2, 167.2, 163.7, 151.0, 149.7 139.5, 134.4, 127.6, 123.5, 121.3, 118.8, 113.9, 94.7, 66.4, 65.7, 55.2, 53.6, 39.1, 23.1; **HRMS (ES)** calculated for $C_{39}H_{45}N_8O_5$ ($[M+H]^+$) m/z: 705.3501,
found 705.3510.

4-(2-(Pyrrolidin-1-yl)ethoxy)-N^2,N^6-*bis*(4-(2-(pyrrolidin-1-yl)ethoxy) quinolin-2-yl)pyridine-2,6 dicarboxamide (26)

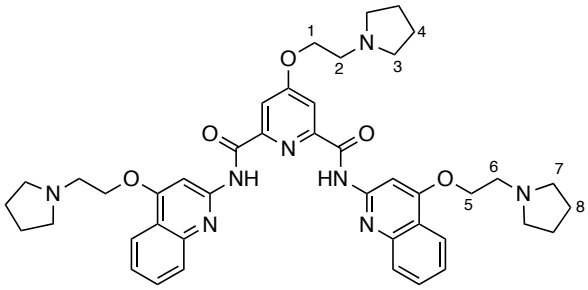

Following procedure **G3**, the TFA salt of **11b** (52 mg, 0.132 mmol), **5b** (70 mg, 0.271 mmol), TEA (40 µl, 0.290 mmol) and 1-chloro-*N*,*N*,2-trimethylpropenyl-amine (38 µl, 0.290 mmol) were reacted to afford the TFA salt of the title compound as a white powder (**26**·3CF_3CO_2H, 88 mg, 0.080 mmol, 61%). **^{1}H-NMR** (400 MHz, CD_3OD) $\boldsymbol{\delta_H}$ 8.47 (2H, *br d*, *J* 8.5 Hz, CH (ar)), 8.22 (2H, *s*, CH (ar)), 8.20 (2H, *s*, CH (ar)), 8.12 (2H, *br d*, *J* 8.5 Hz, CH (ar)), 8.02-7.96 (2H, *m*, CH (ar)), 7.75-7.70 (2H, *m*, CH (ar)), 4.95-4.90 (4H, *m*, OCH_2 (5)), 4.78-4.74 (2H, *m*, OCH_2 (1)), 4.05-3.76 (12H, *m*, $NCH_2(CH_2)_2$, (3,7)), 3.50-3.35 (6H, *m*, OCH_2CH_2 (2,6)), 2.34-2.07 (12H, *m*, $NCH_2CH_2CH_2$ (4,8)); **^{13}C-NMR** (100 MHz, CD_3OD) $\boldsymbol{\delta_C}$ 165.9, 163.1, 151.3, 150.1, 142.0, 133.3, 126.8, 123.1, 119.1,

118.5, 115.5, 113.4, 94.4, 65.8, 64.7, 55.1, 55.0, 54.9, 53.6, 23.0, 22.9; **HRMS (ES)** calculated for $C_{43}H_{51}N_8O_5$ ($[M+H]^+$) m/z: 759.3977, found 759.3980.

N^2,N^6-*bis*(4-(2-Aminoethoxy)quinolin-2-yl)-4-(prop-2-yn-1-yloxy) pyridine-2,6 dicarboxamide (27)

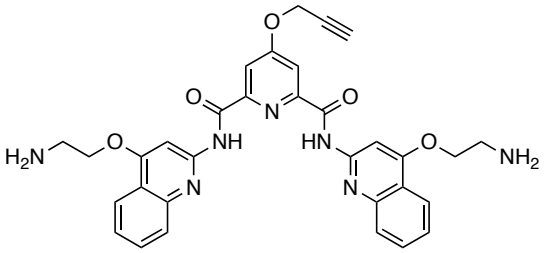

Following procedure **G3**, **11c** (115 mg, 0.520 mmol), **5a** (315 mg, 1.040 mmol), TEA (160 µl, 1.145 mmol) and 1-chloro-*N*,*N*,-2-trimethylpropenyl-amine (151 µl, 1.145 mmol) were reacted to afford the TFA salt of the title compound as a white powder (**27**·$2CF_3CO_2H$, 395 mg, 0.482 mmol, 93%). **^{1}H-NMR** (400 MHz, CD_3OD) $\boldsymbol{\delta_H}$ 8.57 (2H, *br d*, *J* 8.0 Hz, C<u>H</u> (ar)), 8.27-8.24 (4H, *m*, C<u>H</u> (ar)), 8.16 (2H, *br d*, *J* 8.0 Hz, C<u>H</u> (ar)), 8.08-8.02 (2H, *m*, C<u>H</u> (ar)), 7.82-7.76 (2H, *m*, C<u>H</u> (ar)), 5.20-5.17 (2H, *m*, OC<u>H_2</u>C), 4.89-4.85 (4H, *m*, OC<u>H_2</u>), 3.76-3.70 (4H, *m*, OCH_2C<u>H_2</u>), 3.26-3.25 (1H, *m*, C<u>H</u>); **^{13}C-NMR** (100 MHz, CD_3OD) $\boldsymbol{\delta_C}$ 167.7, 167.2, 163.9, 151.3, 149.5, 139.1, 134.1, 127.5, 123.6, 121.4, 118.8, 114.2, 94.6, 78.6, 76.4, 67.4, 56.8, 38.6; **HRMS (ES)** calculated for $C_{33}H_{30}N_7O_5$ ($[M+H]^+$) m/z: 592.2284, found 592.2297.

N^2,N^6-*bis*(4-(3-Aminopropoxy)quinolin-2-yl)-4-(prop-2-yn-1-yloxy) pyridine-2,6 dicarboxamide (28)

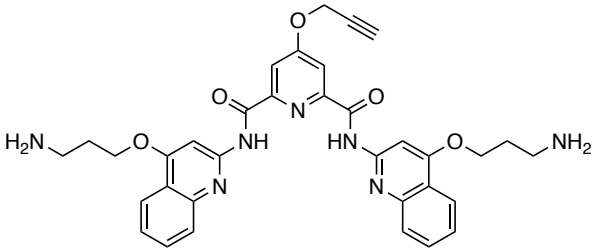

Following procedure **G3**, **11c** (115 mg, 0.520 mmol), **16a** (360 mg, 1.078 mmol), TEA (160 µl, 1.145 mmol) and 1-chloro-*N*,*N*,-2-trimethylpropenyl-amine (151 µl, 1.145 mmol) were reacted to afford the TFA salt of the title compound as a white powder (**28**·2CF_3CO_2H, 350 mg, 0.413 mmol, 79%). **^{1}H-NMR** (400 MHz, CD_3OD) $\boldsymbol{\delta_H}$ 8.38 (2H, *br d*, *J* 8.0 Hz, C<u>H</u> (ar)), 8.24 (2H, *s*, C<u>H</u> (ar)), 8.15-8.11 (4H, *m*, C<u>H</u> (ar)), 8.04-7.99 (2H, *m*, C<u>H</u> (ar)), 7.78-7.72 (2H, *m*, C<u>H</u> (ar)), 5.18-5.16 (2H, *m*, OC<u>H_2</u>C), 4.72-4.67 (4H, *m*, OC<u>H_2</u>), 3.39-3.35 (4H, *m*, OCH_2C<u>H_2</u>), 3.26-3.24 (1H, *m*, C<u>H</u>), 2.52-2.44 (4H, *m*, $O(CH_2)_2C$<u>H_2</u>); **^{13}C-NMR** (100 MHz, CD_3OD) $\boldsymbol{\delta_C}$ 168.1, 167.0, 163.3, 151.4, 149.9, 140.9, 133.5, 127.3, 123.2, 122.5, 119.1, 113.7, 94.3, 78.2, 76.6, 67.8, 57.0, 37.2, 27.0; **HRMS (ES)** calculated for $C_{34}H_{34}N_7O_5$ ($[M+H]^+$) m/z: 620.2621, found 620.2612.

4-Methoxy-N^2,N^6-*bis*(4-(2-(pyrrolidin-1-yl)ethoxy)quinolin-2-yl) pyridine-2,6 dicarboxamide (29)

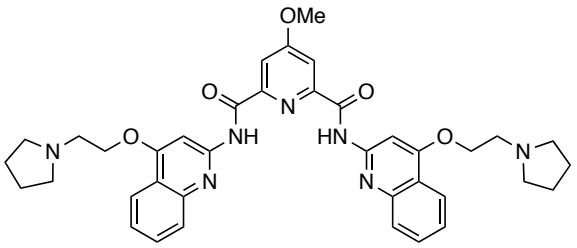

Following procedure **G3**, **15** (50 mg, 0.255 mmol), **5b** (132 mg, 0.510 mmol), TEA (76 µl, 0.546 mmol) and 1-chloro-*N*,*N*,-2-trimethylpropenyl-amine (72 µl,

0.546 mmol) were reacted to afford the TFA salt of the title compound as a white powder (**29**·2CF_3CO_2H, 140 mg, 0.207 mmol, 81%). **^{1}H-NMR** (400 MHz, CD_3OD) $\boldsymbol{\delta_H}$ 8.33 (2H, *br d*, *J* 8.5 Hz, C<u>H</u> (ar)), 8.17 (2H, *s*, C<u>H</u> (ar)), 7.97 (4H, *m*, C<u>H</u> (ar)), 7.82 (2H, *ddd*, *J* 8.5, 7.0, 1.0 Hz, C<u>H</u> (ar)), 7.58 (2H, *ddd*, *J* 8.5, 7.0, 1.0 Hz, C<u>H</u> (ar)), 4.07 (3H, *s*, C<u>H</u>$_3$), 3.87-3.62 (8H, *m*, OC<u>H</u>$_2$, $OCH_2C\underline{H}_2$), 3.32-3.20 (4H, *m*, NC<u>H</u>$_2$$(CH_2)_2$), 2.61-2.51 (4H, *m*, NC<u>H</u>$_2$$(CH_2)_2$), 2.17-1.88 (8H, *m*, $NCH_2C\underline{H}_2CH_2$); **^{13}C-NMR** (100 MHz, CD_3OD) $\boldsymbol{\delta_C}$ 166.1, 162.7, 151.6, 149.7, 148.9, 142.7, 134.0, 128.1, 126.8, 123.4, 119.3, 115.6, 94.6, 66.1, 54.1, 53.5, 45.8, 23.6; **HRMS (ES)** calculated for $C_{38}H_{42}N_7O_5$ ($[M+H]^+$) m/z: 676.3245, found 676.3241.

4-Methoxy-N^2,N^6-*bis*(4-methoxyquinolin-2-yl) pyridine-2,6 dicarboxamide (30)

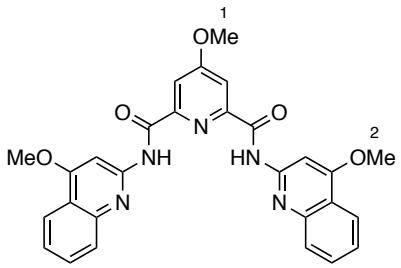

Following procedure **G3**, **15** (100 mg, 0.510 mmol), **17** (178 mg, 1.020 mmol), TEA (152 µl, 1.091 mmol) and 1-chloro-*N*,*N*,-2-trimethylpropenyl-amine (144 µl, 1.091 mmol) were reacted to afford the title compound as a white powder (137 mg, 0.270 mmol, 53%). **^{1}H-NMR** (400 MHz, CD_3OD) $\boldsymbol{\delta_H}$ 8.42 (2H, *br d*, *J* 8.0 Hz, C<u>H</u> (ar)), 8.22 (2H, *s*, C<u>H</u> (ar)), 8.13 (2H, *s*, C<u>H</u> (ar)), 8.06 (2H, *br d*, *J* 8.0 Hz, C<u>H</u> (ar)), 7.94-7.90 (2H, *m*, C<u>H</u> (ar)), 7.70-7.65 (2H, *m*, C<u>H</u> (ar)), 4.87 (6H, *s*, OC<u>H</u>$_3$ (2)), 4.15 (3H, *s*, OC<u>H</u>$_3$ (1)); **^{13}C-NMR** (100 MHz, CD_3OD) $\boldsymbol{\delta_C}$ 162.8, 162.1, 152.6, 151.0, 147.4, 146.8, 131.2, 127.3, 126.4, 125.2, 122.6, 119.5, 95.4, 54.3, 53.2; **HRMS (ES)** calculated for $C_{28}H_{23}N_5O_5$ ($[M+H]^+$) m/z: 510.1777, found 510.1787.

4-Chloro-N^2,N^6-*bis*(4-(2-aminoethoxy)quinolin-2-yl)-pyridine-2,6 dicarboxamide (31)

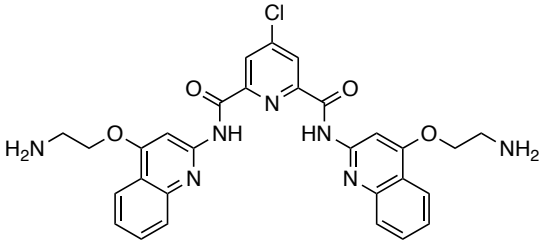

Following procedure **G3**, **13** (100 mg, 0.496 mmol), **5a** (300 mg, 0.989 mmol), TEA (152 µl, 1.091 mmol) and 1-chloro-*N*,*N*,-2-trimethylpropenyl-amine (144 µl, 1.091 mmol) were reacted to afford the TFA salt of the title compound as a white powder (**31**·2CF_3CO_2H, 250 mg, 0.312 mmol, 63%). **^{1}H-NMR** (400 MHz, CD_3OD) $\boldsymbol{\delta_H}$ 8.64 (2H, *s*, C<u>H</u> (ar)), 8.52 (2H, *br d*, *J* 8.5 Hz, C<u>H</u> (ar)), 8.15 (2H, *s*, C<u>H</u> (ar)), 8.10 (2H, *br d*, *J* 8.5 Hz, C<u>H</u> (ar)), 7.97 (2H, *m*, C<u>H</u> (ar)), 7.72 (2H, *m*, C<u>H</u> (ar)), 4.80 (4H, *t*, *J* 5.0 Hz, OC<u>H_2</u>), 4.71 (4H, *t*, *J* 5.0 Hz, $OCH_2C\underline{H_2}$); **^{13}C-NMR** (100 MHz, CD_3OD) $\boldsymbol{\delta_C}$ 166.1, 162.5, 151.4, 149.7, 148.8, 142.4, 133.2, 127.3, 126.6, 123.4, 119.4, 115.1, 94.7, 66.5, 38.8; **HRMS (ES)** calculated for $C_{29}H_{27}ClN_7O_4$ ($[M+H]^+$) m/z: 572.1813, found 572.1824.

4-Chloro-N^2,N^6-*bis*(4-(3-aminopropoxy)quinolin-2-yl)-pyridine-2,6 dicarboxamide (32)

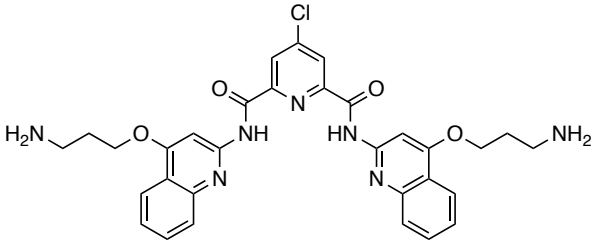

Following procedure **G3**, **13** (50 mg, 0.248 mmol), **16a** (157 mg, 0.495 mmol), TEA (76 µl, 0.546 mmol) and 1-chloro-*N*,*N*,-2-trimethylpropenyl-amine (72 µl, 0.546 mmol) were reacted to afford the TFA salt of the title compound as a

white powder (**32**·2CF_3CO_2H, 164 mg, 0.198 mmol, 80%). **^{1}H-NMR** (400 MHz, CD_3OD) $\boldsymbol{\delta_H}$ 8.59 (2H, *s*, C<u>H</u> (ar)), 8.35-8.31 (2H, *m*, C<u>H</u> (ar)), 8.10-8.04 (4H, *m*, C<u>H</u> (ar)), 8.00-7.93 (2H, *m*, C<u>H</u> (ar)), 7.74-7.68 (2H, *m*, C<u>H</u> (ar)), 4.70-4.62 (4H, *m*, OC<u>H</u>$_2$), 3.40-3.34 (4H, *m*, OCH_2C<u>H</u>$_2$), 2.53-2.43 (4H, *m*, $O(CH_2)_2C$<u>H</u>$_2$); **^{13}C-NMR** (100 MHz, CD_3OD) $\boldsymbol{\delta_C}$ 166.9, 162.4, 151.2, 149.5, 141.1, 133.7, 127.3, 126.8, 123.0, 122.5, 119.2, 115.4, 94.2, 67.9, 37.0, 27.1; **HRMS (ES)** calculated for $C_{31}H_{30}ClN_7NaO_4$ ($[M+Na]^+$) m/z: 601.3145, found 601.3155.

4-Chloro-N^2,N^6-*bis*(4-(2-(pyrrolidin-1-yl)ethoxy)quinolin-2-yl) pyridine-2,6 dicarboxamide (33)

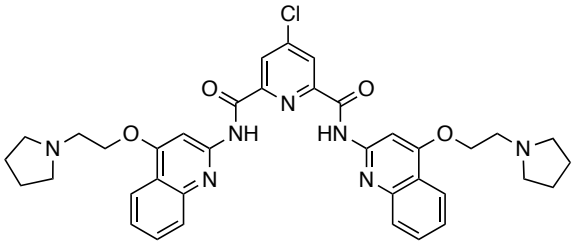

Following procedure **G3**, **13** (100 mg, 0.496 mmol), **5b** (295 mg, 0.991 mmol), TEA (152 µl, 1.091 mmol) and 1-chloro-*N*,*N*,-2-trimethylpropenyl-amine (144 µl, 1.091 mmol) were reacted to afford the TFA salt of the title compound as a white powder (**33**·2CF_3CO_2H, 330 mg, 0.363 mmol, 73%). **^{1}H-NMR** (400 MHz, CD_3OD) $\boldsymbol{\delta_H}$ 8.62 (2H, *s*, C<u>H</u> (ar)), 8.39 (2H, *dd*, *J* 8.5, 1.0 Hz, C<u>H</u> (ar)), 8.20 (2H, *s*, C<u>H</u> (ar)), 8.01 (2H, *dd*, *J* 8.5, 1.0 Hz, C<u>H</u> (ar)), 7.87 (2H, *ddd*, *J* 8.5, 6.5, 1.0 Hz, C<u>H</u> (ar)), 7.64 (2H, *ddd*, *J* 8.5, 6.5, 1.0 Hz, C<u>H</u> (ar)), 4.84 (4H, *t*, *J* 5.5 Hz, OC<u>H</u>$_2$), 3.98 (4H, *t*, *J* 5.5 Hz, OCH_2C<u>H</u>$_2$), 3.95-3.81 (4H, *m*, NC<u>H</u>$_2(CH_2)_2$), 3.48-3.36 (4H, *m*, NC<u>H</u>$_2(CH_2)_2$), 2.35-2.04 (8H, *m*, NCH_2C<u>H</u>$_2CH_2$); **^{13}C-NMR** (100 MHz, CD_3OD) $\boldsymbol{\delta_C}$ 170.5, 163.7, 152.0, 150.4, 145.9, 142.4, 140.4, 131.8, 126.6, 126.1, 125.8, 122.3, 94.9, 64.9, 55.3, 53.8, 23.1; **HRMS (ES)** calculated for $C_{37}H_{39}ClN_7O_4$ ($[M+H]^+$) m/z: 680.2747, found 680.2730.

4-Chloro-N^2,N^6-*bis*(4-(2-(dimethylamino)ethoxy)quinolin-2-yl) pyridine-2,6 dicarboxamide (34)

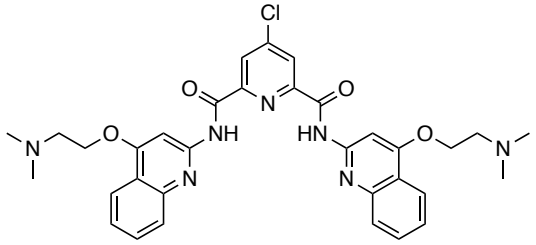

Following procedure **G3**, **13** (50 mg, 0.248 mmol), **16b** (115 mg, 0.498 mmol), TEA (76 µl, 0.546 mmol) and 1-chloro-*N*,*N*,-2-trimethylpropenyl-amine (72 µl, 0.546 mmol) were reacted to afford the TFA salt of the title compound as a white powder (**34**·2CF_3CO_2H, 165 mg, 0.193 mmol, 78%). **^{1}H-NMR** (400 MHz, CD_3OD) $\boldsymbol{\delta_H}$ 8.46 (2H, *s*, C<u>H</u> (ar)), 8.35 (2H, *dd*, *J* 8.0, 1.0 Hz, C<u>H</u> (ar)), 8.16 (2H, *s*, C<u>H</u> (ar)), 7.98 (2H, *dd*, *J* 8.0, 1.0 Hz, C<u>H</u> (ar)), 7.82 (2H, *ddd*, *J* 8.0, 6.5, 1.0 Hz, C<u>H</u> (ar)), 7.57 (2H, *ddd*, *J* 8.0, 6.5, 1.0 Hz, C<u>H</u> (ar)), 4.72-4.68 (4H, *m*, OC<u>H</u>$_2$), 3.81-3.73 (4H, *m*, OCH_2C<u>H</u>$_2$), 3.00 (12H, *s*, C<u>H</u>$_3$); **^{13}C-NMR** (100 MHz, CD_3OD) $\boldsymbol{\delta_C}$ 162.5, 161.7, 152.3, 150.7, 147.2, 146.4, 131.1, 127.1, 126.1, 124.9, 122.2, 119.2, 95.4, 63.2, 55.4, 42.9; **HRMS (ES)** calculated for $C_{33}H_{35}ClN_7O_4$ ($[M+H]^+$) m/z: 628.2439, found 628.2441.

4-Chloro-N^2,N^6-*bis*(4-(3-(dimethylamino)propoxy)quinolin-2-yl) pyridine-2,6 dicarboxamide (35)

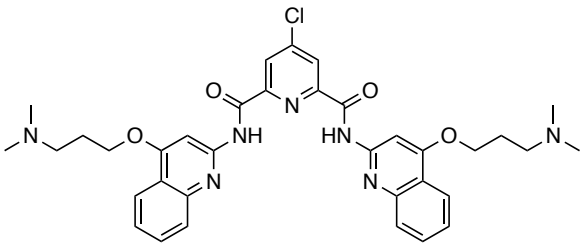

Following procedure **G3**, **13** (50 mg, 0.248 mmol), **16c** (122 mg, 0.498 mmol), TEA (76 µl, 0.546 mmol) and 1-chloro-*N*,*N*,-2-trimethylpropenyl-amine (72 µl,

0.546 mmol) were reacted to afford the TFA salt of the title compound as a white powder (**35**·2CF_3CO_2H, 158 mg, 0.178 mmol, 72%). **^{1}H-NMR** (400 MHz, CD_3OD) $\boldsymbol{\delta_H}$ 8.57 (2H, *s*, C<u>H</u> (ar)), 8.37 (2H, *br d*, *J* 8.0 Hz, C<u>H</u> (ar)), 8.10 (2H, *br d*, *J* 8.0 Hz, C<u>H</u> (ar)), 8.01 (2H, *s*, C<u>H</u> (ar)), 8.00-7.96 (2H, *m*, C<u>H</u> (ar)), 7.76-7.71 (2H, *m*, C<u>H</u> (ar)), 4.68-4.64 (4H, *m*, OC<u>H_2</u>), 3.59-3.52 (4H, *m*, $OCH_2C\underline{H_2}$), 3.05 (12H, *s*, C<u>H_3</u>), 2.60-2.51 (4H, *m*, $O(CH_2)_2C\underline{H_2}$); **^{13}C-NMR** (100 MHz, CD_3OD) $\boldsymbol{\delta_C}$ 167.2, 162.8, 150.9, 149.3, 140.2, 133.9, 127.6, 127.2, 123.1, 121.9, 118.9, 115.4, 94.5, 67.7, 55.2, 42.6, 24.5; **HRMS (ES)** calculated for $C_{35}H_{39}ClN_7O_4$ ($[M+H]^+$) m/z: 656.2736, found 656.2747.

4-(4-Fluorobenzyloxy)-N^2,N^6-*bis*(4-(2-aminoethoxy)quinolin-2-yl) pyridine-2,6 dicarboxamide (36)

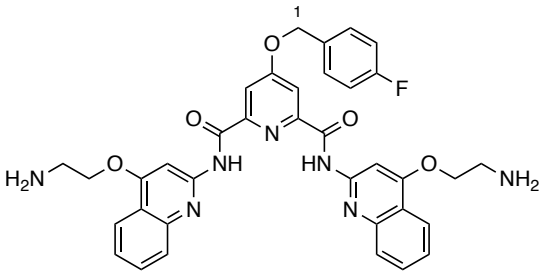

Following procedure **G3**, **11d** (8 mg, 0.024 mmol), **5a** (13 mg, 0.049 mmol), TEA (7 µl, 0.053 mmol) and 1-chloro-*N*,*N*,-2-trimethylpropenyl-amine (7 µl, 0.053 mmol) were reacted to afford the TFA salt of the title compound as a white powder (**36**·2CF_3CO_2H, 15 mg, 0.059 mmol, 61%). **^{1}H-NMR** (500 MHz, CD_3OD) $\boldsymbol{\delta_H}$ 8.46 (2H, *dd*, *J* 8.0, 1.0 Hz, C<u>H</u> (ar)), 8.19 (2H, *s*, C<u>H</u> (ar)), 8.17 (2H, *s*, C<u>H</u> (ar)), 8.05 (2H, *dd*, *J* 8.0, 1.0 Hz, C<u>H</u> (ar)), 7.93 (2H, *d*, *J* 8.5 Hz, C<u>H</u> (ar)), 7.68 (2H, *d*, *J* 8.5 Hz, C<u>H</u> (ar)), 7.61-7.57 (2H, *m*, C<u>H</u> (ar)), 7.20-7.14 (2H, *m*, C<u>H</u> (ar)), 5.44 (2H, *s*, OC<u>H_2</u> (1)), 4.77 (4H, *t*, *J* 4.0 Hz, OC<u>H_2</u>CH_2), 3.68 (4H, *t*, *J* 4.0 Hz, $OCH_2C\underline{H_2}$); **^{13}C-NMR** (125 MHz, CD_3OD) $\boldsymbol{\delta_C}$ 169.8, 166.7, 164.3 (*d*, *J* 245 Hz), 164.2, 152.5, 151.0, 143.7, 134.1, 132.8, 131.2 (*d*, *J* 8 Hz), 127.6, 124.5, 124.1, 120.2, 116.5 (*d*, *J* 22 Hz), 114.5, 95.3, 71.7, 67.6, 39.8; **HRMS (ES)** calculated for $C_{36}H_{33}FN_7O_5$ ($[M+H]^+$) m/z: 662.2521, found 662.2501.

4-(4-Fluorobenzyloxy)-N^2,N^6-*bis*(4-(2-(pyrrolidin-1-yl)ethoxy) quinolin-2-yl)pyridine-2,6 dicarboxamide (37)

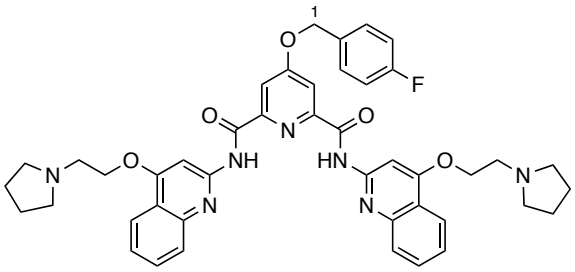

Following procedure **G3**, **11d** (12 mg, 0.041 mmol), **5b** (23 mg, 0.089 mmol), TEA (13 µl, 0.091 mmol) and 1-chloro-*N*,*N*,-2-trimethylpropenyl-amine (12 µl, 0.091 mmol) were reacted to afford the TFA salt of the title compound as a white powder (**37**·2CF_3CO_2H, 26 mg, 0.026 mmol, 63%). **^{1}H-NMR** (400 MHz, CD_3OD) $\boldsymbol{\delta_H}$ 8.42 (2H, *br d*, *J* 8.0 Hz, C<u>H</u> (ar)), 8.20 (2H, *s*, C<u>H</u> (ar)), 8.18 (2H, *s*, C<u>H</u> (ar)), 8.07 (2H, *br d*, *J* 8.0 Hz, C<u>H</u> (ar)), 7.97-7.91 (2H, *m*, C<u>H</u> (ar)), 7.71-7.66 (2H, *m*, C<u>H</u> (ar)), 7.63-7.57 (2H, *m*, C<u>H</u> (ar)), 7.23-7.16 (2H, *m*, C<u>H</u> (ar)), 5.46 (2H, *s*, OC<u>H</u>$_2$ (1)), 4.94-4.87 (4H, *m*, OC<u>H</u>$_2$$CH_2$), 4.04-3.82 (8H, *m*, NC<u>H</u>$_2$$(CH_2)_2$), 3.48-3.36 (4H, *m*, OCH_2C<u>H</u>$_2$), 2.34-2.04 (8H, *m*, NCH_2C<u>H</u>$_2$$CH_2$); **^{13}C-NMR** (100 MHz, CD_3OD) $\boldsymbol{\delta_C}$ 169.0, 165.4 (*d*, *J* 245.0 Hz), 163.3, 151.5, 150.1, 143.3, 133.0, 130.5 (*d*, *J* 8.0 Hz), 126.7, 124.0, 123.5, 122.8, 199.4, 115.9 (*d*, *J* 20.0 Hz), 115.3, 113.3, 94.5, 70.5, 65.6, 55.1, 53.9, 22.9; **HRMS (ES)** calculated for $C_{44}H_{45}N_7O_5F_1$ ($[M+H]^+$) m/z: 770.3461, found 770.3450.

4-((1H-1,2,3-Triazol-4-yl)methoxy)-N^2,N^6-*bis*(4-(2-aminoethoxy) quinolin-2-yl)pyridine-2,6 dicarboxamide (38)

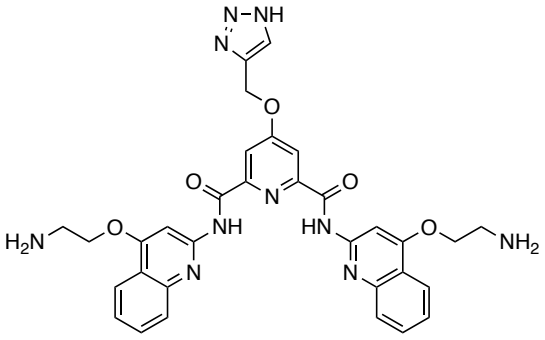

Following procedure **G4**, **27** (20 mg, 0.024 mmol), copper(II) sulfate pentahydrate (1.5 mg, 0.006 mmol), sodium ascorbate (5.3 mg, 0.027 mmol) and sodium azide (1.7 mg, 0.027 mmol) were reacted to afford the TFA salt of the title compound as a pale white solid (**38**·3CF_3CO_2H, 12 mg, 0.014 mmol, 57%). **^{1}H-NMR** (400 MHz, CD_3OD) $\boldsymbol{\delta_H}$ 8.53 (2H, *br d*, *J* 8.0 Hz, C<u>H</u> (ar)), 8.26 (2H, *s*, C<u>H</u> (ar)), 8.15 (2H, *s*, C<u>H</u> (ar)), 8.12 (2H, *br d*, *J* 8.0 Hz, C<u>H</u> (ar)), 8.08 (1H, *s*, C<u>H</u> (ar)), 8.00 (2H, *m*, C<u>H</u> (ar)), 7.74 (2H, *m*, C<u>H</u> (ar)), 5.64 (2H, *s*, C<u>H_2</u>C), 4.83 (4H, *t*, *J* 5.0 Hz, OC<u>H_2</u>CH_2), 3.72 (4H, *t*, *J* 5.0 Hz, OCH_2C<u>H_2</u>); **^{13}C-NMR** (100 MHz, CD_3OD) $\boldsymbol{\delta_C}$ 168.6, 166.6, 163.6, 151.4, 149.8, 141.2, 133.9, 133.3, 127.1, 123.5, 122.6, 119.0, 113.8, 94.2, 66.9, 62.6, 60.5, 38.8; **HRMS (ES)** calculated for $C_{32}H_{31}N_{10}O_5$ ($[M+H]^+$) m/z: 635.2479, found 635.2480.

4-((1H-1,2,3-Triazol-4-yl)methoxy)-N^2,N^6-*bis*(4-(3-aminopropoxy) quinolin-2-yl)pyridine-2,6 dicarboxamide (39)

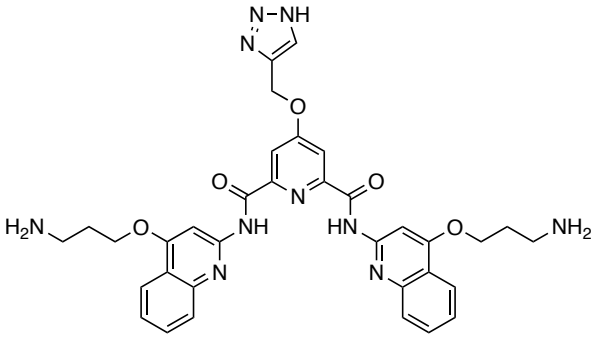

Following procedure **G4**, **28** (20 mg, 0.024 mmol), copper(II) sulfate pentahydrate (1.5 mg, 0.006 mmol), sodium ascorbate (5.3 mg, 0.027 mmol) and sodium azide (1.7 mg, 0.027 mmol) were reacted to afford the TFA salt of the title compound as a pale yellow solid (**39**·3CF_3CO_2H, 14 mg, 0.016 mmol, 67%). **^{1}H-NMR** (400 MHz, CD_3OD) $\boldsymbol{\delta_H}$ 8.37 (2H, *br d*, *J* 8.0 Hz, C<u>H</u> (ar)), 8.26 (2H, *s*, C<u>H</u> (ar)), 8.14 (2H, *s*, C<u>H</u> (ar)), 8.14-8.06 (3H, *m*, C<u>H</u> (ar)), 8.04-7.96 (2H, *m*, C<u>H</u> (ar)), 7.78-7.70 (2H, *m*, C<u>H</u> (ar)), 5.64 (2H, *s*, C<u>H_2</u>C), 4.71-4.65 (4H, *m*, OC<u>H_2</u>CH_2), 3.40-3.33 (4H, *m*, OCH_2C<u>H_2</u>), 2.52-2.43 (4H, *m*, $O(CH_2)_2C$<u>H_2</u>); **^{13}C-NMR** (100 MHz, CD_3OD) $\boldsymbol{\delta_C}$ 168.6, 166.8, 163.5, 151.5, 149.8, 141.2, 133.5, 133.1, 127.5, 123.6, 122.6, 119.2, 113.7, 94.1, 67.5, 62.4, 56.2, 36.9, 27.1; **HRMS (ES)** calculated for $C_{34}H_{35}N_{10}O_5$ ($[M+H]^+$) m/z: 663.2792, found 663.2797.

4-((1H-1,2,3-Triazol-4-yl)methoxy)-N^2,N^6-*bis*(4-(2-aminoethoxy) quinolin-2-yl)pyridine-2,6 dicarboxamide (40)

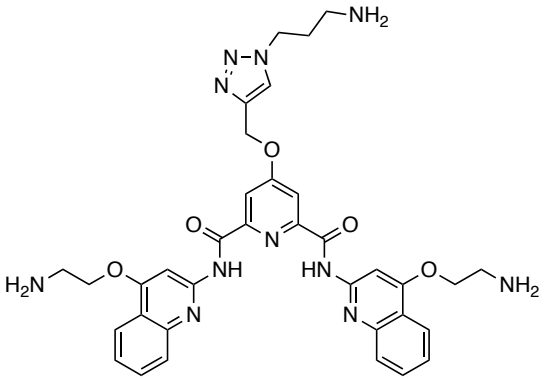

Following procedure **G4**, **27** (22 mg, 0.027 mmol), copper(II) sulfate pentahydrate (0.9 mg, 0.004 mmol), sodium ascorbate (8.1 mg, 0.041 mmol) and 3-azidopropan-1-amine (4.1 mg, 0.041 mmol) were reacted to afford the TFA salt of the title compound as a pale yellow solid (**40**·3CF_3CO_2H, 6 mg, 0.006 mmol, 22%). **^{1}H-NMR** (500 MHz, CD_3OD) $\boldsymbol{\delta_H}$ 8.47 (2H, *br d*, *J* 8.5 Hz, C<u>H</u> (ar)), 8.25 (1H, *s*, C<u>H</u> (ar)), 8.21 (2H, *s*, C<u>H</u> (ar)), 8.15 (2H, *s*, C<u>H</u> (ar)), 8.04 (2H, *br d*, *J* 8.5 Hz, C<u>H</u> (ar)), 7.93-7.89 (2H, *m*, C<u>H</u> (ar)), 7.68-7.63 (2H, *m*, C<u>H</u> (ar)), 5.55 (2H, *s*, OC<u>H_2</u>C), 4.74 (4H, *t*, *J* 5.0 Hz, OC<u>H_2</u>CH_2), 4.61-4.55 (2H, *m*, NC<u>H_2</u>CH_2CH_2), 3.66 (4H, *t*, *J* 5.0 Hz, OCH_2C<u>H_2</u>), 3.04-2.97 (2H, *m*, $N(CH_2)_2$C<u>H_2</u>), 2.33-2.25 (2H, *m*, NCH_2C<u>H_2</u>CH_2); **^{13}C-NMR** (125 MHz, CD_3OD) $\boldsymbol{\delta_C}$ 169.4, 166.5, 164.2, 152.5, 151.2, 144.0, 143.5, 134.0, 127.5, 126.3, 124.8, 124.1, 120.2, 114.3, 95.3, 67.5, 63.5, 54.8, 39.8, 38.1, 29.1; **HRMS (ES)** calculated for $C_{35}H_{38}N_{11}O_5$ ($[M+H]^+$) m/z: 692.3057, found 692.3051.

4-((1-(Meth-4-ylbenzoate)-1,2,3-triazol-4-yl)methoxy)-N^2,N^6-*bis* (4-(2-aminoethoxy)quinolin-2-yl)pyridine-2,6 dicarboxamide (41)

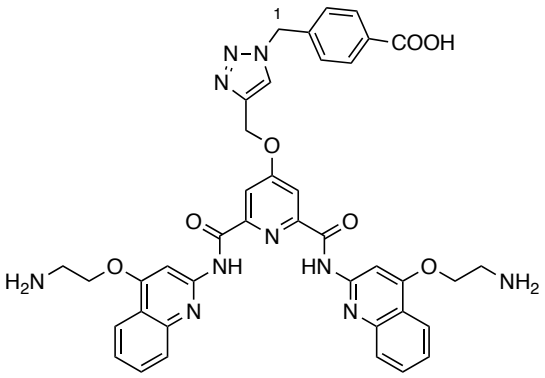

Following procedure **G4**, **27** (19 mg, 0.023 mmol), copper(II) sulfate pentahydrate (0.8 mg, 0.003 mmol), sodium ascorbate (7.1 mg, 0.035 mmol) and 4-(azidomethyl)benzoic acid (6.3 mg, 0.036 mmol) were reacted to afford the TFA salt of the title compound as a pale yellow solid (**41**·2CF_3CO_2H, 10 mg, 0.010 mmol, 43%). **^{1}H-NMR** (400 MHz, CD_3OD) $\boldsymbol{\delta_H}$ 8.49 (2H, *br d*, *J* 8.5 Hz, C<u>H</u> (ar)), 8.30 (1H, *s*, C<u>H</u> (ar)), 8.18 (2H, *s*, C<u>H</u> (ar)), 8.13 (2H, *s*, C<u>H</u> (ar)), 8.07-7.98 (4H, *m*, C<u>H</u> (ar)), 7.97-7.90 (2H, *m*, C<u>H</u> (ar)), 7.71-7.64 (2H, *m*, C<u>H</u> (ar)), 7.42 (2H, *br d*, *J* 8.5 Hz, C<u>H</u> (ar)), 5.76 (2H, *s*, C<u>H_2</u> (1)), 5.59 (2H, *s*, OC<u>H_2</u>C), 4.79 (4H, *t*, *J* 5.0 Hz, OC<u>H_2</u>CH_2), 3.72 (4H, *t*, *J* 5.0 Hz, OCH_2C<u>H_2</u>); **^{13}C-NMR** (100 MHz, CD_3OD) $\boldsymbol{\delta_C}$ 168.4, 168.0, 166.0, 163.2, 151.3, 149.9, 143.9, 143.3, 142.6, 142.2, 140.8, 133.2, 130.3, 128.0, 126.3, 125.4, 123.2, 119.2, 113.7, 94.2, 66.8, 62.6, 53.4, 38.8; **HRMS (ES)** calculated for $C_{40}H_{37}N_{10}O_7$ ($[M+H]^+$) m/z: 769.2826, found 769.2841.

4-((1-(Glucos-2-yl)-1,2,3-triazol-4-yl)methoxy)-N^2,N^6-*bis* (4-(3-aminoethoxy)quinolin-2-yl)-pyridine-2,6 dicarboxamide (42)

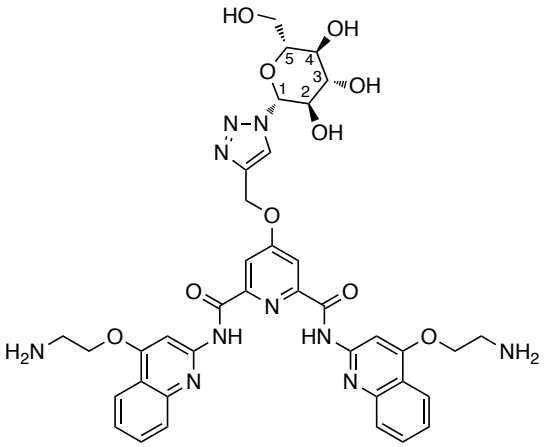

Following procedure **G4**, **27** (20 mg, 0.024 mmol), copper(II) sulfate pentahydrate (0.9 mg, 0.003 mmol), sodium ascorbate (7.4 mg, 0.037 mmol) and 1-azido-1-deoxy-β-D-glucopyranoside (7.7 mg, 0.038 mmol) were reacted to afford the TFA salt of the title compound as a pale yellow solid (**42**·2CF_3CO_2H, 10 mg, 0.010 mmol, 40%). **^{1}H-NMR** (500 MHz, CD_3OD) $\boldsymbol{\delta_H}$ 8.44-8.42 (3H, *m*, C<u>H</u> (ar)), 8.21 (2H, *s*, C<u>H</u> (ar)), 8.16 (2H, *s*, C<u>H</u> (ar)), 8.00 (2H, *br d*, *J* 8.5 Hz, C<u>H</u> (ar)), 7.89-7.86 (2H, *m*, C<u>H</u> (ar)), 7.64-7.61 (2H, *m*, C<u>H</u> (ar)), 5.65-5.63 (1H, *m*, <u>H</u> (1)), 5.56 (2H, *s*, OC<u>H</u>$_2$C), 4.71-4.70 (4H, *m*, OC<u>H</u>$_2$CH_2), 3.91-3.84 (2H, *m*, HOC<u>H</u>$_2$), 4.15-3.55 (4H, *m*, <u>H</u> (2-5)), 3.43-3.37 (4H, *m*, OCH_2C<u>H</u>$_2$); **^{13}C-NMR** (125 MHz, CD_3OD) $\boldsymbol{\delta_C}$ 165.9, 164.1, 152.1, 151.3, 145.0, 142.2, 133.6, 127.2, 125.5, 125.4, 123.9, 120.3, 114.3, 95.4, 89.7, 81.2, 78.5, 74.1, 70.9, 67.2, 63.4, 62.4, 54.8, 39.8; $[\boldsymbol{\alpha}]_{\boldsymbol{D}}^{\boldsymbol{20}}$=21.0° (c 100 µM, H_2O); **HRMS (ES)** calculated for $C_{38}H_{41}N_{10}O_{10}$ ($[M+H]^+$) m/z: 797.3038, found 797.3001.

4-((1-(Glucos-2-yl)-1,2,3-triazol-4-yl)methoxy)-N^2,N^6-*bis*(4-(3-aminopropoxy)quinolin-2-yl)pyridine-2,6 dicarboxamide (43)

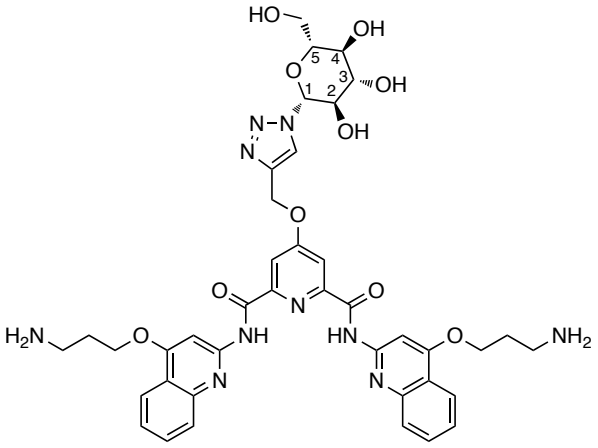

Following procedure **G4**, **28** (28 mg, 0.033 mmol), copper(II) sulfate pentahydrate (2.1 mg, 0.008 mmol), sodium ascorbate (7.2 mg, 0.036 mmol) and 1-azido-1-deoxy-β-D-glucopyranoside (7.3 mg, 0.036 mmol) were reacted to afford the TFA salt of the title compound as a pale white solid (**43**·2CF_3CO_2H, 21 mg, 0.020 mmol, 60%). **^{1}H-NMR** (500 MHz, CD_3OD) $\boldsymbol{\delta_H}$ 8.47 (1H, *s*, C<u>H</u> (ar)), 8.28 (2H, *br d*, *J* 8.5 Hz, C<u>H</u> (ar)), 8.20 (2H, *s*, C<u>H</u> (ar)), 8.10 (2H, *s*, C<u>H</u> (ar)), 8.04 (2H, *br d*, *J* 8.5 Hz, C<u>H</u> (ar)), 7.96-7.91 (2H, *m*, C<u>H</u> (ar)), 7.71-7.65 (2H, *m*, C<u>H</u> (ar)), 5.71-5.65 (1H, *m*, <u>H</u> (1)), 5.58 (2H, *s*, OC<u>H_2</u>C), 4.67-4.59 (4H, *m*, OC<u>H_2</u>CH_2), 4.20-4.15 (1H, *m*, <u>H</u> (2)), 3.98-3.92 (1H, *m*, HOC<u>H_2</u>), 3.90-3.86 (1H, *m*, HOC<u>H_2</u>), 3.74-3.68 (1H, *m*, <u>H</u> (5)), 3.62-3.56 (1H, *m*, <u>H</u> (4)), 3.53-3.49 (1H, *m*, <u>H</u> (3)), 3.35-3.31 (4H, *m*, OCH_2C<u>H_2</u>), 2.47-2.41 (4H, *m*, O$(CH_2)_2$C<u>H_2</u>); **^{13}C-NMR** (125 MHz, CD_3OD) $\boldsymbol{\delta_C}$ 167.9, 166.5, 162.8, 150.6, 149.2, 141.7, 140.2, 133.0, 126.5, 124.1, 122.4, 121.7, 118.5, 113.3, 93.6, 88.1, 79.8, 77.0, 72.6, 69.3, 67.2, 62.0, 60.8, 36.6, 26.5; $[\alpha]_D^{20}$=+20.1° (c 100 μM, H_2O); **HRMS (ES)** calculated for $C_{40}H_{45}N_{10}O_{10}$ ($[M+H]^+$) m/z: 825.3320, found 825.3335.

4-((1-(Galactos-2-yl)-1,2,3-triazol-4-yl)methoxy)-N^2,N^6-*bis*(4-(3-aminopropoxy)quinolin-2-yl)pyridine-2,6 dicarboxamide (44)

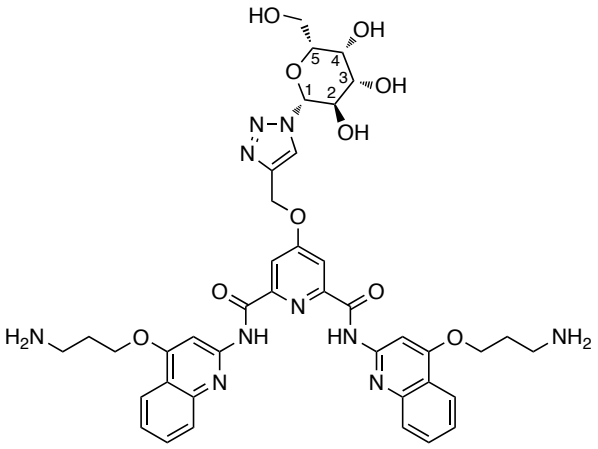

Following procedure **G4**, **28** (18 mg, 0.021 mmol), copper(II) sulfate pentahydrate (1.5 mg, 0.005 mmol), sodium ascorbate (4.6 mg, 0.023 mmol) and 1-azido-1-deoxy-β-D-galactopyranoside (4.7 mg, 0.023 mmol) were reacted to afford the TFA salt of the title compound as a pale white solid (**44**·2CF_3CO_2H, 14 mg, 0.013 mmol, 63%). ^{1}**H-NMR** (500 MHz, CD_3OD) δ_H 8.49 (1H, *s*, C<u>H</u> (ar)), 8.20 (2H, *br d*, *J* 8.5 Hz, C<u>H</u> (ar)), 8.23 (2H, *s*, C<u>H</u> (ar)), 8.17-8.06 (4H, *m*, C<u>H</u> (ar)), 7.98-7.93 (2H, *m*, C<u>H</u> (ar)), 7.72-7.67 (2H, *m*, C<u>H</u> (ar)), 5.65-5.62 (1H, *m*, <u>H</u> (1)), 5.60 (2H, *s*, OC<u>H_2</u>C), 4.69-4.61 (4H, *m*, OC<u>H_2</u>CH_2), 4.22-4.16 (1H, *m*, <u>H</u> (2)), 4.01-3.97 (1H, *m*, HOC<u>H_2</u>), 3.88-3.83 (1H, *m*, HOC<u>H_2</u>), 3.78-3.55 (3H, *m*, <u>H</u> (3-5)), 3.36-3.32 (4H, *m*, OCH_2C<u>H_2</u>), 2.48-2.39 (4H, *m*, $O(CH_2)_2C$<u>H_2</u>); ^{13}**C-NMR** (125 MHz, CD_3OD) δ_C 167.9, 166.5, 162.8, 150.6, 149.2, 141.8, 140.2, 133.0, 126.4, 124.1, 122.4, 121.9, 118.5, 113.3, 93.6, 88.2, 79.8, 76.9, 72.7, 69.5, 67.3, 61.9, 60.8, 36.7, 26.5; $[\boldsymbol{\alpha}]_{\boldsymbol{D}}^{\mathbf{20}}$=+19.0° (c 100 μM, H_2O); **HRMS (ES)** calculated for $C_{40}H_{45}N_{10}O_{10}$ ($[M+H]^+$) m/z: 825.3320, found 825.3353.

4-((1-((2S,3S,5R)-2-(Hydroxymethyl)-5-(5-methyl-2,4-dioxo-3,4-dihydropyrimidin-1(2*H*)-yl)tetrahydrofuran-3-yl)-1,2,3-triazol-4-yl)methoxy)-N^2,N^6-*bis*(4-(2-aminoethoxy)quinolin-2-yl)pyridine-2,6 dicarboxamide (45)

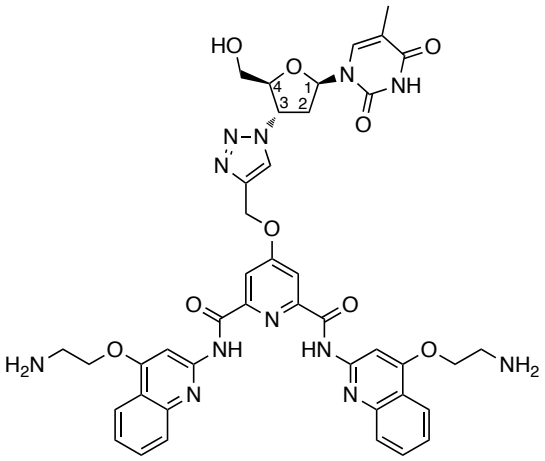

Following procedure **G4**, **28** (30 mg, 0.037 mmol), copper(II) sulfate pentahydrate (3.0 mg, 0.012 mmol), sodium ascorbate (8.0 mg, 0.040 mmol) and zidovudine (12.0 mg, 0.045 mmol) were reacted to afford the TFA salt of the title compound as a pale white solid (**45**·2CF_3CO_2H, 29 mg, 0.027 mmol, 73%). **^{1}H-NMR** (400 MHz, CD_3OD) δ_H 8.52 (2H, *br d*, *J* 8.5 Hz, C<u>H</u> (ar)), 8.44 (1H, *s*, C<u>H</u> (ar)), 8.22 (2H, *s*, C<u>H</u> (ar)), 8.12-8.05 (4H, *m*, C<u>H</u> (ar)), 8.00-7.93 (2H, *m*, C<u>H</u> (ar)), 7.91 (1H, *s*, C<u>H</u> (*T*)), 7.74-7.67 (2H, *m*, C<u>H</u> (ar)), 5.62 (2H, *s*, OC<u>H</u>$_2$C), 4.87-4.80 (4H, *m*, OC<u>H</u>$_2$CH$_2$), 4.44-4.39 (1H, *m*, <u>H</u> (1)), 4.00 (2H, *m*, <u>H</u> (2)), 3.95-3.89 (1H, *m*, HOC<u>H</u>$_2$), 3.87-3.80 (1H, *m*, HOC<u>H</u>$_2$), 3.77-3.71 (4H, *m*, OCH$_2$C<u>H</u>$_2$), 2.97-2.88 (1H, *m*, <u>H</u> (4)), 2.82-2.71 (1H, *m*, <u>H</u> (3)), 1.89 (3H, *s*, C<u>H</u>$_3$); **^{13}C-NMR** (100 MHz, CD_3OD) δ_C 166.8, 165.3, 163.5, 151.4, 151.1, 149.6, 140.3, 137.0, 133.9, 127.1, 125.2, 123.4, 121.8, 118.8, 114.1, 110.9, 94.2, 85.7, 85.5, 85.0, 67.2, 62.6, 61.4, 60.6, 54.2, 38.7, 38.2, 37.3; $[\boldsymbol{\alpha}]_{\boldsymbol{D}}^{\mathbf{20}}$=+22.0° (c 100 μM, H_2O); **HRMS (ES)** calculated for $C_{42}H_{43}N_{12}O_9$ ($[M+H]^+$) m/z: 859.3294, found 859.3294.

4-((1-((2S,3S,5R)-2-(Hydroxymethyl)-5-(5-methyl-2,4-dioxo-3,4-dihydropyrimidin-1(2H)-yl)tetrahydrofuran-3-yl)-1,2,3-triazol-4-yl)methoxy)N^2,N^6-*bis*(4-(3-aminopropoxy)quinolin-2-yl)pyridine-2,6 dicarboxamide (46)

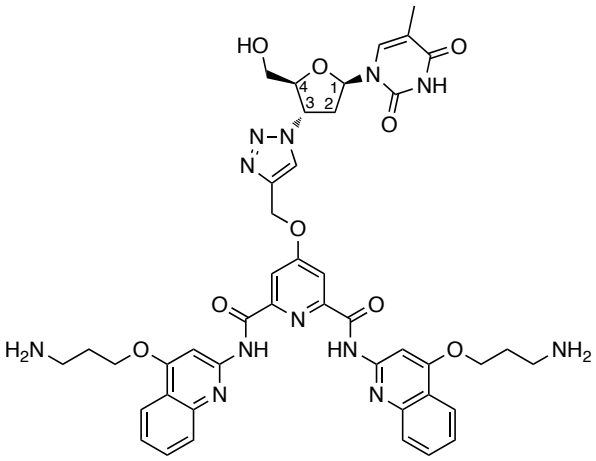

Following procedure **G4**, **28** (33 mg, 0.039 mmol), copper(II) sulfate pentahydrate (3.0 mg, 0.012 mmol), sodium ascorbate (8.0 mg, 0.040 mmol) and zidovudine (13.0 mg, 0.049 mmol) were reacted to afford the TFA salt of the title compound as a pale white solid (**46**·2CF_3CO_2H, 21 mg, 0.019 mmol, 48%). **^{1}H-NMR** (400 MHz, CD_3OD) δ_H 8.42 (1H, *s*, C<u>H</u> (ar)), 8.34 (2H, *br d*, *J* 8.0 Hz, C<u>H</u> (ar)), 8.25 (2H, *s*, C<u>H</u> (ar)), 8.14-8.04 (4H, *m*, C<u>H</u> (ar)), 8.03-7.96 (2H, *m*, C<u>H</u> (ar)), 7.92 (1H, *s*, C<u>H</u> (*T*)), 7.77-7.70 (2H, *m*, C<u>H</u> (ar)), 5.62 (2H, *s*, OC<u>H</u>$_2$C), 4.73-4.66 (4H, *m*, OC<u>H</u>$_2$CH$_2$), 4.45-4.40 (1H, *m*, <u>H</u> (1)), 4.00 (2H, *m*, <u>H</u> (2)), 3.96-3.89 (1H, *m*, HOC<u>H</u>$_2$), 3.86-3.78 (1H, *m*, HOC<u>H</u>$_2$), 3.39-3.34 (4H, *m*, OCH$_2$C<u>H</u>$_2$), 2.98-2.88 (1H, *m*, <u>H</u> (4)), 2.82-2.71 (1H, *m*, <u>H</u> (3)), 2.52-2.41 (4H, *m*, O(CH$_2$)$_2$C<u>H</u>$_2$), 1.91 (3H, *s*, C<u>H</u>$_3$); **^{13}C-NMR** (100 MHz, CD_3OD) δ_C 168.5, 167.3, 163.7, 151.5, 151.2, 149.7, 140.0, 137.0, 133.8, 127.1, 125.1, 122.9, 121.9, 119.0, 114.0, 113.4, 110.7, 94.2, 85.8, 85.5, 68.0, 62.6, 61.4, 60.8, 54.3, 38.1, 37.1, 26.9, 11.5; $[\boldsymbol{\alpha}]_{\boldsymbol{D}}^{\mathbf{20}}$=+23.0° (c 100 μM, H_2O); **HRMS (ES)** calculated for $C_{44}H_{47}N_{12}O_9$ ($[M+H]^+$) m/z: 887.3589, found 887.3554.

4-(2-((+)biotinylamido)ethoxy)N^2,N^6-*bis*(4-(2-aminoethoxy)quinolin-2-yl)pyridine-2,6 dicarboxamide
(47)

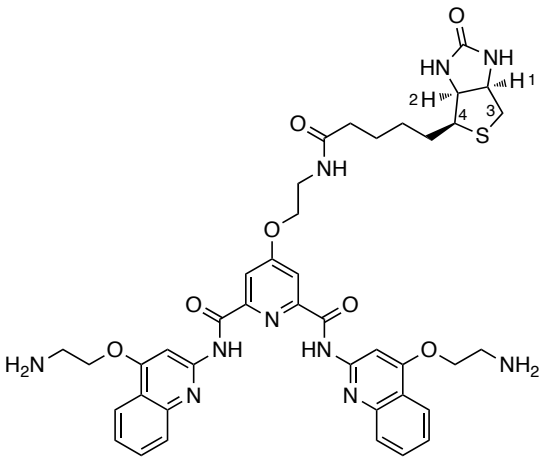

Compound **55** (50 mg, 0.054 mmol) was dissolved in 5 ml MeOH and 5% Pd/C was added. The mixture was stirred under microwave irradiation for 1 h. The mixture was filtered through celite and the solvent removed *in vacuo*. Some of the Cbz-deprotected product was used without further purification for the next step. This compound (**47**·2CF_3CO_2H, 13 mg, 0.016 mmol) and TEA (8 µl, 0.054 mmol) were dissolved in 1 ml DCM and (+)biotin *N*-hydroxysuccinimide ester (6 mg, 0.018 mmol) was added. The solution was stirred for 2 h at rt. The solvent was removed *in vacuo* and the product purified by HPLC (gradient: 10% MeCN/90% H_2O, 0.1% TFA to 100% MeCN, 0.1% TFA over 30 min, R_t=14.5-15.0 min) to yield the TFA salt of the product as a white solid (16 mg, 0.015 mmol, 93%). ^{1}**H-NMR** (500 MHz, D_2O) δ_H 8.49 (2H, *br d*, *J* 8.0 Hz, C<u>H</u> (ar)), 8.19 (2H, *s*, C<u>H</u> (ar)), 8.13 (2H, *s*, C<u>H</u> (ar)), 8.07 (2H, *br d*, *J* 8.0 Hz, C<u>H</u> (ar)), 7.96-7.92 (2H, *m*, C<u>H</u> (ar)), 7.70-7.66 (2H, *m*, C<u>H</u> (ar)), 4.79-4.69 (4H, *m*, OC<u>H</u>$_2$CH_2NH_2), 4.46-4.40 (2H, *m*, OC<u>H</u>$_2$CH_2NH), 4.38-4.33 (1H, *m*, <u>H</u> (1)), 4.24-4.19 (1H, *m*, <u>H</u> (2)), 3.72-3.63 (6H, *m*, OCH_2C<u>H</u>$_2$NH_2, OCH_2C<u>H</u>$_2$NH), 3.17-3.08 (1H, *m*, <u>H</u> (4)), 2.88-2.80 (1H, *m*, <u>H</u> (3)), 2.65-2.56 (1H, *m*, <u>H</u> (3)), 2.27-2.19 (2H, *m*, COC<u>H</u>$_2$), 1.74-1.47 (4H, *m*, COCH_2C<u>H</u>$_2$, CO(CH_2)$_3$C<u>H</u>$_2$), 1.44-1.29 (2H, *m*, CO(CH_2)$_2$C<u>H</u>$_2$); ^{13}**C-NMR** (125 MHz, D_2O) δ_C 176.7, 170.0, 164.4, 152.5, 151.1, 149.8, 144.3, 133.9, 127.4, 124.9, 124.1, 120.1, 116.7, 114.3, 95.5, 67.5, 63.5,

61.5, 56.9, 53.9, 41.2, 39.8, 39.6, 36.7, 29.7, 29.6, 26.9; $[\boldsymbol{\alpha}]_{\boldsymbol{D}}^{\mathbf{20}}$=+57.1° (c 100 μM, H_2O); **HRMS (ES)** calculated for $C_{41}H_{47}N_{10}O_7$ ($[M+H]^+$) m/z: 823.3350, found 823.3314.

4-(2-((+)Biotinylamido)ethoxy)-N^2,N^6-*bis*(4-(3-aminopropoxy)quinolin-2-yl)pyridine-2,6 dicarboxamide (48)

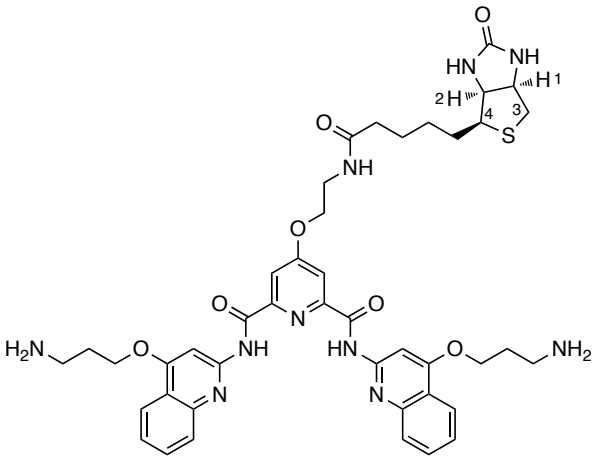

Compound **56** (70 mg, 0.073 mmol) was dissolved in MeOH (5 ml) and 5% Pd/C was added. The mixture was stirred under microwave irradiation for 1 h. The mixture was filtered through celite and the solvent removed *in vacuo*. Some of the Cbz-deprotected product was used without further purification for the next step. This compound (20 mg, 0.024 mmol) and TEA (11 μl, 0.079 mmol) were dissolved in DCM (1 ml) and (+)-biotin *N*-hydroxysuccinimide ester (9 mg, 0.026 mmol) was added. The solution was stirred for 2 h at rt. The solvent was removed *in vacuo* and the product purified by HPLC (gradient: 10% MeCN/90% H_2O, 0.1% TFA to 100% MeCN, 0.1% TFA over 30 min, R_t=14.5-15.0 min) to yield the TFA salt of the product as a white solid (**48**·$2CF_3CO_2H$, 23 mg, 0.022 mmol, 92%). ^{1}**H-NMR** (500 MHz, CD_3OD) δ_H 8.39 (2H, *br d*, *J* 8.0 Hz, C<u>H</u> (ar)), 8.18-8.09 (6H, *m*, C<u>H</u> (ar)), 8.06-7.98 (2H, *m*, C<u>H</u> (ar)), 7.79-7.72 (2H, *m*, C<u>H</u> (ar)), 4.75-4.66 (4H, *m*, OC<u>H</u>$_2$(CH_2)$_2$), 4.50-4.41 (3H, *m*, OC<u>H</u>$_2$$CH_2$NH, (1)), 4.29-4.23 (1H, *m*, <u>H</u> (2)), 3.76-3.67 (2H, *m*, OCH_2C<u>H</u>$_2$NH), 3.41-3.35 (4H, *m*, OCH_2C<u>H</u>$_2$$CH_2$),

3.21-3.13 (1H, *m*, H (4)), 2.92-2.83 (1H, *m*, H (3)), 2.65-2.58 (1H, *m*, H (3)), 2.53-2.44 (4H, *m*, $O(CH_2)_2C\underline{H}_2$), 2.32-2.23 (2H, *m*, $COC\underline{H}_2$), 1.76-1.38 (6H, *m*, $COCH_2(C\underline{H}_2)_3$); **^{13}C-NMR** (125 MHz, CD_3OD) δ_C 175.6, 167.4, 163.5, 151.2, 149.8, 147.4, 140.2, 133.8, 127.2, 123.1, 121.8, 119.0, 116.1, 113.6, 94.3, 68.3, 67.8, 62.3, 60.7, 55.9, 40.0, 38.6, 37.1, 35.9, 30.1, 28.5, 27.1, 25.9; $[\boldsymbol{\alpha}]_{\boldsymbol{D}}^{\mathbf{20}}$=+52.8° (c 100 µM, H_2O); **HRMS (ES)** calculated for $C_{43}H_{51}N_{10}O_7$ ($[M+H]^+$) m/z: 851.3663, found 851.3692.

4-(2-(6-((+)Biotinylamido)hexanamido)ethoxy)-N^2,N^6-*bis*(4-(3-aminopropoxy)quinolin-2-yl)pyridine-2,6 dicarboxamide (49)

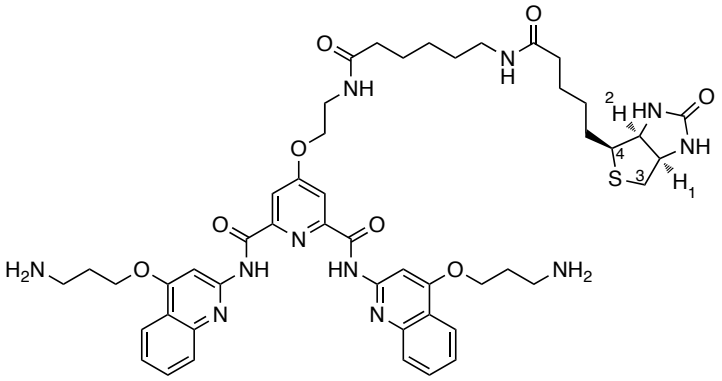

Compound **56** (70 mg, 0.073 mmol) was dissolved in MeOH (5 ml) and 5% Pd/C was added. The mixture was stirred under microwave irradiation for 1 h. The mixture was filtered through celite and the solvent removed *in vacuo*. Some of the Cbz-deprotected product was used as a crude for the next step. This compound (20 mg, 0.024 mmol) and TEA (11 µl, 0.053 mmol) were dissolved in DCM (1 ml) and (+)-biotinamidohexanoic acid *N*-hydroxysuccinimide ester (12 mg, 0.026 mmol) was added. The solution was stirred for 2 h at rt. The solvent was removed *in vacuo* and the product purified by HPLC (gradient: 10% MeCN/90% H_2O, 0.1% TFA to 100% MeCN, 0.1% TFA over 30 min, R_t=14.5-15.0 min) to yield the TFA salt of the product as a white solid (**49**·$2CF_3CO_2H$, 26 mg, 0.022 mmol, 90%). **^{1}H-NMR** (500 MHz, CD_3OD) δ_H 8.45-3.38 (2H, *m*, C$\underline{H}$ (ar)), 8.21-8.12

(4H, *m*, C<u>H</u> (ar)), 8.10-7.98 (4H, *m*, C<u>H</u> (ar)), 7.83-7.75 (2H, *m*, C<u>H</u> (ar)), 4.78-4.69 (4H, *m*, OC<u>H</u>$_2$(CH$_2$)$_2$), 4.51-4.43 (3H, *m*, OC<u>H</u>$_2$CH$_2$NH, (1)), 4.31-4.24 (1H, *m*, <u>H</u> (2)), 3.76-3.70 (2H, *m*, OCH$_2$C<u>H</u>$_2$NH), 3.40-3.35 (4H, *m*, OCH$_2$C<u>H</u>$_2$CH$_2$), 3.18-3.09 (3H, *m*, <u>H</u>, (4, al)), 3.03-2.99 (2H, *m*, <u>H</u>, (al)), 2.90-2.86 (3H, *m*, <u>H</u>, (3, al)), 2.73-2.71 (1H, *m*, <u>H</u>, (3)), 2.70-2.68 (2H, *m*, <u>H</u>, (al)), 2.53-2.43 (4H, *m*, O(CH$_2$)$_2$C<u>H</u>$_2$), 2.32-2.23 (2H, *m*, COC<u>H</u>$_2$(CH$_2$)$_3$CH), 2.19-2.10 (2H, *m*, <u>H</u>, (al)), 1.72-1.40 (6H, *m*, COCH$_2$(C<u>H</u>$_2$)$_3$CH); ^{13}**C-NMR** (125 MHz, CD$_3$OD) δ_C 174.0, 170.0, 168.1, 164.0, 150.9, 149.7, 144.2, 139.1, 138.3, 134.5, 127.6, 123.3, 121.3, 119.0, 113.8, 94.3, 68.1, 62.3, 60.8, 56.0, 54.2, 40.1, 39.2, 38.5, 37.0, 35.7, 29.0, 28.4, 26.9, 26.4, 25.8, 25.5, 25.2, 23.2; $[\boldsymbol{\alpha}]_{\boldsymbol{D}}^{\mathbf{20}}$=+50.3° (c 100 μM, H$_2$O); **HRMS (ES)** calculated for C$_{49}$H$_{62}$N$_{11}$O$_8$ ([M+H]$^+$) m/z: 964.4505, found 964.4512.

4-(2-(+)Biotinylamido)ethoxy)-N^2,N^6-*bis*(4-(2-(pyrrolidin-1-yl)ethoxy)quinolin-2-yl)-pyridine-2,6 dicarboxamide (50)

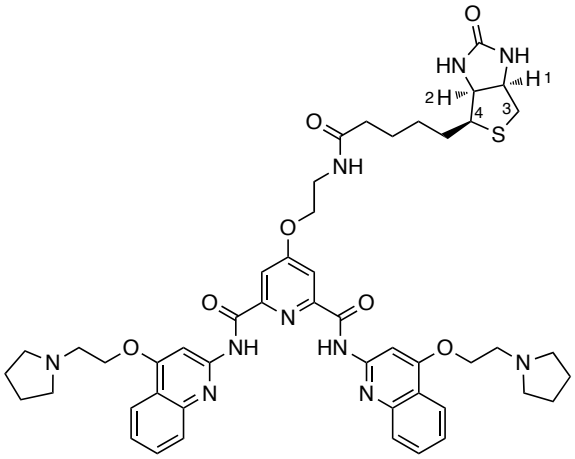

Compound **25** (20 mg,19.1 μmmol) and TEA (13 μl, 0.063 mmol) were dissolved in DCM (1 ml). (+)-biotin *N*-hydroxysuccinimide ester (7 mg, 0.021 mmol) was added and the solution allowed to stir for 2 h. The solvent was removed *in vacuo* and the product purified by HPLC (gradient: 10% MeCN/90% H$_2$O, 0.1% TFA to 100% MeCN, 0.1% TFA over 30 min, R$_t$=15.0-15.5 min) to yield the TFA salt of the product as a white solid (**50**·2CF$_3$CO$_2$H, 22 mg, 0.019 mmol, 99%).

^{1}H-NMR (500 MHz, CD_3OD) δ_H 8.41 (2H, *br d*, *J* 8.0 Hz, C<u>H</u> (ar)), 8.13 (2H, *s*, C<u>H</u> (ar)), 8.10-8.04 (2H, *m*, C<u>H</u> (ar)), 7.97-7.91 (2H, *m*, C<u>H</u> (ar)), 7.71-7.64 (2H, *m*, C<u>H</u> (ar)), 7.70-7.66 (2H, *m*, C<u>H</u> (ar)), 4.49-4.38 (6H, *m*, OC<u>H</u>$_2$), 4.32-4.27 (1H, *m*, <u>H</u> (1)), 4.24-4.19 (1H, *m*, <u>H</u> (2)), 4.01-3.96 (4H, *m*, NC<u>H</u>$_2$(CH$_2$)$_2$), 3.94-3.85 (4H, *m*, NC<u>H</u>$_2$(CH$_2$)$_2$), 3.73-3.68 (2H, *m*, OCH$_2$C<u>H</u>$_2$NH), 3.44-3.33 (4H, *m*, OCH$_2$C<u>H</u>$_2$N), 3.22-3.09 (1H, *m*, <u>H</u> (4)), 3.00-2.95 (1H, *m*, <u>H</u> (3)), 2.86-2.80 (1H, *m*, <u>H</u> (3)), 2.31-2.06 (10H, *m*, COC<u>H</u>$_2$, NCH$_2$C<u>H</u>$_2$CH$_2$), 1.79-1.46 (6H, *m*, COCH$_2$(C<u>H</u>$_2$)$_3$); **^{13}C-NMR** (125 MHz, CD_3OD) δ_C 176.6, 172.0, 170.0, 169.9, 166.8, 164.4, 152.3, 150.9, 143.0, 134.5, 127.9, 124.3, 120.0, 114.4, 95.6, 69.4, 66.8, 63.2, 61.5, 56.9, 56.3, 54.7, 41.1, 39.5, 36.8, 31.6, 29.4, 26.5, 24.0; $[\boldsymbol{\alpha}]_{\boldsymbol{D}}^{\mathbf{20}}$=+60.4° (c 100 μM, H_2O); **HRMS (ES)** calculated for $C_{49}H_{59}N_{10}O_7S$ ($[M+H]^+$) m/z: 931.4283, found 931.4289.

4-(2-(6-((+)Biotinylamido)hexanamido)ethoxy)-N^2,N^6-*bis*(4-(2-(pyrrolidin-1-yl)ethoxy)quinolin-2-yl)pyridine-2,6 dicarboxamide (51)

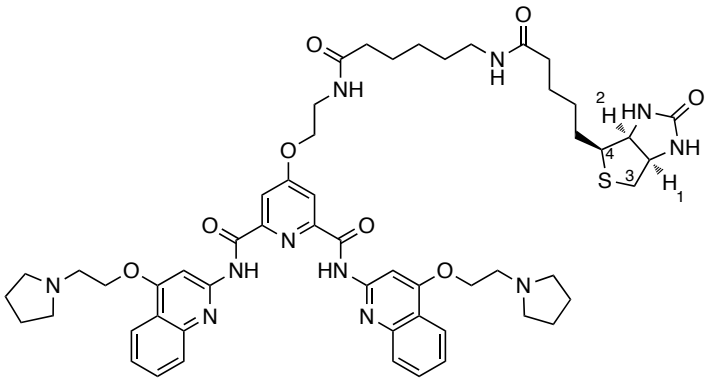

Compound **25** (20 mg, 0.019 mmol) and TEA (13 μl, 0.063 mmol) were dissolved in DCM (1 ml). (+)-biotinamidohexanoic acid *N*-hydroxysuccinimide ester (10 mg, 0.021 mmol) was added and the solution allowed to stir for 2 h. The solvent was removed *in vacuo* and the product purified by HPLC (gradient: 10% MeCN/90% H_2O, 0.1% TFA to 100% MeCN, 0.1% TFA over 30 min, R_t=15.0-15.5 min) to yield the TFA salt of the product as a white solid (**50**·2CF_3CO_2H, 23 mg, 0.018 mmol, 94%). **^{1}H-NMR** (500 MHz, CD_3OD) δ_H 8.45 (2H, *br d*, *J*

8.5 Hz, C<u>H</u> (ar)), 8.16-8.10 (6H, *m*, C<u>H</u> (ar)), 8.02-7.97 (2H, *m*, C<u>H</u> (ar)), 7.76-7.68 (2H, *m*, C<u>H</u> (ar)), 4.94-4.90 (4H, *m*, OC<u>H</u>$_2$CH$_2$NCH$_2$), 4.49-4.45 (1H, *m*, <u>H</u> (1)), 4.44-4.41 (2H, *m*, OC<u>H</u>$_2$CH$_2$NH), 4.26-4.20 (1H, *m*, <u>H</u> (2)), 4.02-3.96 (4H, *m*, NC<u>H</u>$_2$(CH$_2$)$_2$), 3.94-3.86 (4H, *m*, NC<u>H</u>$_2$(CH$_2$)$_2$), 3.73-3.68 (2H, *m*, OCH$_2$C<u>H</u>$_2$NH), 3.42-3.32 (4H, *m*, OCH$_2$C<u>H</u>$_2$NCH$_2$), 3.21-3.04 (4H, *m*, <u>H</u> (al)), 2.94-2.85 (1H, *m*, <u>H</u> (4)), 2.72-2.59 (2H, *m*, <u>H</u> (3)), 2.31-2.04 (12H, *m*, COC<u>H</u>$_2$, NCH$_2$C<u>H</u>$_2$CH$_2$, (al)), 1.68-1.40 (10H, *m*, COCH$_2$(C<u>H</u>$_2$)$_3$CH); **^{13}C-NMR** (125 MHz, CD$_3$OD) δ_C 176.6, 175.9, 171.9, 169.9, 167.3, 164.5, 152.3, 150.8, 141.9, 134.9, 128.2, 124.4, 123.4, 119.9, 114.5, 95.4, 69.3, 67.0, 63.3, 61.6, 57.0, 56.1, 54.6, 41.1, 40.3, 36.9, 36.7, 31.5, 30.1, 29.5, 27.5, 26.9, 26.5, 25.5, 24.1; $[\boldsymbol{\alpha}]_{\boldsymbol{D}}^{\mathbf{20}}$=+52.2° (c 100 µM, H$_2$O); **HRMS (ES)** calculated for $C_{55}H_{70}N_{11}O_8S$ ([M+H]$^+$) m/z: 1044.5124, found 1044.5171.

4-(2-(6-(6-((+)Biotinylamido)hexanamido)hexanamido)ethoxy)-N^2,N^6-*bis*(4-(2-(pyrrolidin-1-yl)ethoxy)quinolin-2-yl)pyridine-2,6 dicarboxamide (52)

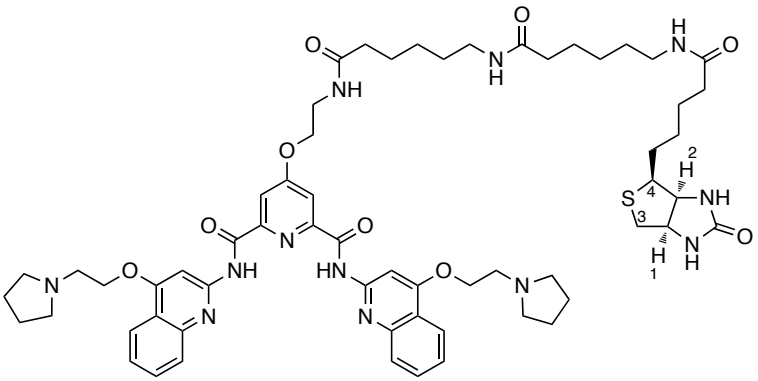

Compound **25** (20 mg, 0.019 mol) and TEA (13 µl, 0.063 mmol) were dissolved in DCM (1 ml). (+)-biotinamidohexanoyl-6-aminohexanoic acid *N*-hydroxysuccinimide ester (12 mg, 0.021 mmol) was added and the solution allowed to stir for 2 h. The solvent was removed *in vacuo* and the product purified by HPLC (gradient: 10% MeCN/90% H$_2$O, 0.1% TFA to 100% MeCN, 0.1% TFA over 30 min, R$_t$=15.0-15.5 min) to yield the TFA salt of the product as a white solid (**50**·2CF$_3$CO$_2$H, 24 mg, 0.017 mmol, 90%). **^{1}H-NMR** (500 MHz, CD$_3$OD) δ_H

8.47 (2H, *br d*, *J* 8.5 Hz, C<u>H</u> (ar)), 8.18-8.10 (6H, *m*, C<u>H</u> (ar)), 8.03-7.98 (2H, *m*, C<u>H</u> (ar)), 7.77-7.71 (2H, *m*, C<u>H</u> (ar)), 4.94-4.90 (4H, *m*, OC<u>H</u>$_2$CH$_2$NCH$_2$), 4.50-4.41 (3H, *m*, OC<u>H</u>$_2$CH$_2$NH, <u>H</u> (1)), 4.30-4.23 (1H, *m*, <u>H</u> (2)), 4.01-3.98 (4H, *m*, NC<u>H</u>$_2$(CH$_2$)$_2$), 3.95-3.85 (4H, *m*, NC<u>H</u>$_2$(CH$_2$)$_2$), 3.72-3.67 (2H, *m*, OCH$_2$C<u>H</u>$_2$NH), 3.42-3.33 (4H, *m*, OCH$_2$C<u>H</u>$_2$NCH$_2$), 3.20-3.07 (7H, *m*, <u>H</u> (4, al)), 2.94-2.85 (1H, *m*, <u>H</u> (3)), 2.71-2.60 (1H, *m*, <u>H</u> (3)), 2.29-2.08 (14H, *m*, COC<u>H</u>$_2$(CH$_2$)$_3$CH, <u>H</u> (al)), 1.77-1.39 (16H, *m*, COCH$_2$(C<u>H</u>$_2$)$_3$CH, NCH$_2$C<u>H</u>$_2$CH$_2$, <u>H</u> (al)); **^{13}C-NMR** (125 MHz, CD$_3$OD) δ_C 175.2, 174.4, 170.4, 168.8, 168.5, 166.0, 163.0, 150.9, 149.4, 140.6, 133.4, 126.6, 122.8, 122.0, 118.5, 112.9, 93.9, 68.0, 65.7, 62.0, 60.5, 55.7, 54.7, 53.2, 39.7, 38.7, 38.1, 35.5, 35.4, 35.3, 28.6, 28.3, 28.1, 26.2, 26.1, 25.6, 25.5, 25.3, 25.1, 23.9, 22.6; $[\boldsymbol{\alpha}]_{\boldsymbol{D}}^{\mathbf{20}}$=+55.5° (c 100 µM, H$_2$O); **HRMS (ES)** calculated for $C_{61}H_{81}N_{12}O_9S$ ([M+H]$^+$) m/z: 1157.5908, found 1157.5965.

4-(5-oxo-(+)Biotinyl)-9,12-dioxa-3,6,15-triazapentadecyloxy)-N^2,N^6-*bis*(4-(2-(pyrrolidin-1 yl)ethoxy) quinolin-2-yl)pyridine-2,6 dicarboxamide (53)

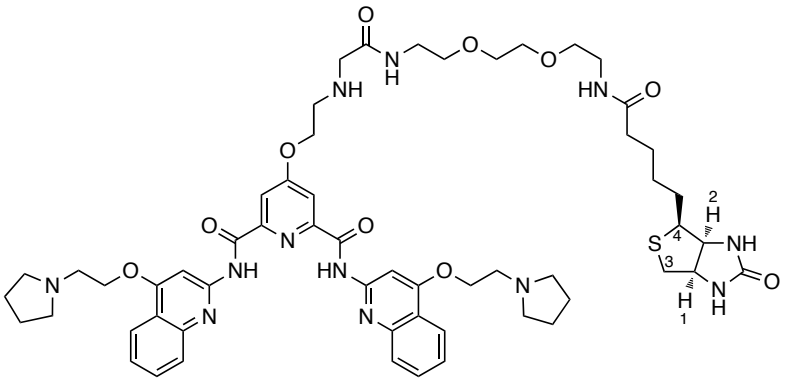

Compound **25** (20 mg, 0.019 mmol) was dissolved in DMF (5 ml). Triethylamine (100 µl, 0.6 mmol) and (+)-biotin polyetheleneoxide iodoacetamide (21 mg, 0.039 mmol) were added. The reaction was stirred for 2 h at 100 °C. The solvent was removed *in vacuo* to yield a yellow oil which was purified by HPLC (gradient: 10% MeCN/90% H$_2$O, 0.1% TFA to 100% MeCN, 0.1% TFA over 30 min, R$_t$=14.0-14.5 min) to yield the TFA salt of the title compound (**53**·3CF$_3$CO$_2$H, 13 mg, 0.009 mmol, 47%) as a light yellow waxy solid. **^{1}H-NMR** (500 MHz, CD$_3$OD)

δ_H 8.46 (2H, *br d*, *J* 8.5 Hz, C<u>H</u> (ar)), 8.27 (2H, *s*, C<u>H</u> (ar)), 8.19 (2H, *s*, C<u>H</u> (ar)), 8.12 (2H, *br d*, *J* 8.5 Hz, C<u>H</u> (ar)), 8.01-7.96 (2H, *m*, C<u>H</u> (ar)), 7.75-7.70 (2H, *m*, C<u>H</u> (ar)), 4.95-4.89 (4H, *m*, OC<u>H</u>$_2$CH$_2$NCH$_2$), 4.75-4.70 (2H, *m*, OC<u>H</u>$_2$CH$_2$NH), 4.54-4.41 (1H, *m*, <u>H</u> (1)), 4.32-4.25 (1H, *m*, <u>H</u> (2)), 4.06-3.98 (6H, *m*, NC<u>H</u>$_2$(CH$_2$)$_2$, <u>H</u> (al)), 3.96-3.88 (4H, *m*, NC<u>H</u>$_2$(CH$_2$)$_2$), 3.73-3.68 (2H, *m*, COC<u>H</u>$_2$NH), 3.67-3.64 (4H, *m*, OCH$_2$C<u>H</u>$_2$N(CH$_2$)$_2$), 3.63-3.54 (6H, *m*, <u>H</u> (al)), 3.53-3.46 (4H, *m*, <u>H</u> (al)), 3.44-3.40 (2H, *m*, OCH$_2$C<u>H</u>$_2$NH), 3.24-3.14 (1H, *m*, <u>H</u> (4)), 2.96-2.86 (1H, *m*, <u>H</u> (3)), 2.72-2.61 (1H, *m*, <u>H</u> (3)), 2.33-2.06 (10H, *m*, COC<u>H</u>$_2$CH$_2$, NCH$_2$C<u>H</u>$_2$CH$_2$), 1.77-1.30 (6H, *m*, COCH$_2$(C<u>H</u>$_2$)$_3$); **^{13}C-NMR** (125 MHz, CD$_3$OD) δ_C 165.2, 162.8, 161.1, 160.6, 151.1, 150.0, 142.4, 132.8, 126.4, 123.4, 122.6, 118.8, 117.6, 116.9, 115.2, 112.8, 94.0, 69.9, 69.2, 68.9, 65.3, 64.6, 62.0, 60.2, 55.6, 54.8, 53.3, 46.3, 39.7, 39.2, 38.8, 35.3, 28.3, 28.1, 25.5, 22.6, 21.3; $[\boldsymbol{\alpha}]_{\boldsymbol{D}}^{\mathbf{20}}$+66.8° (c 100 µM, H$_2$O); **HRMS (ES)** calculated for $C_{57}H_{75}N_{12}O_{10}S$ ([M+H]$^+$) m/z: 1119.5444, found 1119.5452.

4-(2-Benzyloxycarbonylaminoethoxy)pyridine-2,6-dicarboxylic acid (54)

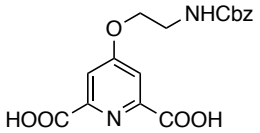

9 (1.0 g, 4.7 mmol), *N*-Cbz-ethanolamine (0.9 ml, 4.6 mmol) and 3.3 g triphenylphosphine polymer bound (1.6 mmol loading/g) were added to freshly distilled THF (50 ml) and cooled to 0 °C. DIAD (1.2 ml, 6.5 mmol) was added dropwise under argon. The mixture was allowed to warm to rt and stirred for 3 d. The solution was filtered and the solvent was removed *in vacuo* and the product purified by column chromatography (80% EtOAc, 20% petroleum ether) to obtain the dimethyl ester of the title compound as a white powder. This compound was dissolved in MeOH (50 ml) and deprotected by slowly adding a solution of NaOH (0.3 g, 7.7 mmol) in H$_2$O (50 ml). The solvent was evaporated *in vacuo* and the remaining solid dissolved in H$_2$O. The solution was acidified with 5% HCOOH (aq.) and extracted with EtOAc. The organic layer was dried

over $MgSO_4$, filtered, and the solvent removed *in vacuo* to obtain the title compound as a white powder (1.0 g, 2.7 mmol, 57%). ^{1}**H-NMR** (500 MHz, CD_3OD) δ_H 7.85 (2H, *s*, C<u>H</u> (ar)), 7.38-7.22 (5H, *m*, C<u>H</u> (Cbz)), 5.07 (2H, *s*, C<u>H</u>$_2$ (Cbz)); 4.28 (2H, *t*, *J* 5.0 Hz, OC<u>H</u>$_2$), 3.57 (2H, *t*, *J* 5.0 Hz, OCH_2C<u>H</u>$_2$); ^{13}**C-NMR** (125 MHz, CD_3OD) δ_C 169.3, 166.9, 159.0, 150.4, 138.3, 129.5, 129.0, 128.8, 115.2, 69.2, 67.6, 41.0; **HRMS (ES)** calculated for $C_{17}H_{16}N_2NaO_7$ ($[M+Na]^+$) m/z: 383.0849, found 383.0850.

4-(2-Benzyloxycarbonylaminoethoxy)-N^2,N^6-*bis*(4-(2-*tert*-butyloxycarbonylamino-ethoxy)quinolin-2-yl)pyridine-2,6 dicarboxamide (55)

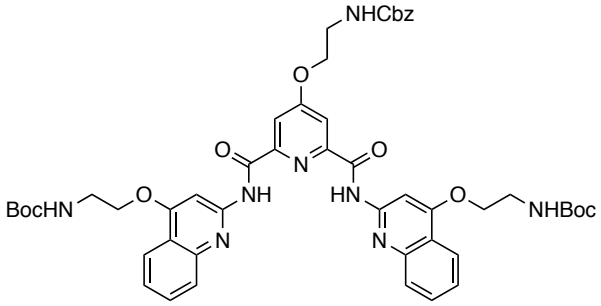

54 (44 mg, 0.115 mmol) was dissolved in DCM (20 ml) and 1-chloro-*N*,*N*,-2-trimethylpropenyl-amine (33 µl, 0.254 mmol) was added slowly and the reaction allowed to stir at rt for 2 h. The solution was then cooled to 0 °C. TEA (35 µl, 0.254 mmol) was added dropwise and the solution was allowed to warm to rt and stirred for 1 h. **5a** (75 mg, 0.247 mmol) was added and the solution stirred under argon at rt overnight. The solvent was removed in *vacuo* and the title compound was precipitated from hot MeCN as a white powder (90 mg, 0.097 mmol, 84%). ^{1}**H-NMR** (400 MHz, CD_3OD) δ_H 8.26 (2H, *br d*, *J* 8.5, C<u>H</u> (ar)), 8.06 (2H, *s*, C<u>H</u> (ar)), 7.96 (2H, *br d*, *J* 8.5 Hz, C<u>H</u> (ar)), 7.93 (2H, *s*, C<u>H</u> (ar)), 7.83-7.77 (2H, *m*, C<u>H</u> (ar)), 7.56-7.50 (2H, *m*, C<u>H</u> (ar)), 7.39-7.27 (5H, *m*, C<u>H</u> (Cbz)), 5.15 (2H, *s*, C<u>H</u>$_2$ (Cbz)), 4.40-4.25 (6H, *m*, OC<u>H</u>$_2$), 3.60-3.47 (6H, *m*, OCH_2C<u>H</u>$_2$), 1.41 (18H, *s*, C<u>H</u>$_3$); ^{13}**C-NMR** (100 MHz, CD_3OD) δ_C 171.3, 167.6, 163.5, 156.7, 156.2, 152.5, 151.2, 146.8, 137.5, 136.1, 131.4, 129.6, 128.7, 128.2,

128.1, 125.2, 122.9, 119.3, 112.6, 95.4, 78.2, 68.6, 67.7, 65.9, 28.6, 28.4; **HRMS (ES)** calculated for $C_{49}H_{54}N_8O_{11}$ ($[M+H]^+$) m/z: 931.3990, found 931.3985.

4-(2-Benzyloxycarbonylaminoethoxy)-N^2,N^6-*bis*(4-(3-*tert*-butyloxycarbonylamino-propoxy)quinolin-2-yl)pyridine-2,6 dicarboxamide (56)

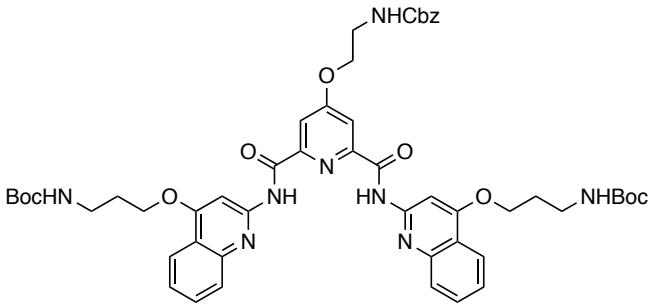

54 (70 mg, 0.141 mmol) was dissolved in DCM (20 ml) and 1-chloro-*N*,*N*,-2-trimethylpropenyl-amine (53 µl, 0.402 mmol) was added slowly and the reaction allowed to stir at rt for 2 h. The solution was then cooled to 0 °C. TEA (56 µl, 0.402 mmol) was added dropwise and the solution was allowed to warm to rt and stirred for 1 h. **16a** (120 mg, 0.310 mmol) was added and the solution stirred under argon at rt overnight. The solvent was removed in *vacuo* and the title compound was precipitated from hot MeCN as a white powder (137 mg, 0.147, mmol, 81%). ^{1}**H-NMR** (400 MHz, CD_3OD) δ_H 8.16 (2H, *dd*, *J* 8.5, 1.5 Hz, C<u>H</u> (ar)), 8.11 (2H, *s*, C<u>H</u> (ar)), 7.95 (2H, *dd*, *J*, C<u>H</u> (ar) 8.5, 1.5 Hz, C<u>H</u> (ar)), 7.92 (2H, *s*, C<u>H</u> (ar)), 7.78 (2H, *ddd*, *J* 8.5, 6.5, 1.5 Hz, C<u>H</u> (ar)), 7.53 (2H, *ddd*, *J* 8.5, 6.5, 1.5 Hz, C<u>H</u> (ar)), 7.39-7.27 (5H, *m*, C<u>H</u> (ar) (Cbz)), 5.06 (2H, *s*, C<u>H$_2$</u> (Cbz)), 4.40-4.29 (6H, *m*, OC<u>H$_2$</u>), 3.54-3.46 (2H, *m*, $OCH_2C\underline{H_2}NHCbz$), 3.28-3.20 (4H, *m*, $OCH_2C\underline{H_2}CH_2$), 2.09-2.01 (4H, *m*, $O(CH_2)_2C\underline{H_2}$), 1.37 (18H, *s*, C<u>H$_3$</u>); ^{13}**C-NMR** (100 MHz, CD_3OD) δ_C 162.0, 161.1, 155.2, 154.6, 151.3, 150.0, 145.9, 140.0, 129.4, 127.2, 126.7, 125.8, 123.4, 120.7, 118.1, 116.8, 113.9, 112.5, 110.8, 93.8, 87.3, 76.5, 65.1, 64.4, 37.7, 27.7, 27.1; **HRMS (ES)** calculated for $C_{51}H_{59}N_8O_{11}$ ($[M+H]^+$) m/z: 959.4455, found 959.4460.

5.2 FRET-melting

100 μM stock solutions of oligonucleotides were prepared in molecular biology grade DNase-free H_2O (Sigma Aldrich®). Further dilutions were carried out in 60 mM potassium cacodylate buffer, pH 7.4. FRET-melting experiments were carried out with a 200 nM oligonucleotide concentration. Six DNA oligonucleotides were used in these experiments: five were dual fluorescently labelled: H-telo (5′-FAM-GGG TTA GGG TTA GGG TTA GGG-TAMRA-3′), C-myc (5′-FAM-TGA GGG TGG GTA GGG TGG GTA A-TAMRA-3′), C-kit1 (5′-FAM-GGG AGG GCG CTG GGA GGA GGG-TAMRA-3′), C-kit2 (5′-FAM-GGG CGG GCG CGA GGG AGG GG-TAMRA-3′), ds-DNA (5′-FAM-TAT AGC TAT A-HEG-T ATA GCT ATA-TAMRA-3′) and one was unlabelled: ds-DNA competitor (5′-CAA TCG GAT CGA ATT CGA TCC GAT TG-3′).

The donor fluorophore was FAM, and the acceptor fluorophore was TAMRA. The dual-labelled oligonucleotides were annealed at a concentration of 400 nM by heating at 94 °C for 10 min followed by slow cooling to rt at a controlled rate of 0.1 °C/min. 96-well plates were prepared by addition of 50 μl of the annealed DNA solution to each well, followed by 50 μl solution of compound at the appropriate concentration. For the competition experiments, ds-DNA competitor was added to the dual-labelled oligonucleotides at an excess of 50 or 200 mole equivalents and annealed in the same solution in order to produce an excess of at least 25 or 100 mole equivalents of double stranded DNA, respectively. Measurements were made in triplicate with an excitation wavelength of 483 nm and a detection wavelength of 533 nm. Final analysis of the data was carried out using OriginPro 7.5 data analysis and graphing software (OriginLab®). All given values were determined graphically from a dose-response fitting of ΔT_m against compound concentration.

5.3 HyperChem® modeling

Molecular modeling calculations were performed for molecules **1a**, **2a** and **3a** using HyperChem®, v 8.1 in order to calculate the rotational barriers for C16-C13, C8-C4, C2-C7 and C10-C15 bonds as depicted in Figure 2.3 for **1a**.

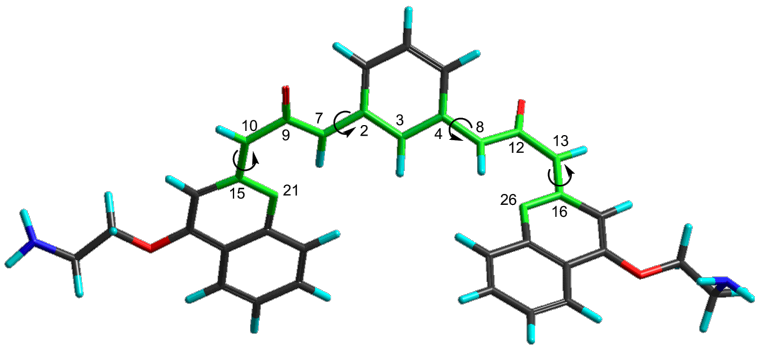

Figure 5.1: labelled bonds of **1a** for the modeling studies.

Conformational search using the PM3 semi-empirical method with convergence criteria of 0.025 kcal/mol/Å was performed for the bonds indicated above (simultaneous rotations). The conformations with the lowest energies were further refined using PM3 with a convergence criteria of 0.01 kcal/mol/Å. The optimised structures were placed in a 42875/Å^3 water box containing 1378 H_2O molecules. The system was optimised using the MM+ force field with a convergence criteria of 0.025 kcal/mol Å. Pictures of the simulation of the molecules in a water box are displayed in Figure 5.2.

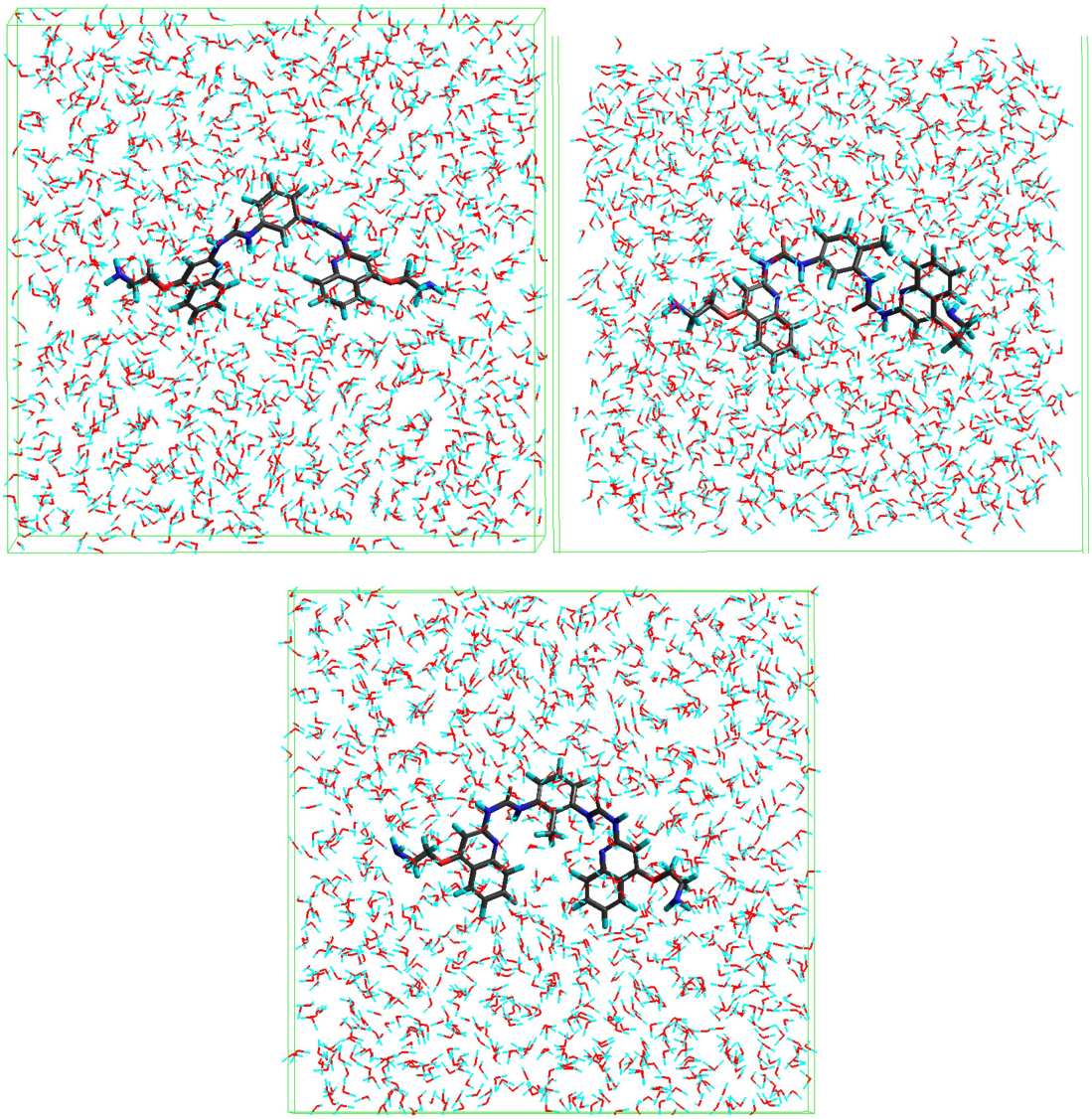

Figure 5.2: Optimised structures of **top left: 1a**; **top right: 2a** and **bottom: 3a** placed in a 42875 Å^3 water box.

5.4 Cell studies

HT-1080 cells were cultured in T-75 flasks in media (DMEM, high L-glucose, L-glutamine) supplemented with 10% fetal calf serum) and split at 70-80% confluency using 0.25% trypsin 0.02% EDTA in 1 × PBS.

5.4.1 Measurements of growth inhibition (GI_{50})

Growth inhibition was determined using the cell viability assay CellTiter-Glo™ (Promega®). HT-1080, HeLa, U2OS or WI-38 cells were plated in 96 well plates at a density of 4,000 cells per well in 100 µl media and incubated for 24 h. Compounds were added in serial dilutions (in a range between 0-40 µM) at a volume of 100 µl per well at the respective concentrations. Cell viability was measured after 72 h using the manufacturers protocol. In brief, the media was removed from the wells, and 100µl of media (rt) was added, followed by 100 µl of the luminescence reagent (rt). Measurements were taken after 20 min incubation at rt. All measurements were made in triplicate and the experiment repeated three times. Luminescent readings were taken on a luminometer. Final analysis of the data was carried out using OriginPro® 7.5 data analysis and graphing software (OriginLab®). The GI_{50} was determined graphically from a dose-response fitting of %luminescent signal against compound concentration.

5.4.2 Long term growth assay and cytotoxicity

HT-1080 cells were cultured in T-25 flasks as stated above and seeded at 300,000 cells per flask initially and incubated with **18-20**, **22**, **23**, **25**, **26**, **31-33**, **35-38**, **44** or **53** at the respective GI_{50} concentrations, or no compound as control. The cells were split after 3 to 4 days, counted with a hemicytometer and reseeded at their initial density of 300,000 cells per flask. PDs were calculated as stated in section 3.6. Toxicity was assessed using a Trypan blue exclusion assay. In brief, 10 µl of cell suspension was mixed with 10 µl of 0.4 % aq. Trypan blue solution and cells counted with a hemicytometer. Dead cells were identified by blue nuclear staining. This procedure was repeated every third day. All experiments were performed in triplicate. Final analysis was done using OriginPro® 7.5 data analysis and graphing software.

5.4.3 β-Galactosidase assay

Senescence was assessed using a senescence β-galactosidase staining kit (Cell Signalling Technology®) according to the manufacturers protocol. In brief, HT-1080 cells were cultured in T-75 flasks for 1 d and incubated with **23**, **25**, **26**, **31**, **33**, **44**

and **53** respectively for 4 d at their respective GI_{50}. As a control, cells were incubated without compound under the same conditions. Cells were split and seeded at 4000 cells per well on a Cover Well™ microscopy slide chamber (Invitrogen®) and incubated with **23**, **25**, **26**, **31**, **33 44** and **53** at the aforementioned concentrations, or in the absence of compound, for another 4 d. Subsequently, the media was removed and the wells washed twice with 1 × PBS. Cells were fixed with 2% formaldehyde and 0.2% glutaraldehyde in 1× PBS for 15 min. This solution was then removed and the wells washed twice with 1 × PBS. Each well was incubated with 800 µl staining solution (40 mM citric acid/sodium phosphate (pH 6.0), 0.15 M NaCl, 2 mM $MgCl_2$, 5 mM potassium ferrocyanide, 5 mM potassium ferricyanide, 1 mg/ml X-gal, 5% DMF) at 37 °C for 16 h. The staining solution was removed and the cells stored in 70% glycerol.

5.5 Genomic DNA isolation

Genomic DNA was extracted from HT-1080 cells using QIAamp™ DNA Mini Kit (Qiagen®) according to the manufacturers protocol. The buffer content of the supplied kit was not provided by the manufacturer. In brief, cells were isolated by centrifugation (up to 5×10^6 per sample) after trypsinisation. 20 µl of proteinase K solution (600 mAU/ml) and 6 µl RNAse A (20 mg/ml, Invitrogen®) were added to each sample. 200 µl of the supplied buffer *AL* were added and the resulting solution mixed thoroughly. The samples were incubated at 56 °C for 10 min. Subsequently, 200 µl of EtOH were added and the resulting solution mixed thoroughly. The solution was transferred into a QIAmp™ mini spin column and centrifuged at 8,000 rpm for 1 min. The supernatant was discarded and 500 µl of buffer *AW1* were added to the column. The sample was centrifuged at 8,000 rpm for 1 min. The supernatant was discarded and 500 µl of buffer *AW2* were added and the column centrifuged at 13,700 rpm for 3 min. The supernatant was discarded. 200 µl of molecular biology grade DNase-free H_2O were added to each column and the column centrifuged at 8,000 rpm for 1 min to elute the final genomic DNA solution.

5.6 Non-denaturing hybridisation assay

To detect the 3′-G-overhang a non-denaturing hybridisation assay was performed. 5 µg of undigested genomic DNA, extracted from cells treated with or without compounds **23**, **25**, **26**, **31**, **33**, **44** or **53** at the respective GI_{50} concentrations and respective time points, were hybridised for 16 h at 50 °C with 0.5 pmol of [γ-^{32}P] ATP-labelled oligonucleotide of the sequence (5′-$(CCCTAA)_3CCC$-3′) in 30 µl hybridisation buffer (20 mM Tris.HCl (pH 8.0), 0.5 mM EDTA, 50 mM NaCl, 10 mM $MgCl_2$). Radioactive oligonucleotides were prepared by incorporating [γ-^{32}P] ATP using T4 polynucleotide kinase with 70-80% labeling efficiency. Labeling was achieved at 37 °C for 1 h and 95 °C for 5 min and a typical labeling reaction solution consisted of: 1.2 µl 10 × PNK buffer, 4.0 µl 5′-$(CCCTAA)_3CCC$-3′ at 1 µM, 0.3 µl T4 polynucleotide kinase solution, 1.2 µl [γ-^{32}P] ATP stock solution and 5.3 µl biology grade H_2O. Hybridisation reactions were stopped by the addition of 9 µl loading buffer (20% glycerol, 1 mM EDTA, 0.2% bromophenol blue) and size-fractioned on a 0.7% agarose gel for 3 h at 45 V. The gels were subsequently stained with EBr. The bottom of the gel was cut to remove unbound probe and thus increase resolution. Gels were dried on Whatman® filter paper at 60 °C and exposed overnight on an autoradiography film. EBr fluorescence and the autoradiography film were scanned with a phosphorimager (Typhoon™ 9210, Amersham Biosciences®). Results were expressed as the relative hybridisation signal normalised to the fluorescent signal of EBr.

5.7 Genomic DNA sonication

Isolated genomic DNA from HT-1080 cells was sheared with a Bioruptor™ (UCD 200) sonicator (Diagenode®). 200 µl of DNA sample was sonicated at 0 °C for 60 min. Sonication was performed at intervals (30 s on and 30 s off). This procedure yielded DNA fragment sizes of approximately 100-500 bp, as assessed by agarose gel electrophoresis.

5.8 Pull-down studies

5.8.1 Pull-down studies on synthetic oligonucleotides

Oligonucleotide stock solutions of 100 μM were prepared using molecular biology grade DNase-free H_2O. Further dilutions were carried out in annealing buffer containing 10 mM Tris.HCl (pH 7.4) and 60 mM KCl. The samples were annealed by heating at 94 °C for 10 min followed by slow cooling to rt at a controlled rate of 0.1 °C/min.

The following protocol was used for the experiments described in section 4.3:

In a pull-down experiment, 50 μl of oligonucleotide at 2 μM was incubated with **47**, **48**, **49**, **50**, **51**, **52** or **53** (0, 1.0, 2.0, 4.0, 6.0, 10.0 and 14.0 μM) for 15 min at rt. The streptavidin-coated magnetic beads (Sigma Aldrich®) isolated by magnetic separation from 100 μl of the supplied suspension were washed twice with 100 μl of annealing buffer. They were then incubated with the DNA/ligand solution for 15 min at rt. The supernatant was separated from beads through magnetic separation and analysed by UV.

The following protocol was used for the experiments described in section 4.4:

In a pull-down experiment, 100 μl of oligonucleotide at 5 μM was incubated with **53** (0, 3.0, 4.5, 6.5, 10.0 and 15.0 μM) for 30 min at rt. In experiments involving G-quadruplex DNA/ds-DNA mixtures, 50 μl of a 5 μM ds-DNA solution was added to 50 μl of a 5 μM G-quadruplex DNA solution, and the mixture was incubated with a defined quantity of **53** (0, 3.0, 4.5, 6.5, 10.0 and 15.0 μM) for 30 min at rt. One vial of streptavidin-coated magnetic beads (Streptavidin MagneSphere™ paramagnetic particles, Promega®), which had been washed twice with 300 μl of annealing buffer, was then incubated with the solution for 30 min at rt. The supernatant was separated from beads through magnetic separation and analysed by UV or gel electrophoresis. In a recovery experiment, the beads collected after pull-down were washed twice with 100 μl of 10 mM Tris.HCl (pH 7.4). For the experiments involving DNA, 100 μl of an 8 M aq. LiCl solution was added per vial of beads and incubated for 30 min at rt. The beads were heated

for 5 min at 60 °C and the solution was separated from beads through magnetic separation. Before analysis by gel electrophoresis, the supernatant was purified using Illustra MicroSpin™ G-25 columns to remove LiCl (GE-Healthcare®). For the experiments involving RNA, 100 µl of an 8 M aq. urea solution was added to each vial of beads and incubated for 30 min at rt. The solution was separated *via* magnetic separation and analysed by UV without further purification. The experiments of longer synthetic oligonucleotides (50-101 mer) were performed with 0, 1 and 3 mole equivalents of **53**. The DNA concentrations used were 5 µM for 50 and 51mers and 1 µM for 100 and 101-mers, respectively. For the experiments in the presence of the complementary strand, the strands had been annealed in a 1:1 mixture of both strands. Experiments were performed with a 1 µM or 5 µM concentration of the resulting double-stranded DNA.

5.8.2 Co-operativity pull-down

Pull-down experiments in the presence of **23** were performed in an analogous manner to the procedures described in section 5.8.1. The DNA was incubated with 0.0, 10.0 or 20.0 µM **23** prior to adding 0.0, 5.0 or 15.0 µM **53**. The UV spectra were blanked against the respective solutions with the appropriate concentrations of **23**.

5.8.3 Pull-down studies on genomic DNA

Sonicated genomic DNA was annealed at a concentration of 0.52 µM in annealing buffer as described in section 5.8.1. In a pull-down experiment, 100 µl of genomic DNA (0.52 µM) were incubated with **53** (0, 2.6, 5.2 and 10.4 µM) for 2 h at rt. The solution was then incubated with one vial of streptavidin-coated magnetic beads, which had been washed twice with 300 µl of annealing buffer, for 1 h at rt. The supernatant was separated from beads through magnetic separation, purified using the QIAquick™ Nucleotide Removal Kit (Qiagen®) In a recovery experiment, the beads collected after pull-down were washed twice with 100 µl of 10 mM Tris.HCl (pH 7.4). A urea solution (100 µl, 8 M aq.) was added to the each vial of beads and the solution was incubated for 30 min at rt. The solutions were recovered through magnetic separation and purified using Illustra MicroSpin™ G-25 (GE-Healthcare®) columns.

5.8.4 Agarose gel electrophoresis

Gels were prepared at the given percentage of agarose (by weight) in TBE buffer by heating in a microwave until a clear solution was obtained. The solution was poured into a gel tank of the appropriate size fitted with a comb, and the gel was left to cool and set at rt between 30 and 60 min. The comb was removed and the tank filled with 1 × TBE buffer. DNA samples (10-60 µl) were loaded and the gel run at the appropriate voltage and time to separate the DNA samples. 6 × loading buffer (20% glycerol, 1 mM EDTA, 0.2% bromophenol blue) was used and diluted as appropriate. DNA was visualised by staining the gels subsequently with Sybr™ Gold or EBr for 15 min.

5.8.5 Polyacrylamide gel electrophoresis

Denaturing polyacrylamide gel electrophoresis was performed by using 20% pre-cast gels (Invitrogen®) and run with the appropriate gel tank. Non-denaturing polyacrylamide gel electrophoresis was performed by pouring the gels (10 × TBE buffer (1 ml) , proto-gel polyacrylamide (6.6 ml), biology grade H_2O (2.7 ml), 50 µl 10% w/v ammonium persulfate and 5 µl TEMED) which were stand to set for 1 h and run in the appropriate gel tank. Samples were loaded using the following 6 × loading buffer: 25 mg bromophenol blue, 25 mg xylene cyanol and 1.5 g Ficoll in biology grade H_2O (10 ml). Gels were pre-run for 30 min and then run at 50-100 V for 1-3 h depending on gel size and DNA fragment sizes. PAGE was performed at 4 °C or rt depending on the separation of the DNA fragments. DNA was visualised by staining the gels subsequently with Sybr™ Gold or EBr for 15 min.

5.9 qPCR studies on genomic DNA

The composition of the PCR reactions performed on telomere and *36B4* control gene were identical except for the primers. In a typical PCR experiment, the final concentration of reagents were 0.2 × Sybr Green I solution, 15 mM TRIS.HCl (pH 8.0), 50 mM KCl, 2 mM $MgCl_2$, 0.2 mM of each dNTP, 5 mM DTT, 1% DMSO, 1.25 U AmpliTaq Goldtextsuperscript™ DNA polymerase and 35 ng of pull-down supernatant genomic DNA in a final volume of 50 µl. The final

telomere primer concentrations were: tel 1: 270 nM and tel 2: 900 nM. The final *36B4* primer concentrations were: 36B4u: 300 nM and 36B4d: 500 nM. The PAGE purified primer sequences were: tel 1 (5′-GGT TTT TGA GGG TGA GGG TGA GGG TGA GGG TGA GGG T-3′), tel 2 (5′-TCC CGA CTA TCC CTA TCC CTA TCC CTA TCC CTA TCC CTA-3′), 36B4u (5′-CAG CAA GTG GGA AGG TGT AAT CC-3′) and 36B4d (5′-CCC ATT CTA TCA TCA ACG GGT ACA A-3′). We performed the following controls in all the PCR reactions performed on the supernatants after pull-down and solutions after recovery from beads: 1) no template DNA; 2) *Escherichia coli* genomic DNA which does not contain telomeres; 3) no primers and 4) no polymerase. The PCR cycle conditions were set as follows: a preincubation step for 10 min at 95 °C to activate the DNA polymerase for both the telomere and *36B4* control gene PCRs followed by 1) 33 cycles at 95 °C for 15 s and 54 °C for 2 min for telomere PCR and 2) 33 cycles at 95 °C for 15 s and 58 °C for 1 min for *36B4* PCR. The number of PCR cycles was set to 22 when the telomere specific qPCR was performed on genomic DNA solutions obtained after recovery from beads. All measurements were performed in triplicate. Cp values were calculated using LightCycler® 480 software using the second derivative method. The ΔC_p values were calculated using the following formula (5.3):

$$\Delta C_p = C_{p.CON} - C_{p.[53]} \tag{5.1}$$

$C_{p.CON} = C_p$ of control experiment, $C_{p.[53]} = C_p$ of an experiment performed with a defined molarity of **53**.

The PCR amplification efficiencies, calculated from standard curves were 1.96 and 1.94 for telomere and *36B4* PCRs, respectively. Relative percentage ratios of telomere and *36B4* in the supernatant obtained after pull-down were calculated by using the following formula (5.2):

$$\%Ratio = p^{-\Delta C_p} \times 100 \tag{5.2}$$

p = primer efficiency.

To assess the significance of the experiment, we performed an unpaired t-test. The p-values were as follows:

[53] in μM	telomere qPCR p-value	*36B4* qPCR p-value
0.0	-	-
2.6	0.0278	0.7122
5.2	0.0100	0.7258
10.4	0.0001	0.2836

Table 5.1: p-values for qPCR experiments

Agarose gel electrophoresis (2%) was carried out to visualise the qPCR amplified product of telomeric DNA recovered from the beads. The gel was run at 80 V for 90 min in 1 × TBE buffer and then stained with EBr.

5.10 Error calculations

Errors were calculated as the standard deviation using the following formula:

$$\sigma = \sqrt[2]{\frac{1}{N}\sum_{i=1}^{N}(x_{\mathrm{i}} - \mu)^2} \tag{5.3}$$

σ = standard deviation, N = sample size, x = sample value, μ = mean value.

Appendix A

Additional FRET-melting data

The FRET melting thermal shift profiles for compounds **18-46** are displayed in Figure A.1, Figure A.2 and Figure A.3. The used targets are: ● H-telo, ● C-kit1, ● C-kit2, ● C-myc, ● Bcl-2 and ● K-ras.

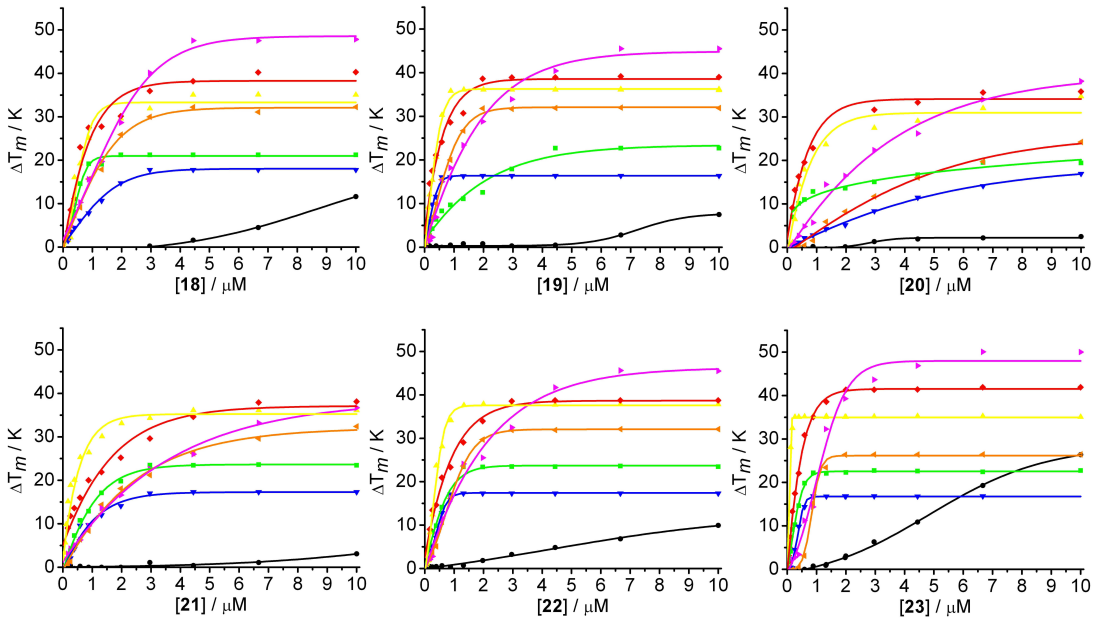

Figure A.1: FRET-melting thermal shift profiles for **18-23**.

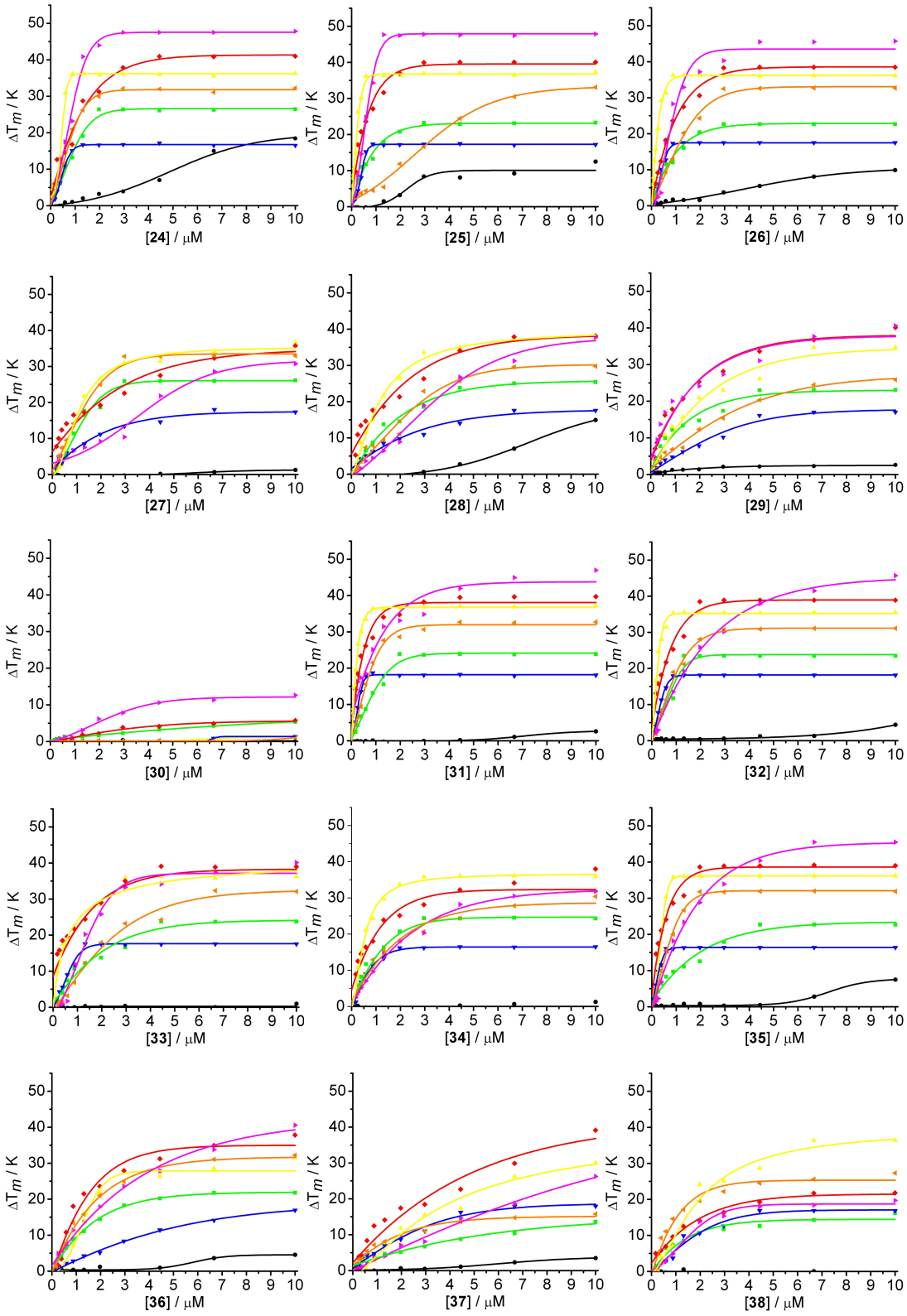

Figure A.2: FRET-melting thermal shift profiles for **24-38**.

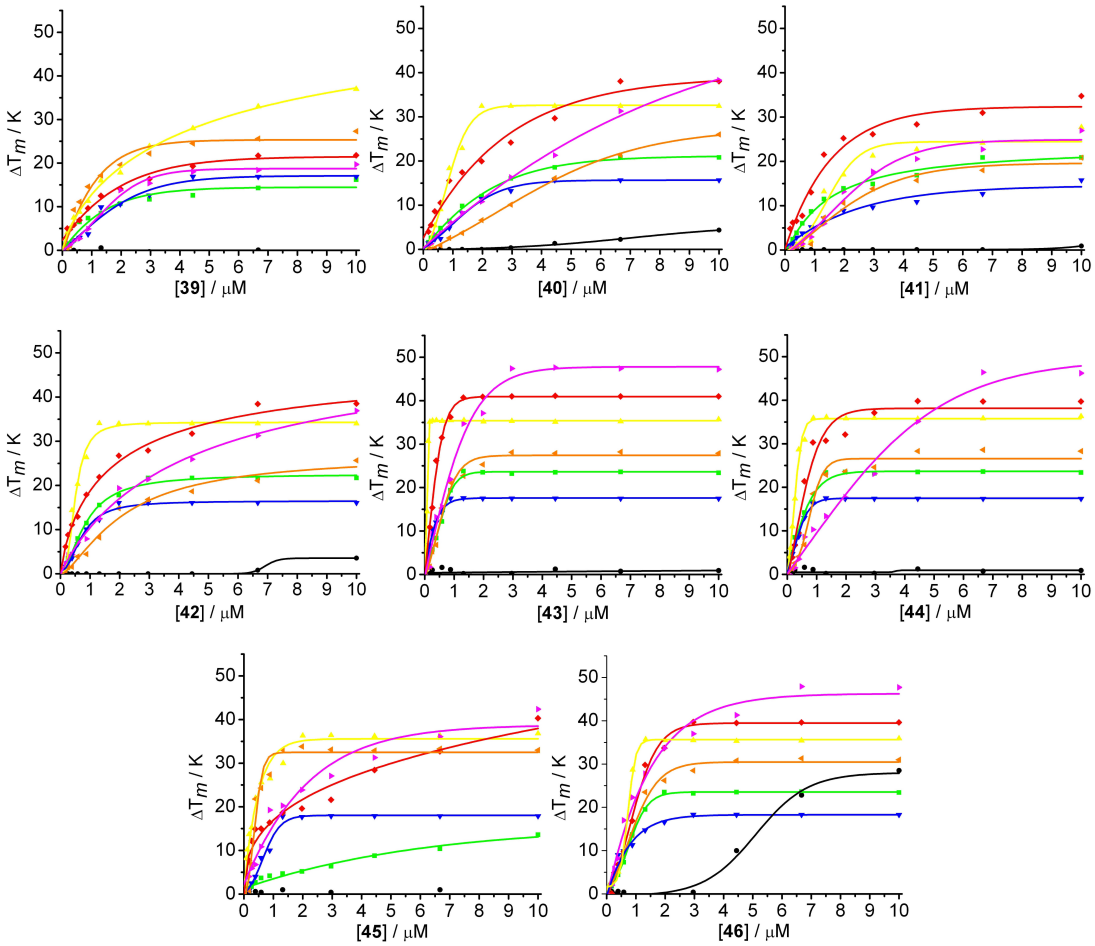

Figure A.3: FRET-melting thermal shift profiles for **39**-**46**.

The ΔT_m-values at 1 μM compound **18-46** are displayed in Table A.1 for C-kit1, C-kit2, C-myc, Bcl-2 and K-ras. The values for H-telo and ds-DNA can be found in Chapter 3 (Table 3.1).

	ΔT_m (K)				
Compound	**C-kit1**	**C-kit2**	**C-myc**	**Bcl-2**	**K-ras**
18	25.6±0.7	19.7±0.5	9.1±0.2	14.7±0.8	15.2±0.7
19	31.8±0.9	9.7±0.5	16.3±0.8	22.7±0.7	18.0±0.8
20	26.2±0.9	12.1±0.9	2.9±0.1	3.5±0.4	8.4±0.9
21	19.2±0.8	14.5±0.7	10.3±0.5	9.9±1.1	9.9±0.4
22	26.8±0.5	19.5±1.2	16.6±0.4	18.2±0.6	16.7±0.4
23	35.0±0.7	22.3±0.7	16.8±0.8	19.2±0.9	20.2±0.8
24	22.2±0.4	16.2±0.7	15.8±0.8	21.0±1.0	29.9±0.9
25	31.2±0.9	16.0±0.5	17.0±0.8	5.9±0.7	40.4±0.9
26	24.5±0.7	14.9±0.7	17.1±0.8	15.6±1.1	25.7±0.7
27	14.6±0.5	11.5±1.0	7.4±0.6	14.6±0.5	5.4±0.4
28	16.5±1.0	9.6±0.4	6.3±0.3	7.5±0.4	4.7±0.3
29	17.7±0.7	11.2±0.6	4.9±0.8	7.1±1.1	17.8±0.7
30	1.2±0.6	1.1±0.5	0.4±0.2	0.3±0.3	2.3±0.3
31	33.3±0.9	14.4±0.6	16.0±1.0	23.1±0.9	25.7±0.7
32	29.1±0.7	17.3±0.3	17.1±0.5	18.9±9.7	15.1±0.9
33	22.2±0.9	9.6±0.7	14.5±0.8	8.6±0.9	12.2±0.6
34	19.6±0.4	13.3±0.4	12.1±0.5	11.5±0.9	10.3±0.5
35	31.6±0.5	9.7±0.5	16.9±0.8	22.7±0.8	18.3±0.4
36	15.5±0.6	9.4±0.3	2.3±0.3	13.2±0.8	10.7±0.5
37	9.1±0.9	3.8±0.4	5.3±0.5	6.7±0.5	3.2±0.4
38	9.9±0.9	7.2±0.6	5.8±0.1	14.4±0.9	5.8±0.5
39	9.8±0.5	7.4±0.3	5.9±0.3	14.3±0.8	5.9±0.5
40	13.5±0.8	7.2±0.4	5.7±0.4	2.5±0.4	5.8±0.3
41	15.5±0.5	9.2±0.5	5.3±0.5	4.2±0.3	4.8±0.4
42	18.5±0.8	13.2±0.3	11.1±0.4	6.5±0.3	10.4±0.4
43	38.1±0.7	20.9±0.9	16.8±0.7	21.6±0.9	26.1±0.5
44	28.7±0.9	19.3±0.8	16.5±1.0	19.6±0.7	9.6±0.3
45	17.1±0.8	3.6±0.7	13.8±0.5	32.0±0.7	16.0±1.1
46	20.1±0.9	15.8±1.1	13.2±0.7	17.1±0.9	22.3±0.9

Table A.1: ΔT_m at 1μM compound **18-46**.

Appendix B

NCI growth arrest data

The data provided by the cell-line screen performed by the NCI are displayed in this appendix. The growth curves of 60 cancer cell lines treated with different doses of **20**, **25**, **26** and **31** are displayed. They were determined from five doses of compound. The appendix also features tables listing the various GI_{50}, TGI and LC_{50} values. Furthermore, the appendix shows the mean values of the aforementioned constants. The accumulative data describes and summarises the effects these compounds have on the growth properties of the cancer cell lines investigated.

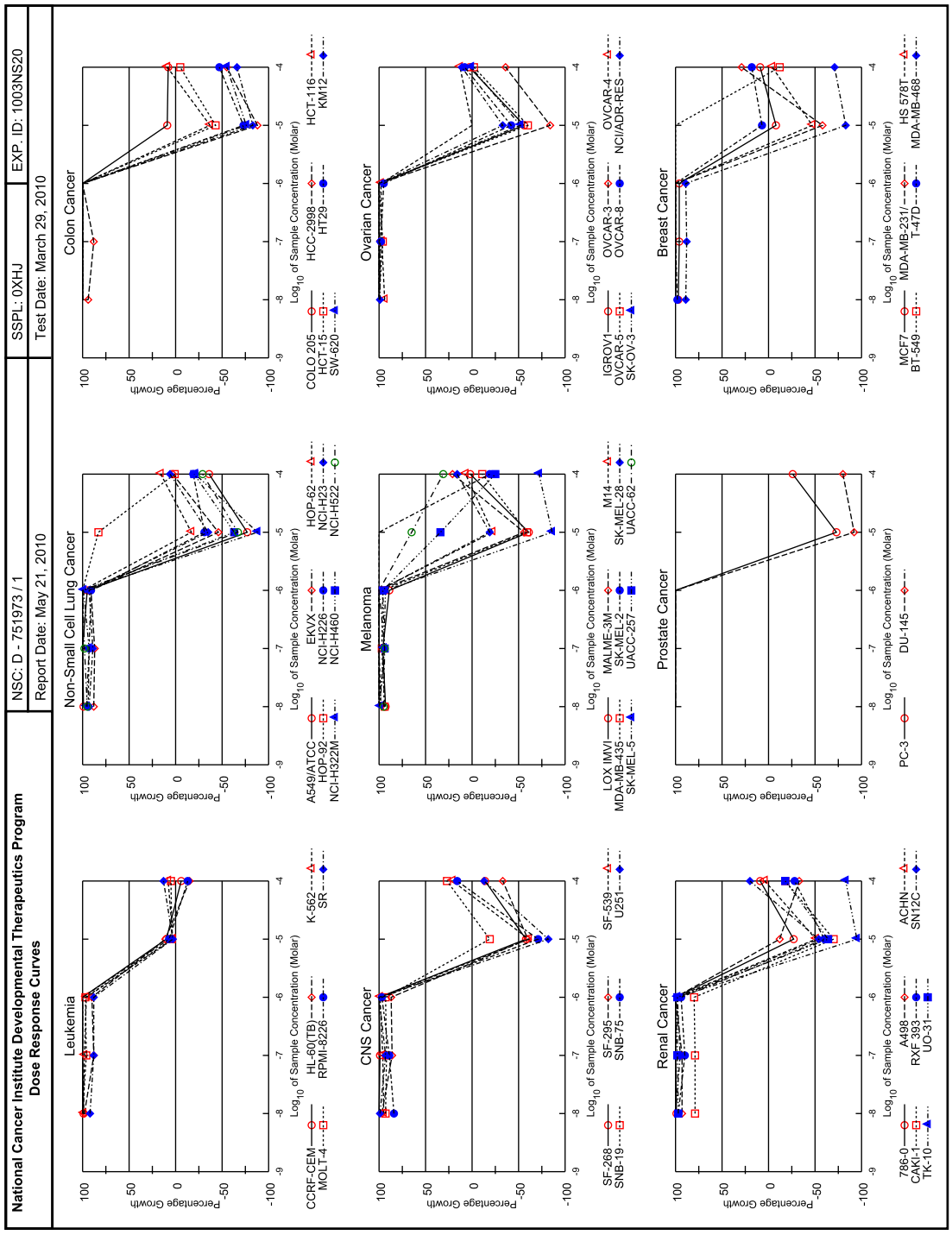

Figure B.1: Growth curves of various cancer cell lines treated with increasing molarities of **20**.

National Cancer Institute Developmental Therapeutics Program
In-Vitro Testing Results

NSC : D - 751973 / 1	Experiment ID : 1003NS20	Test Type : 08	Units : Molar
Report Date : May 21, 2010	Test Date : March 29, 2010	QNS :	MC :
COMI : Raphaine D (84124)	Stain Reagent : SRB Dual-Pass Related	SSPL : 0XHJ	

			Log10 Concentration												
	Time		Mean Optical Densities					Percent Growth							
Panel/Cell Line	Zero	Ctrl	-8.0	-7.0	-6.0	-5.0	-4.0	-8.0	-7.0	-6.0	-5.0	-4.0	GI50	TGI	LC50
Leukemia															
CCRF-CEM	0.498	1.813	1.797	1.829	2.028	0.632	0.470	99	101	116	10	-6	4.22E-6	4.37E-5	> 1.00E-4
HL-60(TB)	0.724	2.736	2.696	2.485	2.526	0.949	0.615	98	88	90	11	-15	3.20E-6	2.66E-5	> 1.00E-4
K-562	0.337	2.278	2.259	2.238	2.210	0.400	0.488	99	98	96	3	8	3.15E-6	> 1.00E-4	> 1.00E-4
MOLT-4	0.891	3.096	3.101	3.014	3.032	0.974	1.002	100	96	97	4	5	3.20E-6	> 1.00E-4	> 1.00E-4
RPMI-8226	0.764	2.206	2.296	2.533	2.536	0.871	0.666	106	123	123	7	-13	4.28E-6	2.31E-5	> 1.00E-4
SR	0.408	1.925	1.803	1.738	1.747	0.452	0.599	92	88	88	3	13	2.81E-6	> 1.00E-4	> 1.00E-4
Non-Small Cell Lung Cancer															
A549/ATCC	0.288	1.514	1.505	1.524	1.453	0.066	0.184	99	101	95	-77	-36	1.83E-6	3.57E-6	.
EKVX	0.645	1.800	1.660	1.647	1.699	0.350	0.681	88	87	91	-46	3	2.00E-6	.	> 1.00E-4
HOP-62	0.451	1.548	1.551	1.620	1.652	0.376	0.632	100	107	110	-17	16	2.96E-6	.	> 1.00E-4
HOP-92	0.988	1.619	1.642	1.670	1.778	1.512	0.992	104	108	125	83	1	2.51E-5	> 1.00E-4	> 1.00E-4
NCI-H226	0.899	2.143	2.069	2.056	2.028	0.620	0.727	94	93	91	-31	-19	2.16E-6	5.56E-6	> 1.00E-4
NCI-H23	0.498	1.717	1.630	1.589	1.629	0.323	0.570	93	89	93	-35	6	2.16E-6	.	> 1.00E-4
NCI-H322M	0.645	1.847	1.795	1.768	1.841	0.080	0.512	96	93	99	-88	-21	1.84E-6	3.40E-6	.
NCI-H460	0.273	2.041	2.095	2.185	2.093	0.102	0.219	103	108	103	-63	-20	2.09E-6	4.18E-6	.
NCI-H522	0.582	1.601	1.554	1.580	1.657	0.191	0.411	95	98	105	-67	-29	2.10E-6	4.08E-6	.
Colon Cancer															
COLO 205	0.294	1.784	1.863	1.884	1.897	0.424	0.410	105	107	108	9	8	3.82E-6	> 1.00E-4	> 1.00E-4
HCC-2998	0.669	1.915	1.841	1.768	1.918	0.081	0.303	94	88	100	-88	-55	1.85E-6	3.41E-6	6.29E-6
HCT-116	0.186	1.934	1.961	1.997	1.957	0.117	0.348	102	104	101	-37	9	2.34E-6	.	> 1.00E-4
HCT-15	0.369	2.501	2.543	2.537	2.526	0.210	0.351	102	102	101	-43	-5	2.26E-6	5.03E-6	> 1.00E-4
HT29	0.184	1.157	1.197	1.238	1.215	0.050	0.097	104	108	106	-73	-47	2.05E-6	3.91E-6	.
KM12	0.447	1.947	2.054	2.013	1.981	0.074	0.154	107	104	102	-83	-66	1.91E-6	3.55E-6	6.61E-6
SW-620	0.297	1.276	1.322	1.315	1.338	0.073	0.133	105	104	106	-76	-55	2.04E-6	3.84E-6	7.23E-6
CNS Cancer															
SF-268	0.388	1.261	1.277	1.250	1.283	0.163	0.334	102	99	103	-58	-14	2.12E-6	4.35E-6	.
SF-295	0.798	1.832	1.799	1.684	1.700	0.318	0.537	97	86	87	-60	-33	1.79E-6	3.91E-6	.
SF-539	0.683	2.228	2.157	2.162	2.218	0.267	1.014	95	96	99	-61	21	2.03E-6	.	.
SNB-19	0.444	1.923	1.827	1.803	1.816	0.361	0.841	93	92	93	-19	27	2.42E-6	.	> 1.00E-4
SNB-75	0.726	1.496	1.376	1.411	1.474	0.209	0.850	84	89	97	-71	16	1.91E-6	.	.
U251	0.294	1.503	1.487	1.418	1.511	0.052	0.257	99	93	101	-82	-13	1.89E-6	3.55E-6	.
Melanoma															
LOX IMVI	0.222	1.597	1.497	1.538	1.449	0.087	0.256	93	96	89	-61	2	1.83E-6	.	.
MALME-3M	0.692	1.463	1.466	1.483	1.511	0.306	0.856	100	103	106	-56	21	2.22E-6	.	.
M14	0.306	1.368	1.351	1.365	1.382	0.239	0.376	98	100	101	-22	7	2.61E-6	.	> 1.00E-4
MDA-MB-435	0.501	1.993	1.908	1.945	1.928	0.204	0.448	94	97	96	-59	-11	1.97E-6	4.14E-6	.
SK-MEL-2	0.843	1.821	1.944	1.860	2.018	2.134	0.679	113	104	120	132	-19	3.48E-5	7.44E-5	> 1.00E-4
SK-MEL-28	0.512	1.625	1.629	1.678	1.663	0.417	0.695	100	105	103	-19	16	2.74E-6	.	> 1.00E-4
SK-MEL-5	0.470	2.238	2.225	2.155	2.123	0.068	0.131	99	95	93	-86	-72	1.75E-6	3.33E-6	6.32E-6
UACC-257	0.733	1.644	1.643	1.590	1.607	1.045	0.548	100	94	96	34	-25	5.56E-6	3.76E-5	> 1.00E-4
UACC-62	0.619	2.451	2.358	2.341	2.449	1.818	1.188	95	94	100	65	31	2.81E-5	> 1.00E-4	> 1.00E-4
Ovarian Cancer															
IGROV1	0.445	2.025	2.095	2.097	2.059	0.197	0.494	104	105	102	-56	3	2.14E-6	.	.
OVCAR-3	0.443	1.183	1.227	1.239	1.232	0.071	0.283	106	108	107	-84	-36	1.98E-6	3.63E-6	.
OVCAR-4	0.538	1.810	1.733	1.766	1.779	0.537	0.703	94	97	98	.	13	3.07E-6	.	> 1.00E-4
OVCAR-5	0.504	1.442	1.480	1.407	1.483	0.202	0.493	104	96	104	-60	-2	2.14E-6	4.31E-6	.
OVCAR-8	0.276	1.243	1.273	1.227	1.199	0.160	0.353	103	98	95	-42	8	2.14E-6	.	> 1.00E-4
NCI/ADR-RES	0.275	0.933	0.926	0.926	0.930	0.183	0.345	99	99	100	-33	11	2.36E-6	.	> 1.00E-4
SK-OV-3	0.572	1.644	1.647	1.731	1.733	0.277	0.578	100	108	108	-52	1	2.31E-6	.	.
Renal Cancer															
786-0	0.534	2.147	2.137	2.163	2.282	0.392	0.676	99	101	108	-27	9	2.71E-6	.	> 1.00E-4
A498	1.013	1.661	1.617	1.616	1.693	0.894	0.675	93	93	105	-12	-33	2.96E-6	7.93E-6	> 1.00E-4
ACHN	0.324	1.645	1.755	1.714	1.702	0.159	0.378	108	105	104	-51	4	2.24E-6	.	.
CAKI-1	0.750	1.889	1.652	1.652	1.660	0.225	0.612	79	79	80	-70	-18	1.58E-6	3.41E-6	.
RXF 393	0.604	1.041	1.027	0.996	1.014	0.242	0.433	97	90	94	-60	-28	1.93E-6	4.07E-6	.
SN12C	0.445	2.050	2.058	1.973	2.016	0.204	0.760	100	95	98	-54	20	2.06E-6	.	.
TK-10	0.511	1.304	1.330	1.318	1.286	0.024	0.088	103	102	98	-95	-83	1.77E-6	3.21E-6	5.82E-6
UO-31	0.763	2.282	2.232	2.253	2.255	0.275	0.622	97	98	98	-64	-18	1.98E-6	4.03E-6	.
Prostate Cancer															
PC-3	0.583	1.816	1.896	1.888	1.983	0.156	0.429	106	106	114	-73	-26	2.19E-6	4.05E-6	.
DU-145	0.336	1.102	1.173	1.155	1.159	0.026	0.066	109	107	107	-92	-80	1.94E-6	3.45E-6	6.14E-6
Breast Cancer															
MCF7	0.350	2.174	2.110	2.095	2.108	0.322	0.512	97	96	96	-8	9	2.78E-6	.	> 1.00E-4
MDA-MB-231/ATCC	0.439	1.248	1.263	1.293	1.302	0.183	0.674	102	106	107	-58	29	2.20E-6	.	.
HS 578T	0.799	1.366	1.388	1.385	1.376	0.424	0.766	104	103	102	-47	-4	2.23E-6	4.83E-6	> 1.00E-4
BT-549	1.092	2.375	2.468	2.495	2.512	2.590	0.961	107	109	111	117	-12	3.30E-5	8.06E-5	> 1.00E-4
T-47D	0.491	1.506	1.484	1.509	1.542	0.559	0.673	98	100	104	7	18	3.57E-6	> 1.00E-4	> 1.00E-4
MDA-MB-468	0.580	1.275	1.201	1.194	1.201	0.099	0.171	89	88	89	-83	-71	1.69E-6	3.30E-6	6.44E-6

Figure B.2: GI_{50}, TGI and LC_{50} values of various cancer cell lines treated with **20**.

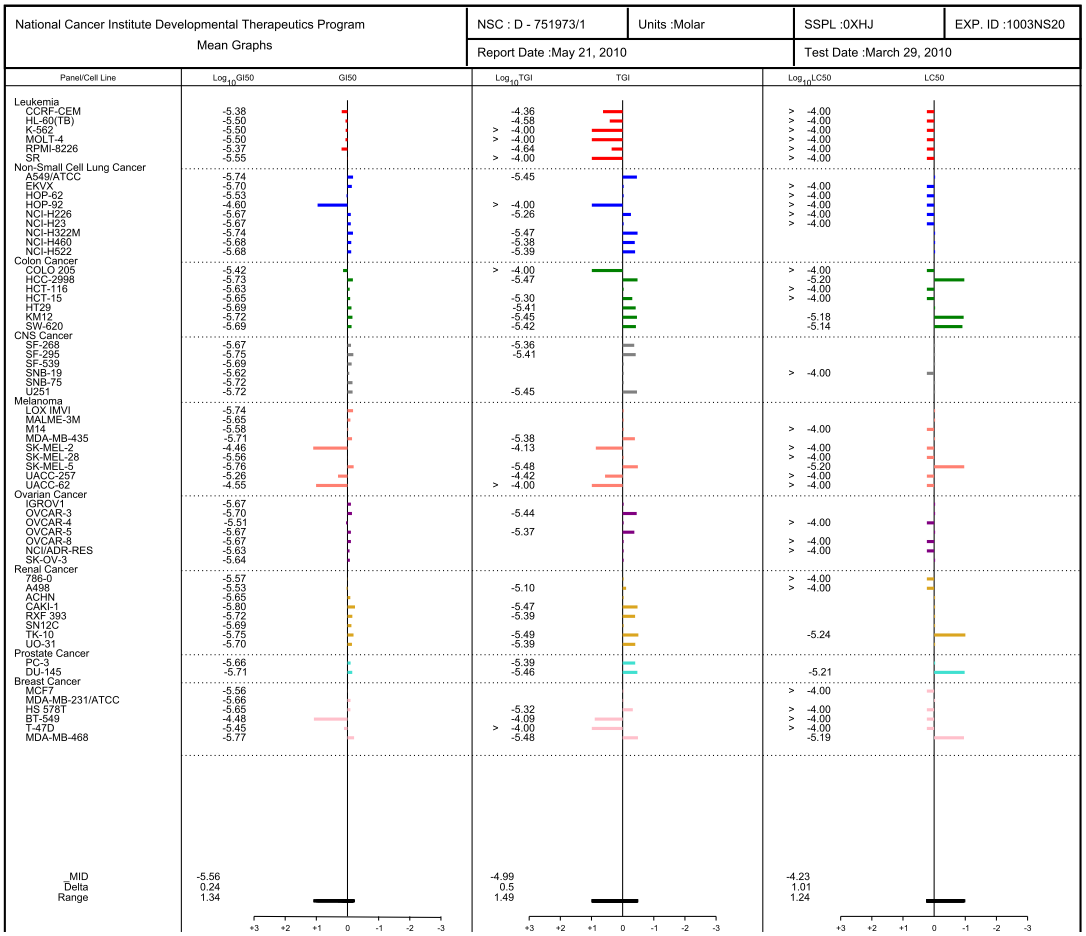

Figure B.3: Mean values of GI_{50}, TGI and LC_{50} against various cancer cell lines treated with **20**.

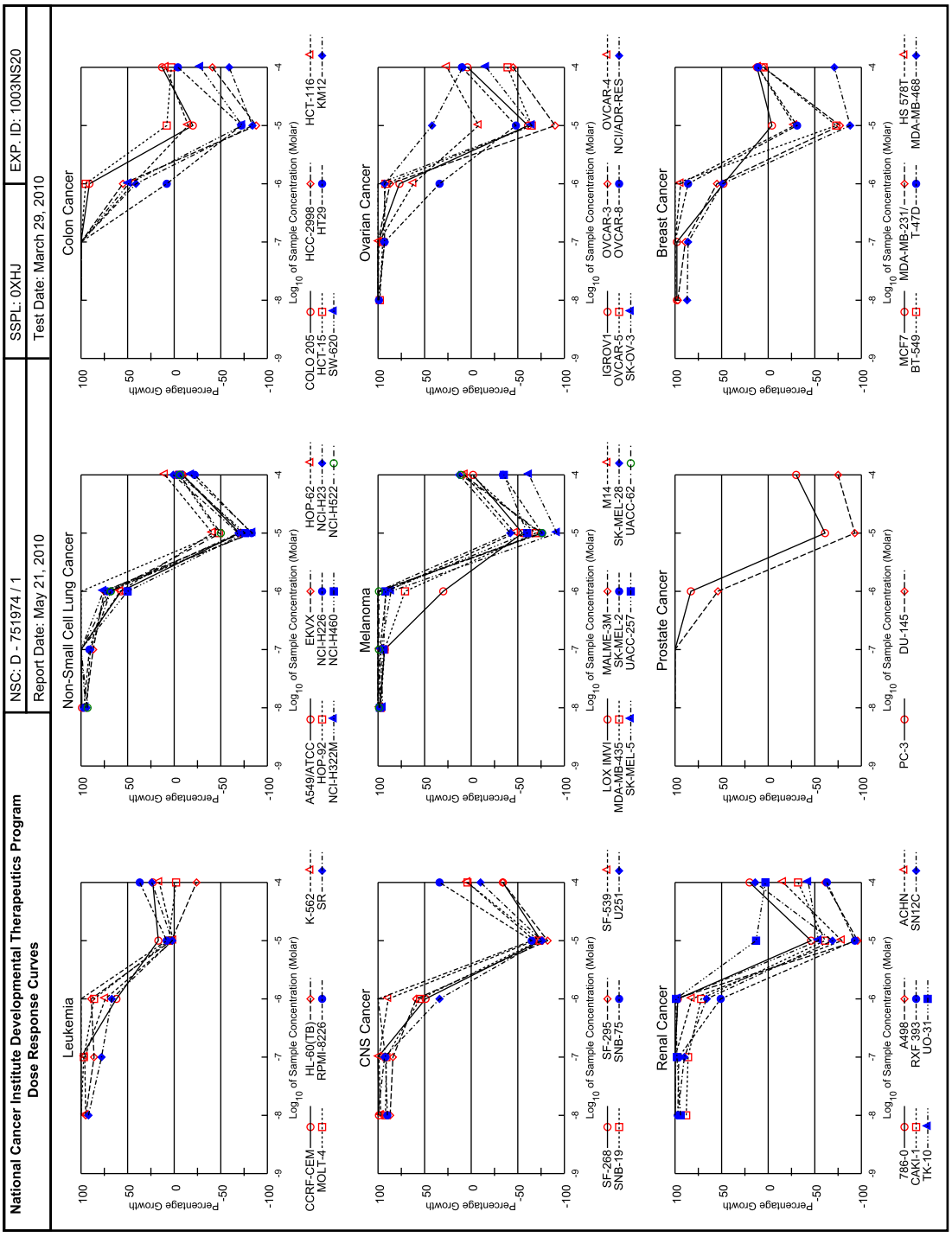

Figure B.4: Growth curves of various cancer cell lines treated with increasing molarities of **25**.

National Cancer Institute Developmental Therapeutics Program
In-Vitro Testing Results

NSC : D - 751974 / 1	Experiment ID : 1003NS20	Test Type : 08	Units : Molar
Report Date : May 21, 2010	Test Date : March 29, 2010	QNS :	MC :
COMI : Raphaine E (84125)	Stain Reagent : SRB Dual-Pass Related	SSPL : 0XHJ	

			Log10 Concentration												
	Time		Mean Optical Densities					Percent Growth							
Panel/Cell Line	Zero	Ctrl	-8.0	-7.0	-6.0	-5.0	-4.0	-8.0	-7.0	-6.0	-5.0	-4.0	GI50	TGI	LC50
Leukemia															
CCRF-CEM	0.498	1.699	1.757	1.996	1.240	0.701	0.778	105	125	62	17	23	1.83E-6	> 1.00E-4	> 1.00E-4
HL-60(TB)	0.724	2.639	2.536	2.375	2.427	0.780	0.554	95	86	89	3	-24	2.83E-6	1.29E-5	> 1.00E-4
K-562	0.337	2.295	2.205	2.208	1.794	0.357	0.646	95	96	74	1	16	2.15E-6	> 1.00E-4	> 1.00E-4
MOLT-4	0.891	3.045	3.040	2.979	2.744	1.011	0.872	100	97	86	6	-2	2.80E-6	5.29E-5	> 1.00E-4
RPMI-8226	0.764	2.226	2.360	2.564	2.241	0.887	1.301	109	123	101	8	37	3.56E-6	> 1.00E-4	> 1.00E-4
SR	0.408	1.869	1.747	1.543	1.385	0.440	0.760	92	78	67	2	24	1.82E-6	> 1.00E-4	> 1.00E-4
Non-Small Cell Lung Cancer															
A549/ATCC	0.288	1.551	1.542	1.550	1.011	0.085	0.263	99	100	57	-70	-9	1.14E-6	2.81E-6	.
EKVX	0.645	1.720	1.670	1.581	1.457	0.177	0.588	95	87	75	-73	-9	1.49E-6	3.23E-6	.
HOP-62	0.451	1.462	1.502	1.542	1.041	0.265	0.555	104	108	58	-41	10	1.21E-6	.	> 1.00E-4
HOP-92	0.988	1.789	1.839	1.875	1.852	0.512	0.936	106	111	108	-48	-5	2.35E-6	4.91E-6	> 1.00E-4
NCI-H226	0.899	2.165	2.123	2.050	1.812	0.152	0.700	97	91	72	-83	-22	1.39E-6	2.92E-6	.
NCI-H23	0.498	1.750	1.671	1.627	1.350	0.154	0.508	94	90	68	-69	1	1.35E-6	.	.
NCI-H322M	0.645	1.804	1.748	1.863	1.529	0.104	0.529	95	105	76	-84	-18	1.46E-6	2.99E-6	.
NCI-H460	0.273	2.002	2.126	2.147	1.131	0.065	0.258	107	108	50	-76	-6	9.85E-7	2.48E-6	.
NCI-H522	0.582	1.665	1.592	1.675	1.321	0.292	0.546	93	101	68	-50	-6	1.43E-6	3.78E-6	> 1.00E-4
Colon Cancer															
COLO 205	0.294	1.749	1.798	1.776	1.618	0.234	0.483	103	102	91	-20	13	2.33E-6	.	> 1.00E-4
HCC-2998	0.669	1.684	1.747	1.696	1.229	0.083	0.395	106	101	55	-88	-41	1.09E-6	2.43E-6	.
HCT-116	0.186	1.960	1.989	2.044	0.964	0.159	0.341	102	105	44	-15	9	7.93E-7	.	> 1.00E-4
HCT-15	0.369	2.387	2.385	2.423	2.285	0.532	0.420	100	102	95	8	3	3.29E-6	> 1.00E-4	> 1.00E-4
HT29	0.184	1.239	1.264	1.240	0.264	0.052	0.177	102	100	8	-72	-4	3.48E-7	1.24E-6	.
KM12	0.447	1.901	1.956	1.949	1.045	0.071	0.182	104	103	41	-84	-59	7.19E-7	2.13E-6	5.34E-6
SW-620	0.297	1.342	1.376	1.392	0.812	0.080	0.214	103	105	49	-73	-28	9.70E-7	2.53E-6	.
CNS Cancer															
SF-268	0.388	1.240	1.230	1.283	0.804	0.096	0.255	99	105	49	-75	-34	9.52E-7	2.47E-6	.
SF-295	0.798	1.793	1.661	1.636	1.390	0.146	0.523	87	84	59	-82	-34	1.17E-6	2.64E-6	.
SF-539	0.683	2.117	2.071	2.099	1.961	0.217	0.745	97	99	89	-68	4	1.77E-6	.	.
SNB-19	0.444	1.734	1.637	1.618	1.156	0.121	0.497	92	91	55	-73	4	1.10E-6	.	.
SNB-75	0.726	1.497	1.417	1.437	1.507	0.256	0.988	90	92	101	-65	34	2.03E-6	.	.
U251	0.294	1.580	1.583	1.485	0.730	0.071	0.265	100	93	34	-76	-10	5.31E-7	2.03E-6	.
Melanoma															
LOX IMVI	0.222	1.647	1.618	1.545	0.656	0.099	0.217	98	93	30	-55	-2	4.86E-7	2.26E-6	.
MALME-3M	0.692	1.416	1.414	1.439	1.485	0.179	0.747	100	103	110	-74	8	2.11E-6	.	.
M14	0.306	1.476	1.452	1.453	1.372	0.164	0.390	98	98	91	-47	7	1.99E-6	.	> 1.00E-4
MDA-MB-435	0.501	2.016	1.972	1.903	1.576	0.156	0.506	97	93	71	-69	.	1.41E-6	.	.
SK-MEL-2	0.843	1.852	1.922	1.963	1.923	0.205	0.553	107	111	107	-76	-34	2.05E-6	3.85E-6	.
SK-MEL-28	0.512	1.600	1.624	1.690	1.661	0.300	0.651	102	108	106	-42	13	2.39E-6	.	> 1.00E-4
SK-MEL-5	0.470	2.226	2.137	2.173	1.976	0.039	0.179	95	97	86	-92	-62	1.59E-6	3.04E-6	5.82E-6
UACC-257	0.733	1.700	1.680	1.646	1.624	0.293	0.479	98	94	92	-60	-35	1.89E-6	4.03E-6	.
UACC-62	0.619	2.279	2.268	2.255	2.257	0.151	0.805	99	99	99	-76	11	1.90E-6	.	.
Ovarian Cancer															
IGROV1	0.445	1.876	1.920	1.908	1.543	0.172	0.503	103	102	77	-61	4	1.56E-6	.	.
OVCAR-3	0.443	1.161	1.188	1.243	1.069	0.043	0.244	104	111	87	-90	-45	1.62E-6	3.10E-6	.
OVCAR-4	0.538	1.799	1.798	1.791	1.322	0.497	0.864	100	99	62	-8	26	1.49E-6	.	> 1.00E-4
OVCAR-5	0.504	1.381	1.363	1.339	1.312	0.179	0.305	98	95	92	-65	-39	1.86E-6	3.87E-6	.
OVCAR-8	0.276	1.325	1.313	1.255	0.632	0.144	0.383	99	93	34	-48	10	5.35E-7	.	> 1.00E-4
NCI/ADR-RES	0.275	1.000	1.029	0.950	0.952	0.577	0.338	104	93	93	42	9	6.90E-6	> 1.00E-4	> 1.00E-4
SK-OV-3	0.572	1.498	1.585	1.584	1.519	0.203	0.478	109	109	102	-65	-16	2.06E-6	4.10E-6	.
Renal Cancer															
786-0	0.534	2.105	2.174	2.130	2.058	0.291	0.855	104	102	97	-46	20	2.14E-6	.	> 1.00E-4
A498	1.013	1.657	1.657	1.660	1.677	0.042	0.398	100	100	103	-96	-61	1.85E-6	3.30E-6	5.88E-6
ACHN	0.324	1.638	1.686	1.710	1.401	0.068	0.272	104	105	82	-79	-16	1.58E-6	3.23E-6	.
CAKI-1	0.750	1.836	1.703	1.683	1.533	0.294	0.513	88	86	72	-61	-32	1.47E-6	3.49E-6	.
RXF 393	0.604	1.050	1.036	1.033	0.833	0.044	0.222	97	96	51	-93	-63	1.02E-6	2.27E-6	5.05E-6
SN12C	0.445	1.943	1.902	1.796	1.435	0.139	0.653	97	90	66	-69	14	1.31E-6	.	.
TK-10	0.511	1.283	1.296	1.300	1.262	0.236	0.293	102	102	97	-54	-43	2.05E-6	4.40E-6	.
UO-31	0.763	2.219	2.138	2.184	2.203	0.949	0.810	94	98	99	13	3	3.69E-6	> 1.00E-4	> 1.00E-4
Prostate Cancer															
PC-3	0.583	1.984	2.024	2.088	1.745	0.228	0.408	103	107	83	-61	-30	1.69E-6	3.77E-6	.
DU-145	0.336	1.118	1.161	1.155	0.757	0.025	0.086	106	105	54	-93	-75	1.06E-6	2.33E-6	5.11E-6
Breast Cancer															
MCF7	0.350	2.144	2.108	2.105	1.215	0.336	0.560	98	98	48	-4	12	9.19E-7	.	> 1.00E-4
MDA-MB-231/ATCC	0.439	1.224	1.197	1.136	0.870	0.102	0.475	97	89	55	-77	5	1.09E-6	.	.
HS 578T	0.799	1.398	1.419	1.441	1.360	0.575	0.865	103	107	94	-28	11	2.29E-6	.	> 1.00E-4
BT-549	1.092	2.275	2.326	2.356	2.424	0.290	1.153	104	107	113	-73	5	2.17E-6	.	.
T-47D	0.491	1.364	1.384	1.410	1.245	0.337	0.589	102	105	86	-31	11	2.04E-6	.	> 1.00E-4
MDA-MB-468	0.580	1.310	1.213	1.211	0.936	0.069	0.169	87	86	49	-88	-71	9.25E-7	2.27E-6	5.27E-6

Figure B.5: GI_{50}, TGI and LC_{50} values of various cancer cell lines treated with **25**.

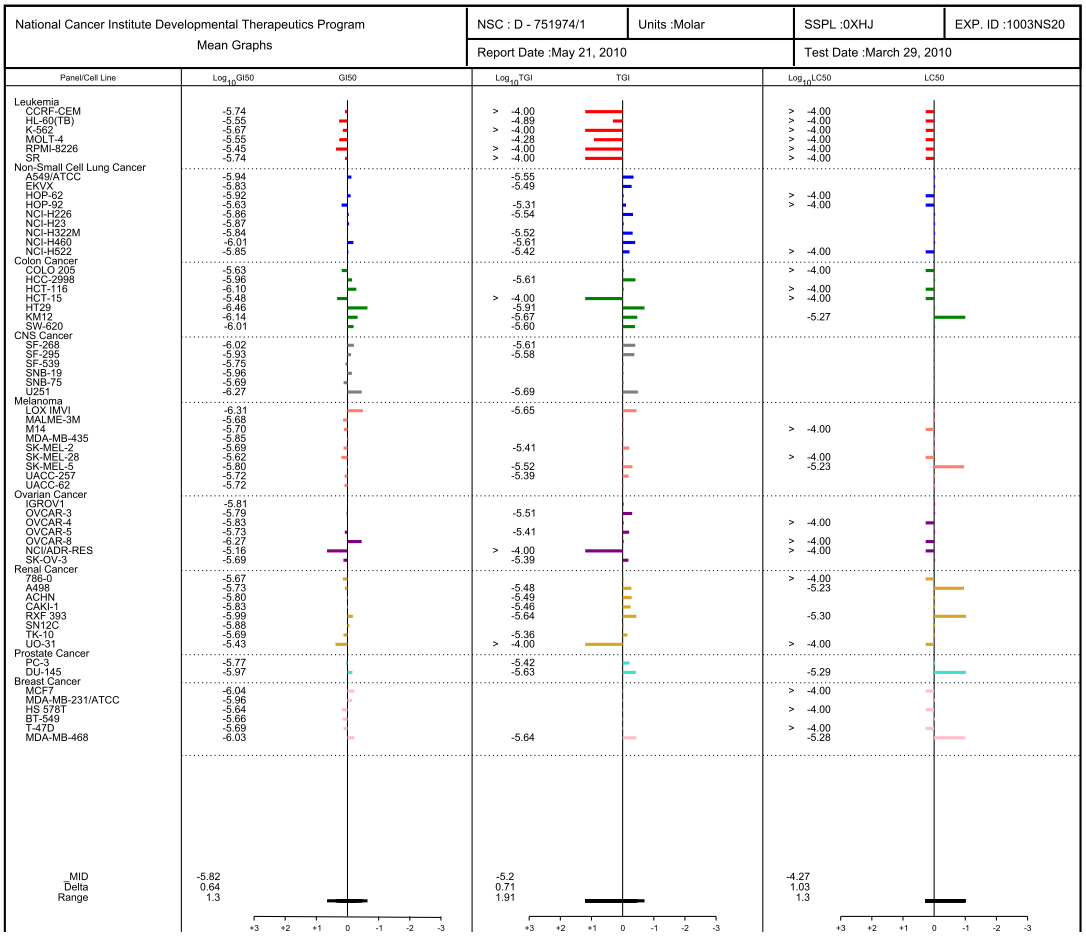

Figure B.6: Mean values of GI_{50}, TGI and LC_{50} against various cancer cell lines treated with **25**.

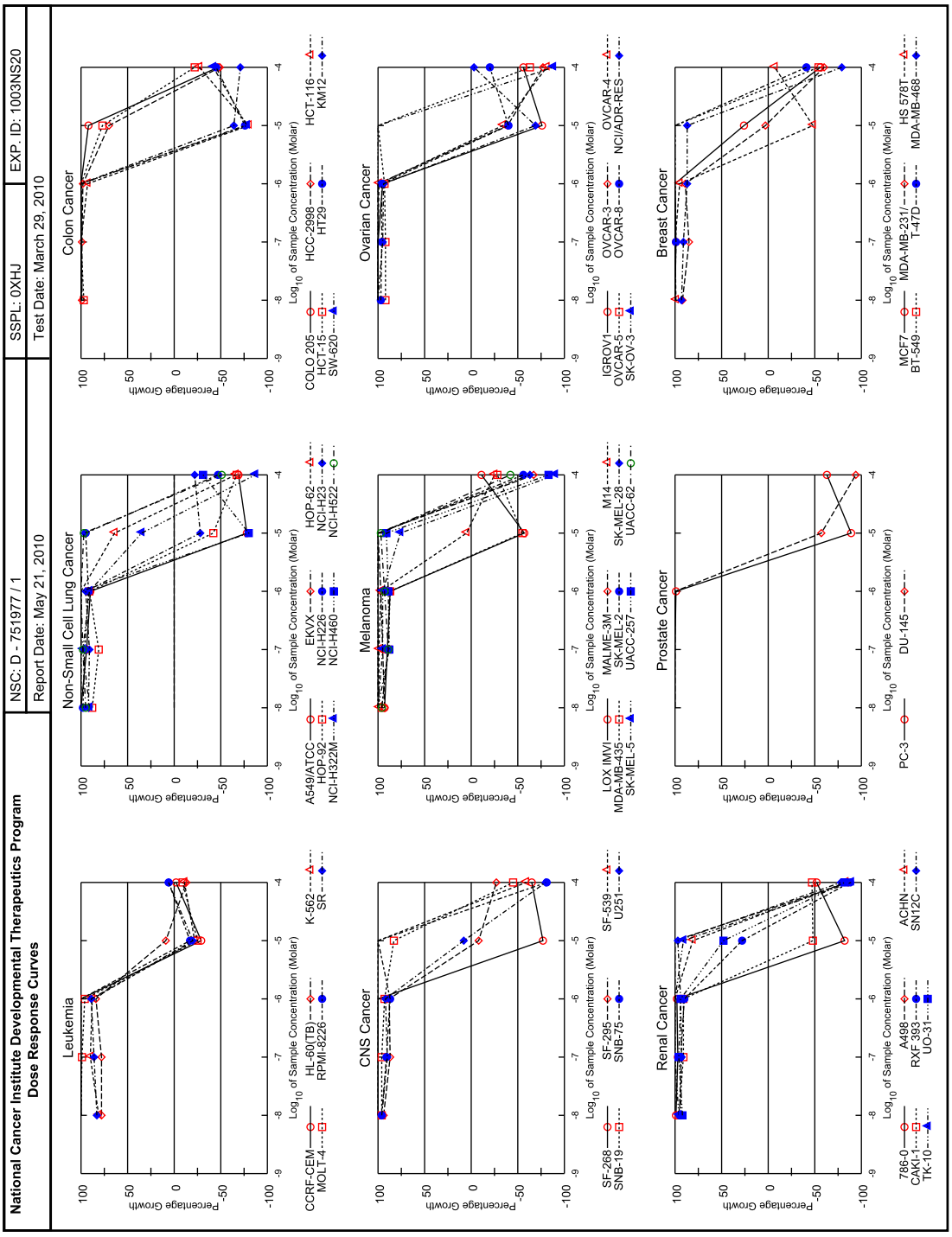

Figure B.7: Growth curves of various cancer cell lines treated with increasing molarities of **26**.

National Cancer Institute Developmental Therapeutics Program
In-Vitro Testing Results

NSC : D - 751977 / 1	Experiment ID : 1003NS20	Test Type : 08	Units : Molar
Report Date : May 21, 2010	Test Date : March 29, 2010	QNS :	MC :
COMI : Raphaine K (84130)	Stain Reagent : SRB Dual-Pass Related	SSPL : 0XHJ	

			Log10 Concentration											
	Time		Mean Optical Densities					Percent Growth						
Panel/Cell Line	Zero	Ctrl	-8.0	-7.0	-6.0	-5.0	-4.0	-8.0	-7.0	-6.0	-5.0	-4.0	GI50	TGI	LC50
Leukemia															
CCRF-CEM	0.498	1.709	1.814	1.753	1.712	0.353	0.486	109	104	100	-29	-2	2.44E-6	5.95E-6	> 1.00E-4
HL-60(TB)	0.724	2.540	2.139	2.143	2.257	0.890	0.627	78	78	84	9	-13	2.86E-6	2.53E-5	> 1.00E-4
K-562	0.337	2.030	1.707	1.860	1.831	0.264	0.300	81	90	88	-22	-11	2.23E-6	6.35E-6	> 1.00E-4
MOLT-4	0.891	2.630	2.654	2.613	2.564	0.669	0.807	101	99	96	-25	-9	2.41E-6	6.23E-6	> 1.00E-4
RPMI-8226	0.764	2.076	2.184	2.418	2.267	0.631	0.842	108	126	114	-17	6	3.08E-6	.	> 1.00E-4
SR	0.408	1.546	1.348	1.388	1.417	0.325	0.479	83	86	89	-20	6	2.26E-6	.	> 1.00E-4
Non-Small Cell Lung Cancer															
A549/ATCC	0.288	1.210	1.216	1.152	1.122	0.063	0.091	101	94	90	-78	-69	1.74E-6	3.44E-6	6.80E-6
EKVX	0.645	1.598	.	.	.	.	.	.	.	.	.	.	.	.	.
HOP-62	0.451	1.179	1.233	1.218	1.184	0.916	0.154	107	105	101	64	-66	1.28E-5	3.10E-5	7.53E-5
HOP-92	0.988	1.455	1.397	1.367	1.414	0.573	0.330	88	81	91	-42	-67	2.04E-6	4.84E-6	2.11E-5
NCI-H226	0.899	2.243	2.213	2.186	2.137	2.181	0.475	98	96	92	95	-47	2.08E-5	4.67E-5	> 1.00E-4
NCI-H23	0.498	1.657	1.564	1.556	1.594	0.359	0.390	92	91	95	-28	-22	2.31E-6	5.92E-6	> 1.00E-4
NCI-H322M	0.645	1.612	1.523	1.591	1.523	0.984	0.082	91	98	91	35	-87	5.40E-6	1.93E-5	4.95E-5
NCI-H460	0.273	1.784	1.866	1.937	1.907	0.055	0.190	105	110	108	-80	-31	2.04E-6	3.76E-6	.
NCI-H522	0.582	1.462	1.419	1.449	1.478	1.434	0.284	95	98	102	97	-51	2.07E-5	4.51E-5	9.81E-5
Colon Cancer															
COLO 205	0.294	1.281	1.358	1.427	1.348	1.200	0.156	108	115	107	92	-47	2.00E-5	4.58E-5	> 1.00E-4
HCC-2998	0.669	2.768	2.747	2.758	2.724	2.131	0.341	99	99	98	70	-49	1.46E-5	3.86E-5	> 1.00E-4
HCT-116	0.186	1.011	1.016	1.014	0.952	0.038	0.135	101	100	93	-80	-27	1.77E-6	3.45E-6	.
HCT-15	0.369	2.365	2.300	2.450	2.614	1.898	0.286	97	104	112	77	-22	1.86E-5	5.93E-5	> 1.00E-4
HT29	0.184	0.960	0.974	0.980	0.966	0.044	0.101	102	103	101	-76	-45	1.94E-6	3.71E-6	.
KM12	0.447	1.848	1.933	1.893	1.922	0.159	0.128	106	103	105	-64	-71	2.12E-6	4.17E-6	8.22E-6
SW-620	0.297	1.254	1.255	1.271	1.261	0.065	0.173	100	102	101	-78	-42	1.92E-6	3.66E-6	.
CNS Cancer															
SF-268	0.388	1.138	1.160	1.147	1.157	0.090	0.138	103	101	103	-77	-65	1.96E-6	3.73E-6	7.08E-6
SF-295	0.798	2.418	2.313	2.207	2.223	0.733	0.581	94	87	88	-8	-27	2.48E-6	8.23E-6	> 1.00E-4
SF-539	0.683	2.108	2.142	2.161	2.193	2.127	0.281	102	104	106	101	-59	2.09E-5	4.29E-5	8.80E-5
SNB-19	0.444	1.663	1.615	1.618	1.572	1.458	0.242	96	96	93	83	-45	1.81E-5	4.43E-5	> 1.00E-4
SNB-75	0.726	1.213	1.195	1.169	1.148	1.237	0.135	96	91	87	105	-81	1.97E-5	3.66E-5	6.78E-5
U251	0.294	1.306	1.267	1.207	1.229	0.380	0.059	96	90	92	8	-80	3.20E-6	1.25E-5	4.58E-5
Melanoma															
LOX IMVI	0.222	1.615	1.513	1.476	1.432	0.096	0.198	93	90	87	-57	-11	1.80E-6	4.02E-6	.
MALME-3M	0.692	1.301	1.261	1.274	1.285	1.419	0.225	93	95	97	119	-67	2.35E-5	4.35E-5	8.06E-5
M14	0.306	1.021	1.014	1.014	1.001	0.339	0.231	99	99	97	5	-25	3.23E-6	1.44E-5	> 1.00E-4
MDA-MB-435	0.501	1.885	1.832	1.736	1.707	0.223	0.363	96	89	87	-55	-28	1.82E-6	4.08E-6	.
SK-MEL-2	0.843	1.860	1.944	1.983	1.970	2.040	0.373	108	112	111	118	-56	2.46E-5	4.77E-5	9.26E-5
SK-MEL-28	0.512	1.248	1.326	1.312	1.332	1.321	0.192	111	109	111	110	-63	2.22E-5	4.34E-5	8.45E-5
SK-MEL-5	0.470	2.359	2.350	2.273	2.266	1.898	0.048	100	95	95	76	-90	1.43E-5	2.86E-5	5.75E-5
UACC-257	0.733	1.312	1.313	1.240	1.249	1.261	0.121	100	88	89	91	-83	1.72E-5	3.33E-5	6.43E-5
UACC-62	0.619	2.383	2.304	2.191	2.255	2.333	0.359	96	89	93	97	-42	2.18E-5	4.99E-5	> 1.00E-4
Ovarian Cancer															
IGROV1	0.445	1.368	1.370	1.401	1.319	0.107	0.196	100	104	95	-76	-56	1.83E-6	3.59E-6	7.04E-6
OVCAR-3	0.443	1.107	1.156	1.179	1.129	0.270	0.101	107	111	103	-39	-77	2.37E-6	5.31E-6	1.92E-5
OVCAR-4	0.538	1.374	1.437	1.388	1.362	0.354	0.105	107	102	99	-34	-81	2.32E-6	5.52E-6	2.18E-5
OVCAR-5	0.504	1.349	1.282	1.283	1.289	1.372	0.188	92	92	93	103	-63	2.08E-5	4.18E-5	8.38E-5
OVCAR-8	0.276	1.173	1.145	1.136	1.136	0.166	0.220	97	96	96	-40	-20	2.18E-6	5.09E-6	> 1.00E-4
NCI/ADR-RES	0.275	0.931	0.932	0.896	0.889	0.084	0.268	100	95	94	-69	-3	1.85E-6	3.75E-6	.
SK-OV-3	0.572	1.238	1.304	1.315	1.266	1.247	0.072	110	112	104	101	-88	1.87E-5	3.44E-5	6.33E-5
Renal Cancer															
786-0	0.534	1.513	1.500	1.482	1.493	0.095	0.255	99	97	98	-82	-52	1.85E-6	3.50E-6	6.62E-6
A498	1.013	1.563	1.572	1.580	1.635	1.647	0.138	102	103	113	115	-86	2.11E-5	3.73E-5	6.60E-5
ACHN	0.324	1.501	1.553	1.568	1.597	1.278	0.055	104	106	108	81	-83	1.55E-5	3.12E-5	6.28E-5
CAKI-1	0.750	1.669	1.629	1.588	1.583	0.390	0.396	96	91	91	-48	-47	1.96E-6	4.50E-6	> 1.00E-4
RXF 393	0.604	1.266	1.236	1.225	1.198	0.788	0.074	95	94	90	28	-88	4.38E-6	1.74E-5	4.71E-5
SN12C	0.445	1.889	1.796	1.793	1.798	1.842	0.099	94	93	94	97	-78	1.85E-5	3.58E-5	6.92E-5
TK-10	0.511	1.201	1.176	1.207	1.205	1.138	0.057	96	101	101	91	-89	1.69E-5	3.20E-5	6.08E-5
UO-31	0.763	1.953	1.855	1.904	1.885	1.331	0.136	92	96	94	48	-82	8.95E-6	2.33E-5	5.65E-5
Prostate Cancer															
PC-3	0.583	1.664	1.665	1.667	1.657	0.064	0.216	100	100	99	-89	-63	1.83E-6	3.37E-6	6.21E-6
DU-145	0.336	1.080	1.121	1.141	1.129	0.145	0.020	106	108	107	-57	-94	2.22E-6	4.49E-6	9.08E-6
Breast Cancer															
MCF7	0.350	1.734	1.736	1.725	1.760	0.717	0.155	100	99	102	26	-56	4.88E-6	2.10E-5	8.49E-5
MDA-MB-231/ATCC	0.439	1.139	1.081	1.037	1.064	0.463	0.174	92	85	89	3	-60	2.87E-6	1.13E-5	6.86E-5
HS 578T	0.799	1.264	1.258	1.262	1.240	0.418	0.742	99	100	95	-48	-7	2.06E-6	4.63E-6	> 1.00E-4
BT-549	1.092	1.679	1.707	1.726	1.698	1.803	0.500	105	108	103	121	-54	2.55E-5	4.91E-5	9.46E-5
T-47D	0.491	1.149	1.151	1.144	1.154	1.171	0.290	100	99	101	103	-41	2.34E-5	5.20E-5	> 1.00E-4
MDA-MB-468	0.580	1.440	1.383	1.365	1.328	1.328	0.120	93	91	87	87	-79	1.67E-5	3.33E-5	6.66E-5

Figure B.8: GI_{50}, TGI and LC_{50} values of various cancer cell lines treated with **26**.

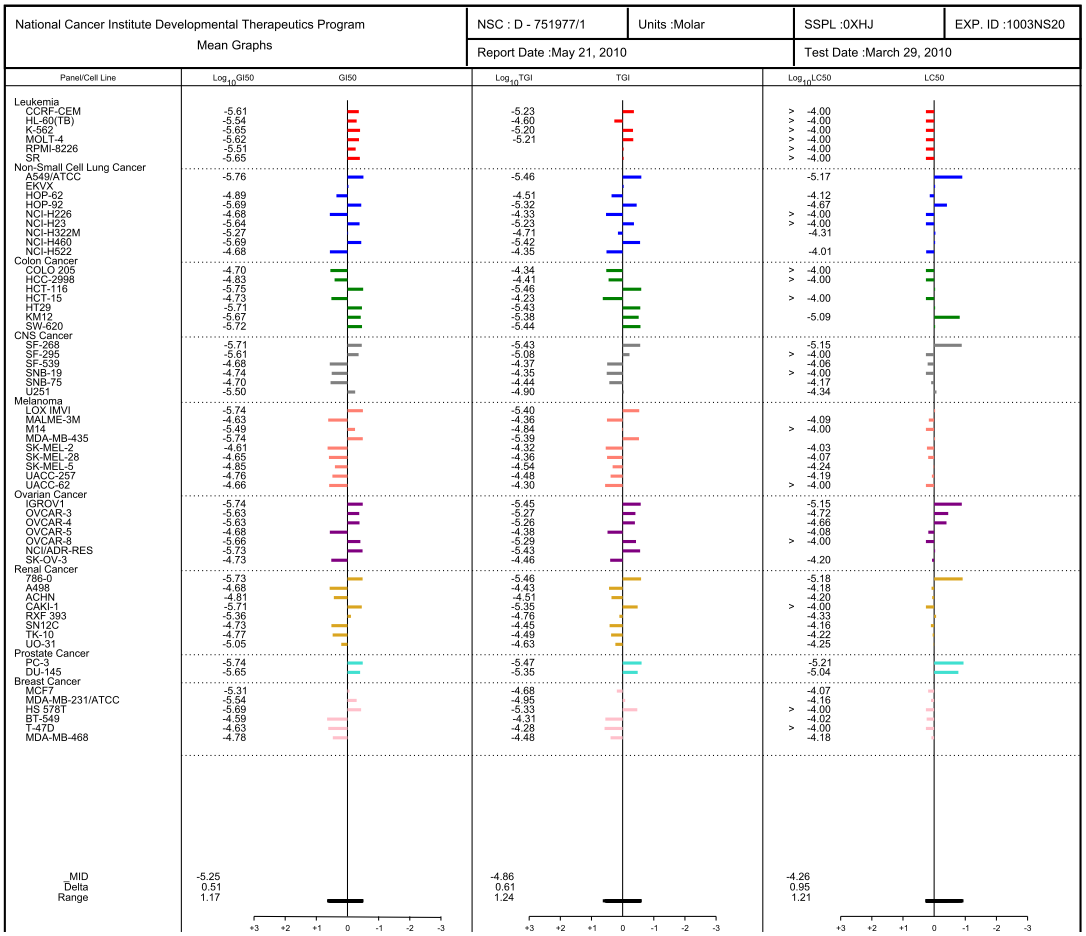

Figure B.9: Mean values of GI_{50}, TGI and LC_{50} against various cancer cell lines treated with **26**.

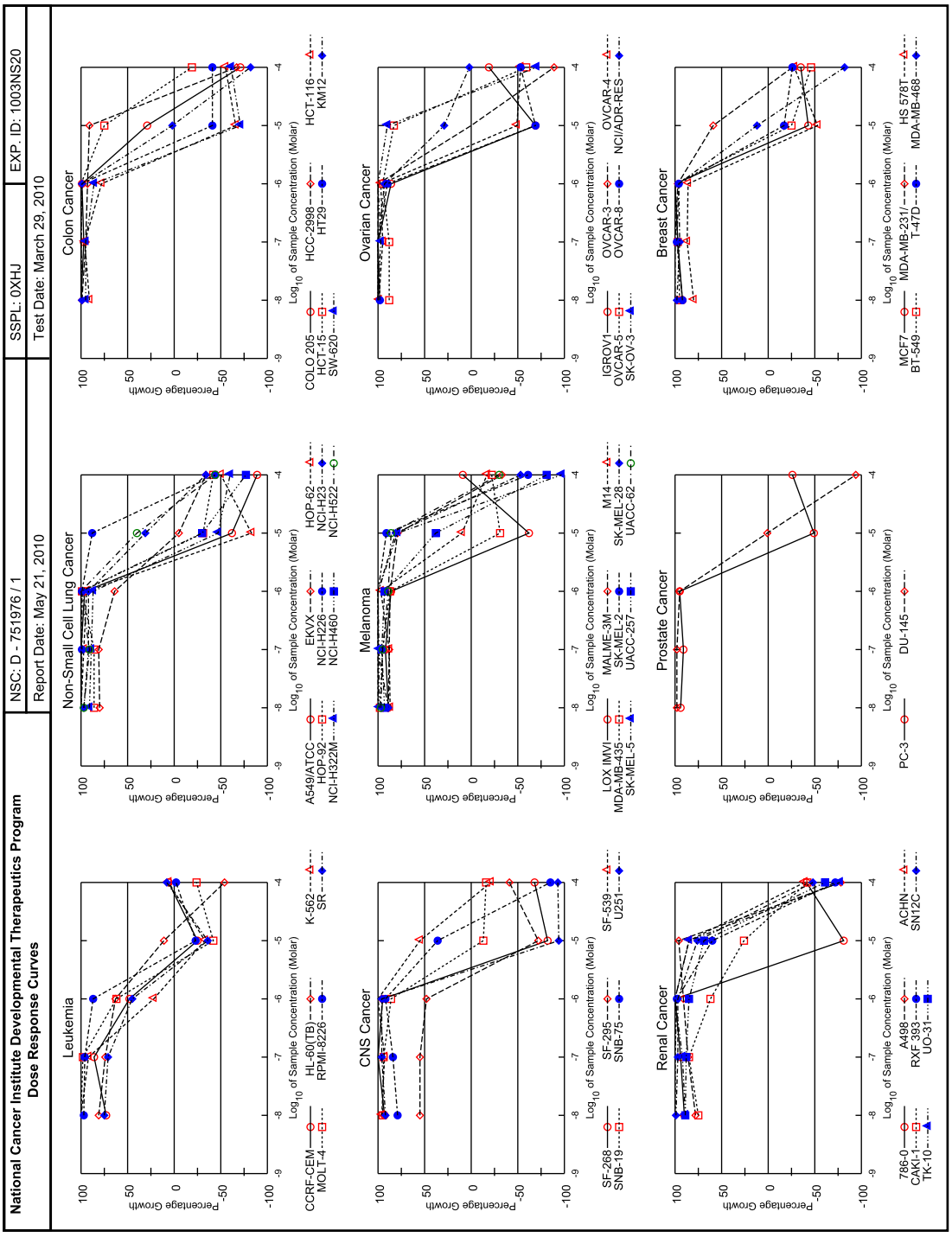

Figure B.10: Growth curves of various cancer cell lines treated with increasing molarities of **31**.

National Cancer Institute Developmental Therapeutics Program
In-Vitro Testing Results

NSC : D - 751976 / 1	Experiment ID : 1003NS20	Test Type : 08	Units : Molar
Report Date : May 21, 2010	Test Date : March 29, 2010	QNS :	MC :
COMI : Raphaine I (84129)	Stain Reagent : SRB Dual-Pass Related	SSPL : 0XHJ	

		Log10 Concentration												
	Time	Mean Optical Densities						Percent Growth						
Panel/Cell Line	Zero	Ctrl	-8.0	-7.0	-6.0	-5.0	-4.0	-8.0	-7.0	-6.0	-5.0	-4.0	GI50	TGI	LC50
Leukemia															
CCRF-CEM	0.498	1.709	1.383	1.536	1.079	0.372	0.572	73	86	48	-25	6	8.82E-7	.	> 1.00E-4
HL-60(TB)	0.724	2.540	2.203	2.067	1.877	0.917	0.331	81	74	63	11	-54	1.80E-6	1.46E-5	8.57E-5
K-562	0.337	2.030	2.039	1.891	0.706	0.227	0.433	101	92	22	-33	6	3.96E-7	.	> 1.00E-4
MOLT-4	0.891	2.630	2.652	2.595	1.976	0.516	0.681	101	98	62	-42	-24	1.31E-6	3.95E-6	> 1.00E-4
RPMI-8226	0.764	2.076	2.041	2.029	1.908	0.589	0.745	97	96	87	-23	-2	2.18E-6	6.19E-6	> 1.00E-4
SR	0.408	1.546	1.264	1.222	0.922	0.262	0.497	75	71	45	-36	8	6.55E-7	.	> 1.00E-4
Non-Small Cell Lung Cancer															
A549/ATCC	0.288	1.210	1.228	1.250	1.177	0.109	0.033	102	104	96	-62	-89	1.96E-6	4.05E-6	8.36E-6
EKVX	0.645	1.598	1.404	1.414	1.259	0.615	0.428	80	81	64	-5	-34	1.62E-6	8.54E-6	> 1.00E-4
HOP-62	0.451	1.179	1.186	1.158	1.136	0.077	0.224	101	97	94	-83	-50	1.77E-6	3.40E-6	6.51E-6
HOP-92	0.988	1.455	1.390	1.390	1.450	0.686	0.570	86	86	99	-31	-42	2.39E-6	5.80E-6	> 1.00E-4
NCI-H226	0.899	2.243	2.268	2.226	2.225	2.078	0.502	102	99	99	88	-44	1.93E-5	4.62E-5	> 1.00E-4
NCI-H23	0.498	1.657	1.620	1.560	1.560	0.853	0.327	97	92	92	31	-34	4.81E-6	2.96E-5	> 1.00E-4
NCI-H322M	0.645	1.612	1.528	1.509	1.486	0.339	0.259	91	89	87	-47	-60	1.88E-6	4.44E-6	1.60E-5
NCI-H460	0.273	1.784	1.846	1.784	1.838	0.192	0.063	104	100	104	-30	-77	2.52E-6	5.99E-6	2.68E-5
NCI-H522	0.582	1.462	1.435	1.381	1.474	0.931	0.329	97	91	101	40	-44	6.79E-6	2.99E-5	> 1.00E-4
Colon Cancer															
COLO 205	0.294	1.281	1.314	1.247	1.267	0.582	0.085	103	97	99	29	-71	5.01E-6	1.95E-5	6.16E-5
HCC-2998	0.669	2.768	2.743	2.673	2.628	2.579	0.221	99	95	93	91	-67	1.82E-5	3.76E-5	7.80E-5
HCT-116	0.186	1.011	0.941	0.982	0.832	0.063	0.085	91	96	78	-66	-55	1.57E-6	3.48E-6	7.70E-6
HCT-15	0.369	2.365	2.415	2.385	2.441	1.862	0.301	103	101	104	75	-19	1.84E-5	6.33E-5	> 1.00E-4
HT29	0.184	0.960	0.986	0.975	1.056	0.109	0.109	103	102	112	-41	-41	2.55E-6	5.40E-6	> 1.00E-4
KM12	0.447	1.848	1.838	1.868	1.833	0.469	0.081	99	101	99	2	-82	3.18E-6	1.04E-5	4.14E-5
SW-620	0.297	1.254	1.202	1.202	1.124	0.087	0.117	95	95	86	-71	-61	1.70E-6	3.55E-6	7.38E-6
CNS Cancer															
SF-268	0.388	1.138	1.087	1.140	1.099	0.070	0.126	93	100	95	-82	-68	1.79E-6	3.43E-6	6.59E-6
SF-295	0.798	2.418	1.689	1.686	1.582	0.220	0.469	55	55	48	-72	-41	5.58E-7	2.51E-6	.
SF-539	0.683	2.108	2.048	2.002	2.220	1.468	0.541	96	93	108	55	-21	1.17E-5	5.31E-5	> 1.00E-4
SNB-19	0.444	1.663	1.607	1.585	1.494	0.385	0.373	95	94	86	-13	-16	2.31E-6	7.34E-6	> 1.00E-4
SNB-75	0.726	1.213	1.112	1.137	1.174	0.904	0.111	79	84	92	36	-85	5.71E-6	2.00E-5	5.17E-5
U251	0.294	1.306	1.229	1.268	1.265	0.017	0.022	92	96	96	-94	-93	1.74E-6	3.19E-6	5.84E-6
Melanoma															
LOX IMVI	0.222	1.615	1.465	1.497	1.417	0.085	0.346	89	92	86	-62	9	1.75E-6	.	.
MALME-3M	0.692	1.301	1.233	1.228	1.223	1.173	0.462	89	88	87	79	-33	1.81E-5	5.05E-5	> 1.00E-4
M14	0.306	1.021	0.928	0.938	1.001	0.380	0.255	87	88	97	10	-17	3.49E-6	2.42E-5	> 1.00E-4
MDA-MB-435	0.501	1.885	1.862	1.811	1.712	0.346	0.389	98	95	87	-31	-22	2.07E-6	5.47E-6	> 1.00E-4
SK-MEL-2	0.843	1.860	1.875	1.882	1.981	1.766	0.332	101	102	112	91	-61	1.86E-5	3.98E-5	8.51E-5
SK-MEL-28	0.512	1.248	1.169	1.247	1.285	1.110	0.240	89	100	105	81	-53	1.71E-5	4.02E-5	9.46E-5
SK-MEL-5	0.470	2.359	2.343	2.334	2.380	1.968	0.013	99	99	101	79	-97	1.47E-5	2.81E-5	5.39E-5
UACC-257	0.733	1.312	1.272	1.286	1.270	0.953	0.139	93	96	93	38	-81	6.04E-6	2.09E-5	5.48E-5
UACC-62	0.619	2.383	2.336	2.286	2.184	2.137	0.431	97	95	89	86	-30	2.04E-5	5.48E-5	> 1.00E-4
Ovarian Cancer															
IGROV1	0.445	1.368	1.388	1.368	1.238	0.137	0.363	102	100	86	-69	-19	1.70E-6	3.58E-6	.
OVCAR-3	0.443	1.107	1.095	1.111	1.122	0.446	0.049	98	101	102	.	-89	3.26E-6	1.01E-5	3.66E-5
OVCAR-4	0.538	1.374	1.362	1.333	1.353	0.273	0.255	99	95	97	-49	-53	2.11E-6	4.62E-6	1.67E-5
OVCAR-5	0.504	1.349	1.249	1.245	1.307	1.202	0.207	88	88	95	83	-59	1.70E-5	3.83E-5	8.63E-5
OVCAR-8	0.276	1.173	1.158	1.191	1.086	0.086	0.131	98	102	90	-69	-53	1.79E-6	3.69E-6	7.61E-6
NCI/ADR-RES	0.275	0.931	0.932	0.959	0.887	0.463	0.286	100	104	93	29	2	4.68E-6	> 1.00E-4	> 1.00E-4
SK-OV-3	0.572	1.238	1.243	1.216	1.239	1.169	0.172	101	97	100	90	-70	1.77E-5	3.65E-5	7.50E-5
Renal Cancer															
786-0	0.534	1.513	1.411	1.455	1.583	0.102	0.317	90	94	107	-81	-41	2.01E-6	3.71E-6	.
A498	1.013	1.563	1.441	1.485	1.515	1.539	0.220	78	86	91	96	-78	1.83E-5	3.55E-5	6.87E-5
ACHN	0.324	1.501	1.510	1.500	1.555	1.320	0.199	101	100	105	85	-39	1.91E-5	4.86E-5	> 1.00E-4
CAKI-1	0.750	1.669	1.442	1.529	1.316	0.988	0.433	75	85	62	26	-42	2.11E-6	2.40E-5	> 1.00E-4
RXF 393	0.604	1.266	1.263	1.268	1.256	1.003	0.171	100	100	98	60	-72	1.20E-5	2.86E-5	6.84E-5
SN12C	0.445	1.889	1.881	1.849	1.844	1.548	0.230	99	97	97	76	-48	1.63E-5	4.09E-5	> 1.00E-4
TK-10	0.511	1.201	1.123	1.143	1.223	1.100	0.119	89	92	103	85	-77	1.65E-5	3.36E-5	6.83E-5
UO-31	0.763	1.953	1.822	1.814	1.771	1.581	0.297	89	88	85	69	-61	1.39E-5	3.38E-5	8.21E-5
Prostate Cancer															
PC-3	0.583	1.664	1.599	1.566	1.613	0.295	0.430	94	91	95	-49	-26	2.06E-6	4.55E-6	> 1.00E-4
DU-145	0.336	1.080	1.065	1.069	1.040	0.346	0.019	98	98	95	1	-94	3.01E-6	1.03E-5	3.43E-5
Breast Cancer															
MCF7	0.350	1.734	1.628	1.699	1.732	0.200	0.227	92	97	100	-43	-35	2.23E-6	5.00E-6	> 1.00E-4
MDA-MB-231/ATCC	0.439	1.139	1.149	1.142	1.121	0.850	0.324	101	100	97	59	-26	1.26E-5	4.90E-5	> 1.00E-4
HS 578T	0.799	1.264	1.172	1.205	1.200	0.376	0.574	80	87	86	-53	-28	1.82E-6	4.16E-6	.
BT-549	1.092	1.679	1.652	1.662	1.706	0.817	0.587	95	97	105	-25	-46	2.64E-6	6.40E-6	> 1.00E-4
T-47D	0.491	1.149	1.097	1.137	1.126	0.409	0.363	92	98	96	-17	-26	2.57E-6	7.12E-6	> 1.00E-4
MDA-MB-468	0.580	1.440	1.422	1.395	1.407	0.680	0.104	98	95	96	12	-82	3.51E-6	1.33E-5	4.55E-5

Figure B.11: GI_{50}, TGI and LC_{50} values of various cancer cell lines treated with **31**.

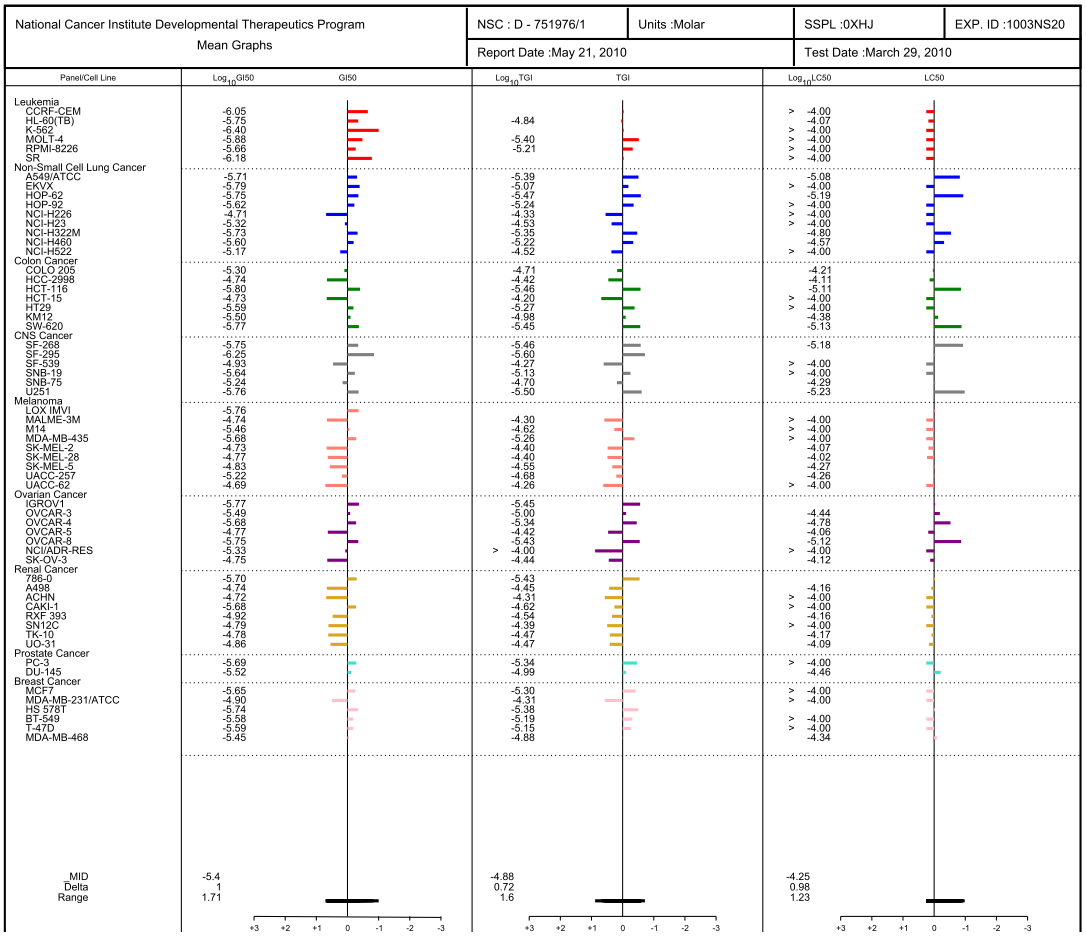

Figure B.12: Mean values of GI_{50}, TGI and LC_{50} against various cancer cell lines treated with **31**.

Appendix C

ADME studies

ADME studies were carried out on compounds **20**, **21**, **22** and **23** by Cancer Research Technology® Ltd. and the results are tabulated hereafter (Table C.1).

test		**target**	**20**	**21**	**22**	**23**
solubility		> 40 μM	151 μM	< 5 μM	158 μM	< 5 μM
permeability	Caco 2-A-B	$>5\times10^6$ cm×s^{-1}	0.38×10^6 cm×s^{-1}	1.10×10^6 cm×s^{-1}	3.96×10^6 cm×s^{-1}	1.64×10^6 cm×s^{-1}
	efflux ratio	<2	0.46	1.09	3.31	0.89
stability	microsome turnover[1]	<80%	2%	45%	0%	0%
	microsome turnover[2]	<80%	48%	61%	22%	59%
plasma protein binding		<99%	100%	100%	100%	99%
CyP450 inhibition	1A2	>1 μM	>10 μM	>10 μM	>10 μM	>10 μM
	2D6	>1 μM	>10 μM	>10 μM	>10 μM	>10 μM
	2C9	>1 μM	>10 μM	>10 μM	>10 μM	>10 μM
	2C19	>1 μM	>10 μM	>10 μM	>10 μM	>10 μM
	3A4	>1 μM	>10 μM	>10 μM	>10 μM	>10 μM
hERG binding inhibition		<50% at 10 μM	n.d.	40%	55%	n.d.

test		**target**	**20**	**21**	**22**	**23**
muscarinic	M1	<50%	n.d.	83%	84%	n.d.
receptor		at 10 μM				
binding	M2	<50%	n.d.	n.d.	78%	n.d.
inhibition		at 10 μM				
	M3	<50%	n.d.	35%	60%	n.d.
		at 10 μM				

Table C.1: ADME results for compounds **20**, **21**, **22** and **23**.

[1] *homo sapiens*
[2] *mus musculus*

References

[1] J. Watson and F. Crick. Molecular structure of nucleic acids. *Nature*, 171: 737–738, 1953. 1

[2] M. H. F. Wilkins, A. R. Stokes, and H. R. Wilson. Molecular structure of deoxypentose nucleic acids. *Nature*, 171:738–740, 1953.

[3] R. E. Franklin and R. G. Gosling. Molecular configuration in sodium thymonucleate. *Nature*, 171:740–741, 1953. 1

[4] I. Bang. Physiological action of guanylic acid. *Z. Physiol. Chem.*, 32:201–213, 1901. 1

[5] M. Gellert, M. N. Lipsett, and D. R. Davies. Helix formation by guanylic acid. *Proc. Natl. Acad. Sci. U.S.A.*, 48:2013–2018, 1962. 1

[6] K. Phillips, Z. Dauter, A. I. Murchie, D. M. Lilley, and B. Luisi. The crystal structure of a parallel-stranded guanine tetraplex at 0.95 Å resolution. *J. Mol. Biol.*, 273:171–182, 1997. 1

[7] M. A. Read and S. Neidle. Structural characterization of a guanine-quadruplex ligand complex. *Biochemistry*, 39:13422–13432, 2000.

[8] G. N. Parkinson, M. P. H. Lee, and S. Neidle. Crystal structure of parallel quadruplexes from human telomeric DNA. *Nature*, 417:876–880, 2002. 2, 3

[9] N. H. Campbell and G. N. Parkinson. Crystallographic studies of quadruplex nucleic acids. *Methods*, 43:252–263, 2007.

[10] S. Neidle and G. N. Parkinson. Quadruplex DNA crystal structures and drug design. *Biochimie*, 90:1184–1196, 2008. 1

[11] Y. Wang and D. J. Patel. Guanine residues in d(T_2AG_3) and d(T_2G_4) form parallel-stranded potassium cation stabilized G-quadruplexes with anti-glycosidic torsion angles in solution. *Biochemistry*, 31:8112–8119, 1992. 1

[12] Y. Wang and D. J. Patel. Solution structure of a parallel-stranded G-quadruplex DNA. *J. Mol. Biol.*, 234:1171–1183, 1993.

[13] M. A. Keniry, G. D. Strahan, E. A. Owen, and R. H. Shafer. Solution structure of the Na^+ form of the dimeric guanine quadruplex $[d(G_3T_4G_3)]_2$. *Eur. J. Biochem.*, 233:631–643, 1995.

[14] Y. Wang and D. J. Patel. Solution structure of the Oxytricha telomeric repeat d$[G_4(T_4G_4)_3]$ G-tetraplex. *J. Mol. Biol.*, 251:76–94, 1995.

[15] A. Ambrus, D. Chen, J. Dai, R. A. Jones, and D. Yang. Solution structure of the biologically relevant G-quadruplex element in the human c-MYC promoter. Implications for G-quadruplex stabilization. *Biochemistry*, 44: 2048–2058, 2005. 1, 14, 31, 46, 76

[16] V. Sasisekharan, S. Zimmerman, and D. R. Davies. The structure of helical 5'-guanosine monophosphate. *J. Mol. Biol.*, 92:171–179, 1975. 1

[17] S. Arnott, R. Chandrasekaran, and C. M. Marttila. Structures for polyinosinic acid and polyguanilyc acid. *Biochem. J.*, 141:537–543, 1974. 1

[18] G. Laughlan, A. I. Murchie, D. G. Norman, M. H. Moore, P. C. Moody, D. M. Lilley, and B. Luisi. The high-resolution crystal structure of a parallel-stranded guanine tetraplex. *Science*, 265:520–524, 1994. 1

[19] J. R. Williamson. G-quartet structures in telomeric DNA. *Annu. Rev. Biophys. Biomol. Struct.*, 23:703–730, 1994. 1

[20] T. Simonsson. G-quadruplex structures - variations on a theme. *Biol. Chem.*, 382:621–628, 2001. 2

[21] S. Burge, G. N. Parkinson, P. Hazel, A. K. Todd, and S. Neidle. Quadruplex DNA: sequence, topology and structure. *Nucleic Acids Res.*, 34:5402–5415, 2006.

[22] J. Dai, M. Carver, and D. Yang. Polymorphism of human telomeric quadruplex structures. *Biochimie*, 90:1172–1183, 2008. 2

[23] D. Miyoshi, A. Nakao, and N. Sugimoto. Structural transition from antiparallel to parallel G-quadruplex of d($G_4T_4G_4$) induced by Ca^{2+}. *Nucleic Acids Res.*, 31:1156–1163, 2003. 2

[24] P. Hazel, J. Huppert, S. Balasubramanian, and S. Neidle. Loop-length-dependent folding of G-quadruplexes. *J. Am. Chem. Soc.*, 126:16405–16415, 2004. 2, 6

[25] A. Bugaut and S. Balasubramanian. A sequence-independent study of the influence of short loop lengths on the stability and topology of intramolecular DNA G-quadruplexes. *Biochemistry*, 47:689–697, 2008. 2, 6

[26] D.-H. Zhang, T. Fujimoto, S. Saxena, H.-Q. Yu, D. Miyoshi, and N. Sugimoto. Monomorphic RNA G-quadruplex and polymorphic DNA G-quadruplex structures responding to cellular environmental factors. *Biochemistry*, 49:4554–4563, 2010. 2

[27] L. Ying, J. J. Green, H. Li, D. Klenerman, and S. Balasubramanian. Studies on the structure and dynamics of the human telomeric G quadruplex by single-molecule fluorescence resonance energy transfer. *Proc. Natl. Acad. Sci. U.S.A.*, 100:14629–14634, 2003. 4

[28] A. M. Zahler, J. R. Williamson, T. R. Cech, and D. M. Prescott. Inhibition of telomerase by G-quartet DNA structures. *Nature*, 350:718–720, 1991. 4, 5, 10, 64

[29] J. L. Huppert and S. Balasubramanian. G-quadruplexes in promoters throughout the human genome. *Nucleic Acids Res.*, 35:406–413, 2007. 4, 13

[30] D. Drygin, A. Siddiqui-Jain, S. O'Brien, M. Schwaebe, A. Lin, J. Bilesath, C. B. Ho, C. Proffitt, K. Trent, J. O. Whitten, J. K. Lim, D. Von Hoff, K. Anderes, and W. G. Rice. Anticancer activity of CX-3543: a direct inhibitor of rRNA biogenesis. *Cancer Res.*, 69:7653–7661, 2009. 4, 7, 10

[31] Y. Wu, K. Shin-ya, and R. M. Brosh Jr. FANCJ helicase defective in Fanconia anemia and breast cancer unwinds G-quadruplex DNA to defend genome stability. *Mol. Cell. Biol.*, 28:4116–4128, 2008. 4, 9, 13

[32] J. Christiansen, M. Kofod, and F. C. Nielsen. A guanosine quadruplex and two stable hairpins flank a major cleavage site in insulin-like growth factor II mRNA. *Nucleic Acids Res.*, 22:5709–5716, 1994. 4, 17

[33] M. Wieland and J. S. Hartig. RNA quadruplex-based modulation of gene expression. *Chem. Biol.*, 14:757–763, 2007.

[34] S. Kumari, A. Bugaut, J. L. Huppert, and S. Balasubramanian. An RNA G-quadruplex in the 5'-UTR of the NRAS proto-oncogene modulates translation. *Nat. Chem. Biol.*, 3:218–221, 2007. 17, 78

[35] J. L. Huppert, A. Bugaut, S. Kumari, and S. Balasubramanian. G-quadruplexes: the beginning and end of UTRs. *Nucleic Acids Res.*, 36: 6260–6268, 2008. 17, 64

[36] A. Bugaut, R. Rodriguez, S. Kumari, S.-T. D. Hsu, and S. Balasubramanian. Small-molecule mediated inhibition of translation by targeting a native RNA-G-quadruplex. *Org. Biomol. Chem.*, 8:2771–2776, 2010. 4, 17, 21, 39, 62

[37] J. L. Huppert and S. Balasubramanian. Prevalence of quadruplexes in the human genome. *Nucleic Acids Res.*, 33:2908–2916, 2005. 5, 19, 64, 84, 95

[38] A. K. Todd, M. Hohnston, and S. Neidle. Highly prevalent putative quadruplex sequence motifs in human DNA. *Nucleic Acids Res.*, 33:2901–2907, 2005. 5, 19

[39] D. Sun, B. Thompson, B. E. Cathers, M. Salazar, S. M. Kerwin, J. O. Trent, T. C. Jenkins, S. Neidle, and L. H. Hurley. Inhibition of human telomerase by a G-quadruplex-interactive compound. *J. Med. Chem.*, 40: 2113–2116, 1997. 5, 6, 19

[40] R. T. Wheelhouse, D. K. Sun, H. Y. Han, F. X. Han, and L. H. Hurley. Cationic porphyrins as telomerase inhibitors: the interaction of tetra-(*N*-

methyl-4-pyridyl)porphine with quadruplex DNA. *J. Am. Chem. Soc.*, 120: 3261–3262, 1998. 5, 6

[41] K. Shin-ya, K. Wierzba, K. Matsuo, T. Ohtani, Y. Yamada, K. Furihata, Y. Hayakwa, and H. Seto. Telomestatin, a novel telomerase inhibitor from *Streptomyces anulatus*. *J. Am. Chem. Soc.*, 123:1262–1263, 2001. 5, 6, 12, 21

[42] D. Gomez, T. Wenner, B. Brassart, C. Douarre, M.-F. O'Donohue, V. El Khoury, K. Shin-ya, H. Morjani, C. Trentesaux, and J.-F. Riou. Telomestatin-induced telomere uncapping is modulated by POT1 through G-overhang extension in HT1080 human tumor cells. *J. Biol. Chem.*, 281: 38721–38729, 2006. 5, 6, 11, 37, 39, 55

[43] R. J. Harrison, S. M. Gowan, L. R. Kelland, and S. Neidle. Human telomerase inhibition by substituted acridine derivatives. *Bioorg. Med. Chem. Lett.*, 9:2463–2468, 1999. 6

[44] S. M. Gowan, J. R. Harrison, L. Patterson, M. Valenti, M. R. Read, S. Neidle, and L. R. Kelland. A G-quadruplex-interactive potent small-molecule inhibitor of telomerase exhibiting *in vitro* and *in vivo* antitumor activity. *Mol. Pharmacol.*, 61:1154–1162, 2002. 7, 39, 56

[45] R. A. Heald, C. Modi, J. C. Cookson, I. Hutchinson, C. A. Laughton, S. M. Gowan, L. R. Kelland, and M. F. Stevens. Antitumour polycyclic acridines. Synthesis and telomerease-inhibitory activity of methylated pentacyclic acridinium salts. *J. Med. Chem.*, 45:590–597, 2002.

[46] A. M. Burger, F. Dai, C. M. Schultes, A. P. Reszka, M. J. Moore, J. A. Double, and S. Neidle. The G-quadruplex-interactive molecule BRACO-19 inhibits tumor growth, consistent with telomere targeting and interference with telomerase function. *Cancer Res.*, 65:1486–1496, 2005. 7, 11, 12

[47] M. J. B. Moore, C. M. Schultes, J. Cuesta, F. Cuenca, M. Gunaratnam, F. A. Tanious, W. D. Wilson, and S. Neidle. Trisubstituted acridines as G-quadruplex telomere targeting agents. Effects of extensions of the 3,6 and 9-side chains on quadruplex binding, telomerase activity, and cell proliferation. *J. Med. Chem.*, 49:582–599, 2006.

[48] M. Gunaratnam, O. Greciano, C. Martins, A. P. Reszka, C. M. Schultes, H. Morjani, J.-F. Riou, and S. Neidle. Mechanism of acridine-based telomerase inhibition and telomere shortening. *Biochem. Pharmacol.*, 74:679–689, 2007. 11, 12, 39

[49] C. Martins, M. Gunaratnam, J. Stuart, V. Makwana, O. Greciano, A. P. Reszka, L. R. Kelland, and S. Neidle. Structure-based design of benzylamino-acridine compounds as G-quadruplex DNA telomere targeting agents. *Bioorg. Med. Chem. Lett.*, 17:2293–2298, 2007.

[50] R. Rodriguez, G. D. Pantoş, D. P. N. Gonçalves, J. K. M. Sanders, and S. Balasubramanian. Ligand-driven G-quadruplex conformational switching by using an unusual mode of interaction. *Angew. Chem. Int. Ed.*, 46: 5404–5407, 2007. 20

[51] M. Laronze-Cochard, Y.-M. Kim, B. Brassart, J.-F. Riou, J.-Y. Laronze, and J. Sapi. Synthesis and biological evaluation of novel 4,5-bis(dialkylaminoalkyl)-substituted acridines as potent telomeric G-quadruplex ligands. *Eur. J. Med. Chem.*, 44:3880–3888, 2009. 6

[52] P. J. Perry, S. M. Gowan, A. P. Reszka, P. Polucci, T. C. Jenkins, L. R. Kelland, and S. Neidle. 1,4- and 2,6-disubstituted amidoanthracene-9,10-dione derivatives as inhibitors of human telomerase. *J. Med. Chem.*, 41: 3253–3260, 1998. 6

[53] P. J. Perry, A. P. Reszka, A. A. Wood, M. A. Read, S. M. Gowan, H. S. Dosanjh, J. O. Trent, T. C. Jenkins, L. R. Kelland, and S. Neidle. Human telomerase inhibition by regioisomeric disubstituted amidoanthracene-9,10-diones. *J. Med. Chem.*, 41:4873–4884, 1998. 6

[54] P. J. Perry, M. A. Read, R. T. Davies, S. M. Gowan, A. P. Reszka, A. A. Wood, L. R. Kelland, and S. Neidle. 2,7-disubstituted amidofluorenone derivatives as inhibitors of human telomerase. *J. Med. Chem.*, 42:2679–2684, 1999. 6

[55] F. Koeppel, J.-F. Riou, A. Laoui, P. B. Arimondo, D. Labit, O. Petitgenet, C. Hélène, and J.-L. Mergny. Ethidium derivatives bind to G-quartets,

inhibit telomerase and act as fluorescent probes for quadruplexes. *Nucleic Acids Res.*, 29:1087–1096, 2001. 6

[56] A. Maraval, S. Franco, C. Vialas, G. Pratviel, M. A. Blasco, and B. Meunier. Porphyrin-aminoquinoline conjugates as telomerase inhibitors. *Org. Biomol. Chem.*, 1:921–927, 2003. 6

[57] M. Y. Kim, M. Gleason-Guzman, E. Izbicka, D. Nishioka, and L. H. Hurley. The different biological effects of telomestatin and TMPyP4 can be attributed to their selectivity for interaction with intramolecular or intermolecular G-quadruplex structures. *Cancer Res.*, 63:3247–3256, 2003. 6, 39, 56

[58] J. Seenisamy, S. Bashyam, V. Gokhale, H. Vankayalapati, D. Sun, A. Siddiqui-Jain, N. Streiner, K. Shin-ya, E. White, W. D. Wilson, and L. H. Hurley. Design and synthesis of an expanded porphyrin that has selectivity for the c-MYC G-quadruplex structure. *J. Am. Chem. Soc.*, 127: 2944–2959, 2005. 7, 14, 31

[59] G. N. Parkinson, R. Ghosh, and S. Neidle. Structural basis for binding of porphyrin to human telomeres. *Biochemistry*, 46:2390–2397, 2007. 6, 19

[60] J.-L. Mergny, L. Lacroix, M.-P. Teulade-Fichou, C. Hounsou, L. Guittat, M. Hoarau, P. B. Arimondo, J.-P. Vigneron, J.-M. Lehn, J.-F. Riou, T. Gerestier, and C. Hélène. Telomerase inhibitors based on quadruplex ligands selected by a fluorescence assay. *Proc. Natl. Acad. Sci. U.S.A.*, 98:3062–3067, 2001. 6

[61] R. Samudrala, X. Zhang, R. M. Wadkins, and D. L. Mattern. Synthesis of a non-cationic, water-soluble perylenetetracarboxylic diimide and its interactions with G-quadruplex-forming DNA. *Bioorg. Med. Chem.*, 15:186–193, 2007. 6

[62] C. Pivetta, L. Lucatello, A. P. Krapcho, B. Gatto, M. Palumbo, and C. Sissi. Perylene side chains modulate G-quadruplex conformation in biologically relevant DNA sequences. *Bioorg. Med. Chem.*, 16:9331–9339, 2008. 6

[63] J. H. Kim, J. H. Kim, G. E. Lee, S. W. Kim, and I. K. Jung. Identification of a quinoxaline derivative that is a potent telomerase inhibitor leading to cellular senescence of human cancer cells. *Biochem. J.*, 373:523–529, 2003. 6

[64] V. Caprio, B. Guyen, Y. Opoku-Boahen, J. Mann, S. M. Gowan, L. M. Kelland, M. A. Read, and S. Neidle. A novel inhibitor of human telomerase derived from 10*H*-indolo[3,2*b*]quinoline. *Bioorg. Med. Chem. Lett.*, 10:2063–2066, 2000. 6, 20

[65] W. C. Drewe, R. Nanjunda, M. Gunaratnam, M. Beltran, G. N. Parkinson, A. P. Reszka, W. D. Wilson, and S. Neidle. Rational design of substituted diarylureas: a scaffold for binding to G-quadruplex motifs. *J. Med. Chem.*, 51:7751–7767, 2008. 6, 8, 30

[66] W. C. Drewe and S. Neidle. Click chemistry assembly of G-quadruplex ligands incorporating a diarylurea scaffold and triazole linkers. *Chem. Commun.*, pages 5295–5297, 2008. 6, 45

[67] M. Bejugam, S. Sewitz, P. S. Shirude, R. Rodriguez, R. Shahid, and S. Balasubramanian. Trisubstituted isoalloxazines as a new class of G-quadruplex binding ligands: small molecule regulation of c-kit oncogene expression. *J. Am. Chem. Soc.*, 129:11890–11891, 2007. 6, 14, 64

[68] K. Jantos, R. Rodriguez, S. Ladame, P. S. Shirude, and S. Balasubramanian. Oxazole-based peptide macrocycles: A new class of G-quadruplex binding ligands. *J. Am. Chem. Soc.*, 128:13662–13663, 2006. 6, 20, 32

[69] G. S. Minhas, D. S. Pilch, J. E. Kerrigan, E. J. LaVoie, and J. E. Rice. Synthesis and G-quadruplex stabilizing properties of a series of oxazole-containing macrocycles. *Bioorg. Med. Chem. Lett.*, 16:3891–3895, 2006.

[70] D. A. Pilch, C. M. Barbieri, S. G. Rzuczek, E. J. Lavoie, and J. E. Rice. Targting human telomeric G-quadruplex DNA with oxazole-containing macrocyclic compounds. *Biochimie*, 90:1233–1249, 2008.

[71] A. Bugaut, K. Jantos, J.-L. Wietor, R. Rodriguez, J. K. M. Sanders, and S. Balasubramanian. Exploring the differential recognition of DNA G-

quadruplex targets by small molecules using dynamic combinatorial chemistry. *Angew. Chem. Int. Ed.*, 47:2677–2680, 2008. 6, 20

[72] J.-F. Riou, L. Guittat, P. Mailliet, A. Laoui, E. Renou, P. Petitgenet, F. Megnin-Chanet, C. Hélène, and J.-L. Mergny. Cell senescence and telomere shortening induced by a new series of specific G-quadruplex DNA ligands. *Proc. Natl. Acad. Sci. U.S.A.*, 99:2672–2677, 2002. 6, 8, 12, 39, 56, 58

[73] D. Gomez, N. Aouali, A. Londono-Vallejo, L. Lacroix, F. Megnin-Chanet, T. Lemarteleur, C. Douarre, K. Shin-ya, P. Mailliet, C. Trentesaux, H. Morjani, J.-L. Mergny, and J.-F. Riou. Resistance to the short term antiproliferative activity of the G-quadruplex ligand 12459 is associated with telomerase overexpression and telomere capping alteration. *J. Biol. Chem.*, 278: 50554–50562, 2003. 6, 12

[74] R. J. Harrison, A. P. Reszka, S. M. Haider, B. Romagnoli, J. Morrell, M. A. Read, S. M. Gowan, C. M. Incles, L. R. Kelland, and S. Neidle. Evaluation of disubstituted acridone derivatives as telomerase inhibitors: the importance of G-quadruplex binding. *Bioorg. Med. Chem. Lett.*, 14: 5845–5849, 2004. 6

[75] F. Cuenca, M. J. B. Moore, K. Johnson, B. Guyen, A. De Cian, and S. Neidle. Design, synthesis and evaluation of 4,5-di-substituted acridone ligands with high G-quadruplex affinity and selectivity, together with low toxicity to normal cells. *Bioorg. Med. Chem. Lett.*, 19:5109–5113, 2009. 6, 8

[76] M. P. Teulade-Fichou, C. Carrasco, L. Guittat, C. Bailly, P. Alberti, J.-L. Mergny, A. David, J.-M. Lehn, and W. D. Wilson. Selective recognition of G-quadruplex telomeric DNA by a bis(quinacridine). *Proc. Natl. Acad. Sci. U.S.A.*, 98:3062–3067, 2001. 6

[77] C. Hounsou, L. Guittat, D. Monchaud, M. Jourdan, N. Saettel, J.-L. Mergny, and M.-P. Teulade-Fichou. G-quadruplex recognition by quinacridines: a SAR, NMR and biological study. *ChemMedChem*, 2:655–666, 2007.

[78] H. Bertrand, S. Bombard, D. Monchaud, and M.-P. Teulade-Fichou. A platinum-quinacridine hybrid as a G-quadruplex ligand. *J. Biol. Inorg. Chem.*, 12:1003–1014, 2007. 6

[79] Z. A. E. Waller, P. S. Shirude, R. Rodriguez, and S. Balasubramanian. Triarylpyridines: a versatile small molecule scaffold for G-quadruplex recognition. *Chem. Commun.*, pages 1467–1469, 2008. 6, 32

[80] C. Leonetti, S. Amodei, C. D'Angelo, A. Rizzo, B. Banassi, A. Antonelli, R. Elli, M. F. Stevens, M. D'Incalci, G. Zupi, and G. Biroccio. Biological activity of the G-quadruplex ligand RHPS4 (3,11-difluoro-6,8,13-trimethyl-8*H*-quino[4,3,2-*kl*]acridinium methosulfate) is associated with telomere capping alteration. *Mol. Pharmacol.*, 66:1138–1146, 2004. 6, 7

[81] M. A. Read, A. A. Wood, J. R. Harrison, S. M. Gowan, L. R. Kelland, H. S. Dosanjh, and S. Neidle. Molecular modeling studies on G-quadruplex complexes of telomerase inhibitors: structure-activity relationships. *J. Med. Chem.*, 42:4538–4546, 1999.

[82] W. Duan, A. Rangan, H. Vankayalapati, M. Y. Kim, Q. Zeng, D. Sun, H. Han, O. Y. Fedoroff, D. Nishioka, S. Y. Rha, E. Izbicka, D. D. Von Hoff, and L. H. Hurley. Design and synthesis of fluoroquinophenoxazines that interact with human telomeric G-quadruplexes and their biological effects. *Mol. Cancer Ther.*, 1:103–120, 2001. 39, 56

[83] M. A. Read, R. J. Harrison, B. Romagnoli, F. A. Tanious, S. M. Gowan, A. P. Reszka, W. D. Wilson, L. R. Kelland, and S. Neidle. Structure-based design of selective and potent G-quadruplex-mediated telomerase inhibitors. *Proc. Natl. Acad. Sci. U.S.A.*, 98:4844–4849, 2001.

[84] A. Siddiqui-Jain, C. L. Grand, D. J. Bearss, and L. H. Hurley. Direct evidence for a G-quadruplex in a promoter region and its targeting with a small molecule to repress c-MYC transcription. *Proc. Natl. Acad. Sci. U.S.A.*, 99:11593–11598, 2002. 14, 15, 31, 46, 64

[85] S. Ladame, J. A. Schouten, J. Stuart, J. Roldan, S. Neidle, and S. Balasubramanian. Tetrapeptides induce selective recognition for G-quadruplexes

when conjugated to a DNA-binding platform. *Org. Biomol. Chem.*, 2:2925–2931, 2004.

[86] A. T. Phan, V. Kuryavyi, H. Y. Gaw, and D. J. Patel. Small-molecule interaction with a five-guanine-tract G-quadruplex structure from the human *MYC* promoter. *Nat. Chem. Biol.*, 1:167–173, 2005. 6, 14, 31, 46

[87] D. Sun, K. Guo, J. J. Rusche, and L. H. Hurley. Facilitation of a structural transition in the polypurine/polypyrimidine tract within the proximal promoter region of the human VEGF gene by the presence of potassium and G-quadruplex-interactive agents. *Nucleic Acids Res.*, 33:6070–6080, 2005. 14

[88] J.-L. Zhou, Y.-J. Lu, T.-M. Ou, J.-M. Zhou, Z.-S. Huang, X.-F. Zhu, C.-J. Du, X.-Z. Bu, L. Ma, L.-Q. Gu, Y.-M. Li, and A. S.-C. Chan. Synthesis and evaluation of quindoline derivatives as G-quadruplex inducing and stabilizing ligands and potential inhibitors of telomerase. *J. Med. Chem.*, 48: 7315–7321, 2005.

[89] D. P. N. Gonçalves, R. Rodriguez, S. Balasubramanian, and J. K. M. Sanders. Tetramethylpryidiniumporphyrazines - a new class of G-quadruplex inducing and stabilising ligands. *Chem. Commun.*, pages 4685–4687, 2006.

[90] J. Hooda, D. Bednarski, L. Irish, and S. M. Firestine. Synthesis and testing of a triaza-cyclopenta[*b*]phenanthrene scaffold as a DNA binding agent. *Bioorg. Med. Chem.*, 14:1902–1909, 2006.

[91] J. E. Reed, A. A. Arnal, S. Neidle, and R. Vilar. Stabilization of G-quadruplex DNA and inhibition of telomerase activity by square-planar nickel (II) complexes. *J. Am. Chem. Soc.*, 128:5992–5993, 2006.

[92] T. Ou, Y. J. Lu, C. Zhang, Z. S. Huang, X. D. Wang, J. H. Tan, Y. Chen, D. L. Ma, K. Y. Wong, J. C. Tang, A. S. Chan, and L. Q. Gu. Stabilization of G-quadruplex DNA and down-regulation of oncogene c-myc by quindoline derivatives. *J. Med. Chem.*, 50:1465–1474, 2007. 14, 31

[93] D. Monchaud and M.-P. Teulade-Fichou. A hitchhiker's guide to G-quadruplex ligands. *Org. Biomol. Chem.*, 6:627–636, 2007. 20, 21, 32

[94] A. De Cian, E. DeLemos, J.-L. Mergny, M.-P. Teulade-Fichou, and D. Monchaud. Highly efficient G-quadruplex recognition by bisquinolinium compounds. *J. Am. Chem. Soc.*, 129:1856–1857, 2007.

[95] G. Zagatto, C. Sissi, S. Moro, D. Dal Ben, G. N. Parkinson, K. R. Fox, S. Neidle, and M. Palumbo. Amide bond direction modulates G-quadruplex recognition and telomerase inhibition by 2,6 and 2,7 bis-substituted anthracenedione derivatives. *Bioorg. Med. Chem.*, 16:354–361, 2008. 20

[96] J. Dash, P. S. Shirude, and S. Balasubramanian. G-quadruplex recognition by bis-indole carboxamides. *Chem. Commun.*, pages 3055–3057, 2008. 32

[97] J. Dash, P. S. Shirude, S.-T. D. Hsu, and S. Balasubramanian. Diarylethynyl amides that recognize the parallel conformation of genomic promoter DNA G-quadruplexes. *J. Am. Chem. Soc.*, 130:15950–15956, 2008. 20

[98] J.-H. Tan, T.-M. Ou, J.-Q. Hou, Y.-J. Lu, S.-L. Huang, H.-B. Luo, J.-Y. Wu, Z.-S. Huang, K.-Y. Wong, and L.-Q. Gu. Isaindigotone derivatives: a new class of highly selective ligands for telomeric G-quadruplex DNA. *J. Med. Chem.*, 52:2825–2835, 2009.

[99] Q. Li, J. Xiang, X. Li, L. Chen, X. Xu, Y. Tang, Q. Zhou, L. Li, H. Zhang, X. Sun, A. Guan, Q. Yang, S. Yang, and G. Xu. Stabilising parallel G-quadruplex DNA by a new class of ligands: two non-planar alkaloids through interaction in lateral grooves. *Biochimie*, 91:811–819, 2009. 6, 19

[100] J. Debray, W. Zeghida, M. Jourdan, D. Monchaud, M.-L. Dheu-Andries, P. Dumy, M.-P. Teulade-Fichou, and M. Demeunynck. Synthesis and evaluation of fused bispyrimidinoacridines as novel pentacyclic analogues of quadruplex-binder BRACO-19. *Org. Biomol. Chem.*, 7:5219–5228, 2009.

[101] J. E. Moses, D. J. Ritson, F. Zhang, C. M. Lombardo, S. Haider, N. Oldham, and S. Neidle. A click chemistry approach to C_3 symmetric, G-quadruplex stabilising ligands. *Org. Biomol. Chem.*, 8:2926–2930, 2010. 45

[102] M. Satyanarayana, Y.-A. Kim, S. G. Rzuczek, D. S. Pilch, A. A. Liu, L. F. Liu, J. E. Rice, and E. J. LaVoie. Macroyclic hexaoxazoles: influence of aminoalkyl substituents on RNA and DNA G-quadruplex stabilization and cytotoxicity. *Bioorg. Med. Chem. Lett.*, 20:3150–3154, 2010.

[103] S. G. Rzuczek, D. S. Pilch, A. Liu, L. Liu, E. J. LaVoie, and J. E. Rice. Macrocyclic pyridyl polyoxazoles: selective RNA and DNA G-quadruplex ligands as antitumor agents. *J. Med. Chem.*, 53:3632–3644, 2010.

[104] M. Bejugam, M. Gunaratnam, S. Müller, D. A. Sanders, S. Sewitz, J. A. Fletcher, S. Neidle, and S. Balasubramanian. Targeting the c-Kit promoter quadruplexes with 6-substituted indenoisoquinolines, a novel class of G-quadruplex stabilising small molecule ligands. *ACS Med. Chem. Lett.*, DOI: 10.1021/ml100062z, 2010. 6, 14, 19

[105] E. Gavathiotis, R. A. Heald, M. F. Stevens, and M. S. Searle. Drug recognition and stabilisation of the parallel-stranded DNA quadruplex $(TTAGGGT)_4$ containing the human telomeric repeat. *J. Mol. Biol.*, 334: 25–36, 2003. 6, 7

[106] N. H. Campbell, M. Patel, C. B. Tofa, R. Ghosh, G. N. Parkinson, and S. Neidle. Selectivity in ligand recognition of G-quadruplex loops. *Biochemistry*, 48:1675–1680, 2009. 6, 19

[107] S. Cosconati, L. Marinelli, R. Trotta, A. Virno, S. De Tito, R. Romagnoli, B. Pagano, V. Limongelli, C. Giancola, P. G. Baraldi, L. Mayol, E. Novellino, and A. Randazzo. Structural and conformational requisites in DNA quadruplex groove binding: another piece to the puzzle. *J. Am. Chem. Soc.*, 132:6425–6433, 2010. 6, 19

[108] J. Ren and J. B. Chaires. Sequence and structural selectivity of nucleic acid binding ligands. *Biochemistry*, 38:16067–16075, 1999. 6

[109] P. Wang, L. Ren, H. He, F. Liang, X. Zhou, and Z. Tan. A phenol quaternary ammonium porphyrin as a potent telomerase inhibitor by selective interaction with quadruplex DNA. *ChemBioChem*, 7:1155–1159, 2006. 6

[110] P. S. Shirude, E. R. Gillies, S. Ladame, F. Godde, K. Shin-ya, I. Huc, and S. Balasubramanian. Macrocyclic and helical oligoamides as a new class of G-quadruplex ligands. *J. Am. Chem. Soc.*, 46:5404–5407, 2007. 6, 21, 32

[111] W. G. Rice, J. K. C. Lim, M. K. Schwabe, A. Siddiqui-Jain, N. H. Streiner, K. B. Trent, J. P. Whitten, L. H. Hurley, and D. D. Von Hoff. Design of CX-3543, a novel multi-targeting antitumor agent. *Proc. Amer. Assoc. Cancer. Res.*, 46, 2005. 7

[112] A. Rizzo, E. Salvati, M. Porru, C. D'Angelo, M. F. Stevens, M. D'Incalci, C. Leonetti, E. Gilson, G. Zupi, and A. Biroccio. Stabilization of quadruplex DNA perturbs telomere replication leading to the activation of an ATR-dependent ATM signaling pathway. *Nucleic Acids Res.*, 37:5353–5364, 2009. 7, 13, 64

[113] E. Salvati, C. Leonetti, A. Rizzo, M. Scarsella, M. Mottolese, R. Galati, I. Sperduti, M. F. Stevens, M. D'Incalci, M. Blasco, G. Chiorino, S. Bauwens, B. Horard, E. Gilson, A. Stoppacciaro, G. Zupi, and A. Biroccio. Telomere damage induced by the G-quadruplex ligand $RHPS_4$ has an antitumor effect. *J. Clin. Invest.*, 117:3236–3247, 2007. 7, 11

[114] C. Leonetti, M. Scarsella, G. Riggio, A. Rizzo, E. Salvati, M. D'Incalci, L. Staszewsky, R. Frapolli, M. F. Stevens, A. Stoppacciaro, M. Mottolese, B. Antoniani, E. Gilson, G. Zupi, and A. Biroccio. G-quadruplex ligand RHPS4 potentiates the antitumor activity of camptothecins in preclinical models of solid tumors. *Clin. Cancer. Res*, 14:7284–7291, 2008. 7

[115] P. Yang, A. De Cian, M.-P. Teulade-Fichou, J.-L. Mergny, and D. Monchaud. Engineering bisquinolinium/thiazole orange conjugates for fluorescent sensing of G-quadruplex DNA. *Angew. Chem. Int. Ed.*, 48:2188–2191, 2009. 8

[116] Y.-C. Tsai, H. Qui, C.-P. Lin, R.-K. Lin, J. E. Kerrigan, S. G. Rzuczek, E. J. LaVoie, J. E. Rice, D. S. Pilch, Y. L. Lyu, and L. F. Lui. A G-quadruplex stabilizer induces M-phase cell cycle arrest. *J. Biol. Chem.*, 284:22535–22543, 2009. 8

[117] G. Pennarun, C. Granotier, L. R. Gauthier, D. Gomez, F. Hoffschir, E. Mandine, J.-F. Riou, J.-L. Mergny, P. Mailliet, and F. D. Boussin. Apoptosis related to telomere instability and cell cycle alterations in human glioma cells treated by new highly selective G-quadruplex ligands. *Oncogene*, 24:2917–2928, 2005. 8, 21

[118] H. J. Lipps and D. Rhodes. G-quadruplex structures: *in vivo* evidence and function. *Trends in Cell Biol.*, 19:414–422, 2009. 9

[119] C. Schaffitzel, I. Berger, J. Postberg, J. Hanes, H. J. Lipps, and A. Plückthun. *In vitro* generated antibodies specific for telomeric guanine-quadruplex DNA react with *Stylonychia lemnae* macronuclei. *Proc. Natl. Acad. Sci. U.S.A.*, 98:8572–8577, 2001. 9

[120] K. Paeschke, T. Simonsson, J. Postberg, D. Rhodes, and H. J. Lipps. Telomere end-binding proteins control the formation of G-quadruplex DNA structures *in vivo*. *Nat. Struct. Mol. Biol.*, 12:847–854, 2005. 9

[121] G. Fang and T. R. Cech. The β subunit of Oxytricha telomere-binding protein promotes G-quartet formation by telomeric DNA. *Cell*, 74:875–885, 1993. 9

[122] G. Fang and T. R. Cech. Characterization of a G-quartet formation reaction promoted by the β-subunit of the Oxytricha telomere-binding protein. *Biochemistry*, 32:11646–11657, 1993. 9

[123] H. Sun, J. K. Karow, I. D. Hickson, and N. Maizels. The Bloom's syndrome helicase unwinds G4 DNA. *J. Biol. Chem.*, 273:27587–27592, 1998. 9, 13

[124] M. Fry and L. A. Loeb. Human Werner syndrome DNA helicase unwinds tetrahelical structures of the fragile X syndrome repeat sequence $\mathrm{d(CGG)}_n$. *J. Biol. Chem.*, 274:12797–12802, 1999. 9, 13

[125] V. A. Soldatenkov, A. A. Vetcher, T. Duka, and S. Ladame. First evidence of a functional interaction between DNA quadruplexes and poly(ADP-ribose) polymerase-1. *ACS Chem. Biol.*, 3:214–219, 2008. 9

[126] C. Schaeffer, B. Bardoni, J.-L. Mandel, B. Ehresmann, C. Ehresmann, and H. Moine. The fragile X mental retardation protein binds specifically to its mRNA via a purine quartet motif. *EMBO J.*, 20:4803–4813, 2001. 9, 17

[127] S. J. McKay and H. Cooke. hnRNP A2/B1 binds specifically to single stranded vertebrate telomeric repeat $(TTAGGG)_n$. *Nucleic Acids Res.*, 20: 6461–6464, 1992. 10

[128] M. Paramasivam, A. Membrino, S. Cogoi, H. Fukada, H. Nakagama, and L. E. Xodo. Protein hnRNP A1 and its derivative Up1 unfold quadruplex DNA in the human *KRAS* promoter: implications for transcription. *Nucleic Acids Res.*, 37:2841–2853, 2009. 10

[129] V. González, K. Guo, L. H. Hurley, and D. Sun. Identification and characterization of nucleolin as a *c-myc* G-quadruplex binding protein. *J. Biol. Chem.*, 284:23622–23635, 2009. 10

[130] D. Liu, M. S. O'Connor, J. Qin, and Z. Sonyang. Telosome, a mammalian telomere-associated complex formed by multiple telomeric proteins. *J. Biol. Chem.*, 279:51338–51342, 2004. 10

[131] T. de Lange. Shelterin: the protein complex that shapes and safeguards human telomeres. *Genes. Dev.*, 19:2100–2110, 2005. 10

[132] E. H. Blackburn. Structure and function of telomeres. *Nature*, 350:569–573, 1991. 10

[133] J. D. Henson, A. A. Neumann, T. R. Yaeger, and R. R. Reddel. Alternative lengthening of telomeres in mammalian cells. *Oncogene*, 21:598–610, 2002. 10

[134] S. A. Steward and R. A. Weinberg. Telomeres: cancer to human aging. *Annu. Rev. Cell. Dev. Biol.*, 22:531–557, 2006. 10

[135] A. Sancer, L. A. Lindsey-Boltz, K. Unsal-Kaçmaz, and S. Linn. Molecular mechanisms of mammalian DNA repair and the DNA damage checkpoints. *Ann. Rev. Biochem.*, 73:39–85, 2004. 11

[136] A. De Cian, L. Lacroix, C. Douarre, N. Temime-Smaali, C. Trentesaux, J.-F. Riou, and J.-L. Mergny. Targeting telomeres and telomerase. *Biochimie*, 90:131–155, 2008. 11

[137] P. Phatak, J. C. Cookson, F. Dai, V. Smith, R. B. Gartenhaus, M. F. Stevens, and A. M. Burger. Telomere uncapping by the G-quadruplex ligand RHPS4 inhibits clonogenic tumour cell growth. *Br. J. Cancer*, 96: 1223–1233, 2007. 11

[138] T. Tauchi, K. Shin-Ya, G. Sashida, M. Sumi, A. Nakajima, T. Shimamoto, J. H. Ohyashiki, and K. Ohyashiki. Activity of a novel G-quadruplex-interactive telomerase inhibitor, telomestatin (SOT-095), against human leukemia cells: involvement of ATM-dependent DNA damage response pathways. *Oncogene*, 22:5338–5347, 2003. 11, 39, 56

[139] N. Temime-Smaali, L. Guittat, A. Sidibe, K. Shin-ya, C. Trentesaux, and J.-F. Riou. The G-quadruplex ligand telomestatin impairs binding of topoisomerase IIIα to G-quadruplex-forming oligonucleotides and uncaps telomeres in ALT cells. *PLOS*, 4:e6919, 2009. 12

[140] D. Gomez, T. Lemarteleur, L. Lacroix, P. Mailliet, J.-L. Mergny, and J.-F. Riou. Telomerase downregulation induced by the G-quadruplex ligand 12459 in A549 cells is mediated by hTERT RNA alternative splicing. *Nucleic Acids Res.*, 32:371–379, 2004. 12

[141] D. Gomez, A. Guédin, J.-L. Mergny, B. Salles, J.-F. Riou, M.-P. Teulade-Fichou, and P. Calsou. A G-quadruplex structure in the 5'-UTR of TRF2 mRNA represses translation in human cells. *Nucleic Acids Res.*, 2010 doi:10.1093/nar/gkq563. 12, 17, 62

[142] J. D. Griffith, L. Comeau, S. Rosenfield, R. M. Stansel, A. Bianchi, H. Moss, and T. de Lange. Mammalian telomeres end in a large duplex loop. *Cell*, 97:503–514, 1999. 12

[143] R. M. Stansel, T. de Lange, and J. D. Griffith. T-loop assembly *in vitro* involves binding of TRF2 near the 3' telomeric overhang. *EMBO J.*, 20: 5532–5540, 2001. 12

[144] R. Rodriguez, S. Müller, J. A. Yeoman, C. Trentesaux, J.-F. Riou, and S. Balasubramanian. A novel small molecule that alters shelterin integrity and triggers a DNA-damage response at telomeres. *J. Am. Chem. Soc.*, 130:15758–15759, 2008. 12, 21, 32, 36, 37, 38, 39, 53, 55, 61, 62, 90, 95

[145] S. Neidle. Human telomeric G-quadruplexes: the current status of telomeric G-quadruplexes as therapeutic targets in human cancer. *FEBS J.*, 277: 1118–1125, 2010. 12

[146] A. T. Phan, Y. S. Modi, and D. J. Patel. Propeller-type parallel-stranded G-quadruplexes in the human c-myc promoter. *J. Am. Chem. Soc.*, 126: 8710–8716, 2004. 14, 31, 46

[147] S. Rankin, A. P. Reszka, J. L. Huppert, M. Zloh, G. N. Parkinson, A. K. Todd, S. Ladame, and S. Balasubramanian. Putative DNA quadruplex formation within the human c-kit oncogene. *J. Am. Chem. Soc.*, 127:10584–10589, 2005. 14, 31

[148] A. T. Phan, V. Kuryavyi, S. Burge, S. Neidle, and D. J. Patel. Structure of an unprecedented G-quadruplex scaffold in the human c-kit promoter. *J. Am. Chem. Soc.*, 129:4386–4392, 2007. 46

[149] H. Fernando, A. P. Reszka, J. L. Huppert, S. Ladame, S. Rankin, A. R. Venkitaraman, S. Neidle, and S. Balasubramanian. A conserved quadruplex motif located in a transcription activation site of the human c-kit oncogene. *Biochemistry*, 45:7845–7860, 2006. 14, 31, 46

[150] J. Dai, D. Chen, R. A. Jones, L. H. Hurley, and D. Yang. NMR solution structure of the major G-quadruplex structure formed in the human BCL2 promoter region. *Nucleic Acids Res.*, 34:5133–5144, 2006. 14, 46

[151] T. S. Dexheimer, D. Sun, and L. H. Hurley. Deconvoluting the structural and drug-recognition complexity of the G-quadruplex-forming region upstream of the bcl-2 P1 promoter. *J. Am. Chem. Soc.*, 128:5404–5415, 2006. 14

[152] S. Cogoi and L. E. Xodo. G-quadruplex formation within the promoter of the KRAS proto-oncogene and its effect on transcription. *Nucleic Acids Res.*, 34:2536–2549, 2006. 14, 31, 46

[153] S. Cogoi, M. Paramasivam, B. Spolaore, and L. E. Xodo. Structural polymorphism within a regulatory element of the human *KRAS* promoter: formation of G4-DNA recognized by nuclear proteins. *Nucleic Acids Res.*, 36: 3765–3780, 2008. 14, 31, 46

[154] Y. Qin, J. S. Fortin, D. Tye, M. Gleason-Guzman, T. A. Brooks, and L. H. Hurley. Molecular cloning of the human platelet-derived growth factor receptor β (PDGFR-β). Promoter and drug targeting of the G-quadruplex-forming region to repress PDGFR-β expression. *Biochemistry*, 49:4208–4219, 2010. 14

[155] R. M. Howell, K. J. Woodford, M. N. Weitzmann, and K. Usdin. The chicken-globin gene promoter forms a novel "cinched" tetrahelical structure. *J. Biol. Chem.*, 271:5208–5214, 1996. 14

[156] S. P. Clark, C. D. Lewis, and G. Felsenfield. Properties of BGP1, a poly(dG)-binding protein from chicken erythrocytes. *Nucleic Acids Res.*, 18:5119–5126, 1990. 14

[157] T. Shalaby, A. O. von Bueren, M.-L. Hürlimann, G. Fiaschetti, D. Castalletti, T. Masayuki, K. Nagasawa, A. Arcaro, I. Jelesarov, K. Shin-ya, and M. Grotzer. Disabling *c-Myc* in childhood medulloblastoma and atypical tetratoid/rhabdoid tumor cells by the potent G-quadruplex interactive agent S2T1-6OTD. *Mol. Cancer Ther.*, 9:167–179, 2010. 14

[158] M. Gunaratnam, S. Swank, S. M. Haider, K. Galesa, A. P. Reszka, M. Beltran, F. Cuenca, J. A. Fletcher, and S. Neidle. Targeting human gastrointestinal stromal tumor cells with a quadruplex-binding small molecule. *J. Med. Chem.*, 52:3774–3783, 2009. 14

[159] X.-D. Wang, T.-M. Ou, Y.-J. Lu, Z. Li, Z. Xu, C. Xi, J.-H. Tan, S.-L. Huang, L.-K. An, D. Li, L.-Q. Gu, and Z.-S. Huang. Turning off transcription of the *bcl-2* gene by stabilizing the *bcl-2* promoter quadruplex with quindoline derivatives. *J. Med. Chem.*, 53:4390–4398, 2010. 14

[160] P. Bucek, J. Jaumot, Avino, R. Eritja, and R. Gargallo. pH-Modulated Watson-Crick duplex-quadruplex equilibria of guanine-rich and cytosine-rich DNA sequences 140 base pairs upstream of the *c-kit* transcription initiation site. *Chem. Eur. J.*, 15:12663–12671, 2009. 15

[161] D. Sun and L. H. Hurley. The importance of negative superhelicity in inducing the formation of the G-quadruplex and i-motif structures in the c-Myc promoter: Implications for drug targeting and control of gene expression. *J. Med. Chem.*, 52:2863–2874, 2009. 15

[162] S. Dhakal, J. D. Schonhoft, D. Koirala, Z. Yu, S. Basu, and H. Mao. Coexistence of an ILPR i-motif and a partially folded structure with comparable mechanical stability revealed at the single-molecule level. *J. Am. Chem. Soc.*, 2010: DOI: 10.1021/ja100944j. 15

[163] E. F. Michelotti, T. Tomonaga, H. Krutzsch, and D. Levens. Cellular nucleic acid binding protein regulates the CT element of the human *c-Myc* protooncogene. *J. Biol. Chem.*, 270:9494–9499, 1995. 15

[164] M. Takimoto, T. Tomonaga, M. Matunis, M. Avignan, H. Krutzsch, G. Dreyfuss, and D. Levensevens. Specific binding of heterogeneous ribonucleoprotein particle protein K to the human *c-Myc* promoter, *in vitro*. *J. Biol. Chem.*, 268:18249–18258, 1993. 15

[165] G. A. Michelotti, E. F. Michelotti, A. Pullner, R. C. Duncan, D. Eick, and D. Levens. Multiple single-stranded *cis* elements are associated with activated chromatin of the human *c-Myc* gene *in vivo*. *Mol. Cell. Biol.*, 16: 2656–2669, 1996. 15

[166] G. Pesole, F. Mignone, C. Gissi, G. Grillo, F. Licciulli, and S. Liuni. Structural and funtional features of eukaryotic mRNA translated regions. *Gene*, 276:73–81, 2001. 16

[167] B. Mazumder, V. Seshadri, and P. L. Fox. Translational control by the 3'-UTR: the ends specify the means. *Trends Biochem. Sci.*, 28:91–98, 2003. 16

[168] S. Kumari, A. Bugaut, and S. Balasubramanian. Position and stability are determining factors for translation repression by an RNA G-quadruplex-forming sequence within the 5'-UTR of the *NRAS* proto-oncogene. *Biochemistry*, 47:12664–12669, 2008. 17

[169] M. J. Morris and S. Basu. An unusually stable G-quadruplex within the 5'-UTR of the MT3 matrix metalloproteinase mRNA represses translation in eukaryotic cells. *Biochemistry*, 47:53193–5319, 2009. 17

[170] G. D. Balkwill, K. Derecka, T. P. Garner, C. Hodgman, A. P. F. Flint, and M. S. Searle. Repression of translation of human estrogen receptor α by G-quadruplex formation. *Biochemistry*, 48:11487–11495, 2009. 17

[171] M. J. B. Moore, F. Cuenca, M. Searcey, and S. Neidle. Synthesis of distamycin A polyamides targeting G-quadruplex DNA. *Org. Biomol. Chem.*, 4:3479–3488, 2006. 19, 20

[172] E. M. Rexler, J. Seenisamy, S. Bashyam, M.-Y. Kim, E. White, D. Wilson, and L. H. Hurley. Telomestatin and diseleno sapphyrin bind selectively to two different forms of the human telomeric G-quadruplex structure. *J. Am. Chem. Soc.*, 127:9439–9447, 2005. 20

[173] C. Granotier, G. Pennarun, L. Riou, F. Hoffschir, L. R. Gauthier, A. De Cian, D. Gomez, E. Mandine, J.-F. Riou, J.-L. Mergny, P. Mailliet, B. Dutrillaux, and F. D. Boussin. Preferential binding of a G-quadruplex ligand to human chromosome ends. *Nucleic Acids Res.*, 33:4182–4190, 2005. 21, 37

[174] S. Müller, S. Kumari, R. Rodriguez, and S. Balasubramanian. Small molecule-mediated G-quadruplex isolation from human cells. *Nature Chem.*, 2010 *in press*. 21

[175] V. Berl, I. Huc, R. G. Khoury, and J.-M. Lehn. Helical molecular programming: supramolecular double helices by dimerization of helical oligopyridine-dicarboxamide strands. *Chem.-Eur. J.*, 7:2810–2820, 2001. 21

[176] H. Liang, J.-M. Leger, and I. Huc. Aromatic delta-peptides. *J. Am. Chem. Soc.*, 125:3448–3449, 2003. 23

[177] L. Xing, U. Ziener, T. C. Sutherland, and L. A. Cuccia. Hydrogen bond directed synthesis of pyridazine and naphthyridine containing macrocycles. *Chem. Commun.*, pages 5751–5753, 2005. 21

[178] S. Yagi, I. Yonekura, M. Awakura, M. Ezoe, and T. Tagagishi. Facile synthesis of cofacial porphyrin dimer and trimer using a diarylurea linkage. *Chem. Commun.*, pages 557 – 558, 2001. 21

[179] J. J. P. Steward. Optimization of parameters for semiempirical methods I. Method. *J. Comput. Chem.*, 10:209–220, 1989. 24

[180] J. J. P. Steward. Optimization of parameters for semiempirical methods II. Applications. *J. Comput. Chem.*, 10:221–264, 1989. 24

[181] J.-L. Mergny and J.-C. Maurizot. Fluorescence resonance energy transfer as a probe for G-quartet formation by a telomeric repeat. *ChemBioChem*, 2:124–132, 2001. 29, 32

[182] V. Berl, I. Huc, R. G. Khoury, M. J. Krische, and J.-M. Lehn. Interconversion of single and double helices formed from synthetic molecular strands. *Nature*, 407:720–723, 2000. 36

[183] S. L. Jain, P. Bhattacharyya, H. L. Milton, A. M. Z. Slawin, J. A. Crayston, and J. D. Woollins. New pyridine carboxamide ligands and their complexation to copper(II). X-ray structures of mono-, di,- tri- and tetranuclear copper complexes. *Dalton Trans.*, pages 862–871, 2004. 36

[184] G. Chessa, G. Marangoni, and B. Pitteri. Cross-linked polystyrene resins with 2,6-diformylpyridine bis(2'-pyridylhydrazone) groups. Synthesis and metal ion chelation properties. *Reactive Polymers*, 12:219–228, 1990. 41, 106

[185] Protocol (Promega): http://www.promega.com/tbs/tb288/tb288.pdf. 49

[186] W. F. Scherer, J. T. Syverton, and G. O. Gey. Studies on the propagation *in vitro* of poliomyelitis viruses: IV. Viral multiplication in a stable strain of

human malignant epithelial cells (strain HeLa) derived from an epidermoid carcinoma of the cervix. *J. Exp. Med.*, 97:695–715, 1953. 49

[187] S. Rasheed, W. A. Nelson-Rees, E. M. Toth, P. Arnstein, and M. B. Gardner. Characterization of a newly derived human sarcoma cell line (HT-1080). *Cancer*, 33:1027–1033, 1973. 49

[188] J. Pontén and E. Saksela. Two established *in vitro* cell lines from human mesenchymal tumours. *Int. J. Cancer*, 2:434–447, 1967. 49

[189] L. Hayflick and P. S. Moorhead. The serial cultivation of human diploid cell strains. *Exp. Cell. Res.*, 25:585–621, 1961. 49

[190] A. J. Nakamura, Y. J. Chiang, K. S. Hathcock, I. Horikawa, O. A. Sedelnikova, R. J. Hodes, and W. M. Bonner. Both telomeric and non-telomeric DNA damage are determinants of mammalian cellular senescence. *Epigen. Chrom.*, 1, 2008. 49

[191] T. Velderman, K. T. Etheridge, and C. M. Counter. Loss of hPot1 function leads to telomere instability and a *cut*-like phenotype. *Curr. Biol.*, 14: 2264–2270, 2004. 56

[192] G. P. Dimri, C. Lee, G. Basile, M. Acosta, G. Scott, C. Roskelly, E. E. Medrano, M. Linskens, I. Rubelj, O. Pereira-Smith, M. Peacocke, and J. Campisi. A biomarker that identifies senescent human cells in culture and in aging skin *in vivo*. *Proc. Natl. Acad. Sci. U.S.A.*, 92:9363–9367, 1995. 56

[193] A. G. Bodnar, M. Ouelette, M. Frolkis, S. E. Holt, C. P. Chiu, G. B. Morin, C. B. Harley, J. W. Shay, S. Lichtsteiner, and W. E. Wright. Extension of life-span by introduction of telomerase into normal human cells. *Science*, 279:349–352, 1998. 58, 90

[194] NCI website: http://dtp.cancer.gov/branches/btb/ivclsp.html. 58, 59

[195] M. C. Sanguinetti and M. Tristani-Firouzi. Review article hERG potassium channels and cardiac arrhythmia. *Nature*, 440:463–469, 2006. 61

[196] J. Taunton, C. A. Hassig, and S. L. Schreiber. A mammalian histone deacetylase related to the yeast transcriptional regulator Rpd3p. *Science*, 272:408–411, 1996. 64

[197] D. R. Bentley *et al.* Accurate whole human genome sequencing using reversible terminator chemistry. *Nature*, 456:53–59, 2008. 64, 96

[198] A. Barski, S. Cuddapah, K. Cui, D. E. Schones T.-Y. Roh, Z. Wang, G. Wei, L. Chepelev, and K. Zhao. High-resolution profiling of histone methylations in the human genome. *Cell*, 129:823–837, 2007. 64, 65, 77, 79

[199] D. S. Johnson, A. Mortazavi, R. M. Myers, and B. Wold. Genome-wide mapping of *in vivo* protein-DNA interactions. *Science*, 316:1497–1502, 2007. 64, 65, 77, 79

[200] P. C. Weber, D. H. Ohlendorf, J. J. Wendoloski, and F. R. Slemme. Structural origins of high-affinity biotin binding to streptavidin. *Science*, 243: 85–88, 1989. 66

[201] I. V. Smirnov and R. H. Shafer. Electrostatics dominate quadruplex stability. *Biopolymers*, 85:91–101, 2006. 76

[202] A. Wong and G. Wu. Selective binding of monovalent cations to the stacking G-quartet structure formed by guanosine 5‘-monophosphate: a solid-state NMR study. *J. Am. Chem. Soc.*, 125:13895–13905, 2003. 76

[203] C. Cawthon. Telomere measurement by quantitative PCR. *Nucleic Acids Res.*, 30:e47, 2002. 94